Fall 2021

Teaching an Old Dog New Tricks: Synthesis and Applications Of Novel Polybenzimidazole (PBI) Membranes

Laura Ann Murdock

TEACHING AN OLD DOG NEW TRICKS: SYNTHESIS AND APPLICATIONS OF NOVEL POLYBENZIMIDAZOLE (PBI) MEMBRANES

by

Laura Ann Murdock

Bachelor of Science
University of South Carolina, 2016

Submitted in Partial Fulfillment of the Requirements

For the Degree of Doctor of Philosophy in

Chemistry

College of Arts and Sciences

University of South Carolina

2022

Accepted by:

Brian C. Benicewicz, Major Professor

Chuanbing Tang, Committee Member

Donna A. Chen, Committee Member

William E. Mustain, Committee Member

Tracey L. Weldon, Interim Vice Provost and Dean of the Graduate School

DEDICATION

I would like to dedicate this to my 5 wonderful Grandparents – Sylvia Jackson, Nancy and Gus Hurd, and Frank and Helen Murdock.

ACKNOWLEDGEMENTS

First and foremost, I would like to express my sincerest gratitude to my advisor, Dr. Brian Benicewicz. It has been the greatest honor working with you over the past 5 years. From your mentorship, I have learned skills to develop me into a scientist and leader. Thank you for letting me explore my creativity, for giving me space to learn from my mistakes and try new thing, and for always advocating for me. I will always remember my time in the BB lab fondly, thank you very much for the opportunities you have given me.

I would next like to thank my committee members, Dr. Chuanbing Tang, Dr. Donna Chen, and Dr. William Mustain. Each of you have challenged me and provided insights and feedback to help develop my research skills. I want to thank Dr. Morgan Stefik, who's lab I did undergraduate research in, for the opportunity to get involved in research and for encouraging me to apply to graduate school.

I would like to thank the Benicewicz group, including previous and current lab members – Dr. Zaid Abbas, Dr. Maan Al-Ali, Dr. Amin Daryaei, Dr. Ben Howard, Dr. Fei Huang, Dr. Yucheng Huang, Dr. Ishwor Karki, Dr. Mohammad Khani, Dr. Andrew Pingitore, Dr. Julia Pribyl, Dr. Lihui Wang, Richard Ly, Caroline Rohlfing and Eric Ruzicka. I would especially like to thank Dr. Julia Pribyl for encouraging me and believing in me since day 1, your continued support has meant so much to me. I would also like to thank Dr. Andrew Pingitore for training me and teaching me the skills I needed to succeed during my PhD. To Dr. Zaid Abbas, thank you for reminding me that there is life outside of the lab to

be enjoyed, your humor and encouragement really helped me when the hard lab days hit. I want to thank Dr. Fei Huang for teaching this organic chemist electrochemistry with great patience. To the unsung hero of the BB Group, Miss Susan Hipp, thank you so much for your support and encouragement over the past 5 years, for advocating for me and being there for me.

I'd like give a big thank you to my friends and fellow graduate students that I've had the opportunity to meet while here. In particular, I would like to thank Dr. Zachary Marsh, who mentored me as an undergraduate researcher in the Stefik Group, Dr. Meghan Lamm for her guidance and support, and Dr. Tianyu Zhu for his encouragement and for making the late laboratory nights less lonely. I would like to thank the many friends I've made throughout the department.

I want to thank my amazing collaborators that I've had the opportunity to work with. To Dr. Carsten Henschel and Dr. Jörg Belack at BASF New Business, Dr. Daniel Malko, Dr. Evgeny Larionov, Detlef Ott, and Andrea Krebs at BASF, I am so thankful for your support, encouragement, excitement, and feedback. The whole BASF team has treated me like a respected colleague since day 1. I'm very grateful to have had the opportunity to work with you all, it has been so much fun.

Lastly, I would like to thank my amazing family and friends for their continued support. To my parents, Cindy and Greg, my siblings Kyle, Kelly, and Meredith, and 14 year old dog Upton, thank you for the constant support and love. I wouldn't have been able to do this without your support. To my good friends and housemates, Madison Kennette and Cecilia Depret-Bixio, your support has meant so much to me, thank you for celebrating every single achievement with me and encouraging me to have fun outside of the lab.

ABSTRACT

Polybenzimidazoles (PBIs) represent a class of performance polymers that display exceptional thermal and oxidative stability. For almost thirty years, PBI membranes have been investigated as promising candidates for next-generation alternative energy devices, including high temperature polymer electrolyte membrane fuel cells (HT-PEMFCs) and vanadium redox flow batteries (VRBs). Issues with the production of PBI membranes arise from their inherent low solubility in organic solvents. Thus, conventional approaches typically yield membranes that have limited molecular weight and generate significant waste in preparation, due to the large quantity of solvent required to dissolve PBIs for membrane casting.

Presented herein is the development of a new process, adapted from the sol-gel polyphosphoric acid (PPA) Process, to yield dense PBI films for the first time without the use of organic solvents. This significantly reduces the waste generated in making PBI films and allows much higher molecular weights to be achieved. Included in this work is the fabrication and characterization of dense PBI films produced by this method and applications in two electrochemical devices. In the case of HT-PEMFCs, the PBI membranes produced have demonstrated the ability to maintain high proton conductivities (>0.20 S cm^{-1}) with lower levels of phosphoric acid. These new membranes also contain double the solids content and a five times enhancement in the creep resistance, compared to

the previous membrane method. Thus, cell operation at high current densities was achieved with a very low degradation rate. This advanced membrane offers great potential in aviation and heavy-duty vehicle applications.

For VRBs, PBI membranes produced using the outlined technique result in two orders of magnitude reduction in vanadium permeability. This process also gives PBI membranes with higher ionic conductivity than those that are cast from an organic solvent and doped in acid, or the "conventionally imbibed" PBIs. Membranes produced according to this method thus have impressive cell cycling results and show great promise in grid-scale energy storage.

TABLE OF CONTENTS

LIST OF TABLES

LIST OF FIGURES

LIST OF SYMBOLS

X	Acid Doping Level
P	Cell Pressure
ΔV	Change in Voltage
J(t)	Creep Compliance
F	Faraday Constant
η_{ihh}	Inherent Viscosity
σ	Ionic Conductivity
E_{ohmic}	Ohmic Overpotential
R_m	Ohmic Resistance
p_{anode}	Partial Pressure of Hydrogen at Anode
$p_{cathode}$	Partial Pressure of Hydrogen at Cathode
$E_{polarization}$	Polarization Overpotential
$E_{required}$	Required EHS Cell Potential
P_s	Salt Permeability
J_s^0	Steady-State Creep Compliance
T	Temperature
R	Universal Gas Constant
v/v	Volume Percentage
wt%	Weight Percent

LIST OF ABBREVIATIONS

AEM ..... Anion Exchange Membrane

BET ..... Brunauer-Emmett-Teller

BEVs ..... Battery Electric Vehicles

BP ..... Back Pressure

CE ..... Coulombic Efficiency

CEM ..... Cation Exchange Membrane

DCA ..... Dicarboxylic Acid

DMAc ..... N,N′-Dimethylacetamide

DPIP ..... Diphenyl Isophthalate

EDS ..... Energy Dispersive X-Ray Spectroscopy

EE ..... Energy Efficiency

EHS ..... Electrochemical Hydrogen Separation

EIS ..... Electrochemical Impedance Spectroscopy

GDE ..... Gas Diffusion Electrode

GDL ..... Gas Diffusion Layer

HFR ..... High Frequency Resistance

HT-PEMFC ..... High Temperature Polymer Electrolyte Membrane Fuel Cell

IEM ..... Ion Exchange Membrane

IV ..... Inherent Viscosity

IPA ..... Isophthalic Acid

LiCl ..... Lithium Chloride

LT-PEMFC ..... Low Temperature Polymer Electrolyte Membrane Fuel Cell

m-PBI ..... Meta Polybenzimidazole

m/p-PBI ..... Meta/Para Polybenzimidazole

MEA ..... Membrane Electrode Assembly

$MgSO_4$ ..... Magnesium Sulfate

NaOH ..... Sodium Hydroxide

NIST ..... National Institute of Standards and Technology

OCV ..... Open Circuit Voltage

p-PBI ..... Para Polybenzimidazole

PA ..... Phosphoric Acid

PBI ..... Polybenzimidazole

PEM ..... Polymer Electrolyte Membrane

PEMFC ..... Polymer Electrolyte Membrane Fuel Cell

PFSA ..... Perfluorosulfonic Acid

PPA ..... Polyphosphoric Acid

PRU ..... Polymer Repeat Unit

PTFE ..... Polytetrafluoroethylene

RH ..... Relative Humidity

s-PBI ..... Sulfonated Polybenzimidazole

SA ..... Sulfuric Acid

SEM ..... Scanning Electron Microscope

STPA ..... 2-Sulfoterephthalic Acid Monosodium Salt

TAB ..... 3,3′,4,4′-Tetraamine-(1,1′-Biphenyl)

TGA ..... Thermogravimetric Analysis

TPA ..... Terephthalic Acid

UTRC ..... United Technologies Research Center

$VOSO_4$ ..... Vanadium (IV) Sulfate

VRB ..... Vanadium Redox Flow Battery

WAXS ..... Wide-Angle X-ray Scattering

2D 2-Dimensional

2OH-PBI ..... Dihydroxy Polybenzimidazole

2OH-TPA ..... 2,5-Dihydroxyterephthalic Acid

5S-IPA ..... 5-Sulfoisophthalic Acid Monosodium Salt

CHAPTER 1

INTRODUCTION

1.1 ENERGY CRISIS

Greenhouse gases, such as carbon dioxide, are gases in the atmosphere that absorb radiation from the sun and interfere with our Earth's naturally balanced greenhouse effect. Increasing levels of greenhouse gases in the atmosphere traps in heat to further warm the Earth. Global carbon dioxide emissions from the burning of fossil fuels for energy production have significantly risen since the late 1800's, as demonstrated in **Figure 1.1**.[1] As of 2015, fossil fuels accounted for 80% of the world's primary energy consumption.[2] The demand for energy is rising due to technology innovations and increasing world population. However, fossil fuels are a finite resource and damaging to the environment. The steadily rising temperatures on Earth has been linked to environmental conditions including depletion of ice sheets, rising sea levels, increasing and intensifying extreme weather events, and ocean acidification.[3-8] Thus, there is a great need to develop alternative energy sources and advanced energy storage to meet the growing energy demands of our ever-advancing world.

1.2 FUEL CELLS

A fuel cell converts the chemical energy of a fuel, typically hydrogen into electrical energy. The first working fuel cell was developed by Sir William Grove in 1839.[9] Advantages of fuel cells include no production of greenhouse gases or air pollutants, broad selection of fuels can be used, there is no need for recharging, and they have a high energy conversion efficiency (no Carnot cycle limitations).[10-12] In a hydrogen fuel cell (**Figure 1.2**[13]), hydrogen gas is fed to the negative electrode, known as the anode, where a catalyst oxidizes hydrogen into protons and electrons. The electrons travel through an external circuit to generate

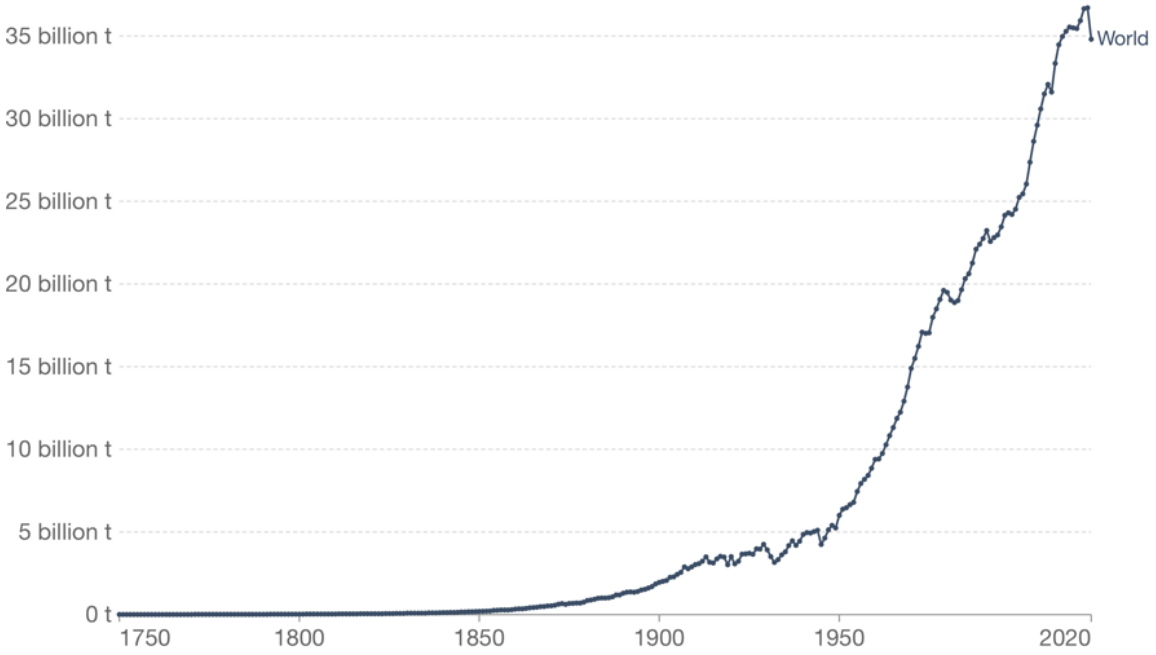

Figure 1.1. Global annual carbon dioxide emissions from the burning of fossil fuels for energy and cement production.[1]

electricity, while protons are transported through the polymer membrane, located in the center of the cell. Reduction occurs at the positive electrode, the cathode, where protons, electrons and oxygen are combined to produce water and heat. The electrochemical reactions are displayed below:

$$\text{Anode: } 2\,H_2 \rightarrow 4\,H^+ + 4\,e^-$$

$$\text{Cathode: } O_2 + 4\,e^- + 4\,H^+ \rightarrow 2\,H_2O$$

$$\text{Overall: } 2\,H_2 + O_2 \rightarrow 2\,H_2O$$

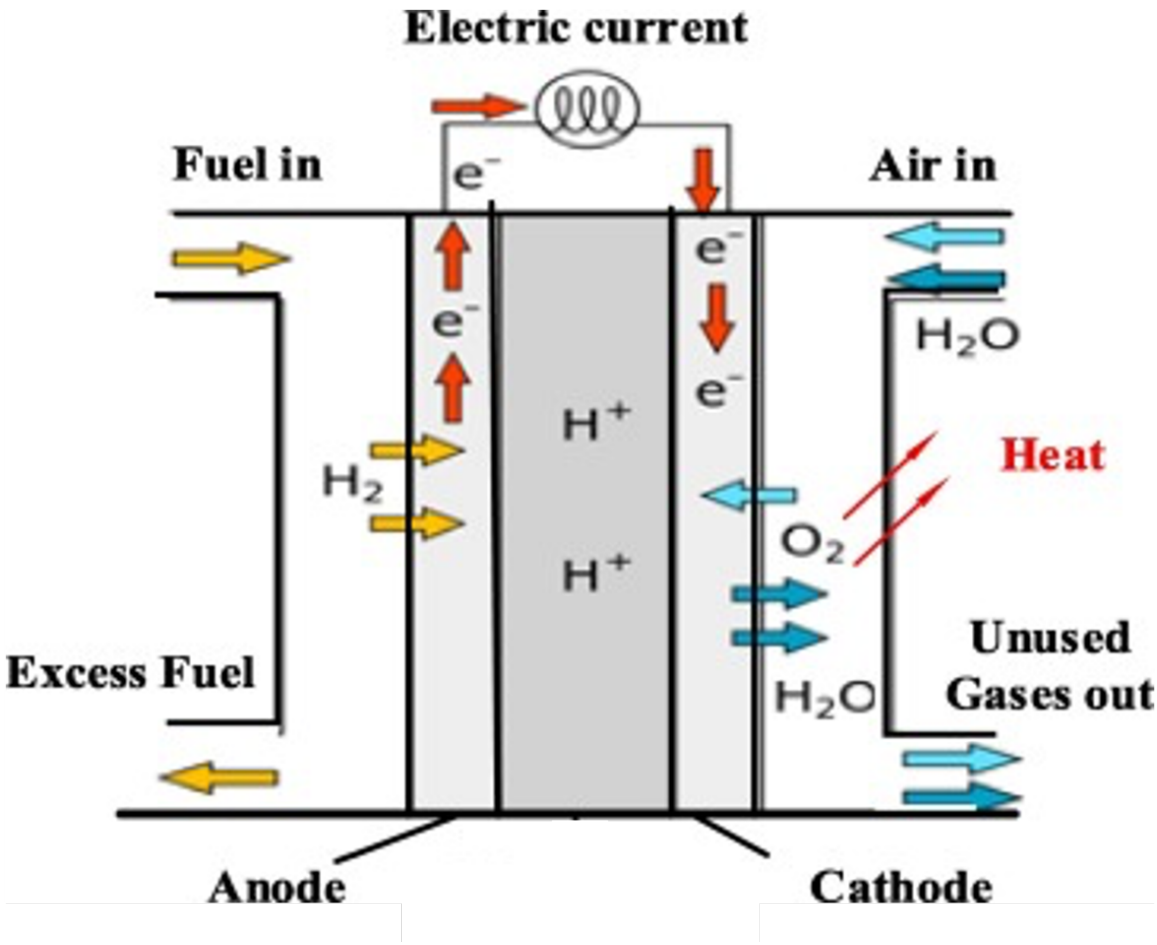

Figure 1.2. The basic operation of a hydrogen fuel cell.[13]

Fuel cells are typically classified by their electrolyte, including polymer membrane, alkaline, phosphoric acid, molten carbonate, and solid oxide. Polymer electrolyte membrane fuel cells, or proton exchange membrane fuel cells (PEMFCs) offer potential applications in portable power, transportation, and residential power generation applications.[14-16]

PEMFCs utilize semipermeable membranes which are responsible for proton transportation and conduction, while also limiting transmission of gases and electrons. At the heart of a PEMFC is the membrane electrode assembly

(MEA). MEAs consists of the polymer membrane sandwiched between two electrodes. The electrochemical reactions occur at the surface of the catalyst, in the interface between the electrolyte and the membrane. The MEA is built into the fuel cell with other components (**Figure 1.3**[17]), including gas diffusion layers, gaskets, graphite plates, current collectors, and end plates.

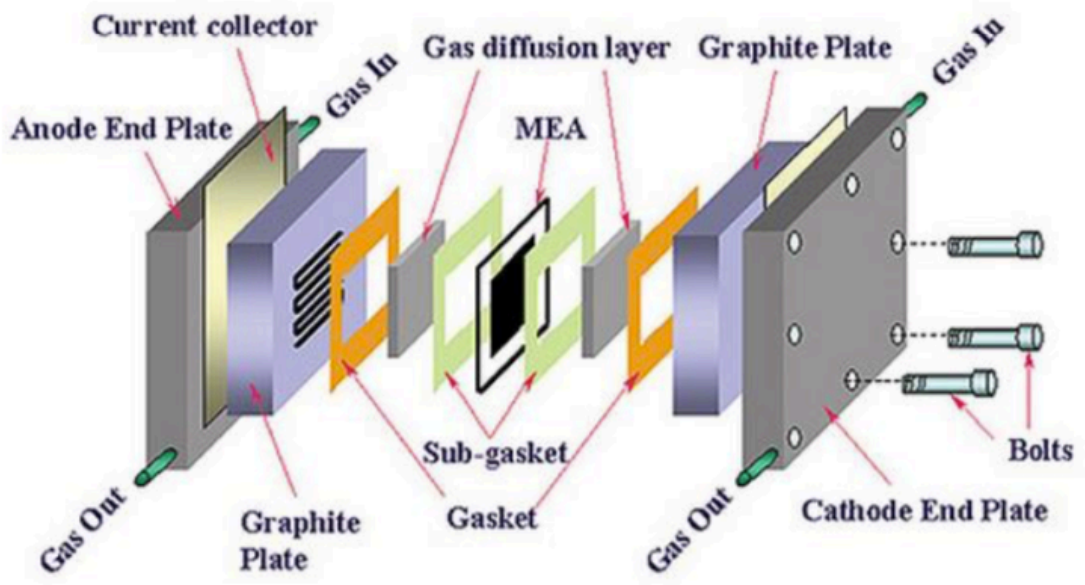

Figure 1.3. Fuel cell components.[17]

Low temperature polymer electrolyte membrane fuel cells (LT-PEMFCs) typically utilize perfluorinated sulfonic acid (PFSA) membranes, such as Nafion®.[18] PFSA membranes are dependent on water to conduct protons, and are thus limited to fuel cell operating temperatures below 100 °C.[19] While LT-PEMFCs benefit from quick start-up, high power density, and easy scale-up, they have several limitations.[20] Due to the dependence on water, large heat exchangers are required to adequately manage the water and heat within the cell stack. Fuel cell operation at low temperatures also requires very pure fuels, as some impurities

such as 10 ppm of carbon monoxide will competitively and irreversible bind to the catalyst, eventually poisoning it.

High temperature polymer electrolyte membrane fuel cells (HT-PEMFCs) are operated from 120-200 °C and provide many enticing benefits. HT-PEMFCs display enhanced tolerance to fuel impurities,[19, 21-24] faster electrode kinetics,[25-27] and simplified water management.[28, 29] HT-PEMFCs typically utilize phosphoric acid doped polybenzimidazole membranes, due to their significant ionic conductivity at elevated temperatures, excellent chemical and thermal stability in the fuel cell environment, low gas permeability, and nearly zero water drag coefficient.[22, 30-38]

1.3 ELECTROCHEMICAL HYDROGEN SEPARATION

Electrochemical Hydrogen Separation (EHS) is a technique to efficiently purify, pump, and pressurize hydrogen at low to moderate flow rates, which is needed to advance the hydrogen economy. Existing technologies for hydrogen purification include cryogenic distillation,[39-41] pressure swing adsorption,[42-45] and membrane separation.[40, 46-48] However, each of these methods requires significant energy and associated costs, as well as multiple vessels, high maintenance, or significant venting of excess hydrogen.[40, 46, 49]

EHS was originally reported and developed in the 1960's based on low-temperature PEMs.[50, 51] As displayed in **Figure 1.4**, a hydrogen containing gas stream is fed to the anode and the hydrogen is oxidized to protons and electrons. The electrons travel through the external circuit to the cathode, while protons are driven through the membrane by the applied potential difference between the anode and the cathode. The protons and electrons are combined at the cathode to

re-form molecular hydrogen. EHS and fuel cells are very similar, however, EHS is operated in electrolytic mode while fuel cells are operated in galvanic mode, meaning that EHS requires power to complete the chemical reactions and does not generate power as is done in galvanic mode. Low temperature PEMs are limited to EHS operation with gas streams that do not contain molecules that will poison the platinum catalyst or diffuse through the membrane.[52-58] However, high temperature PEMs, such as phosphoric acid doped PBI membranes, can mitigate the issues that surround EHS operation with low temperature PEMs.[59-63]

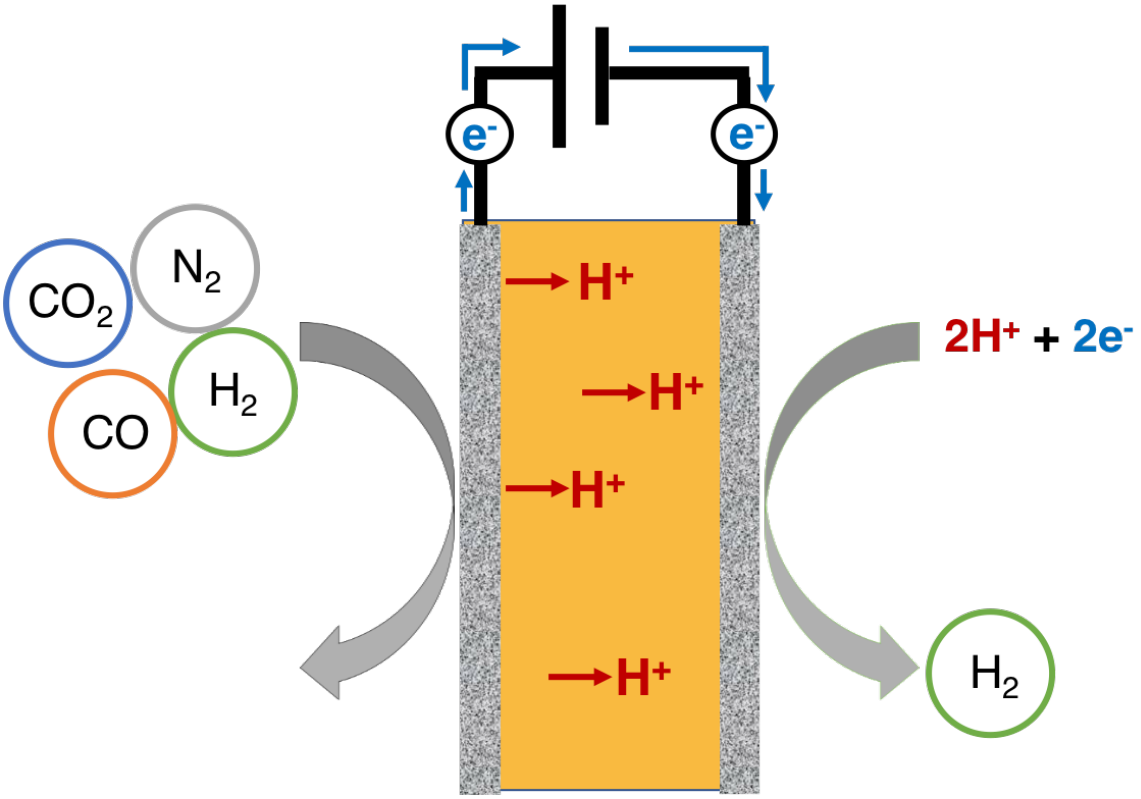

Figure 1.4. Basic operation of an electrochemical hydrogen pump.

1.4 VANADIUM REDOX FLOW BATTERIES

The vanadium redox flow battery (VRB) is a rechargeable, all liquid battery, with application in large-scale energy storage. VRBs store and release energy through conversion of chemical energy and electrical energy. Advantages of VRBs include longevity, active thermal management, and liberation from energy and power rankings.[64] VRBs offers potential applications in grid energy storage, especially in conjunction with renewable energy sources such as solar or wind energy. In a typical VRB (**Figure 1.5**[65]), there are two electrolyte tanks, each containing a vanadium redox couple (2+/3+ and 4+/5+) dissolved in 2-4 M sulfuric acid, and a cell stack situated between the two tanks.[66] The charge-discharge process involves oxidation or reduction of the active species to bring about conversion of the chemical energy and electrical energy.[67] Charging occurs while the V^{3+} species is reduced on the anode to form V^{2+} and while the VO^{2+}(V^{4+}) species is oxidized to the VO_2^+(V^{5+}) species on the anode. A standard potential of 1.25 V is produced by VRBs through the following reactions:

$$\text{Anode: } V^{3+} + e^- \leftrightarrow V^{2+} \quad E^\circ = -0.25 \text{ V}$$

$$\text{Cathode: } VO^{2+} + H_2O - e^- \leftrightarrow VO_2^+ + 2\,H^+ \quad E^\circ = 1.00 \text{ V}$$

$$\text{Cell: } VO^{2+} + H_2O + V^{3+} \leftrightarrow VO_2^+ + 2\,H^+ + V^{2+} \quad E^\circ = 1.25 \text{ V}$$

A key component of the VRB is the ion exchange membrane (IEM), found in the center of the cell stack to confine each electrolyte solution to their respective half-cell. The IEM has two main functions in a VRB, to transfer ions from the anode to the cathode, and to prevent cross-over of the anolyte and catholyte solutions.[68]

Thus, the transport properties of protons and vanadium ions in a selected membrane must be fundamentally understood to maximize the great potential of the VRB.

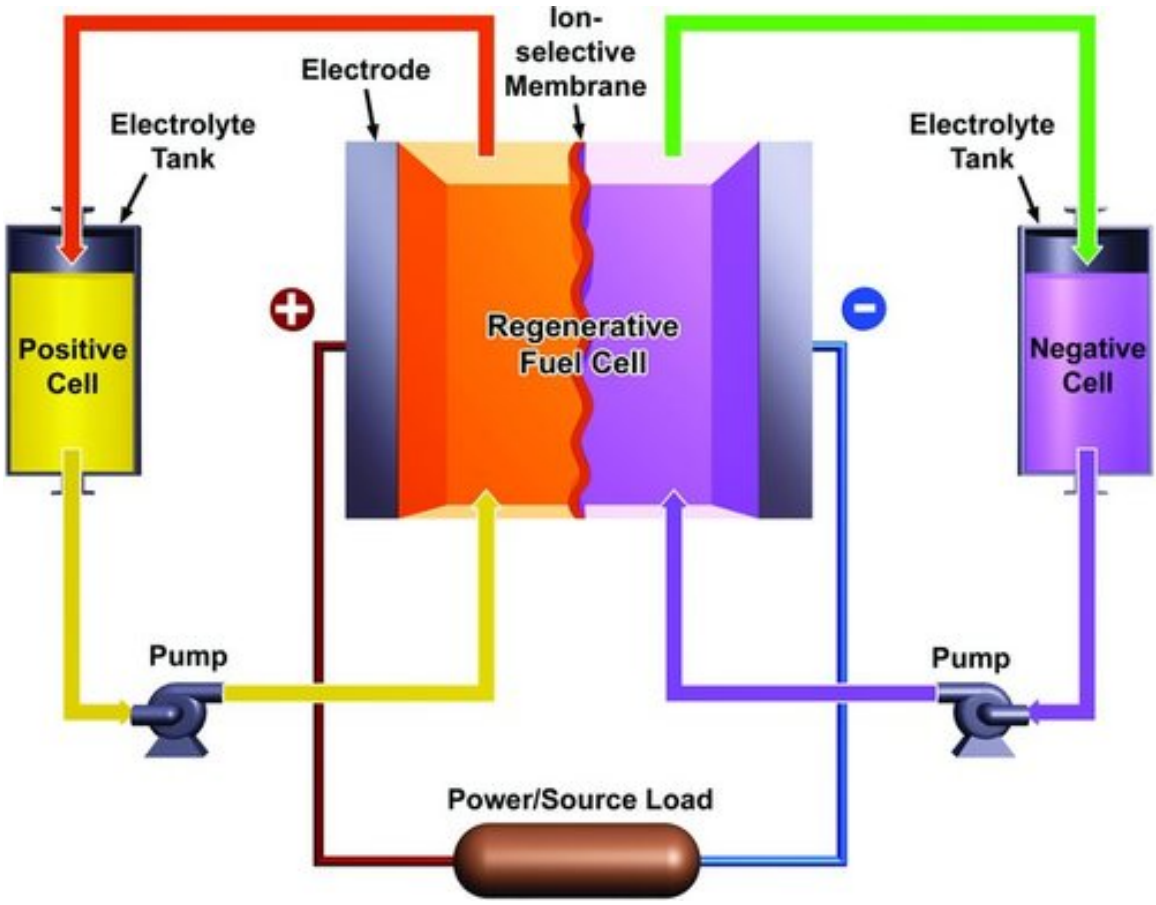

Figure 1.5. Illustration of a VRB.[65]

VRBs typically employ well-known and commercially available PFSA-based materials as the membrane separator. While PFSAs generally display high ionic conductivities, they are cation permeable by nature, and thus display high vanadium permeability.[69-71] Furthermore, PFSAs are expensive, accounting for up to 40% of the total cost of the cell stack, and there are environmental concerns about their production and disposal.[72-77] Therefore, the development of

nonperfluorinated membranes that display high ionic conductivity, low vanadium permeability, and excellent oxidative stability are needed.

1.5 POLYBENZIMIDAZOLES

Polybenzimidazoles (PBIs) are a class of performance polymers originally synthesized in 1959, the first wholly aromatic PBI was synthesized in 1961 by Vogel and Marvel.[78, 79] Aromatic PBIs display high thermal stability, nonflammability, and excellent chemical resistance. However, due to the rigid nature of the wholly aromatic backbone, the solubility and processability of PBIs remains a challenge. The general structure of PBI is displayed in **Figure 1.6**. The most heavily investigated PBI is poly(2,2′-*m*-(phenylene)-5,5′-bibenzimidazole (m-PBI), which exhibits both excellent thermal stability and processability. It was commercialized by Hoechst Celanese in the 1980's under the trademark Celazole®. PBI has been investigated for applications as adhesives and composites, molded parts, fibers, and membranes. PBI membranes and films have been used as membranes for liquid and gas separations,[80-86] nanofiltration,[87-89] and ion-exchange membranes in electrochemical devices.[90, 91]

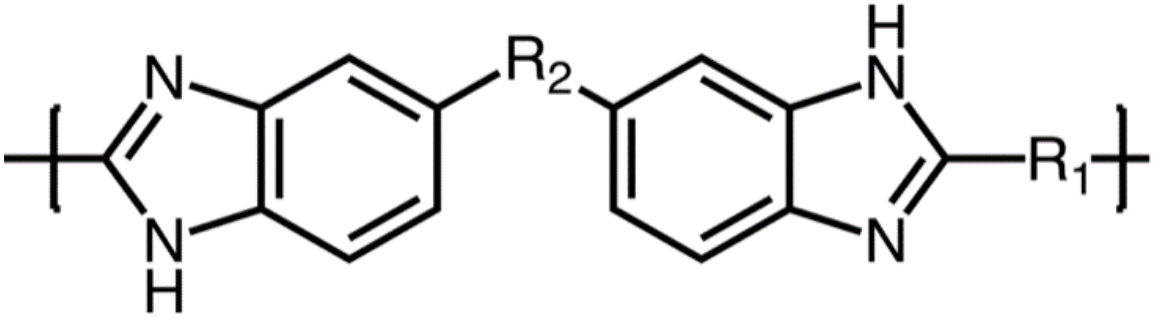

Figure 1.6. General structure of a polybenzimidazole repeat unit.

1.6 SYNTHESIS OF POLYBENZIMIDAZOLES

PBI membranes can be produced following a two stage melt/solid polycondensation reaction or a solution polymerization. The general synthetic route to produce PBI is shown in **Figure 1.7**. In the two stage melt/solid polycondensation reaction, commercial production of m-PBI is carried out using 3,3',4,4'-tetramaminobiphenyl (TAB) and diphenyl isophthalate (DPIP).[92] In the first stage, PBI pre-polymers are produced with a low molecular weight. In the second stage, the pre-polymers are crushed and heated to high temperatures (>300 ºC) to produce the high molecular weight m-PBI. In this method, no organic solvents are required, and post-polymerization is relatively easy. However, due to inherent limitations of heterogeneous reactions, the inherent viscosity (IV) is limited to 0.5-0.8 dL g^{-1}.[93, 94] PBIs can also be polymerization in a solution polymerization of dicarboxylic acids and tetramines, in solvents such as polyphosphoric acid (PPA), methane sulfonic acid and phosphorus pentoxide, and N, N-dimethylacetamide (DMAc).[17, 95, 96]

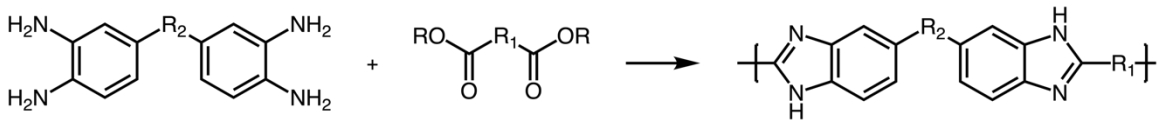

Figure 1.7. General synthetic scheme of polybenzimidazoles.

1.7 POLYBENZIMIDAZOLE MEMBRANE PREPARATION

1.7.1 Conventional Imbibing Method

The most frequently reported method to produce acid doped PBI membranes is the "conventional imbibing method," as shown in **Figure 1.8**.[30, 91, 97,

[98] In this method, PBI is extracted after polymerization and purified by dissolving in DMAc and lithium chloride (LiCl) under pressures of 80-100 psi and high temperatures. The solution is then filtered and cast as a film, from which the solvent is evaporated. After evaporation and drying, dense PBI films are formed which must undergo additional washing in boiling water to remove remaining DMAc. After drying, the dense PBI films are doped in phosphoric acid.

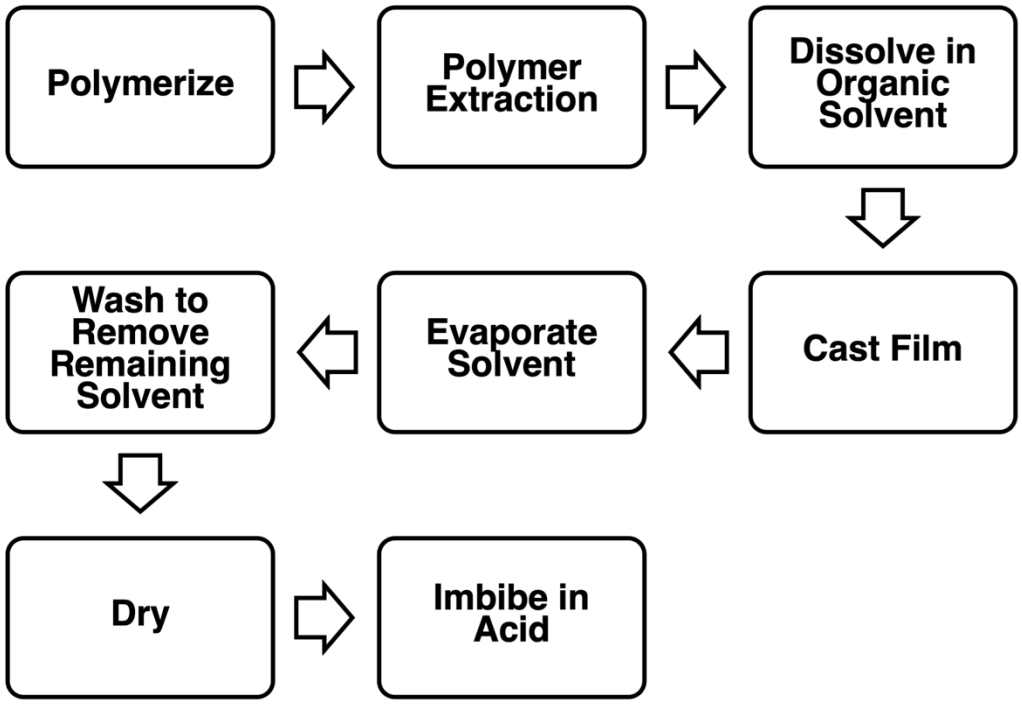

Figure 1.8. Steps in the conventional imbibing method to produce acid imbibed dense PBI membranes.

The conventional imbibing technique involves multiple steps, harsh conditions, and generates a significant amount of waste. This method also has limitations including limited PBI backbone structures that can be prepared in this method, and limited molecular weights due to solubility limitations. PBIs that

contain a more rigid backbone structure, such as p-PBI, are much less soluble in organic solvents than m-PBI due to closer packing of polymer chains.[79, 99]

PBIs produced in the conventional imbibing method were doped in phosphoric acid for application in HT-PEMFCs and EHS. Acid doping levels of 6-10 moles of phosphoric acid per polymer repeat unit were achieved and ionic conductivity at 150 °C was 0.04-0.08 S cm^{-1}.[93] Efforts to increase the acid doping levels and ionic conductivities of membranes produced in this method were not successful, as the mechanical properties of the membranes worsen as the acid doping levels are increased.[100] PBIs produced in the conventionally imbibed process were doped in a sulfuric acid solution to investigate application in VRBs. PBIs produced in this method displayed a very low vanadium permeability, and a very low ionic conductivity.[101-104]

1.7.2 PPA Process

In 2005, Xiao et al. reported on a method to utilize polyphosphoric acid (PPA) as both the condensation reagent and casting solvent to produce gel PBI membranes doped in phosphoric acid, and termed the PPA Process.[105] In the PPA Process (**Figure 1.9**), dicarboxylic acids and tetramines are polymerized in PPA at temperatures of 195-220 °C to produce high molecular weight PBI polymers. Upon completion of the polymerization, the PBI polymers in solution with PPA are cast directly onto a suitable substrate, typically glass plates. PBI and PPA are both hygroscopic and will absorb moisture in the air, hydrolyzing PPA to phosphoric acid (PA). However, while PPA is a good solvent for PBI, PA is a poor solvent for PBI and a sol-to-gel phase transition occurs (**Figure 1.10**).

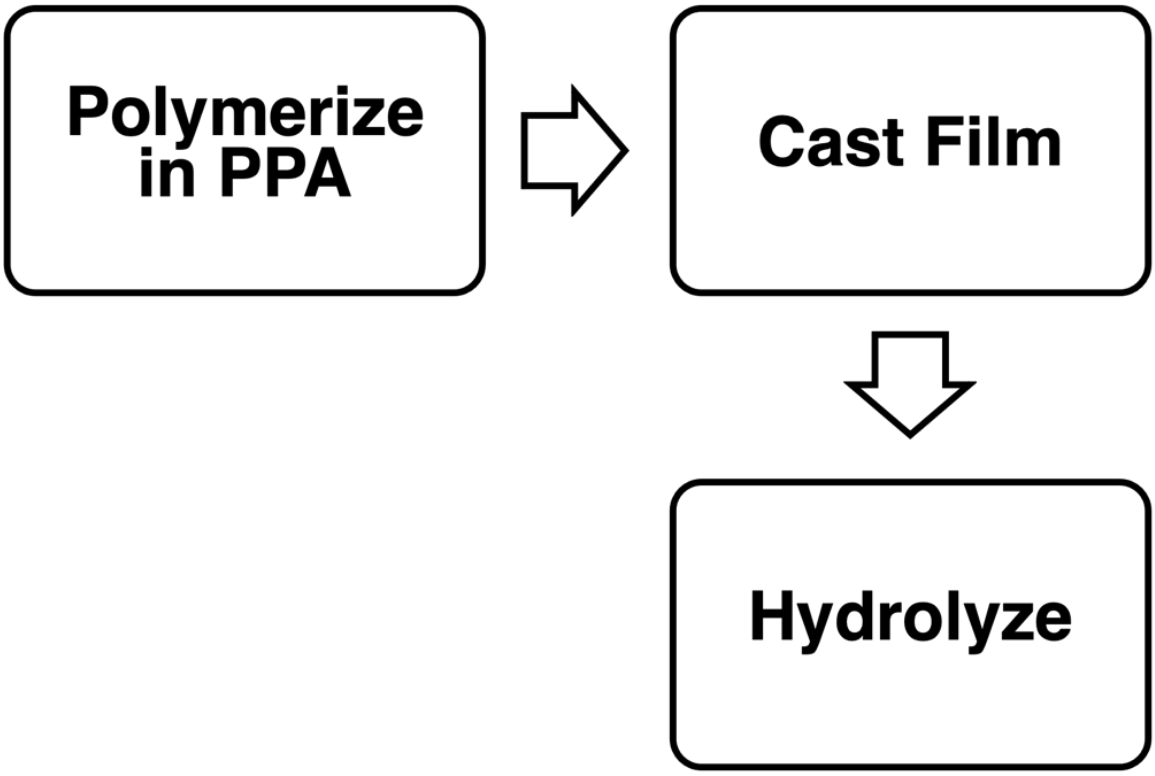

Figure 1.9. Steps in the PPA Process to produce acid-doped gel PBI membranes.

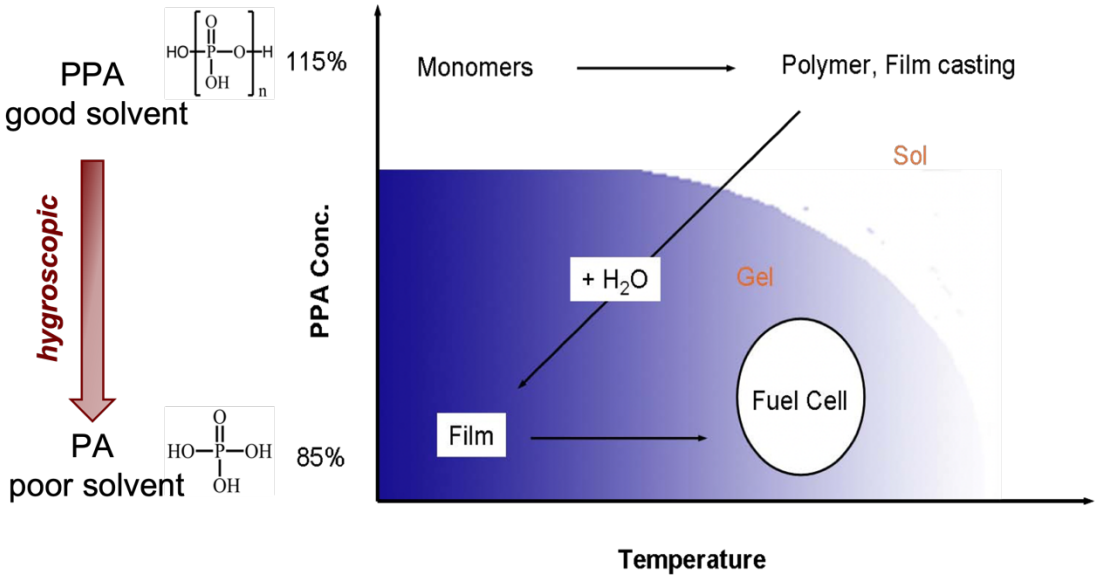

Figure 1.10. The sol-gel process that occurs in the PPA Process.

The PPA Process is quicker, generates less waste, and is cheaper than the conventional imbibing technique. Also, PBIs produced in the PPA Process have been shown to display better properties for electrochemical devices, such as higher acid doping levels and ionic conductivities at elevated temperatures. [105-114] In a comparative study of m-PBI produced in the conventional imbibing method and the PPA Process, the conventionally imbibed m-PBI displayed a lower IV, acid doping level, and conductivity at elevated temperatures. PPA Process m-PBI was able to achieve an ionic conductivity of 0.14 S cm^{-1} at 180 °C, compared to an ionic conductivity of 0.08 S cm^{-1} at 180 °C for the conventionally imbibed m-PBI.[61] Furthermore, since the PPA Process does not require any organic solvents, PBIs with more rigid backbone structure's, such as p-PBI can be produced. It was found that p-PBI membranes produced in the PPA Process contain an acid doping level of 30-40 moles of phosphoric acid per polymer repeat unit, and ionic conductivities of ~0.26 S cm^{-1} at 180 °C.[114]

Despite the high acid doping levels and ionic conductivities achieved using the PPA Process, membranes produced in this method have been found to suffer from membrane creep.[115] Creep and stress relaxation occur in the PBI gel membranes, as they contain very little solids content and mostly liquid (~95 wt%). Creep affects the performance in fuel cells, causing loss of intimate contact with electrodes that is needed. Creep thinning can eventually cause pinholes and catastrophic failure of the fuel cell. Methods were attempted to improve the creep properties of gel PBI membranes.[111, 116, 117] For example, in 2019 Pingitore et al. reported on a meta/para-PBI copolymer membrane with improved creep properties, and stable cell performance over 17,000 hours.[111] However, the ionic

conductivity of the m/p-PBI copolymer membrane was lower than the p-PBI gel membrane, 0.17 S cm^{-1} and 0.26 S cm^{-1}, respectively. This led to a lower performance of the fuel cell, although the performance durability was improved. Similar issues with creep were investigated for EHS operation.[61, 62]

Gel PBI membranes produced in the PPA Process have also been investigated for application in VRBs.[118] Wang et al. investigated s-PBI gel membranes and crosslinking reactions on flow battery ex-situ properties and cell performance. The s-PBI gel membranes displayed very high ionic conductivities (>500 mS cm^{-1} in 2.6 M sulfuric acid), but very high vanadium permeabilities (~5 x 10^{-7} cm^2 s^{-1}). They compared this to conventionally imbibed m-PBI membrane, which showed roughly an order of magnitude lower ionic conductivity (13 mS cm^{-1} in 2.6 M sulfuric acid) and 4 orders of magnitude lower vanadium permeability (2.5 x 10^{-11} cm^2 s^{-1}). While the permeability of the s-PBI gel membranes were too high, the high iconic conductivities of the gel PBI membranes allowed for flow battery charge and discharge processes to occur at higher current densities, up to 500 mA cm^{-2}. Meanwhile, conventionally imbibed m-PBI could only operate at ~100 mA cm^{-2} since it had a much lower ionic conductivity. Overall, there remains a trade-off of vanadium permeability and ionic conductivity. PBI membranes that can overcome this trade-off and achieve high ionic conductivity and low vanadium permeability are still needed.

1.8 DISSERTATION OUTLINE

This dissertation focuses on the synthesis, processing and properties of PBI membranes for applications in electrochemical devices. The principles and

limitations to production of PBI membranes, discussed here in Chapter 1, guided the development of a new processing technique to produce dense PBI films without organic solvents.

Chapter 2 focuses on the process to make dense PBI films and the development of a new processing technique to produce dense PBI films without the use of organic solvents. Various dense PBI films with rigid para-oriented backbone structures were prepared and compared to dense meta-PBI films produced by casting from an organic solvent. The dense PBI films produced in the new solvent-free process displayed excellent thermal stability and mechanical properties.

Chapter 3 expanded on the work in Chapter 2 by investigating application of dense PBI films produced in the solvent-free process in VRBs. Compared to the original gel PBIs, the dense PBIs prepared exhibited significantly lower vanadium permeability, but also lower ionic conductivity. The dense PBI films produced in the new process were stable during cell testing for over 7 months.

Chapter 4 explored the application of the dense PBI films in HT-PEMFCs and EHS. The new processing technique allowed for high ionic conductivity to be achieved at high temperatures and for better mechanical properties. This allowed for improved fuel cell and EHS performance under various operating conditions. The better properties and performance of the dense PBIs was attributed to a difference in the morphology of the PBI membranes with different processing techniques.

Chapter 5 deviates from the process to make dense PBI films, and investigates the synthesis of novel copolymer gel PBI membranes. Optimization of the polymerization was completed as well as studies on application in HT-PEMFCs and VRBs.

1.9 REFERENCES

[1] Ritchie, H.; Roser, M. CO_2 and greenhouse gas emissions, 2020. Our World in Data Web site. https://ourworldindata.org/co2-emissions?utm_source=squamish%20chief&utm_campaign=squamish%20chief&utm_medium=referral (accessed Feb 16, 2022).

[2] Mohr, S.; Wang, J.; Ellem, G.; Ward, J.; Giurco, D. Projection of World Fossil Fuels by Country. *Fuel* **2015,** *141*, 120-135.

[3] Nerem, R. S.; Beckley, B. D.; Fasullo, J. T.; Hamlington, B. D.; Masters, D.; Mitchum, G. T. Climate-Change–Driven Accelerated Sea-Level Rise Detected in the Altimeter Era. *Proceedings of the National Academy of Sciences* **2018,** *115* (9), 2022-2025.

[4] Wuebbles, D. J.; Fahey, D. W.; Hibbard, K. A. *Climate Science Special Report: Fourth National Climate Assessment, Volume I;* U.S. Global Change Research Program: Washington, DC, 2017; pp 470.

[5] Dilmore, R.; Zhang, L. Greenhouse Gases and Their Role in Climate Change. In *Greenhouse Gases and Clay Minerals*. Green; Romanov, V., Ed.; Springer, 2018; pp 15-32. DOI: 10.1007/978-3-319-12661-6_2

[6] Doney, S. C.; Fabry, V. J.; Feely, R. A.; Kleypas, J. A. Ocean Acidification: The Other CO2 Problem. *Annual Review of Marine Science* **2009,** *1*, 169-192.

[7] Manabe, S.; Broccoli, A. The Influence of Continental Ice Sheets on the Climate of an Ice Age. *Journal of Geophysical Research: Atmospheres* **1985,** *90* (D1), 2167-2190.

[8] Jentsch, A.; Kreyling, J.; Beierkuhnlein, C. A New Generation of Climate-Change Experiments: Events, Not Trends. *Frontiers in Ecology and the Environment* **2007,** *5* (7), 365-374.

[9] Grove, W. R. XXIV. On voltaic series and the combination of gases by platinum. *The London, Edinburgh, and Dublin Philosophical Magazine and Journal of Science* **1839,** *14* (86-87), 127-130.

[10] Yeager, E. Fuel Cells: They produce more electricty per pound of fuel than any other nonnuclear method of power production. *Science* **1961,** *134* (3486), 1178-1186.

[11] Larminie, J.; Dicks, A. *Fuel Cell Systems Explained*, 2nd ed.; J. Wiley & Sons Ltd, 2003. DOI: 10.1002/9781118878330

[12] Srinivasan, S. *Fuel Cells : From Fundamentals to Applications*, 1st ed.; Springer, 2006. DOI: 10.1007/0-387-35402-6

[13] *PEM Fuel Cells with Bio-Ethanol Processor Systems: A Multidisciplinary Study of Modelling, Simulation, Fault Diagnosis and Advanced Control*, 1st ed.; Basualdo, M. S.; Feroldi, D.; Outbib, R., Eds.; Springer, 2011. DOI: 10.1007/978-1-84996-184-4

[14] Böddeker, K. W.; Peinemann, K. V.; Nunes, S. P. Membranes in Fuel Cells. *Journal of Membrane Science* **2001,** *185* (1), 1.

[15] Satyapal, S. *U.S. Department of Energy Hydrogen and Fuel Cells Program; 2011 Annual Merit Review and Peer Evaluation Report*; NREL/BK-6A20-74379; DOE/GO-102019-5199; Arlington, Virginia, 2011.

[16] Wang, Y.; Chen, K. S.; Mishler, J.; Cho, S. C.; Adroher, X. C. A review of polymer electrolyte membrane fuel cells: Technology, applications, and needs on fundamental research. *Applied Energy* **2011,** *88* (4), 981-1007.

[17] Fishel, K. Hydroxy polybenzimidazoles for high temperature fuel cells and the solution polymerization of polybenzimidazole. Ph.D. Dissertation, University of South Carolina, Columbia, SC, 2015.

[18] Grot, W. G. Perfluorinated ion exchange polymers and their use in research and industry. *Macromolecular Symposia* **1994**, *82* (1), 161-172.

[19] Garsany, Y.; Gould, B. D.; Baturina, O. A.; Swider-Lyons, K. E. Comparison of the Sulfur Poisoning of PBI and Nafion PEMFC Cathodes. *Electrochemical and Solid-State Letters* **2009,** *12* (9), B138.

[20] Wang, Y.; Diaz, D. F. R.; Chen, K. S.; Wang, Z.; Adroher, X. C. Materials, technological status, and fundamentals of PEM fuel cells – A review. *Materials Today* **2020,** *32*, 178-203.

[21] Song, C.; Hui, S.; Zhang, J. High-temperature PEM Fuel Cell Catalysts and Catalyst Layers. In *PEM Fuel Cell Electrocatalysts and Catalyst Layers: Fundamentals and Applications*, Zhang, J., Ed. Springer, 2008; pp 861-888. DOI: 10.1007/978-1-84800-936-3_18

[22] Li, Q.; He, R.; Gao, J.-A.; Jensen, J. O.; Bjerrum, N. J. The CO Poisoning Effect in PEMFCs Operational at Temperatures up to 200°C. *Journal of The Electrochemical Society* **2003,** *150* (12), A1599.

[23] Asensio, J. A.; Sánchez, E. M.; Gómez-Romero, P. Proton-conducting membranes based on benzimidazole polymers for high-temperature PEM fuel cells. A chemical quest. *Chemical Society Reviews* **2010,** *39* (8), 3210-3239.

[24] Bose, S.; Kuila, T.; Nguyen, T. X. H.; Kim, N. H.; Lau, K.-t.; Lee, J. H. Polymer membranes for high temperature proton exchange membrane fuel cell: Recent advances and challenges. *Progress in Polymer Science* **2011,** *36* (6), 813-843.

[25] Chandan, A.; Hattenberger, M.; El-kharouf, A.; Du, S.; Dhir, A.; Self, V.; Pollet, B. G.; Ingram, A.; Bujalski, W. High temperature (HT) polymer electrolyte membrane fuel cells (PEMFC) – A review. *Journal of Power Sources* **2013,** *231*, 264-278.

[26] Clouser, S. J.; Huang, J. C.; Yeager, E. Temperature dependence of the Tafel slope for oxygen reduction on platinum in concentrated phosphoric acid. *Journal of Applied Electrochemistry* **1993,** *23* (6), 597-605.

[27] Zhu, Y.; Zhu, W. H.; Tatarchuk, B. J. Performance comparison between high temperature and traditional proton exchange membrane fuel cell stacks using electrochemical impedance spectroscopy. *Journal of Power Sources* **2014,** *256*, 250-257.

[28] Zhang, C.; Zhang, L.; Zhou, W.; Wang, Y.; Chan, S. H. Investigation of water transport and its effect on performance of high-temperature PEM fuel cells. *Electrochimica Acta* **2014,** *149*, 271-277.

[29] He, R.; Li, Q.; Xiao, G.; Bjerrum, N. J. Proton conductivity of phosphoric acid doped polybenzimidazole and its composites with inorganic proton conductors. *Journal of Membrane Science* **2003,** *226* (1), 169-184.

[30] Wainright, J. S.; Wang, J. T.; Weng, D.; Savinell, R. F.; Litt, M. Acid-Doped Polybenzimidazoles: A New Polymer Electrolyte. *Journal of The Electrochemical Society* **1995,** *142* (7), L121-L123.

[31] Kim, H.-J.; Lim, T.-H. PBI Derivatives: Polymer Electrolyte Fuel Cell Membrane for High Temperature Operation. *Journal of Industrial and Engineering Chemistry* **2004,** *10* (7), 1081-1085.

[32] Samms, S. R.; Wasmus, S.; Savinell, R. F. Thermal Stability of Proton Conducting Acid Doped Polybenzimidazole in Simulated Fuel Cell Environments. *Journal of The Electrochemical Society* **1996,** *143* (4), 1225-1232.

[33] Kerres, J.; Ullrich, A.; Meier, F.; Häring, T. Synthesis and characterization of novel acid–base polymer blends for application in membrane fuel cells. *Solid State Ionics* **1999,** *125* (1), 243-249.

[34] Cassidy, P. E. Polybenzimidazoles. In *Thermally Stable Polymers: Synthsis and Properties*, Marcel Dekker, 1980; pp 163-173.

[35] Ma, Y. L.; Wainright, J. S.; Litt, M. H.; Savinell, R. F. Conductivity of PBI Membranes for High-Temperature Polymer Electrolyte Fuel Cells. *Journal of The Electrochemical Society* **2004,** *151* (1), A8.

[36] Bouchet, R.; Siebert, E. Proton conduction in acid doped polybenzimidazole. *Solid State Ionics* **1999,** *118* (3), 287-299.

[37] Mekhilef, S.; Saidur, R.; Safari, A. Comparative study of different fuel cell technologies. *Renewable and Sustainable Energy Reviews* **2012,** *16* (1), 981-989.

[38] Zeis, R. Materials and characterization techniques for high-temperature polymer electrolyte membrane fuel cells. *Beilstein Journal of Nanotechnology* **2015,** *6*, 68-83.

[39] Huang, C.; Ali, T. Analyses of one-step liquid hydrogen production from methane and landfill gas. *Journal of Power Sources* **2007,** *173* (2), 950-958.

[40] Adhikari, S.; Fernando, S. Hydrogen membrane separation techniques. *Industrial & Engineering Chemistry Research* **2006,** *45* (3), 875-881.

[41] Park, D.; Urm, J. J.; Lee, J.-U.; Chang, M. H.; Lee, J. M. Dynamic optimization of cryogenic distillation operation for hydrogen isotope separation in fusion power plant. *International Journal of Hydrogen Energy* **2021,** *46* (47), 24135-24148.

[42] Grande, C. A.; Lopes, F. V.; Ribeiro, A. M.; Loureiro, J. M.; Rodrigues, A. E. Adsorption of off-gases from steam methane reforming (H2, CO2, CH4, CO and N2) on activated carbon. *Separation Science and Technology* **2008,** *43* (6), 1338-1364.

[43] Ribeiro, A. M.; Grande, C. A.; Lopes, F. V.; Loureiro, J. M.; Rodrigues, A. E. A parametric study of layered bed PSA for hydrogen purification. *Chemical Engineering Science* **2008,** *63* (21), 5258-5273.

[44] Sircar, S.; Golden, T. Purification of hydrogen by pressure swing adsorption. *Separation Science and Technology* **2000,** *35* (5), 667-687.

[45] Lopes, F. V.; Grande, C. A.; Rodrigues, A. E. Activated carbon for hydrogen purification by pressure swing adsorption: Multicomponent breakthrough curves and PSA performance. *Chemical Engineering Science* **2011,** *66* (3), 303-317.

[46] Ockwig, N. W.; Nenoff, T. M. Membranes for hydrogen separation. *Chemical Reviews* **2007,** *107* (10), 4078-4110.

[47] Li, H.; Song, Z.; Zhang, X.; Huang, Y.; Li, S.; Mao, Y.; Ploehn, H. J.; Bao, Y.; Yu, M. Ultrathin, molecular-sieving graphene oxide membranes for selective hydrogen separation. *Science* **2013,** *342* (6154), 95-98.

[48] Yun, S.; Oyama, S. T. Correlations in palladium membranes for hydrogen separation: A review. *Journal of Membrane Science* **2011,** *375* (1-2), 28-45.

[49] Hatlevik, Ø.; Gade, S. K.; Keeling, M. K.; Thoen, P. M.; Davidson, A.; Way, J. D. Palladium and palladium alloy membranes for hydrogen separation and production: History, fabrication strategies, and current performance. *Separation and Purification Technology* **2010,** *73* (1), 59-64.

[50] Langer, S. H.; Haldeman, R. G. Electrolytic hydrogen purification and recovery of same. U.S. Patent #3,475,302. October 28, 1969.

[51] Maget, H. J. R. Process for gas purification. U.S. Patent #3,489,670. January 13, 1970.

[52] Winnick, J. Electrochemical separation of Gases. *Advances in Electrochemical Science and Engineering* **1990,** *1*, 205-248.

[53] Langer, S. H.; Haldeman, R. G. Hydrogen: Electrolytic Technique for Purifying It and Removing It from a Gas Stream. *Science* **1963,** *142* (3589), 225-226.

[54] Onda, K.; Ichihara, K.; Nagahama, M.; Minamoto, Y.; Araki, T. Separation and compression characteristics of hydrogen by use of proton exchange membrane. *Journal of Power Sources* **2007,** *164* (1), 1-8.

[55] Sedlak, J.; Austin, J.; LaConti, A. Hydrogen recovery and purification using the solid polymer electrolyte electrolysis cell. *International Journal of Hydrogen Energy* **1981,** *6* (1), 45-51.

[56] Ströbel, R.; Oszcipok, M.; Fasil, M.; Rohland, B.; Jörissen, L.; Garche, J. The compression of hydrogen in an electrochemical cell based on a PE fuel cell design. *Journal of Power Sources* **2002,** *105* (2), 208-215.

[57] Rohland, B.; Eberle, K.; Ströbel, R.; Scholta, J.; Garche, J. Electrochemical hydrogen compressor. *Electrochimica Acta* **1998,** *43* (24), 3841-3846.

[58] Lee, H. K.; Choi, H. Y.; Choi, K. H.; Park, J. H.; Lee, T. H. Hydrogen separation using electrochemical method. *Journal of Power Sources* **2004,** *132* (1), 92-98.

[59] Fishel, K.; Qian, G.; Eisman, G.; Benicewicz, B. C. Electrochemical Hydrogen Pumping. In *High Temperature Polymer Electrolyte Membrane Fuel Cells*; Li, Q.; Aili, D.; Hjuler, H. A.; Jensen, J. O., Eds.; Springer, 2016; pp 527-540. DOI: 10.1007/978-3-319-17082-4_24

[60] Perry, K. A.; Eisman, G. A.; Benicewicz, B. C. Electrochemical hydrogen pumping using a high-temperature polybenzimidazole (PBI) membrane. *Journal of Power Sources* **2008,** *177* (2), 478-484.

[61] Huang, F.; Pingitore, A. T.; Benicewicz, B. C. Electrochemical hydrogen separation from reformate using high-temperature polybenzimidazole (PBI) membranes: the role of chemistry. *ACS Sustainable Chemistry & Engineering* **2020,** *8* (16), 6234-6242.

[62] Huang, F.; Pingitore, A. T.; Benicewicz, B. C. High Polymer Content m/p-Polybenzimidazole Copolymer Membranes for Electrochemical Hydrogen Separation under Differential Pressures. *Journal of the Electrochemical Society* **2020,** *167* (6), 063504.

[63] Thomassen, M.; Sheridan, E.; Kvello, J. Electrochemical hydrogen separation and compression using polybenzimidazole (PBI) fuel cell technology. *Journal of Natural Gas Science and Engineering* **2010,** *2* (5), 229-234.

[64] Kear, G.; Shah, A. A.; Walsh, F. C. Development of the all-vanadium redox flow battery for energy storage: a review of technological, financial and policy aspects. *International Journal of Energy Research* **2012,** *36* (11), 1105-1120.

[65] Li, L.; Kim, S.; Wang, W.; Vijayakumar, M.; Nie, Z.; Chen, B.; Zhang, J.; Xia, G.; Hu, J.; Graff, G. A stable vanadium redox-flow battery with high energy density for large-scale energy storage. *Advanced Energy Materials* **2011,** *1* (3), 394-400.

[66] Skyllas-Kazacos, M.; Kazacos, G.; Poon, G.; Verseema, H. Recent advances with UNSW vanadium-based redox flow batteries. *International Journal of Energy Research* **2010,** *34* (2), 182-189.

[67] Ponce de León, C.; Frías-Ferrer, A.; González-García, J.; Szánto, D. A.; Walsh, F. C. Redox flow cells for energy conversion. *Journal of Power Sources* **2006,** *160* (1), 716-732.

[68] Skyllas-Kazacos, M.; Chakrabarti, M. H.; Hajimolana, S. A.; Mjalli, F. S.; Saleem, M. Progress in Flow Battery Research and Development. *Journal of The Electrochemical Society* **2011,** *158* (8), R55.

[69] Jiang, B.; Yu, L.; Wu, L.; Mu, D.; Liu, L.; Xi, J.; Qiu, X. Insights into the impact of the nafion membrane pretreatment process on vanadium flow battery performance. *ACS Applied Materials & Interfaces* **2016,** *8* (19), 12228-12238.

[70] Jiang, B.; Wu, L.; Yu, L.; Qiu, X.; Xi, J. A comparative study of Nafion series membranes for vanadium redox flow batteries. *Journal of Membrane Science* **2016,** *510*, 18-26.

[71] Chen, D.; Wang, S.; Xiao, M.; Meng, Y. Preparation and properties of sulfonated poly (fluorenyl ether ketone) membrane for vanadium redox flow battery application. *Journal of Power Sources* **2010,** *195* (7), 2089-2095.

[72] Yuan, Z.; Duan, Y.; Zhang, H.; Li, X.; Zhang, H.; Vankelecom, I. Advanced porous membranes with ultra-high selectivity and stability for vanadium flow batteries. *Energy & Environmental Science* **2016,** *9* (2), 441-447.

[73] Schwenzer, B.; Zhang, J.; Kim, S.; Li, L.; Liu, J.; Yang, Z. Membrane Development for Vanadium Redox Flow Batteries. *ChemSusChem* **2011,** *4* (10), 1388-1406.

[74] Minke, C.; Turek, T. Economics of vanadium redox flow battery membranes. *Journal of Power Sources* **2015,** *286*, 247-257.

[75] Aziz, M. A.; Shanmugam, S. Ultra-high proton/vanadium selectivity of a modified sulfonated poly (arylene ether ketone) composite membrane for all vanadium redox flow batteries. *Journal of Materials Chemistry A* **2017,** *5* (32), 16663-16671.

[76] Xu, H.; Wang, X.; Shao, Z.; Hsing, I. Recycling and regeneration of used perfluorosulfonic membranes for polymer electrolyte fuel cells. *Journal of Applied Electrochemistry* **2002,** *32* (12), 1337-1340.

[77] Yang, S.; Ahn, Y.; Kim, D. Poly (arylene ether ketone) proton exchange membranes grafted with long aliphatic pendant sulfonated groups for vanadium redox flow batteries. *Journal of Materials Chemistry A* **2017,** *5* (5), 2261-2270.

[78] Brinker, K. C.; Robinson, I. M. Polybenzimidazoles. U.S. Patent #2,895,948. July 21, 1959.

[79] Vogel, H.; Marvel, C. S. Polybenzimidazoles, new thermally stable polymers. *Journal of Polymer Science* **1961,** *50* (154), 511-539.

[80] Kumbharkar, S. C.; Karadkar, P. B.; Kharul, U. K. Enhancement of gas permeation properties of polybenzimidazoles by systematic structure architecture. *Journal of Membrane Science* **2006,** *286* (1-2), 161-169.

[81] Wang, K. Y.; Chung, T.-S. Fabrication of polybenzimidazole (PBI) nanofiltration hollow fiber membranes for removal of chromate. *Journal of Membrane Science* **2006,** *281* (1), 307-315.

[82] Yang, T.; Xiao, Y.; Chung, T.-S. Poly-/metal-benzimidazole nano-composite membranes for hydrogen purification. *Energy & Environmental Science* **2011,** *4* (10), 4171-4180.

[83] Han, Y.-J.; Wang, K.-H.; Lai, J.-Y.; Liu, Y.-L. Hydrophilic chitosan-modified polybenzoimidazole membranes for pervaporation dehydration of isopropanol aqueous solutions. *Journal of Membrane Science* **2014,** *463*, 17-23.

[84] Pesiri, D. R.; Jorgensen, B.; Dye, R. C. Thermal optimization of polybenzimidazole meniscus membranes for the separation of hydrogen, methane, and carbon dioxide. *Journal of Membrane Science* **2003,** *218* (1), 11-18.

[85] Singh, R. P.; Li, X.; Dudeck, K. W.; Benicewicz, B. C.; Berchtold, K. A. Polybenzimidazole based random copolymers containing hexafluoroisopropylidene functional groups for gas separations at elevated temperatures. *Polymer* **2017,** *119*, 134-141.

[86] Stevens, K. A.; Moon, J. D.; Borjigin, H.; Liu, R.; Joseph, R. M.; Riffle, J. S.; Freeman, B. D. Influence of temperature on gas transport properties of tetraaminodiphenylsulfone (TADPS) based polybenzimidazoles. *Journal of Membrane Science* **2020,** *593*, 117427.

[87] Wang, K. Y.; Chung, T.-S. Polybenzimidazole nanofiltration hollow fiber for cephalexin separation. *AIChE Journal* **2006,** *52* (4), 1363-1377.

[88] Lv, J.; Wang, K. Y.; Chung, T.-S. Investigation of amphoteric polybenzimidazole (PBI) nanofiltration hollow fiber membrane for both cation and anions removal. *Journal of Membrane Science* **2008,** *310* (1), 557-566.

[89] Valtcheva, I. B.; Kumbharkar, S. C.; Kim, J. F.; Bhole, Y.; Livingston, A. G. Beyond polyimide: Crosslinked polybenzimidazole membranes for organic solvent nanofiltration (OSN) in harsh environments. *Journal of Membrane Science* **2014,** *457*, 62-72.

[90] Fishel, K.; Qian, G.; Benicewicz, B. C. PBI Membranes Aia the PPA Process. In *High Temperature Polymer Electrolyte Membrane Fuel Cells*; Li, Q.; Aili, D.; Hjuler, H. A.; Jensen, J. O., Eds.; Springer, 2016; pp 217-238. DOI: 10.1007/978-3-319-17082-4_10

[91] Aili, D.; Jensen, J. O.; Li, Q. Polybenzimidazole Membranes by Post Acid Doping. In *High Temperature Polymer Electrolyte Membrane Fuel Cell*s; Li, Q.; Aili, D.; Hjuler, H. A.; Jensen, J. O., Eds. Springer, 2016; pp 195-215. DOI: 10.1007/978-3-319-17082-4_9

[92] Sandor, R. B. PBI (Polybenzimidazole): Synthesis, Properties and Applications. *High Performance Polymers* **1990,** *2* (1), 25-37.

[93] Mader, J.; Xiao, L.; Schmidt, T. J.; Benicewicz, B. C. Polybenzimidazole/Acid Complexes as High-Temperature Membranes. In *Fuel Cells II: Advances in Polymer Science,* Vol. 216; Scherer, G. G., Ed.; Springer, 2008; pp 63-124. DOI: 10.1007/12_2007_129

[94] Choe, E.-W. Catalysts for the preparation of polybenzimidazoles. *Journal of Applied Polymer Science* **1994,** *53* (5), 497-506.

[95] Iwakura, Y.; Uno, K.; Imai, Y. Polyphenylenebenzimidazoles. *Journal of Polymer Science Part A: General Papers* **1964,** *2* (6), 2605-2615.

[96] Eaton, P. E.; Carlson, G. R.; Lee, J. T. Phosphorus pentoxide-methanesulfonic acid. Convenient alternative to polyphosphoric acid. *The Journal of Organic Chemistry* **1973,** *38* (23), 4071-4073.

[97] Yang, H. *Aromatic high-strength fibers*. John Wiley and Sons, Inc., 1989.

[98] Powers, E. J.; Serad, G. A. History and Development of Polybenzimidazoles. In *High Performance Polymers: Their Origin and Development*; Seymour, R. B.; Kirshenbaum, G. S., Eds.; Springer, 1986; pp 355-373. DOI: 10.1007/978-94-011-7073-4_34

[99] Kumbharkar, S. C.; Islam, M. N.; Potrekar, R. A.; Kharul, U. K. Variation in acid moiety of polybenzimidazoles: Investigation of physico-chemical properties towards their applicability as proton exchange and gas separation membrane materials. *Polymer* **2009,** *50* (6), 1403-1413.

[100] He, R.; Li, Q.; Bach, A.; Jensen, J. O.; Bjerrum, N. J. Physicochemical properties of phosphoric acid doped polybenzimidazole membranes for fuel cells. *Journal of Membrane Science* **2006,** *277* (1-2), 38-45.

[101] Zhou, X. L.; Zhao, T. S.; An, L.; Wei, L.; Zhang, C. The use of polybenzimidazole membranes in vanadium redox flow batteries leading to increased coulombic efficiency and cycling performance. *Electrochimica Acta* **2015,** *153*, 492-498.

[102] Luo, T.; David, O.; Gendel, Y.; Wessling, M. Porous poly(benzimidazole) membrane for all vanadium redox flow battery. *Journal of Power Sources* **2016,** *312*, 45-54.

[103] Peng, S.; Yan, X.; Zhang, D.; Wu, X.; Luo, Y.; He, G. A H_3PO_4 preswelling strategy to enhance the proton conductivity of a H_2SO_4-doped polybenzimidazole membrane for vanadium flow batteries. *RSC Advances* **2016,** *6* (28), 23479-23488.

[104] Peng, S.; Wu, X.; Yan, X.; Gao, L.; Zhu, Y.; Zhang, D.; Li, J.; Wang, Q.; He, G. Polybenzimidazole membranes with nanophase-separated structure induced by non-ionic hydrophilic side chains for vanadium flow batteries. *Journal of Materials Chemistry A* **2018,** *6* (9), 3895-3905.

[105] Xiao, L.; Zhang, H.; Scanlon, E.; Ramanathan, L. S.; Choe, E.-W.; Rogers, D.; Apple, T.; Benicewicz, B. C. High-Temperature Polybenzimidazole Fuel Cell Membranes via a Sol−Gel Process. *Chemistry of Materials* **2005,** *17* (21), 5328-5333.

[106] Perry, K. A.; More, K. L.; Payzant, E. A.; Meisner, R. A.; Sumpter, B. G.; Benicewicz, B. C. A comparative study of phosphoric acid-doped m-PBI membranes. *Journal of Polymer Science Part B: Polymer Physics* **2014,** *52* (1), 26-35.

[107] Yu, S.; Benicewicz, B. C. Synthesis and Properties of Functionalized Polybenzimidazoles for High-Temperature PEMFCs. *Macromolecules* **2009,** *42* (22), 8640-8648.

[108] Molleo, M.; Schmidt, T. J.; Benicewicz, B. C. Polybenzimidazole Fuel Cell Technology. In *Encyclopedia of Sustainability Science and Technology;* Meyers, R. A., Ed.; Springer, 2012; pp 8173-8201. DOI: 10.1007/978-1-4419-0851-3

[109] Yu, S.; Xiao, L.; Benicewicz, B. C. Durability Studies of PBI-based High Temperature PEMFCs. *Fuel Cells* **2008,** *8* (3-4), 165-174.

[110] Mader, J. A.; Benicewicz, B. C. Sulfonated Polybenzimidazoles for High Temperature PEM Fuel Cells. *Macromolecules* **2010,** *43* (16), 6706-6715.

[111] Pingitore, A. T.; Huang, F.; Qian, G.; Benicewicz, B. C. Durable High Polymer Content m/p-Polybenzimidazole Membranes for Extended Lifetime Electrochemical Devices. *ACS Applied Energy Materials* **2019,** *2* (3), 1720-1726.

[112] Xiao, L.; Zhang, H.; Jana, T.; Scanlon, E.; Chen, R.; Choe, E.-W.; Ramanathan, L.; Yu, S.; Benicewicz, B. Synthesis and characterization of pyridine-based polybenzimidazoles for high temperature polymer electrolyte membrane fuel cell applications. *Fuel Cells* **2005,** *5* (2), 287-295.

[113] Qian, G.; Benicewicz, B. C. Synthesis and characterization of high molecular weight hexafluoroisopropylidene-containing polybenzimidazole for high-temperature polymer electrolyte membrane fuel cells. *Journal of Polymer Science Part A: Polymer Chemistry* **2009,** *47* (16), 4064-4073.

[114] Yu, S.; Zhang, H.; Xiao, L.; Choe, E.-W.; Benicewicz, B. C. Synthesis of Poly (2,2′-(1,4-phenylene) 5,5′-bibenzimidazole) (para-PBI) and Phosphoric Acid Doped Membrane for Fuel Cells. *Fuel Cells* **2009,** *9* (4), 318-324.

[115] Chen, X.; Qian, G.; Molleo, M. A.; Benicewicz, B. C.; Ploehn, H. J. High temperature creep behavior of phosphoric acid-polybenzimidazole gel membranes. *Journal of Polymer Science Part B: Polymer Physics* **2015,** *53* (21), 1527-1538.

[116] Molleo, M.; Chen, X.; Ploehn, H. J.; Benicewicz, B. C. High Polymer Content 2, 5-Pyridine-Polybenzimidazole Copolymer Membranes with Improved Compressive Properties. *Fuel Cells* **2015,** *15* (1), 150-155.

[117] Molleo, M.; Chen, X.; Ploehn, H. J.; Fishel, K.; Benicewicz, B. C. High Polymer Content 3, 5-Pyridine-Polybenzimidazole Copolymer Membranes with Improved Compressive Properties. *Fuel Cells* **2014,** *14* (1), 16-25.

[118] Wang, L.; Pingitore, A. T.; Xie, W.; Yang, Z.; Perry, M. L.; Benicewicz, B. C. Sulfonated PBI Gel Membranes for Redox Flow Batteries. *Journal of The Electrochemical Society* **2019,** *166* (8), A1449-A1455.

CHAPTER 2

NOVEL SYNTHETIC ROUTE TO DENSE POLYBENZIMIDAZOLE FILMS WITHOUT ORGANIC SOLVENTS

2.1 ABSTRACT

A new post-polymerization processing technique was developed in which gel polybenzimidazole (PBI) membranes are converted into dense PBI films. Using the Polyphosphoric acid (PPA) Process, gel PBIs were prepared and underwent acid removal followed by a controlled densification step. This new process demonstrated for the first time that PBI films could be prepared without casting from an organic solvent. It was also the first time that more rigid PBI backbone structures, such as para-PBI, were prepared as a dense film from high molecular weight polymers. The novel approach to produce dense PBI films from gel PBIs can allow for new PBI structures to be produced as dense films, and holds potential in various applications of PBI films. The new technique also provided lower associated costs, time, waste generation and energy consumption, compared to previous methods. The new process will be described and characterization of the resulting dense PBI films will be discussed.

2.2 INTRODUCTION

Polybenzimidazoles (PBIs) are a class of heterocyclic performance polymers known for their excellent thermal stability and nonflammability. Polybenzimidazoles were first synthesized in the late 1950's and commercially developed by Celanese in 1983.[1] Fully aromatic PBIs have a very high decomposition temperature, above 500 ºC and exhibit melting points above decomposition temperature, or do not melt due to lack of crystallinity.[2] Due to their excellent properties, PBIs are used today as textile fibers, machined parts, and membranes. PBI membranes have been investigated for various processes

including gas separation[3-6], nanofiltration[7-9], and as an ion-exchange membranes in electrochemical devices.[10, 11]

PBIs are typically synthesized in a polycondensation reaction of a tetra-amine and a dicarboxylic acid or derivative. This can be completed in a two-step melt/solid polymerization[12] or solution polymerization. In the two-step melt/solid polymerization used commercially, no organic solvents are required to produce the PBI powder, and post-polymerization processing is relatively easy, however, the molecular weight of PBIs produced in this method is limited, with inherent viscosities (IV) between 0.5 and 0.8 dL g^{-1}, due to inherent limitations of heterogeneous reactions.[13, 14] In solution polymerizations of PBI, high polarity solvents such as N,N-dimethylacetamide (DMAc) have been utilized.[15, 16]

Dense PBI films have been produced commercially using the same method for almost 40 years.[17, 18] In this method, PBI is extracted as powder after polymerization and purified to remove any unreacted monomers and low-molecular weight units. Afterwards, the purified PBI powder is dissolved in an organic solvent, typically DMAc and LiCl which is added to aid in dissolution of PBI, and the solution is cast as a film.[19] The solvent is then evaporated using an oven, and the resulting film is washed in boiling water to remove residual solvent. After drying, a dense PBI film is formed.

This approach for producing PBI films by dissolving in an organic solvent has some limitations. The method is not environmentally friendly, since the organic solvent is added and then fully removed, a significant amount of waste is generated. The procedure also involves many tedious steps and it takes a

significant amount of time as well as cost to produce the PBI films. Furthermore, this film preparation method limits the PBI backbone structures that can be made into dense films as well as the molecular weight of the PBI films. PBI backbones that are more rigid in nature will thus have a lower solubility in organic solvents. While meta-PBI is commercially produced in the organic solvent casting procedure, para-PBI, which contains a more linear and rigid backbone, has very low solubility in organic solvents and cannot be produced as a dense film by casting from organic solvent solutions.[20] Furthermore, as the molecular weight of PBI is increased, the solubility is reduced. Thus, it is difficult to make dense PBI films with high molecular weight (IV > 1 dL g^{-1}), due to the requirement of casting from an organic solvent.

While there are plenty of reports on the synthesis of various PBI backbone structures and their use in several applications, reports that fundamentally question and alter the PBI film fabrication method developed since the 1960's is lacking. Herein, a new method to produce dense PBI films without organic solvents is reported. This new method is practical for commercial production, reduces the amount of waste that is accumulated, and allows for new PBI structures with high molecular weights to be incorporated into dense polymer films for the first time.

The novel organic solvent-free method is based on the PPA Process, which was published in 2005.[21] In the PPA Process, a one-pot technique is used to generate gel PBI membranes that are highly doped in phosphoric acid for use in high temperature polymer electrolyte membrane fuel cells. PPA is utilized as the polymerization solvent to form PBI from a tetraamine and a dicarboxylic acid. The

polymerized solution in PPA is cast directly onto a substrate, thus PPA is also utilized as the casting solvent in the PPA Process. Upon absorption of moisture, PPA is hydrolyzed in situ to form phosphoric acid (PA) and water. PA is a poor solvent for many PBIs, and a solution-to-gel phase transition occurs as PPA is hydrolyzed to PA, as depicted in **Figure 2.1**. This resulted in a mechanically stable gel PBI membrane that is highly doped in phosphoric acid. Since this one-pot synthesis does not require dissolving monomers or resulting polymer in an organic solvent, more rigid para-oriented PBIs with high molecular weight were accessed for the first time with better properties in fuel cells.[22]

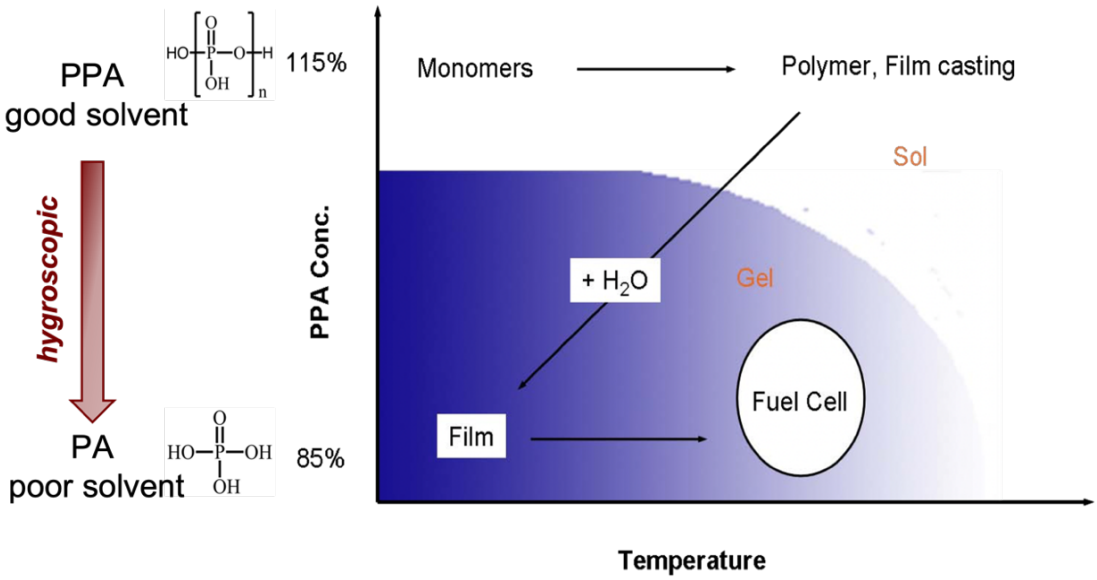

Figure 2.1. The solution-to-gel state diagram for PBIs produced in the PPA Process.

Using the PPA process as a basis, a novel procedure was developed to convert the gel PBI membranes that are highly swollen in phosphoric acid into dense PBI films using an additional two-step physical transformation. This is the first report of an organic solvent-free method to produce dense PBI films, and

allows the formation and investigation of more rigid PBI backbones with high molecular weight. This chapter aims to introduce the new method with three different PBI structures prepared according to the new process and compares them to meta-PBI (m-PBI) films produced in the organic solvent casting method.

2.3 EXPERIMENTAL

2.3.1 Materials

Terephthalic acid (TPA, >99% purity) and isophthalic acid (IPA, >99% purity) were purchased from Amoco. 2-Sulfoterephthalic acid monosodium salt (STPA, >98% purity) and 2,5-dihydroxyterephthalic acid (2OH-TPA, >98% purity) were purchased from TCI America. Poly(phosphoric acid) (PPA, 115%) was purchased from Innophos, technical grade sulfuric acid was purchased from Fisher Chemical, and 3,3′,4,4′-tetraaminobiphenyl (TAB, polymer grade, ~97.5%) was kindly donated by BASF Fuel Cell, Inc. Meta-polybenzimidazole was donated by PBI Performance Products, and was washed in boiling water three times followed by dying in vacuo to removing any remaining DMAc in the sample. All other chemicals and reagents were used as received without further purification.

2.3.2 Polymer Synthesis and Fabrication of Acid-imbibed PBI Gel Membranes

The synthesis of p-PBI, 2OH-PBI and s-PBI were completed as previously reported, depicted in **Figure 2.2**.[11-13] In a typical polymerization, equal molar equivalents of diacid and TAB were added to a reaction kettle under a nitrogen atmosphere, followed by PPA. Equipped with an overhead mechanical stirrer, the reaction mixture was stirred and purged in a nitrogen environment throughout the polymerization. A programmable temperature controller with ramp and soak

features was used to control the polymerization temperature. Typically, polymerizations were completed over a 18-48 hour period, monitored by visual inspection of viscosity, and had a final polymerization temperature of about 195 - 220 °C. The viscous solution of polymer in PPA was cast directly onto a glass substrate, by using a doctor blade with a control gate thickness set to 15 mils. The cast polymer solution was hydrolyzed to form self-supporting membranes by placing in a controlled humidity chamber set to 55% relative humidity for 24 hours.

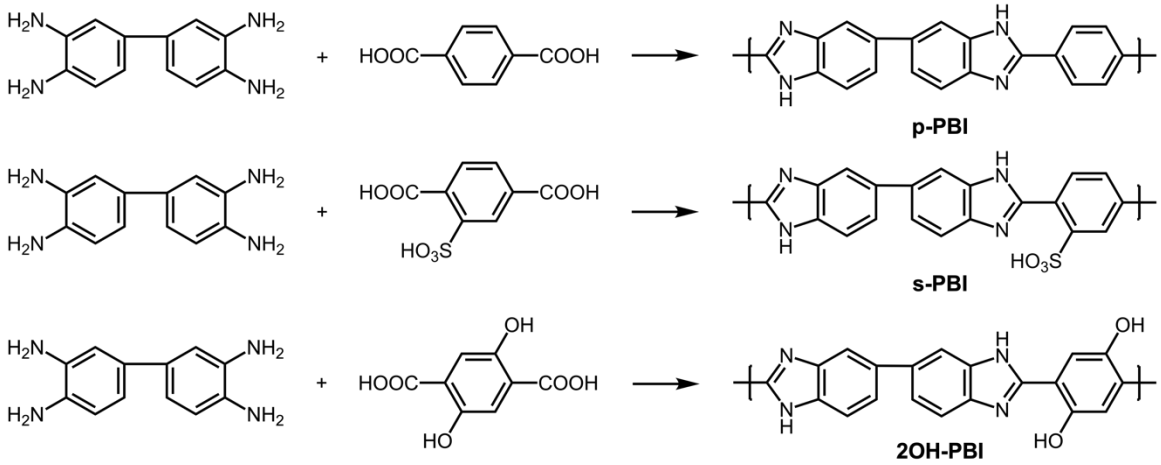

Figure 2.2. Monomers and resulting PBI structures that were prepared in the PPA Process.

2.3.3 Inherent Viscosity

Measurements of the inherent viscosity (IV) were collected for each polymer sample by isolating a small amount of polymer in water. The sample was then pulverized and neutralized with concentrated ammonium hydroxide. The polymer pieces were isolated and the sample was washed with distilled water and vacuum dried. Polymer samples were weighed out to about 0.05 g and dissolved

in concentrated sulfuric acid to achieve a concentration of ~0.2 g dL^{-1}. The polymer solution was filtered through a 0.45 μm syringe filter into a 200 μm Ubbelohde viscometer, and placed in a water bath set at 30 °C for 30 minutes to equilibrate the viscometer to the bath temperature. Sample and control flow times were measured and recorded for three runs each. The control was measured using pristine concentrated sulfuric acid. The average flow time obtained for the sample was compared to the average flow time of the control using the following equation to calculate the inherent viscosity:

$$\eta_{inh} = \frac{\ln\left(t/t_o\right)}{c}$$

Where t was the sample flow time (s), t_o was the control flow time (s), c was the concentration of polymer sample dissolved in sulfuric acid (g dL^{-1}), and η_{inh} was the calculated inherent viscosity (dL g^{-1}). IV's were not able to be obtained for the 2OH-PBI sample, as it was unable to dissolve in concentrated sulfuric acid, due to the formation of phosphate ester bridges.[23]

2.3.4 Post-polymerization Modification

The PBI gel membranes were then subjected to a novel post-polymerization modification technique, beginning with the removal of PA. Membranes were washed in a series of deionized water baths to remove the PA and pH indication paper was used to ensure removal of free phosphoric acid before proceeding. The water-imbibed gel membranes were taken from the water bath and clamped between the porous sheets and left for 12-24 hours to allow remaining water to evaporate, resulting in high quality dense PBI films. In this study, 3.2 mm thick porous polyethylene sheets were used with an average porosity of 45-90 μm.

2.3.5 Membrane Composition Analysis

Titration was used to determine the composition of phosphoric acid, water, and polymer in the gel PBI membranes produced in the PPA Process, and after washing with water to remove the phosphoric acid. Membrane samples were weighed, placed in a beaker with ~50 mL of deionized water, and stirred at room temperature overnight. The beakers were titrated the following day using a Metrohm 888 DMS Titrando autotitrator, with a standard 0.1 N sodium hydroxide solution. The remaining polymer sample was collected after titration, washed with deionized water, and dried in a vacuum oven for 24 hours before weighing. The polymer weight percent (*polymer wt%*) and phosphoric acid weight percent (*acid wt%*) were calculated respectively:

$$Polymer\ wt\% = \frac{W_{dry}}{W_{sample}} \cdot 100$$

$$Acid\ wt\% = \frac{M_{acid} \cdot V_{NaOH} \cdot c_{NaOH}}{W_{sample}} \cdot 100$$

Where W_{sample} was the weight of the sample before titration, W_{dry} was the weight of the final dried sample after titration, M_{acid} was the molecular weight of phosphoric acid, V_{NaOH} and C_{NaOH} was the volume and concentration of sodium hydroxide required to neutralize phosphoric acid to the first equivalence point, respectively.

The phosphoric acid doping level, or the number of moles of phosphoric acid per mole of PBI repeat unit (PRU), *X*, was calculated according to the following equation:

$$X = \frac{V_{NaOH} \cdot c_{NaOH}}{\left({W_{dry}}/{M_{polymer}}\right)}$$

Where V_{NaOH} and C_{NaOH} were the volume and concentration of sodium hydroxide needed to neutralize the phosphoric acid, W_{dry} was the weight of the final dried sample after titration, and $M_{polymer}$ was the molecular weight of the polymer repeat unit.

2.3.6 Tensile Testing

Stress-strain curves were obtained using an Instron 5843 tensile tester equipped with a 100 N load cell. Tensile testing was performed on dumb-bell shaped samples cut to the ASTM standard D638 (type V) specifications which were pre-loaded to 0.1 N and tested with crosshead speed of 10 mm min^{-1}. Three tensile tests were performed on each sample of the same type.

2.3.7 Thermogravimetric Analysis

Thermogravimetric analysis (TGA) was performed on a Hitachi STA7200 Thermal Analysis System under nitrogen. Samples were pre-heated to 100 °C at 10 °C min^{-1} and cooled to room temperature. Data was then collected while heating from room temperature to 750 °C with a heating ramp rate of 10 °C min^{-1}.

2.3.8 Energy Dispersive X-Ray Spectroscopy

Energy dispersive X-ray spectroscopy (EDS) was collected on PBI films mounted on an SEM stub with carbon tape. Elemental analysis was completed with a Tescan Vega-3 SEM instrument equipped with a Thermo EDS attachment. The SEM was operated in low-vacuum mode with a 20 kV accelerating voltage and a 30 s accumulation time.

2.3.9 Wide-Angle X-Ray Scattering

Wide-Angle X-Ray Scattering (WAXS) was performed at the South Carolina SAXS Collaborative using a SAXSLab Ganesha instrument (SAXSLab, Holyoke, MA, USA). A copper target with a Xenocs GeniX 3D microfocus source was used to produce a monochromatic beam with a wavelength of 0.154 nm. The instrument was calibrated using 640d silicon powder reference material from the National Institute of Standards and Technology (NIST) prior to use. The reference peak position was $2\theta = 28.44°$, where 2θ represents the total scattering angle. The two-dimensional (2D) scattering pattern was collected with a Pilatus 300 K detector (Dectris, Baden-Daettwil, Switzerland), which exhibited a nominal pixel dimension of 172 x 172 μm^2. WAXS data was collected with an x-ray flux of ~40 million photons per second incident upon the sample with a sample-to-detector distance of 104.5 mm. The 2D images were azimuthally integrated to yield the scattering vector intensity. Peak positions were fitted using custom MATLAB (Version 2020b, Mathworks, Natick, MA, USA). WAXS simulations were conducted using SASFit.

2.4 RESULTS AND DISCUSSION

Three types of PBIs were selected to demonstrate the new process and compared to a commercially available m-PBI film prepared by the organic solvent casting method. **Figure 2.3** displays a general PBI polymerization, the four PBI structures that will be discussed, and two polymerization methods. Meta-PBI (m-PBI) was prepared using Method 1, the organic solvent casting method, while para-PBI (p-PBI), sulfonated-PBI (s-PBI) and dihydroxy-PBI (2OH-PBI), were prepared using Method 2, the new organic solvent-free process. Method 1

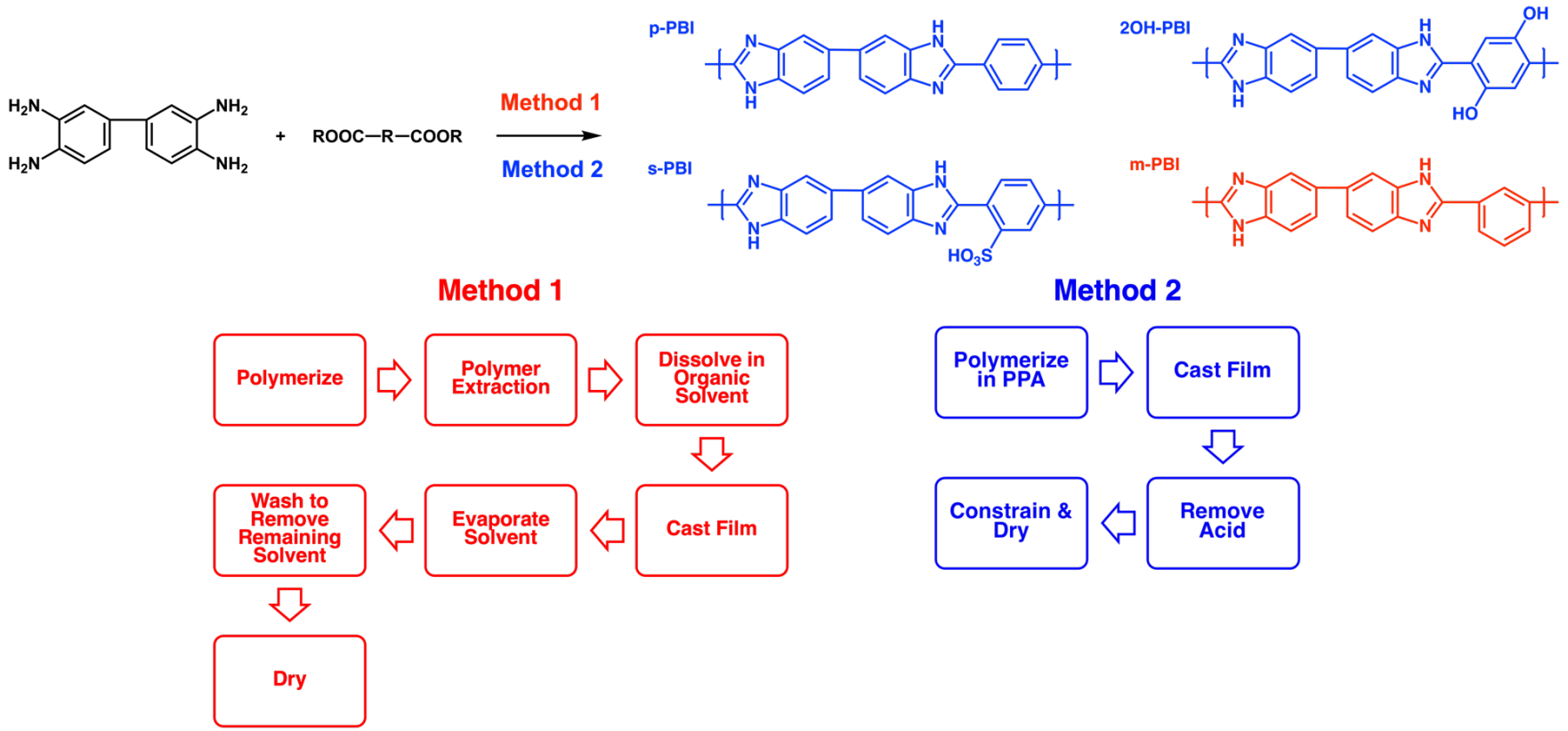

Figure 2.3. Chemical structures of dense PBI films under investigation. m-PBI was a commercially available PBI film, prepared by casting from an organic solvent (Method 1), while p-PBI, s-PBI, and 2OH-PBI, in blue, were prepared using the novel solvent-free technique (Method 2).

involves polymerization of PBI using either the two-step melt/solid polymerization or solution polymerization. The resulting polymer is then dissolved in an organic solvent such as DMAc, cast, and removal of the solvent. In Method 2, the p-PBI, s-PBI and 2OH-PBI samples were prepared in the PPA Process, as previously reported.[22-24] The gel PBI membranes that result from the PPA process contain water, phosphoric acid, and polymer. Each type of gel PBI prepared in the PPA process have a polymer solids content less than 10%, and contain a greater concentration of acid and water compared to polymer. The composition of each type of PBI prepared in the PPA Process can be found in **Table 2.1**.

Table 2.1. Polymer and membrane properties of gel PBI membranes selected for comparative studies.

Sample	IV (dL g^{-1})	Thickness (μm)	Acid Doping Level (PA/PRU)	PBI Content (wt %)
p-PBI[22]	1.4 – 3.8	350	30 – 40	3.0 – 6.0
s-PBI[24]	1.0 – 2.0	273	30 – 35	2.5 – 6.0
2OH-PBI[23]	N/A	335	25.4	5.31

2.4.1 Acid Removal

In order to transform the gel PBI membranes into dense PBI films according to Method 2, the acid and water must be removed and a load-bearing polymer film must remain. The acid was removed by washing in water baths, exchanging the water frequently, until pH indication paper showed the water bath was at a neutral pH. The neutralized gel PBI samples were titrated to determine the acid

content remaining in the gel membrane. It was found that the acid doping level was 1.6 ± 0.2 mol PA/PRU and the acid content in the membrane was 4.5 ± 0.7 wt% of phosphoric acid.

An alternative acid removal procedure was examined where the membranes were placed in a bath of 50% v/v methanol after the initial water bath. The samples were left in the same 50% v/v methanol bath for 24 hours at room temperature. Membrane samples were titrated and found to have less acid. The acid doping level was 0.92 ± 0.03 mol PA/PRU and the acid content was 3.6 ± 0.3 wt% phosphoric acid. Thus, soaking the membrane samples in 50% v/v methanol after the water baths was effective in further removal of phosphoric acid before drying. Results in the following sections are reported on films made using the water washing procedure.

2.4.2 Controlled Drying

In the next phase of the new process, the water-doped gel PBIs were dried to transform the gel membranes into dense polymer films. This was accomplished by clamping the wet gel membrane samples between a porous substrate and drying in an oven. **Figure 2.4** depicts the effect of drying the gel PBI membrane freely (unrestrained) on the benchtop (right) versus while secured between porous plates (left). The PBI sample that underwent controlled drying formed a nice transparent film with a uniform thickness. However, the sample that was left to dry freely was not uniform, as indicated by the darker coloring, and does not offer practical usage. By securing the gel PBI samples between porous sheets and subsequent drying, the structure is constrained in the x- and y-directions, forcing

the membrane to collapse only in the z-direction as water evaporates through the porous material. The physical transformation of gel PBI membranes into uniform dense PBI films is dependent on the controlled drying step. The thickness of the samples after drying were between 25 to 35 μm, which corresponds to an 88-93% reduction in thickness from the original gel PBI.

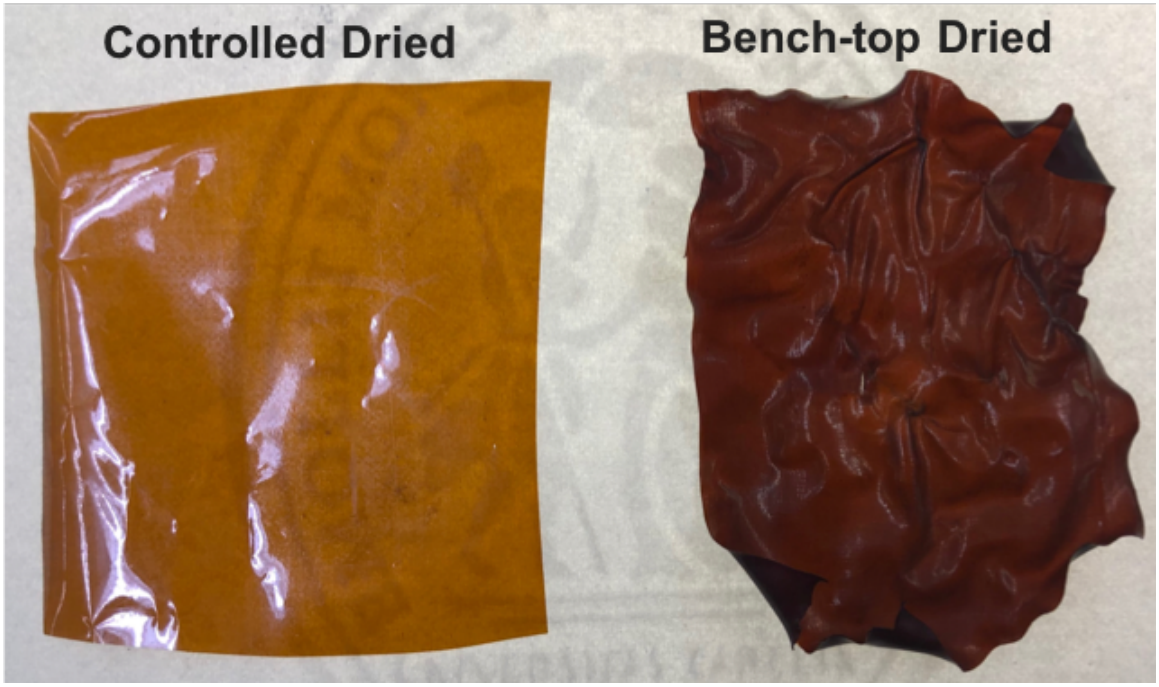

Figure 2.4. Effect of drying gel PBI membranes by securing between porous plates, according to this report (left) and by leaving the membrane on the benchtop to freely dry (right).

2.4.3 Dimensional Changes

Table 2.2 shows the dimensional changes of the PBI membranes throughout the drying process. The first step represented the conversion of an acid doped p-PBI gel membrane into a neutralized water doped p-PBI gel membrane. The sample contracted in the x and y direction by the same amount, roughly 6% during this step, and the total volume decreased by 13.7%. The second step was

the conversion of a water doped p-PBI gel membrane into a dense p-PBI film. During step 2, the sample lost over 92% of its volume, which was mostly from the thickness. Since the membrane was constrained in the x and y direction (length and width), contraction in these directions were minimal (2 - 6%) and dominated by contraction in the z-direction (thickness) which was reduced by 91.9% during step 2. Overall, when the acid doped gel p-PBI membranes underwent the novel processing technique, p-PBI samples experienced a 93.5% reduction in volume, mostly in the z-direction (thickness), which was reduced by 92.1%.

Table 2.2. Dimensional changes measured in each direction for p-PBI after neutralization (step 1) and densification (step 2).

	Length (%)	**Width (%)**	**Thickness (%)**	**Volume (%)**
Step 1	-5.88	-5.98	-2.46	-13.7
Step 2	-5.70	-2.54	-91.9	-92.5
Overall	-11.2	-8.37	-92.1	-93.5

2.4.4 Thermal Analysis of Dense PBI Films

TGA was conducted on the solvent-free dense PBI films and the commercially available m-PBI film in a nitrogen environment, as shown in **Figure 2.5**. The m-PBI sample, which was prepared in Method 1, the conventional solvent casting method, displayed the greatest thermal stability. At 200 ºC, there is only a 1.3% weight loss, probably from a small amount of water remaining in the sample. The m-PBI sample has a noticeable dip in weight loss from 400 ºC to 600 ºC, during which the sample goes from 1.6% weight loss to 4.0% weight loss. This is likely due to traces of DMAc, which is known to be held tightly in PBI and difficult to

remove by simple washing.[25] At around 600 ºC a visible rapid degradation begins, which was ascribed to backbone degradation, and the final weight loss at 750 ºC is 13.1%.

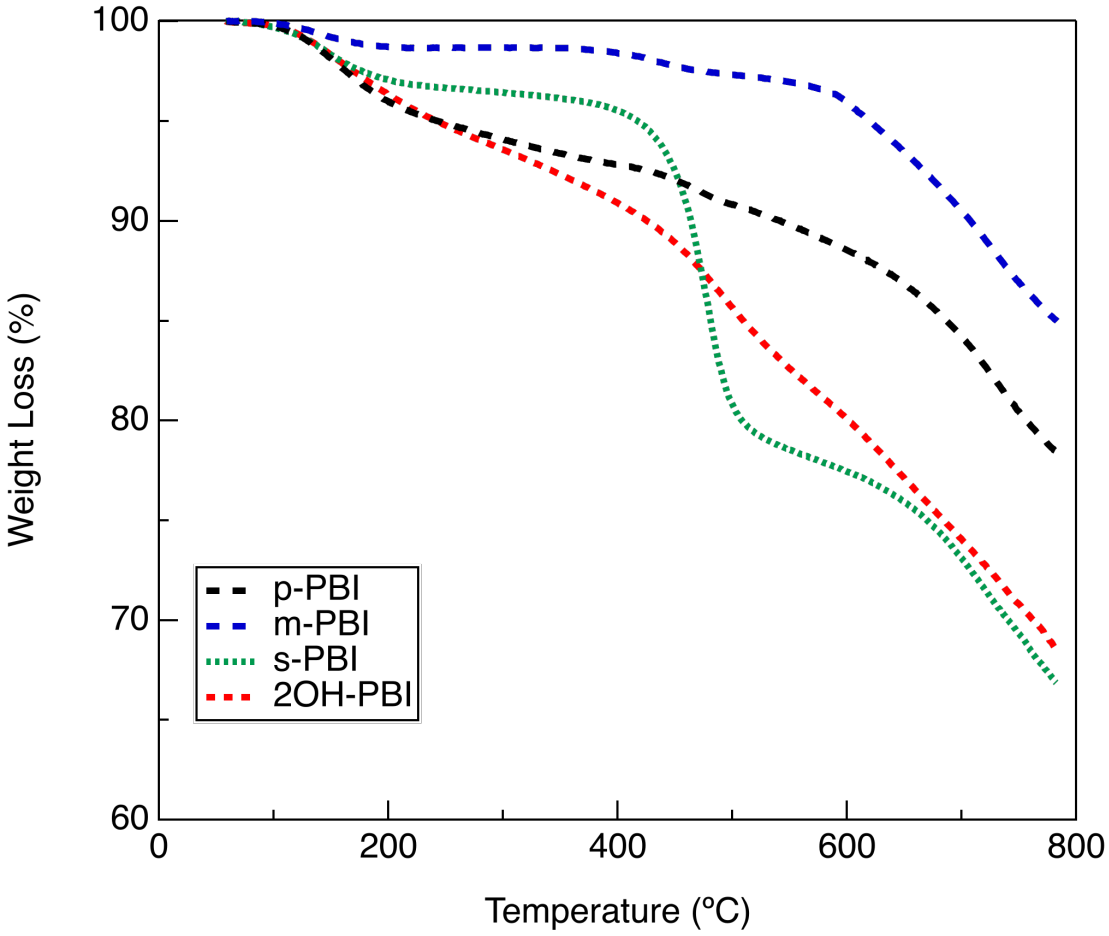

Figure 2.5. TGA measured in a nitrogen atmosphere for each type of PBI film.

The p-PBI sample, which was prepared according to the solvent-free Method 2, displayed good thermal stability. At 200 ºC, there is a 4.0%weight loss, likely from water remaining in the sample. The sample then displays a linear loss of mass up to about 600 ºC, where the total weight loss reaches 11.5%. A second, more rapid degradation is observed above 600 ºC. The final weight loss at 750 ºC

is 19.5%. The two functionalized PBIs, s-PBI and 2OH-PBI, which were both prepared in the solvent-free method, displayed lower thermal stability than the non-functionalized samples. The s-PBI sample displayed stable thermal behavior from 200 °C to 400 °C, where the weight loss reaches 4.4%. However, significant weight is lost from about 425 to 500 ºC, and the total weight loss reaches 19.1%.

This is consistent with the decomposition of sulfonic acid groups in the s-PBI sample, and in agreement with literature reports of their decomposition at about 425 °C.[24, 26-35] The sample then experiences rapid degradation at 600 ºC, with a final weight loss of 30.6% at 750 ºC. The 2OH-PBI samples looks to had two degradation regions. The first is from 100 to 400 ºC, where the weight loss reaches 9.1%, and the second is from 400 ºC to the highest temperature, about 800 ºC. The 2OH-PBI sample had a final weight loss of 29.2% at 750 ºC.

Comparing the TGA results of samples made in both methods, the sample prepared in the conventional solvent casting method had the greatest thermal stability. However, the degradation observed from about 100 to 600 ºC in the samples prepared using the solvent-free method is likely affected by the small amount of phosphoric acid remaining in the samples after the acid removal step. This will be discussed in more detail later in the chapter.

2.4.5 Mechanical Properties of Dense PBI Films

The mechanical properties of the various dense PBI films were determined from the stress strain curves shown in **Figure 2.6** and tabulated in **Table 2.3**. Each sample that underwent the solvent-free process described in Method 2 displayed a lower stress at break compared to the m-PBI sample prepared in Method 1. The

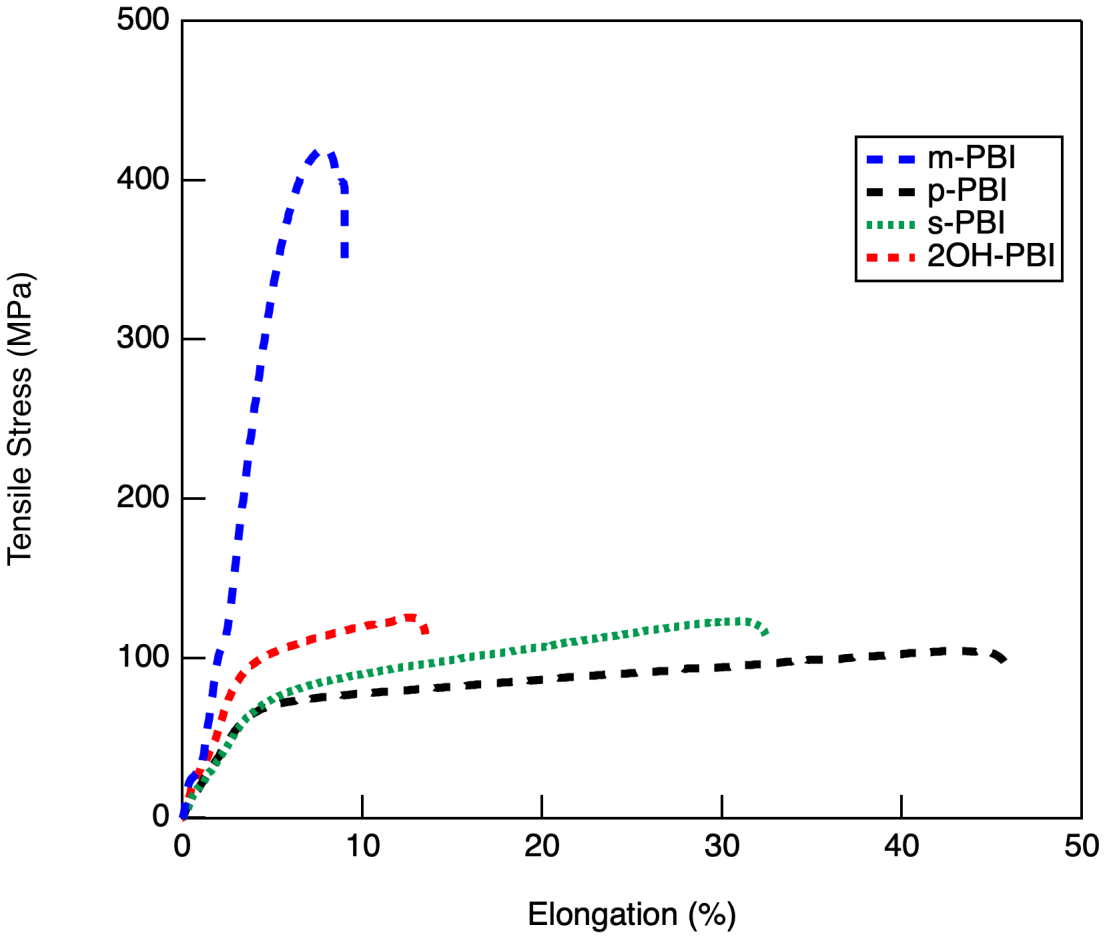

Figure 2.6. Tensile testing results for dense PBI films.

Table 2.3. Young's modulus, strain at break, and elongation at break for each type of dense PBI film.

PBI Type	Young's Modulus (MPa)	Stress at Break (MPa)	Elongation at break (%)
m-PBI	3509 ± 474	408 ± 21	9.8 ± 1.1
p-PBI	2099 ± 191	105 ± 2.5	46 ± 5.8
s-PBI	1928 ± 138	116 ± 11	30 ± 4.2
2OH-PBI	3034 ± 303	127 ± 9.9	11 ± 2.8

m-PBI sample prepared in Method 1 was the stiffest polymer tested, as it displayed the largest value for Young's Modulus. This sample was relatively brittle, as it did

not display plastic deformation at the end of the linear-elastic region of the curve, and fractured when elongation reached 9.8%. The 2OH-PBI sample, which was prepared in the solvent-free procedure, was also relatively stiff with a high Young's Modulus. However, this sample has a greater elongation at break than m-PBI and showed more ductile behavior than the m-PBI sample. The p-PBI sample was less stiff than the m-PBI and 2OH-PBI samples. However, p-PBI displayed the most ductile properties, with an elongation at break of 46%, which was well beyond the yield point. Lastly, s-PBI was the least stiff sample tested, with the lowest Young's Modulus. The s-PBI was also ductile, with an elongation at break of 30% and had a relatively high tensile strength of 116 MPa.

To demonstrate the effect of converting the gel-PBI into a dense film, **Figure 2.7** and **Table 2.4** compare the tensile properties of the gel para-PBI membrane and the dense para-PBI film prepared by Method 2. **Figure 2.7A** contains the full tensile curves, while **Figure 2.7B** displays the curves with a maximum elongation of 50% and maximum tensile stress of 1.0 MPa, to better compare the linear elastic region of the curves.

These results clearly indicate that the p-PBI sample before and after undergoing post-treatment according to Method 2 have very different tensile properties. The p-PBI sample before treatment behaves as an elastic gel, with very low values for Young's Modulus and stress at break, and high values for elongation at break. On the other hand, the p-PBI sample after undergoing Method 2 displays stiffer and stronger material properties and less elasticity. This is indicated by the high value measured for Young's Modulus. The stress at break for the sample after treatment was much higher than the gel sample. While the

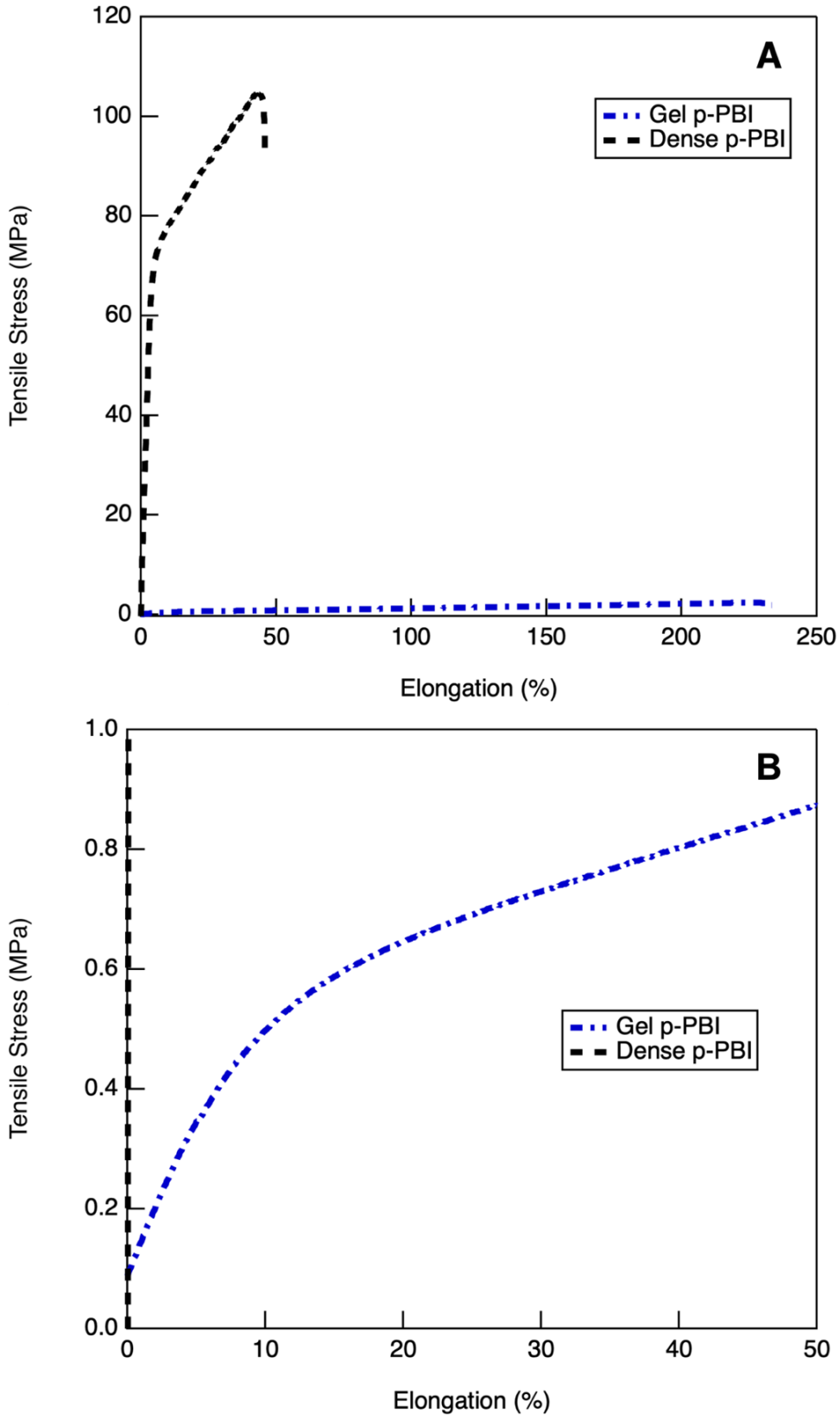

Figure 2.7. Tensile properties of gel para-PBI compared to dense para-PBI.

Table 2.4. Young's modulus, strain at break, and elongation at break for gel and dense p-PBI films.

PBI Type	Young's Modulus (MPa)	Stress at Break (MPa)	Elongation at Break (%)
Gel p-PBI	14.7 ± 0.3	2.6 ± 0.3	251 ± 27
Dense p-PBI	2099 ± 191	105 ± 2.5	46 ± 5.8

elongation at break after treatment is smaller, it is still beyond the linear elastic region. It is clear from this work that the physical transformation of a low polymer content (< 10 wt% polymer solids) gel membrane to a high quality dense film can be conducted by the Method 2 described herein. The z-direction collapse of the gel network of chains into homogeneous dense films produces large area films with excellent mechanical properties that may be useful in many possible applications.

2.4.6 Phosphorus Analysis

As previously mentioned, it is possible that the samples that underwent Method 2 processing have some levels of phosphorus remaining within the samples. It has been previously reported that phosphorus binds strongly with PBI,[36] thus the effect of the phosphorus content that remains in the samples should be studied.

The phosphorus content was measured in each sample after undergoing treatment according to Method 2 using EDS, and the results are displayed in **Table 2.5.** Each sample that underwent Method 2 treatment had some phosphorus remaining, although the amount varied by sample. The s-PBI film contained about

0.27 wt% phosphorus, the least amount of phosphorus detected among the samples. The p-PBI sample was found to contain higher levels of phosphorus, about 1.31 wt%. The 2OH-PBI contained 3.28 wt% phosphorus, which was the most of all of the samples. It was previously reported that 2OH-PBI contains relatively short 2OH-PBI chains that are cross-linked by the formation of phosphate ester bridges.[23] The formation of this covalent cross-linked network with phosphate ester bridges might explain why the 2OH-PBI sample had the highest amount of phosphorus remaining in the sample.

Table 2.5. Phosphorus content, measured as element weight %, collected using EDS for each type of PBI film.

Sample	P (Element wt %)
p-PBI	1.31 ± 0.09
s-PBI	0.27 ± 0.04
2OH-PBI	3.28 ± 0.09

Although the amount of phosphorus remaining in each sample was relatively small, we conducted a study to determine the effects of the retained phosphorus on the properties of the produced films. The remaining phosphorus was completely removed from each PBI sample to study this effect. This was done by washing the dense PBI films in 1 M NaOH for 24 hours at 65 ºC. The samples were then washed in boiling water three times to remove excess salt, and dried in vacuo at 120 ºC to fully dry state before testing. According to EDS results, this procedure is effective in removing the remaining phosphorus, as each sample had no detectable levels of phosphorus.

TGAs of each PBI that did not contain any detectable phosphorus were collected and compared to the previous samples, as shown in **Figure 2.8** and **Table 2.6**. In the dense p-PBI sample, which initially contained 1.31 wt% phosphorus, complete removal of phosphorus had a noticeable impact on the thermal stability. When the phosphorus was completely removed, there was only 1.60% total weight loss at 600 ºC, while the sample with phosphorus displayed a 11.45% weight loss at 600 ºC. However, for the s-PBI sample which contained only 0.27 wt% phosphorus, complete removal of phosphorus had little impact on the thermal stability. For the dense 2OH-PBI sample which initially contained 3.28 wt% phosphorus and displayed 29.18% total weight loss at 750 ºC, complete removal of phosphorus led to a weight loss of 23.32% at 750 ºC. This indicates that even small amounts of phosphorus in the sample can have a significant effect on the thermal stability of the polymer.

The tensile properties of p-PBI with full removal of phosphorus were also studied and compared to the dense p-PBI sample that contained 1.31 wt% phosphorus, shown in **Figure 2.9** and **Table 2.7**. There was a remarkable change in the stress-strain curve upon removal of the small amount of phosphorus. The elongation at break decreased from 462% to 8% and the stress at break increased from 105 MPa to 561 MPa, indicating that the phosphorus species provide a large plasticizer effect, even when present at small amounts.

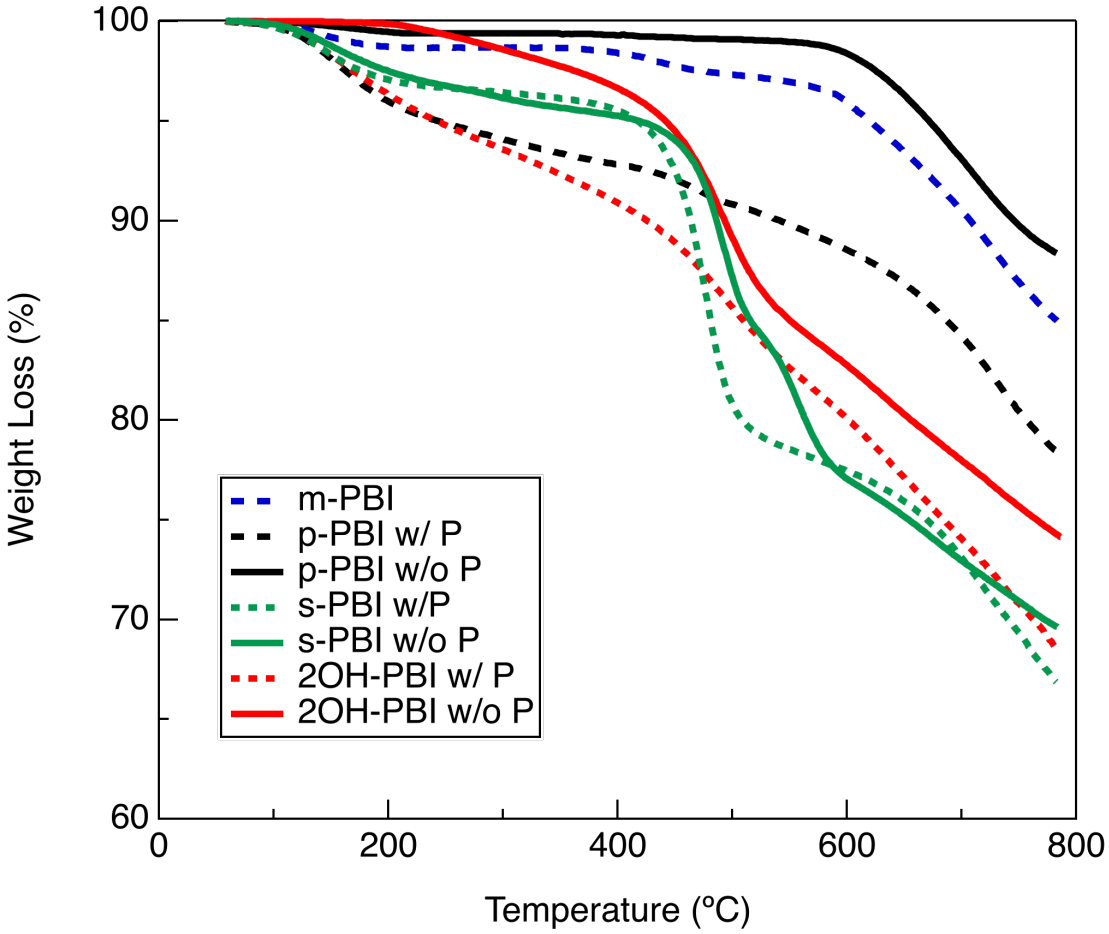

Figure 2.8. TGA of PBIs with complete removal of phosphorus, measured under nitrogen.

Table 2.6. Weight loss % for each sample at 200, 400, 600, and 750 °C, measured using TGA under nitrogen.

Sample	200 °C	400 °C	600 °C	750 °C
m-PBI	1.27 wt%	1.58 wt%	4.03 wt%	13.05 wt%
p-PBI w/ P	4.03 wt%	7.17 wt%	11.45 wt%	19.52 wt%
p-PBI w/o P	0.52 wt%	0.70 wt%	1.60 wt%	10.23 wt%
s-PBI w/ P	2.92 wt%	4.44 wt%	22.54 wt%	30.63 wt%
s-PBI w/o P	2.48 wt%	4.74 wt%	22.91 wt%	29.09 wt%
2OH-PBI w/ P	3.65 wt%	9.10 wt%	19.94 wt%	29.18 wt%
2OH-PBI w/o P	0.13 wt%	3.35 wt%	17.24 wt%	23.32 wt%

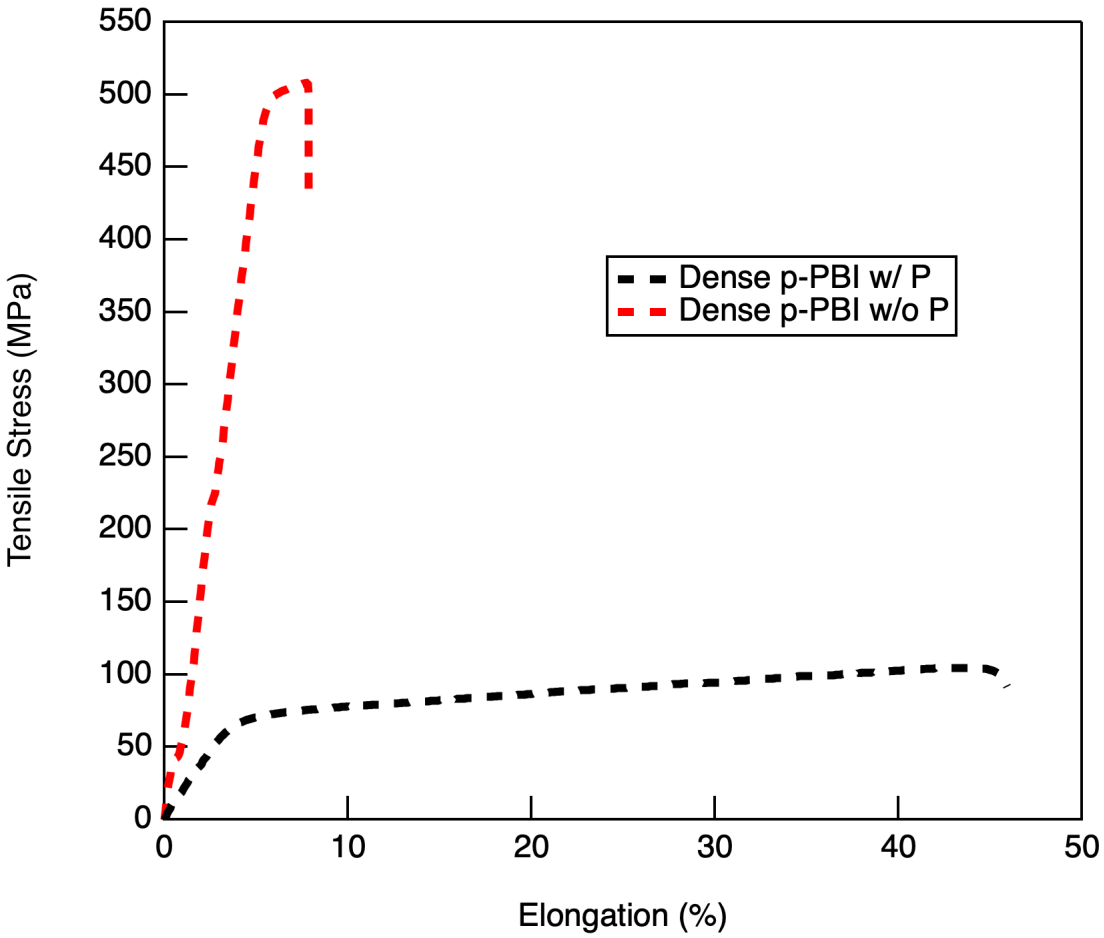

Figure 2.9. Tensile properties of dense p-PBI with 1.31 wt% phosphorus, and dense p-PBI with no phosphorus.

Table 2.7. Young's modulus, strain at break, and elongation at break for p-PBI with and without phosphorus.

PBI Type	Young's Modulus (MPa)	Stress at Break (MPa)	Elongation at break (%)
Dense p-PBI w/ P	2099 ± 191	105 ± 2.5	46 ± 5.8
Dense p-PBI w/o P	6883 ± 1248	561 ± 45	8.0 ± 2.1

The tensile properties of dense p-PBI without phosphorus were also compared to m-PBI prepared in the organic solvent casting method, in **Figure 2.10** and **Table 2.8**. The stress-strain curves were more similar in their features, although the p-PBI film showed higher Young's Modulus and stress at break, which could be due to the more rigid nature of the p-PBI chemistry.

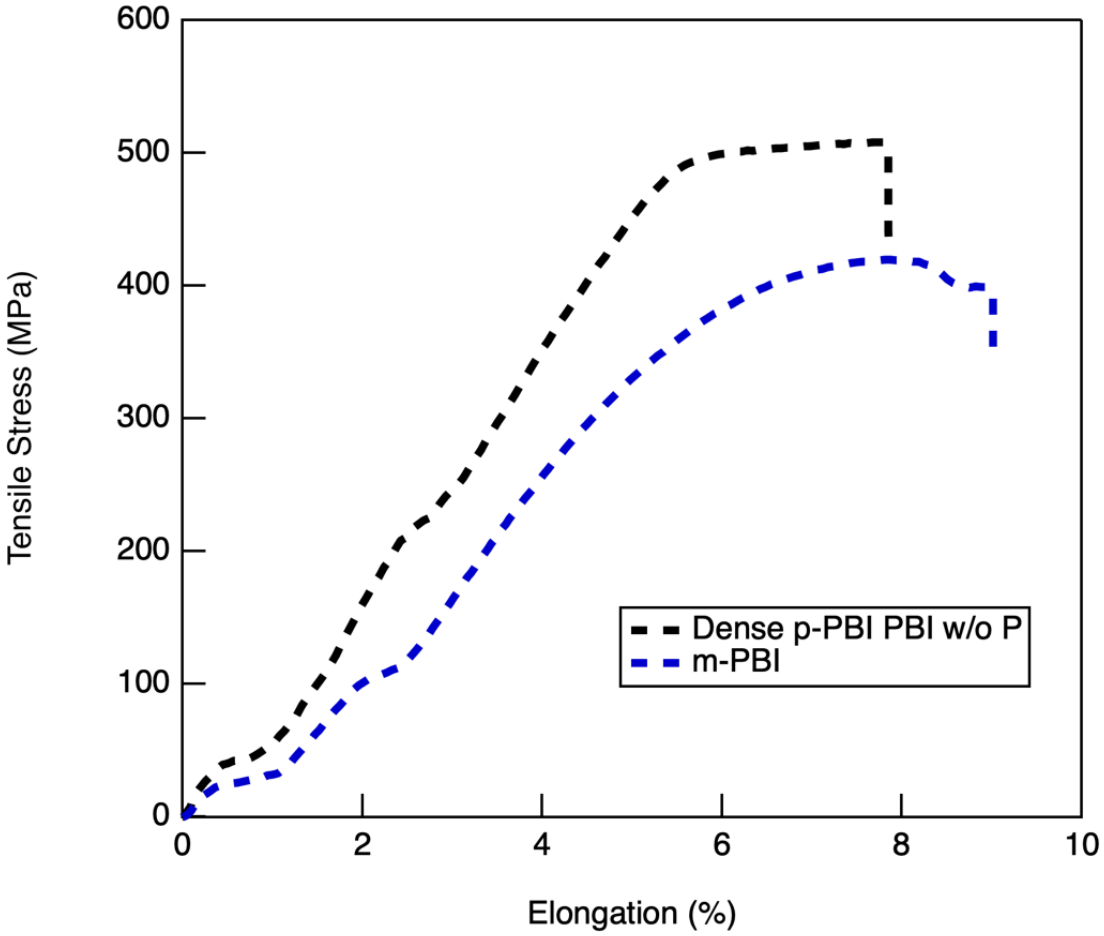

Figure 2.10. Tensile of p-PBI with complete removal of phosphorus, compared to m-PBI.

Table 2.8. Young's modulus, strain at break, and elongation at break for p-PBI without phosphorus and meta-PBI prepared in the organic solvent casting method.

PBI Type	Young's Modulus (MPa)	Stress at Break (MPa)	Elongation at break (%)
Dense p-PBI w/o P	6883 ± 1248	561 ± 45	8.0 ± 2.1
m-PBI	3509 ± 474	408 ± 21	9.8 ± 1.1

2.4.7 WAXS

WAXS was collected on the gel p-PBI membrane, the gel p-PBI in water, and the dense p-PBI membrane sample. The radially integrated 2θ plots are shown in **Figure 2.11**, and the WAXS 2D images are shown in **Figure 2.12** for each membrane sample. The gel p-PBI and gel p-PBI in water samples display an intense and broad peak centered at 2θ = 25°. As reported in literature, this results from convolution of amorphous and crystalline scattering in the gel membranes.[34] This is likely due to the formation of hydrogen bonding structures within the gel membranes. The dense p-PBI samples displays a more distinct but less intense peak at 2θ = 25°, which indicated that there was increased scattering from the amorphous region, compared to the crystalline region, upon undergoing densification.

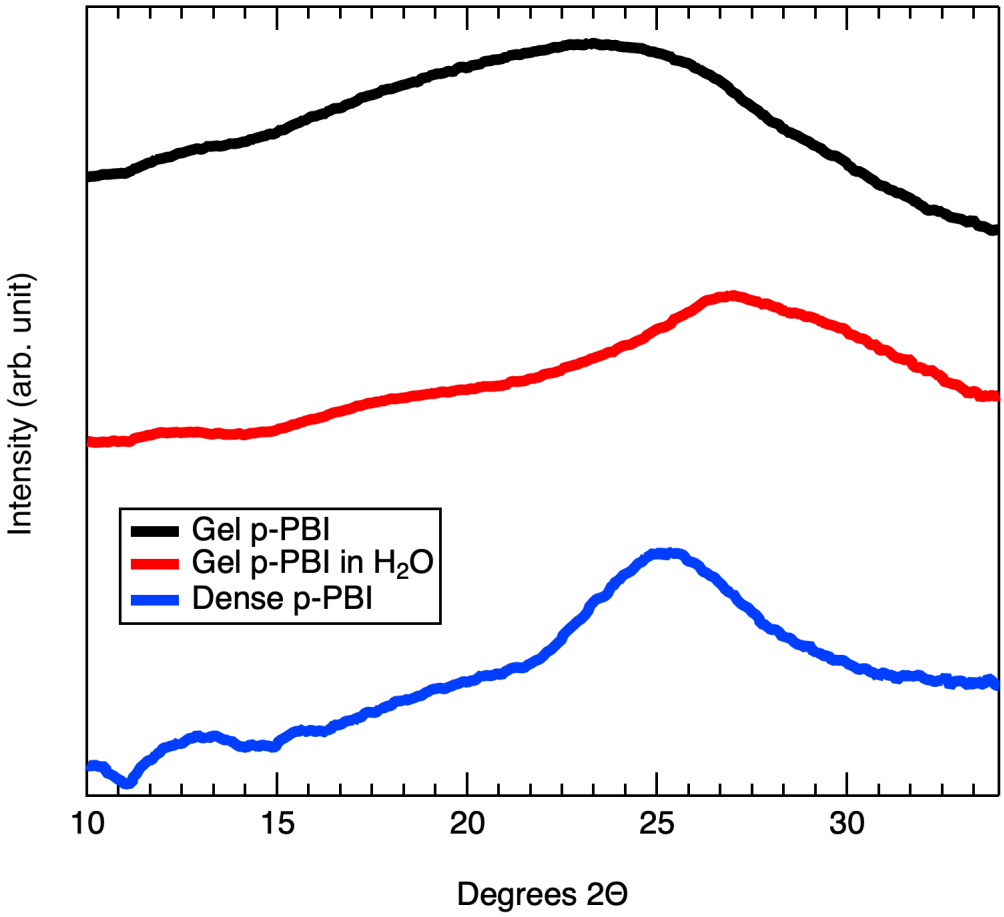

Figure 2.11. Radially integrated 2θ plots of gel p-PBI (black), gel p-PBI in water (red), and dense p-PBI (blue).

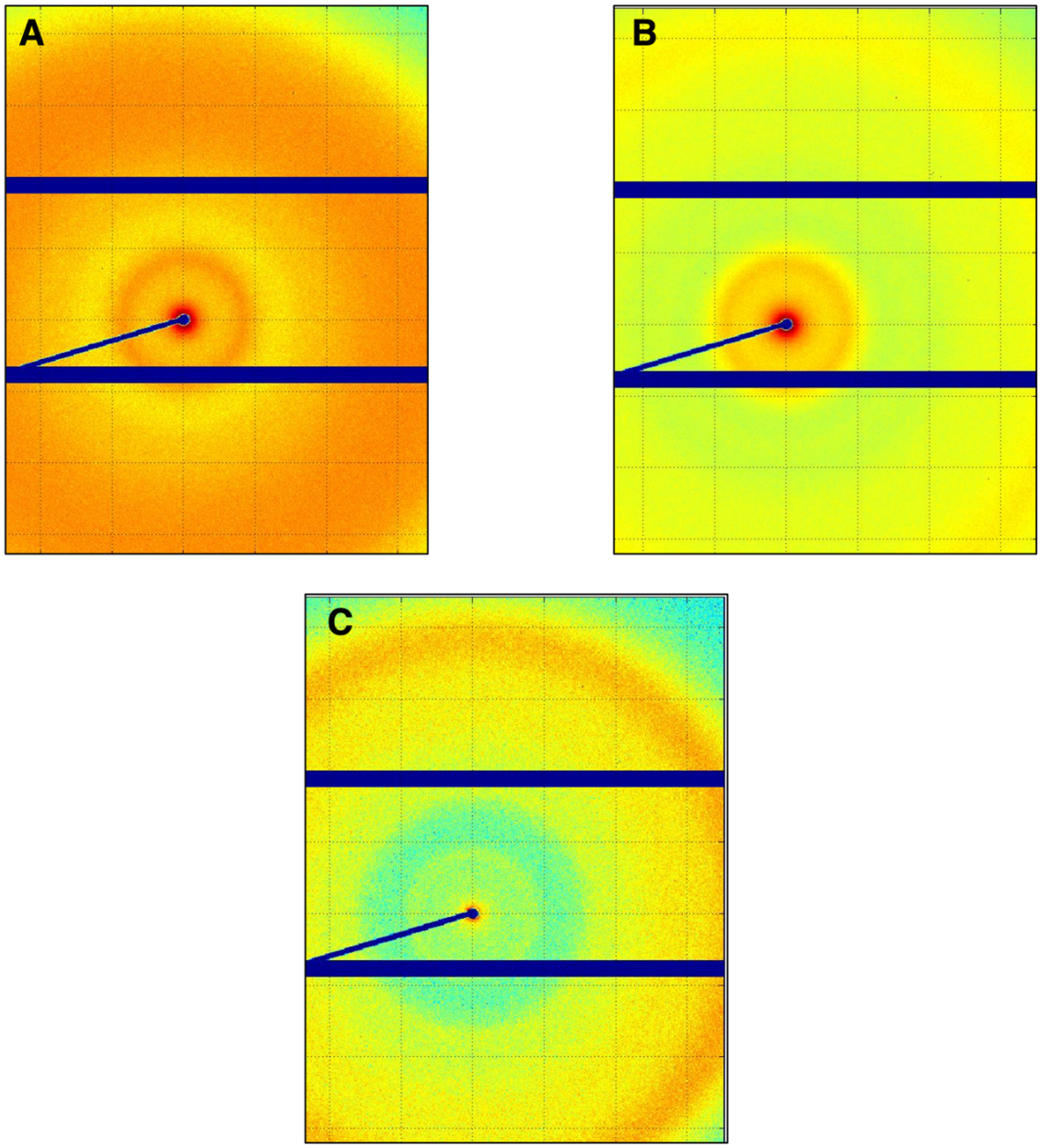

Figure 2.12. WAXS 2D images of A) Gel p-PBI B) Gel p-PBI neutralized in water C) Dense p-PBI.

2.5 CONCLUSIONS

Dense PBI films were prepared for the first time without the use of organic solvents. This was achieved through a process innovation that piggybacks onto the commercially developed PPA Process. By removing the phosphoric acid and

controlled drying of the wet membrane, a physical transformation of a gel PBI membrane into a dense polymer film takes place. These dense PBI films contained a small amount of residual phosphorus in the dense films. The remaining phosphorus was completely removed by additional treatment in base. The TGA and tensile results of p-PBI with and without phosphorus indicate that small amounts of phosphoric acid act as a plasticizer in PBI films. Compared to m-PBI films commercially produced from the organic solvent casting method, the p-PBI films produced in the solvent-free method display higher thermal stability, as well as better mechanical properties. This is due to the more rigid backbone structure of linear p-PBI, compared to m-PBI. An organic solvent-free method to produce high quality, large area dense PBI films has been developed that is applicable to many PBI chemistries which exhibit low or no solubility in organic solvents.

2.6 ACKNOWLEDGEMENTS

We gratefully acknowledge Eric Williams and Dr. Morgan Stefik for their help in collecting the SAXS data.

2.7 REFERENCES

[1] Brinker, K. C. ; Robinson, I. M. Polybenzimidazoles. U.S. Patent #2,895,948. July 21, 1959.

[2] Wainright, J. S.; Wang, J. T.; Weng, D.; Savinell, R. F.; Litt, M. Acid-Doped Polybenzimidazoles: A New Polymer Electrolyte. *Journal of The Electrochemical Society* **1995,** *142* (7), L121-L123.

[3] Pesiri, D. R.; Jorgensen, B.; Dye, R. C. Thermal optimization of polybenzimidazole meniscus membranes for the separation of hydrogen, methane, and carbon dioxide. *Journal of Membrane Science* **2003,** *218* (1), 11-18.

[4] Kumbharkar, S. C.; Islam, M. N.; Potrekar, R. A.; Kharul, U. K. Variation in acid moiety of polybenzimidazoles: Investigation of physico-chemical properties towards their applicability as proton exchange and gas separation membrane materials. *Polymer* **2009,** *50* (6), 1403-1413.

[5] Singh, R. P.; Li, X.; Dudeck, K. W.; Benicewicz, B. C.; Berchtold, K. A. Polybenzimidazole based random copolymers containing hexafluoroisopropylidene functional groups for gas separations at elevated temperatures. *Polymer* **2017,** *119*, 134-141.

[6] Stevens, K. A.; Moon, J. D.; Borjigin, H.; Liu, R.; Joseph, R. M.; Riffle, J. S.; Freeman, B. D. Influence of temperature on gas transport properties of tetraaminodiphenylsulfone (TADPS) based polybenzimidazoles. *Journal of Membrane Science* **2020,** *593*, 117427.

[7] Wang, K. Y.; Chung, T.-S. Polybenzimidazole nanofiltration hollow fiber for cephalexin separation. *AIChE Journal* **2006,** *52* (4), 1363-1377.

[8] Lv, J.; Wang, K. Y.; Chung, T.-S. Investigation of amphoteric polybenzimidazole (PBI) nanofiltration hollow fiber membrane for both cation and anions removal. *Journal of Membrane Science* **2008,** *310* (1), 557-566.

[9] Valtcheva, I. B.; Kumbharkar, S. C.; Kim, J. F.; Bhole, Y.; Livingston, A. G. Beyond polyimide: Crosslinked polybenzimidazole membranes for organic solvent nanofiltration (OSN) in harsh environments. *Journal of Membrane Science* **2014,** *457*, 62-72.

[10] Fishel, K.; Qian, G.; Benicewicz, B. C. PBI Membranes Aia the PPA Process. In *High Temperature Polymer Electrolyte Membrane Fuel Cells*; Li, Q.; Aili, D.; Hjuler, H. A.; Jensen, J. O., Eds.; Springer, 2016; pp 217-238. DOI: 10.1007/978-3-319-17082-4_10

[11] Aili, D.; Jensen, J. O.; Li, Q. Polybenzimidazole Membranes by Post Acid Doping. In *High Temperature Polymer Electrolyte Membrane Fuel Cells*; Li, Q.; Aili, D.; Hjuler, H. A.; Jensen, J. O., Eds. Springer, 2016; pp 195-215. DOI: 10.1007/978-3-319-17082-4_9

[12] Sandor, R. B. PBI (Polybenzimidazole): Synthesis, Properties and Applications. *High Performance Polymers* **1990,** *2* (1), 25-37.

[13] Mader, J.; Xiao, L.; Schmidt, T. J.; Benicewicz, B. C. Polybenzimidazole/Acid Complexes as High-Temperature Membranes. In *Fuel Cells II: Advances in Polymer Science,* Vol. 216; Scherer, G. G., Ed.; Springer, 2008; pp 63-124. DOI: 10.1007/12_2007_129

[14] Choe, E.-W. Catalysts for the preparation of polybenzimidazoles. *Journal of Applied Polymer Science* **1994,** *53* (5), 497-506.

[15] Hedberg, F.; Marvel, C. A new single-step process for polybenzimidazole synthesis. *Journal of Polymer Science: Polymer Chemistry Edition* **1974,** *12* (8), 1823-1828.

[16] Higgins, J.; Marvel, C. Benzimidazole polymers from aldehydes and tetraamines. *Journal of Polymer Science Part A-1: Polymer Chemistry* **1970,** *8* (1), 171-177.

[17] Yang, H. *Aromatic high-strength fibers*. John Wiley and Sons, Inc., 1989.

[18] Powers, E. J.; Serad, G. A. History and Development of Polybenzimidazoles. In *High Performance Polymers: Their Origin and Development*; Seymour, R. B.; Kirshenbaum, G. S., Eds.; Springer, 1986; pp 355-373. DOI: 10.1007/978-94-011-7073-4_34

[19] Molleo, M.; Schmidt, T. J.; Benicewicz, B. C. Polybenzimidazole Fuel Cell Technology. In *Encyclopedia of Sustainability Science and Technology;* Meyers, R. A., Ed.; Springer, 2012; pp 8173-8201. DOI: 10.1007/978-1-4419-0851-3

[20] Neuse, E. W. Aromatic polybenzimidazoles. Syntheses, properties, and applications. In *Synthesis and Degradation Rheology and Extrusion. Advances in Polymer Science,* Vol. 47; Springer, **1982**; pp 1-42.

[21] Xiao, L.; Zhang, H.; Scanlon, E.; Ramanathan, L. S.; Choe, E.-W.; Rogers, D.; Apple, T.; Benicewicz, B. C. High-Temperature Polybenzimidazole Fuel Cell Membranes via a Sol−Gel Process. *Chemistry of Materials* **2005,** *17* (21), 5328-5333.

[22] Yu, S.; Zhang, H.; Xiao, L.; Choe, E.-W.; Benicewicz, B. C. Synthesis of Poly (2,2′-(1,4-phenylene) 5,5′-bibenzimidazole) (para-PBI) and Phosphoric Acid Doped Membrane for Fuel Cells. *Fuel Cells* **2009,** *9* (4), 318-324.

[23] Yu, S.; Benicewicz, B. C. Synthesis and Properties of Functionalized Polybenzimidazoles for High-Temperature PEMFCs. *Macromolecules* **2009,** *42* (22), 8640-8648.

[24] Mader, J. A.; Benicewicz, B. C. Sulfonated Polybenzimidazoles for High Temperature PEM Fuel Cells. *Macromolecules* **2010,** *43* (16), 6706-6715.

[25] Steenberg, T.; Hjuler, H. A.; Terkelsen, C.; Sánchez, M. T.; Cleemann, L. N.; Krebs, F. C. Roll-to-roll coated PBI membranes for high temperature PEM fuel cells. *Energy & Environmental Science* **2012,** *5* (3), 6076-6080.

[26] Ariza, M. J.; Jones, D. J.; Rozière, J. Role of post-sulfonation thermal treatment in conducting and thermal properties of sulfuric acid sulfonated poly(benzimidazole) membranes. *Desalination* **2002,** *147* (1), 183-189.

[27] Asensio, J. A.; Borrós, S.; Gómez-Romero, P. Proton-conducting polymers based on benzimidazoles and sulfonated benzimidazoles. *Journal of Polymer Science Part A: Polymer Chemistry* **2002,** *40* (21), 3703-3710.

[28] Bai, Z.; Price, G. E.; Yoonessi, M.; Juhl, S. B.; Durstock, M. F.; Dang, T. D. Proton exchange membranes based on sulfonated polyarylenethioethersulfone and sulfonated polybenzimidazole for fuel cell applications. *Journal of Membrane Science* **2007,** *305* (1), 69-76.

[29] Glipa, X.; El Haddad, M.; Jones, D. J.; Rozière, J. Synthesis and characterisation of sulfonated polybenzimidazole: a highly conducting proton exchange polymer. *Solid State Ionics* **1997,** *97* (1), 323-331.

[30] Jouanneau, J.; Mercier, R.; Gonon, L.; Gebel, G. Synthesis of Sulfonated Polybenzimidazoles from Functionalized Monomers: Preparation of Ionic Conducting Membranes. *Macromolecules* **2007,** *40* (4), 983-990.

[31] Peron, J.; Ruiz, E.; Jones, D. J.; Rozière, J. Solution sulfonation of a novel polybenzimidazole: A proton electrolyte for fuel cell application. *Journal of Membrane Science* **2008,** *314* (1), 247-256.

[32] Qing, S.; Huang, W.; Yan, D. Synthesis and characterization of thermally stable sulfonated polybenzimidazoles. *European Polymer Journal* **2005,** *41* (7), 1589-1595.

[33] Rikukawa, M.; Sanui, K. Proton-conducting polymer electrolyte membranes based on hydrocarbon polymers. *Progress in Polymer Science* **2000,** *25* (10), 1463-1502.

[34] Staiti, P.; Lufrano, F.; Aricò, A. S.; Passalacqua, E.; Antonucci, V. Sulfonated polybenzimidazole membranes — preparation and physico-chemical characterization. *Journal of Membrane Science* **2001,** *188* (1), 71-78.

[35] Xu, H.; Chen, K.; Guo, X.; Fang, J.; Yin, J. Synthesis of novel sulfonated polybenzimidazole and preparation of cross-linked membranes for fuel cell application. *Polymer* **2007,** *48* (19), 5556-5564.

[36] Quartarone, E.; Mustarelli, P. Polymer fuel cells based on polybenzimidazole/H_3PO_4. *Energy & Environmental Science* **2012,** *5* (4), 6436-6444.

CHAPTER 3

DENSIFIED PBI MEMBRANES WITH ENHANCED PERFORMANCE IN VANADIUM REDOX FLOW BATTERIES

3.1 ABSTRACT

A novel method has been developed in which PBI gel membranes are transformed into dense PBI films. When doped in sulfuric acid, the dense PBI membranes display great potential in vanadium redox flow batteries (VRBs). While the PBI gel membranes display vanadium permeabilities in the range of 49 to 73 x 10^{-8} cm^2 s^{-1}, dense PBI membranes of the reported process exhibit at least an order of magnitude reduction in vanadium permeability, measured between 0.78 to 6.7 x 10^{-8} cm^2 s^{-1}. Previously, dense PBI membranes have been prepared in the "conventionally imbibed" process, which involves casting from an organic solvent and doping in 2.6 M sulfuric acid. The conventionally imbibed PBI membranes display low ionic conductivities of 10 to 20 mS cm^{-1} and cell operation is limited to 200 mA cm^{-2}. However, when dense PBI membranes are prepared according to the new process and doped in the same concentration of sulfuric acid, the ionic conductivity is much higher, between 78 to 139 mS cm^{-1}. Due to the significantly enhanced ionic conductivity, cells constructed with dense PBI membranes prepared using the new technique achieve operation at current densities up to 500 mA cm^{-2}, and the cell performance was found to be stable over a 7-month period. The excellent electrochemical properties combined with a straightforward solvent-free process, demonstrate the great technical potential of dense PBI membranes prepared using this novel technique.

3.2 INTRODUCTION

The vanadium redox flow battery (VRB) is a rechargeable, all liquid battery that holds great potential in large-scale energy storage.[1] VRBs display distinct

advantages including long lifetimes, active thermal management, and liberation from energy and power rankings.[2-4] In a VRB, the four oxidation states of vanadium (V^{2+}, V^{3+}, V^{4+}, and V^{5+}) are employed to convert between chemical energy and electrical energy to charge and discharge the battery. In a typical VRB, two electrolyte tanks contain a vanadium redox couple (2+/3+ and 4+/5+) dissolved in a supporting electrolyte of sulfuric acid, with the cell stack situated between the electrolyte tanks.[5] The V^{4+} / V^{5+} redox couple is located in the posolyte tank, while the V^{2+} / V^{3+} redox couple is in the negolyte tank. Charge-discharge processes involves oxidation or reduction of the active vanadium species to bring about conversion of the chemical and electrical energy.[6] Since VRBs contain only one element as the redox couple, capacity losses due to electrolyte crossover commonly observed in flow batteries containing multiple redox-active elements, are largely eliminated.[7]

A significant hurdle to wide-spread commercialization of VRBs is the high cost associated with manufacture. VRBs typically employ well-known commercially available perfluorosulfonic acid (PFSA)-based materials as the membrane separator, which can account for up to 40% of the total cost in a cell stack, and 10-15% of the whole battery system.[8-10] Therefore, many efforts have been made to develop less expensive, non-fluorinated alternatives that exhibit high vanadium selectivity and tunable ionic conductivity.[2, 6, 11]

Cation exchange membranes (CEMs), such as sulfonated hydrocarbon membranes, have shown high selectivity, tunable ion conductivity, and good energy efficiency compared to PFSA-based membranes.[2, 12-14] However, during periods of charging, excess oxidative V^{5+} is produced which is known to

chemically degrade many hydrocarbon-based membranes.[15] Thus, the long-term stability of such membranes at extended operation time remains a challenge.

Anion exchange membranes (AEMs) have also been investigated as separators in VRBs.[16-18] AEMs take advantage of the Donnan exclusion effect to achieve exceptionally low vanadium crossover, since the positively charged functional groups in the membrane repel vanadium ions through electrostatic repulsion.[19] The low vanadium crossover of AEMs allows for cells to achieve high coulombic efficiencies (CEs). However, the ionic conductivity of AEMs is significantly lower than PFSA-based membranes, mostly reported below 30 mS cm^{-1}, with typical values less than 10 mS cm^{-1}.[19, 20] The high internal resistance of AEMs leads to low energy efficiencies (EEs), demonstrating a trade-off between low vanadium crossover and high ionic conductivity on cell performance.[15, 19] Other than low ionic conductivity, AEMs also have the disadvantage of poor chemical stability.[19]

More recently, polybenzimidazole (PBI) membranes have shown exceptional stability in VRBs.[21-25] Historically, PBI membranes have been investigated for applications in nano-filtration,[26-28] gas separation,[29] and most commonly in high-temperature proton exchange membrane fuel cells.[30-32] Most of the available literature on application of PBI membranes in VRBs has been focused on "conventionally imbibed" PBI membranes.[21-24] In the conventionally imbibed process, dense PBI membranes are cast from a solution of PBI dissolved in an organic solvent and after undergoing tedious solvent removal processes, the dense PBI films are doped in sulfuric acid. Zhang et al. first reported the superior performance of conventionally imbibed PBI membranes over PFSA-based

membranes, with substantially enhanced CEs and capacity decay rates as low as 0.3% per cycle, compared to 1.3% per cycle for PFSA-based membranes.[21] Their work demonstrated that the conventionally imbibed PBI membranes contain low vanadium crossover, but also a low ionic conductivity of 15.8 mS cm^{-1}. Thus, research on PBIs for VRBs has been heavily focused on improving the ionic conductivity of membranes produced in the conventionally imbibed process.[22-24]

Wessling et al. utilized a water vapor induced phase inversion process which led to a slightly enhanced conductivity of 16.6 mS cm^{-1} in 2.5 M sulfuric acid.[22] He et al. first reported on pre-swelling PBIs in phosphoric acid followed by immersion in sulfuric acid, which led to increased acid doping levels and ionic conductivity while maintaining substantially high selectivity.[23] Later, He et al. designed conventionally imbibed PBIs with a nanophase-separated structure prepared by grafting non-ionic hydrophilic side chains, which led to the formation of hydrophilic clusters that acted as effective proton transfer pathways and improved the ionic conductivity.[24] Although these efforts on conventionally imbibed PBIs explored many interesting techniques, the ionic conductivities were raised only slightly above those achieved by PFSA-based membranes. In all types of membranes that have been explored for VRBs, the trade-off between ionic conductivity and vanadium permeability is a recurring theme.

Previously, it was demonstrated that PBI gel membranes have superior performance to the conventionally imbibed PBIs in high-temperature proton exchange membrane fuel cells.[31, 33] PBI gel membranes are generated in a one-pot polymerization of monomers in polyphosphoric acid (PPA). Upon completion of polymerization, membranes are cast directly from the formed PPA/PBI mixture

and subsequent hydrolysis of the PPA to phosphoric acid (PA) induces a sol-to-gel transition. This process, discovered by Benicewicz et al. in 2005 was termed the PPA Process and leads to PBI gel membranes highly swollen in phosphoric acid.[33]

In 2019, Benicewicz et al. reported using sulfonated PBI (s-PBI) gel membranes in VRBs after acid switching the imbibed dopant from phosphoric acid to sulfuric acid.[25] Upon investigation for VRB applications, the s-PBI gel membranes were found to exhibit different properties than those of the conventionally imbibed PBIs. The s-PBI gel membranes and their crosslinked counterparts were much more conductive than conventionally imbibed PBIs, with conductivities ranging from 537 to 593 mS cm^{-1} in 2.6 M sulfuric acid. Due to the enhanced conductivity, VRB cells were operated at current densities ranging from 75 to 500 mA cm^{-2}. Conventionally imbibed PBIs are typically limited to operation below 200 mA cm^{-2} due to their comparatively low ionic conductivity. The s-PBI gel membranes also displayed excellent stability in the oxidative V^{5+} environment even after extended soaking. However, the vanadium crossover of the s-PBI gel membranes was much higher than those measured in conventionally imbibed PBIs due to the open gel structure of the PPA Process membranes.

Herein, we report a method in which PBI gel membranes are converted to dense PBI films and subsequently doped in sulfuric acid. Surprisingly, this facile process leads to relatively high ionic conductivity and low vanadium permeability. VRB cells were constructed and showed excellent VRB performance at high current densities. In VRB testing over a 7-month period, stable performance indicated low vanadium crossover achieved by membranes produced with the new process. Additionally, the novel membrane formation technique required no

organic solvents, no additional chemicals, and is compatible with commercial production techniques. The striking differences between the properties achieved by conventionally imbibed dense PBIs, and dense PBIs made in the reported process suggest that new approaches to membrane formation can offer pathways to overcome the traditional trade-off of conductivity and permeability.

3.3 EXPERIMENTAL

3.3.1 Materials

Terephthalic acid (TPA, >99% purity) was purchased from Amoco. 2-sulfoterephthalic acid monosodium salt (STPA, >98% purity) and 2,5-dihydroxyterephthalic acid (2OH-TPA, >98% purity) were purchased from TCI America. Poly(phosphoric acid) (PPA, 115%) was purchased from Innophos, vanadium (IV) sulfate hydrate was purchased from BeanTown Chemicals, technical grade sulfuric acid (SA) was purchased from Fisher Chemical, and 3,3',4,4'-tetraaminobiphenyl (TAB, polymer grade, ~97.5%) was kindly donated by BASF Fuel Cell, Inc. All chemicals and reagents were used as received without further purification.

3.3.2 Polymer Synthesis and Acid-Imbibed Gel Membrane Fabrication

The synthesis of p-PBI, 2OH-PBI, s-PBI, and m/p-PBI were completed as previously reported.[32, 34-37] The general synthesis of PBI through reaction of diacids and tetraamines is displayed in **Figure 3.1**. In a typical polymerization, equal molar equivalents of the selected dicarboxylic acid and tetraamine (TAB) were added to a reaction kettle under a nitrogen atmosphere, followed by PPA. Equipped with an overhead mechanical stirrer, the reaction mixture was stirred

and purged in a nitrogen environment throughout the polymerization. A programmable temperature controller with ramp and soak features was used to control the polymerization temperature. Polymerizations were completed over a 18-48 hour period and monitored by visual inspection of viscosity. The final polymerization temperature was between 190 and 220 °C. Each viscous solution of polymer in PPA was cast directly onto a glass substrate using a doctor blade with a controlled gate thickness of 15 mils. The cast polymer solution was hydrolyzed in a controlled humidity chamber set to 55% RH to induce the sol-to-gel transition. Gel membranes formed in the PPA Process were self-supporting and heavily imbibed with PA.

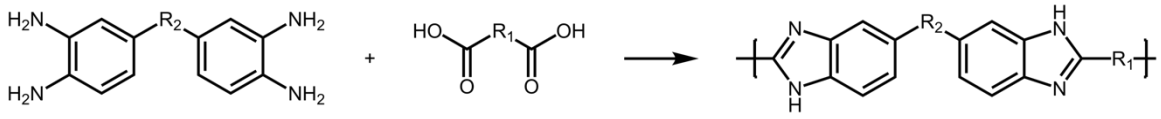

Figure 3.1. General synthetic procedure for the preparation of PBIs by reaction of tetraamines and dicarboxylic acids.

3.3.3 Post-Polymerization Modification

The PBI gel membranes were then subjected to a novel post-polymerization modification technique, beginning with the removal of PA. Membranes were washed in a series of deionized water baths to remove the PA, and pH indication paper was used to ensure removal before proceeding. The water-imbibed p-PBI and s-PBI gel membranes were stretched in one-direction from 0 (non-stretched) to 200% of the original length. An Instron Tensile Tester equipped with a 100 N load cell and a crosshead speed of 20 mm min^{-1} was used to unidirectionally stretch

the water-imbibed PBI gel membranes. Membranes were left in the stretched position between the grips for 30 minutes. Upon removal from the grips, the membranes were immediately placed between porous sheets and the perimeter was secured with clamps.

The similarly prepared water-imbibed p-PBI, 2OH-PBI, and s-PBI membranes also underwent post-treatment, but without stretching. The water-imbibed gel membranes were taken directly from the water bath and clamped between the porous sheets to undergo post-polymerization drying without stretching. The stretched and non-stretched membrane samples were left between the porous sheets for 12-24 hours to allow remaining water to evaporate. The dried densified PBI films were then placed in a solution of 2.6 M sulfuric acid for at least 24 hours before characterization.

The water-imbibed gel PBIs were also tested without post-treatment by directly doping in 2.6 M sulfuric acid for 24 hours. These samples served as a control, in order to determine the effect of post-treatment with and without stretching. The porous sheets used in these studies were composed of porous polyethylene with a thickness of 3.2 mm and an average porosity of 45-90 μm.

3.3.4 Membrane Composition Analysis

Titration was utilized to determine the acid doping level and composition of acid, water, and polymer within each membrane. A small membrane sample was isolated and weighed before adding ~50 mL of deionized water and stirring at room temperature overnight. The mixture was then titrated with a standard 0.1 N sodium hydroxide solution using a Metrohm 888 DMS Titrando autotitrator.

After titration, the sample was washed with deionized water and dried in a vacuum oven overnight, the dried polymer samples were then weighted. The polymer weight percent (*polymer wt%*) and sulfuric acid weight percent (*acid wt%*) were calculated using the following equations:

$$Polymer\ wt\% = \frac{W_{dry}}{W_{sample}} \cdot 100$$

$$Acid\ wt\% = \frac{M_{acid} \cdot V_{NaOH} \cdot c_{NaOH}}{2 \cdot W_{sample}} \cdot 100$$

Where W_{sample} was the weight of the sample before titration, W_{dry} was the weight of the final dried sample after titration, M_{acid} was the molecular weight of sulfuric acid, V_{NaOH} and C_{NaOH} was the volume and concentration of sodium hydroxide required to neutralize sulfuric acid to the first equivalence point, respectively. Although the second proton in sulfuric acid is much less acidic than the first (pK_{a1} = -3 and pK_{a2} = 2), it is still strong enough to cause both protons to be titrated simultaneously.

The sulfuric acid doping level (or the number of moles of sulfuric acid per mole of PBI repeat unit, *X*) was calculated according to the following equation:

$$X = \frac{V_{NaOH} \cdot c_{NaOH}}{2 \cdot \left({W_{dry}}/{M_{polymer}} \right)}$$

Where V_{NaOH} and C_{NaOH} were the volume and concentration of sodium hydroxide needed to neutralize the sulfuric acid, W_{dry} was the weight of the final dried sample after titration, and $M_{polymer}$ was the molecular weight of the polymer repeat unit.

3.3.5 Ionic Conductivity

In-plane conductivity was measured with a four-probe electrochemical impedance spectroscopy (EIS) method. A FuelCon (TrueData EIS PCM) electrochemical workstation was used over a frequency range of 1 Hz to 50 kHz. The samples were cut to roughly 1.0 cm x 4.0 cm and placed in the 4-electrode sample holder. Ionic conductivity (σ) was calculated as follows:

$$\sigma = \frac{d}{l \cdot w \cdot R_m}$$

Where d was the distance between the two inner probes, l was the thickness of the membrane, w was the width of the membrane, and R_m was the ohmic resistance, determined by model fitting. Measurements were conducted at room temperature.

3.3.6 Vanadium Permeability

Measurements for vanadium ($VOSO_4$) permeability were completed with a PermeGear "side-by-side" direct permeation cell. The cell had two chambers, each with a volume capacity of 45 mL, and separated by the membrane under test. The temperature during testing was regulated with a recirculating water bath set to 25 °C. A typical test experiment contained 1.5 M $VOSO_4$ in 2.6 M sulfuric acid in the donor chamber and 1.5 M $MgSO_4$ in 2.6 M sulfuric acid in the receptor chamber. Vanadium (IV) has a strong UV absorption characteristic at 248 nm; utilizing this property, the concentration of the receptor chamber was measured with a Shimadzu UV-2450 UV/Vis spectrometer at various time intervals. The VO^{2+} permeability was calculated using Fick's law of diffusion:

$$P_s t = \ln\left[1 - 2\frac{c_r(t)}{c_r(0)}\right]\left[-\frac{V \cdot d}{A}\right]$$

Where $c_r(0)$ was the initial concentration of $VOSO_4$ in the donor chamber, V was the volume of solution added to each chamber, d was the membrane thickness, A was the active area of the membrane, $c_r(t)$ was the concentration of $VOSO_4$ in the receptor chamber at time t, and P_s was the calculated salt permeability.

3.3.7 Single-Cell Flow Battery Testing

VRB test cells with 23 cm^2 active area and interdigitated flow fields for liquid electrolyte solutions machined into carbon (Tokai G347B), designed and assembled by United Technologies Research Center (UTRC), were utilized. Membranes were sandwiched between identical carbon paper electrodes provided by UTRC that were heat treated to 400 °C for 30 hours in air, and gasketed with polytetrafluoroethylene (PTFE). The flow battery cells were equipped with two reservoirs containing 100 mL of VRB electrolyte from Riverside Specialty Chemicals (NYC, NY), which consisted of 1.60 M of vanadium species with a +3.55 average oxidation state and 3.8 M total sulfur content. Cells were charged via a two-step process, where: [1] the positive and negative electrolytes (posolyte and negolyte) were prepared by charging the initial solution containing $VOSO_4$ (V^{4+}) in sulfuric acid forming V^{3+} and VO_2^+ (V^{5+}). The posolyte solution was then replaced with the initial solution and [2] charging was repeated to generate V^{2+} and V^{5+}. Electrolytes were fed to the cell with KNF diaphragm liquid pumps at a constant 120 mL min^{-1} flow rate. Electrolyte solution temperature was not controlled and was approximately 20 °C. The electrolyte tanks were equipped with a nitrogen purge inlet and outlet. OCV was limited between 1.50 and 1.30 V during

cycling. Cells were cycled between 0.7 and 1.65 V at various current densities and cells were cycles 25 times or until electrolyte utilization was below 35%.

3.4 RESULTS AND DISCUSSION

PBI membranes (2OH-PBI, s-PBI, p-PBI, (**Figure 3.2**) were synthesized using the PPA Process, in which PPA acts as both the polycondensation agent and the polymerization solvent, starting from TAB and the selected dicarboxylic acid, TPA, STPA, or 2OH-TPA. The resulting p-PBI polymer IVs ranged from 1.5 to 3.0 dL g^{-1} and 2.0 to 3.0 dL g^{-1} for s-PBI polymers. 2OH-PBI was not soluble in concentrated sulfuric acid, as previously reported[36], and IV measurements were unable to be obtained. However, the 2OH-PBI membranes had sufficient mechanical properties to be further handled, indicating sufficient molecular weight was achieved for these PBIs.

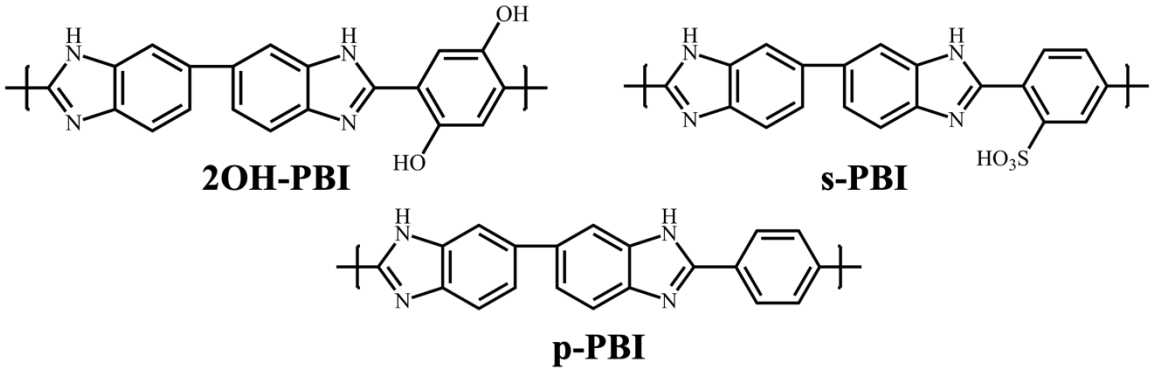

Figure 3.2. Chemical structure of the PBIs under study, p-PBI, 2OH-PBI, and s-PBI.

Typically, an IV greater than 1.0 dL g^{-1} is considered as high molecular weight, thus, PPA readily served as an efficient polycondensation agent and facilitated the synthesis of PBIs with considerable molecular weight. The sol-to-gel

transition induced in the PPA Process is depicted in **Figure 3.3**.[33] The PPA/PBI solution was cast directly after polymerization while the solution was still hot. The as-cast solution (gate thickness 15 mils) was cooled and exposed to moisture from the air which induced the sol-to-gel transition, resulting in stable PBI gel membranes highly swollen in phosphoric acid.

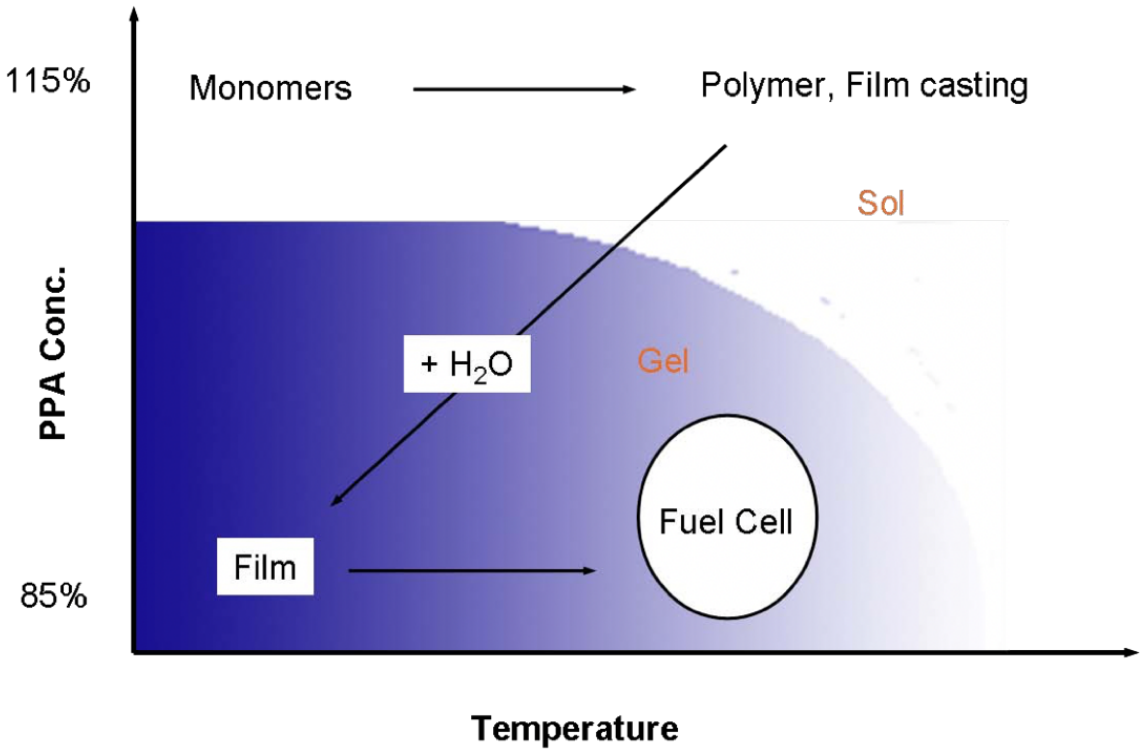

Figure 3.3. Sol-to-gel transition that occurs upon casting from PPA in the PPA Process.[33]

The PBI gels were first neutralized by removing the phosphoric acid in a series of water baths, followed by post-polymerization modification by either controlled drying or stretching and controlled drying. The drying process was able to densify the PBI gels by controlling the collapsing structure. Benchtop drying was attempted without utilizing porous plates or clamps, and the polymer

membranes shriveled up (**Figure 3.4)** in an uncontrolled manner, resulting in a non-uniform shape with no practical use. By placing the membrane between porous sheets and clamping the edges the membrane was restrained in the x- and y-direction and only collapsed in the z-direction, producing a beautiful sheet of dense PBI film. The densification process can be visualized in **Figure 3.5**. Stretching and drying was investigated to determine if induced order of polymer backbone chains could alter the transport properties of the resulting re-imbibed membranes.

Figure 3.4. Dried PBI film produced in the drying process between porous sheets (right) and benchtop drying of an unconstrainted water-imbibed PBI gel membrane (left).

Table 3.1 contains the dimensional characteristics and membrane thickness changes of the p-PBI, s-PBI and 2OH-PBI gel membranes under different processing conditions and then doped in 2.6 M sulfuric acid. The p-PBI samples were selected for additional stretching experiments and were stretched to 150% (p-PBI-150) and 200% (p-PBI-200). It is clear that in all cases the post-processing technique of drying (both stretched and non-stretched) results in a polymer film

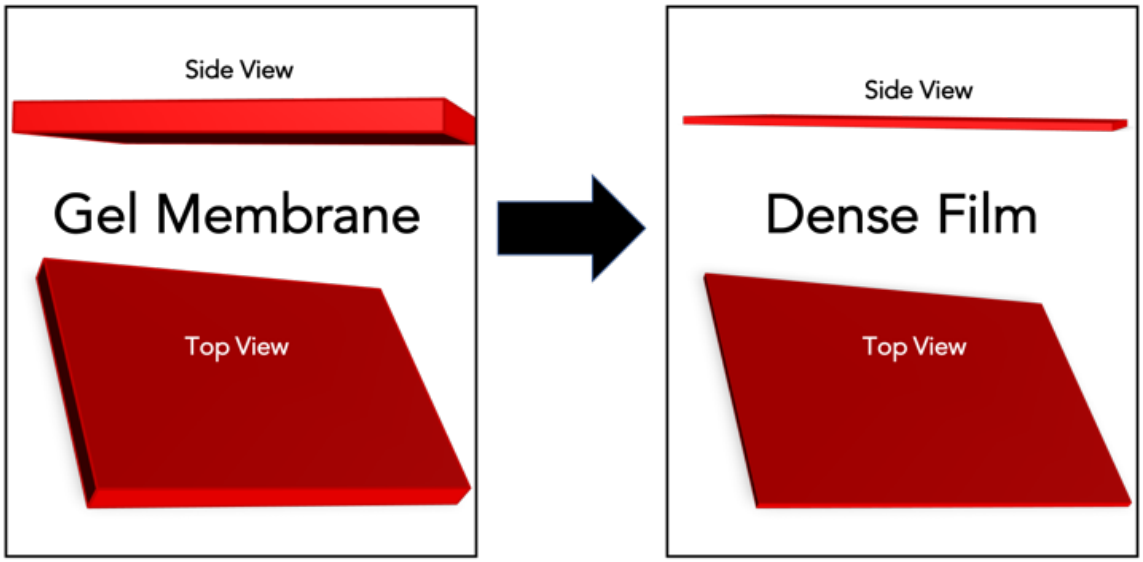

Figure 3.5. Depiction of densification process starting from acid-imbibed PBI gel membranes (left) and transforming into dense PBI films (right).

Table 3.1. Stretching ratios, dry membrane thickness, and thickness of acid-imbibed samples.

PBI Sample	Stretched	Dry Thickness (μm)	Thickness in 2.6 M H_2SO_4 (μm)
p-PBI gel	-	-	295
p-PBI-0	0.0x	30	53.3
p-PBI-150	1.50x	37	51.5
p-PBI-200	2.0x	29	44
s-PBI gel	-	-	220.2
s-PBI-0	0.0x	35	50
2OH-PBI gel	-	-	410
2OH-PBI-0	0.0x	33	70

that does not re-expand into its original thickness when re-doped in 2.6 M sulfuric acid. The sulfuric acid doped membrane thicknesses were much lower than the control samples, which were membrane samples washed with water and then directly placed in sulfuric acid for doping (no intermediate drying step). For the stretched p-PBI samples, further decreases in thickness were observed after drying and doping in 2.6 M sulfuric acid. Another potential advantage of this process is the formation of dry PBI films from a variety of chemistries without the use of organic solvents, even if the PBI chemistries display little or no solubility in organic solvents.

PBI is not conductive on its own and relies on the imbibed electrolyte to achieve substantial ionic conductivity. Thus, each PBI was doped in 2.6 M sulfuric acid and titrated to determine the acid doping level, polymer content, sulfuric acid content, water content, and acid molarity within the membrane, as displayed in **Table 3.2**. Each of the doped membranes that underwent post-treatment drying contained a greater polymer content than the control (gel) PBI membrane. In the p-PBI samples, the polymer content increased further as the samples were stretched. The molarity measured in each membrane sample was higher than the acid bath it was doped in (2.6 M sulfuric acid), indicating that PBI has more of an affinity towards sulfuric acid than water. Interestingly, each sample that underwent post treatment had a higher molarity of sulfuric acid within the membrane than the original gel PBIs, despite the acid doping level being lower for the samples that underwent post-treatment. The phenomenon likely indicates that the morphology of the membranes had been altered due to post-polymerization processing.

Table 3.2. Acid doping level, composition, and molarity of each membrane obtained through titration.

PBI Sample	Acid Doping Level (mol SA/PRU)	Polymer Content (wt%)	H_2SO_4 Content (wt%)	H_2O Content (wt%)	Molarity (M)
p-PBI gel	6.67 ± 0.2	10.7 ± 0.6	22.2 ± 0.5	67.1 ± 1.0	2.85
p-PBI-0	3.07 ± 0.9	29.4 ± 8.5	27.2 ± 1.4	43.5 ± 7.4	4.68
p-PBI-150	2.21 ± 0.1	36.4 ± 2.6	25.1 ± 0.2	38.6 ± 2.7	4.87
p-PBI-200	2.79 ± 0.5	35.9 ± 3.7	31.0 ± 1.8	33.0 ± 1.9	6.32
s-PBI gel	10.50 ± 2.1	8.2 ± 1.6	20.9 ± 0.3	70.8 ± 1.5	2.58
s-PBI-0	4.26 ± 0.7	23.3 ± 4.0	24.1 ± 0.9	52.6 ± 4.0	3.71
2OH-PBI gel	14.7 ± 2.5	5.2 ± 1.0	21.3 ± 0.1	73.4 ± 1.1	2.55
2OH-PBI-0	1.89 ± 0.1	43.6 ± 2.6	23.4 ± 2.0	33.0 ± 4.6	5.17

Ex-situ properties including ionic conductivity (doped in 2.6 M sulfuric acid and 1.5 M $VOSO_4$ + 2.6 M sulfuric acid) and $VOSO_4$ permeability are reported in **Table 3.3** for each sample. The vanadium permeability was reduced with post-modification by at least an order of magnitude for each type of PBI. However, the ionic conductivity was also reduced in the post-modification technique. The vanadium permeability and ionic conductivity of PBI gels before and after post-treatment are further described in **Figures 3.6 & 3.7**.

Table 3.3. Ex-situ properties including polymer solids, acid content, ionic conductivity, and $VOSO_4$ permeability.

PBI Sample	σ (in 2.6 M H_2SO_4) (mS cm^{-1})	σ (in 2.6 M H_2SO_4 + 1.5 M $VOSO_4$) (mS cm^{-1})	$VOSO_4$ Permeability (cm^2 s^{-1})
p-PBI gel	398.0	343	69.3 x 10^{-8}
p-PBI-0	95.2	79.7	2.65 x 10^{-8}
p-PBI-150	129.6	109.4	4.04 x 10^{-8}
p-PBI-200	127.0	89.4	6.71 x 10^{-8}
s-PBI gel	592.7	242.1	489 x 10^{-9}
s-PBI-0	78.2	55.8	7.76 x 10^{-9}
2OH-PBI gel	640.4	408.3	72.3 x 10^{-8}
2OH-PBI-0	139.0	113.7	3.92 x 10^{-8}

Figure 3.6 contains data comparing the $VOSO_4$ permeability of the PBI gels and dense PBIs after post-modification. In **Figure 3.6A**, the permeability of the various p-PBI membranes subjected to post-treatment were between 2.65 x 10^{-8} and 6.71 x 10^{-8} cm^2 s^{-1}, approximately an order of magnitude lower than the p-PBI gel membrane, which was 69.3 x 10^{-8} cm^2 s^{-1}. Of the p-PBI samples that underwent post-treatment, the p-PBI-0 sample (non-stretched) contained the lowest $VOSO_4$ permeability. As the p-PBI samples were stretched further, there was a slight increase in permeability observed with stretching. We hypothesize that polymer backbone order induced by stretching the membranes provided a less tortuous path for vanadium ions to travel through, which accounts for the slight increase in vanadium permeability that was recorded with stretching.

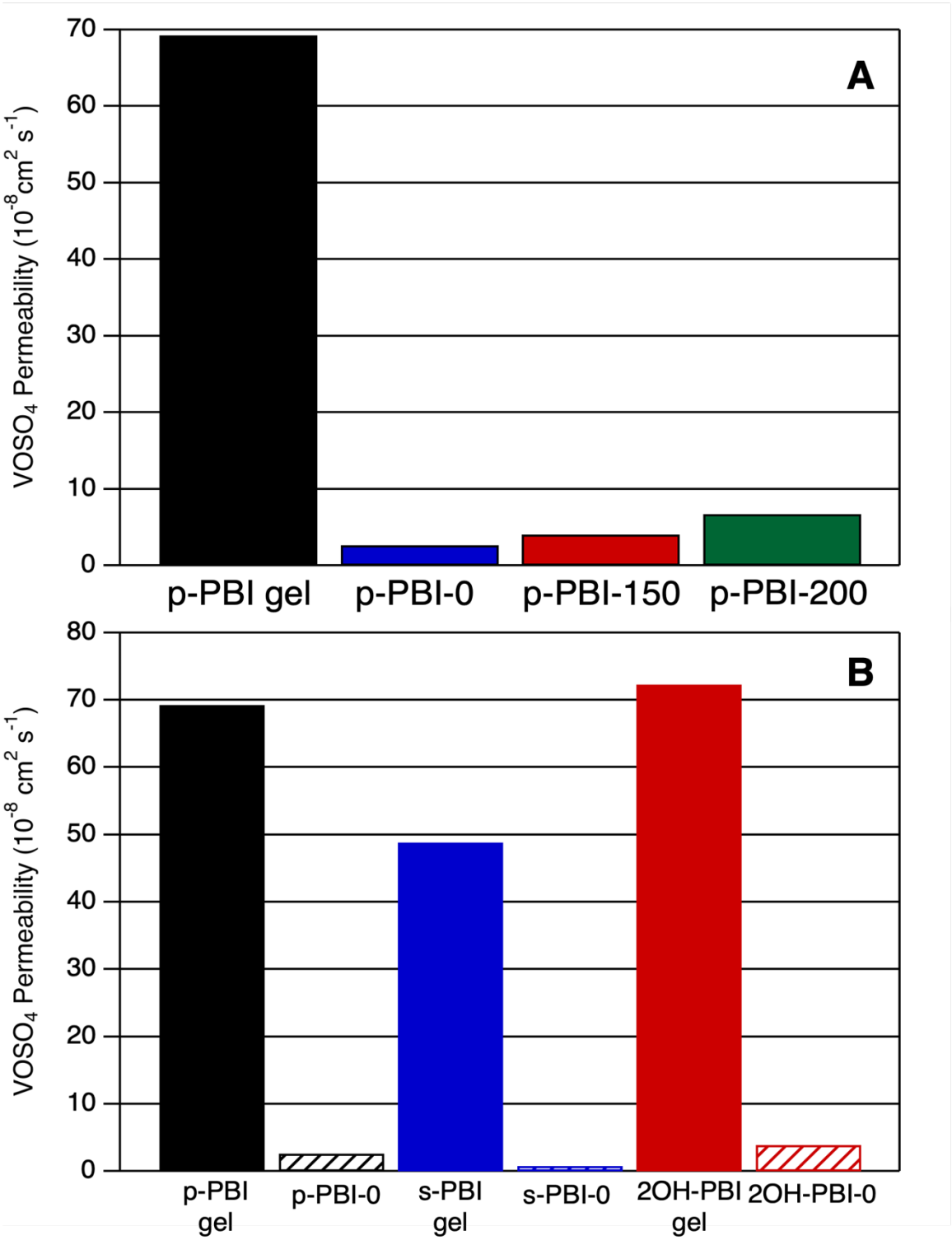

Figure 3.6. Vanadium ($VOSO_4$) permeability of A) p-PBI samples as the gel membranes and after post-treatment with and without stretching and B) each type of PBI chemistry before and after post-treatment of the non-stretched samples.

Figure 3.6B contains the $VOSO_4$ permeability measured for each PBI chemistry before and after post-polymerization modification. In each case, the permeability was dramatically reduced with treatment of the PBI gels, demonstrating that the novel technique is applicable to PBI membranes with various backbone chemistries. Overall, the s-PBI-0 sample displayed the lowest $VOSO_4$ permeability of 7.76 x 10^{-9} cm^2 s^{-1}, which was about 1.5 orders of magnitude lower than the s-PBI gel membrane (489 x 10^{-9} cm^2 s^{-1}). Post-polymerization modification via the controlled drying process is a useful tool to reduce vanadium crossover by densifying the open gel structure of PPA Process PBI gel membranes.

While post-treatment was successful in limiting the $VOSO_4$ crossover, the ionic conductivity was also reduced. **Figure 3.7** contains data of the ionic conductivity for each sample doped in 2.6 M sulfuric acid. The ionic conductivity for each p-PBI sample is shown in **Figure 3.7A**. After post-treatment, each sample displayed a lower ionic conductivity than the original p-PBI gel membrane. Of the p-PBI samples that underwent post-treatment, p-PBI-150 measured the highest ionic conductivity of 246 mS cm^{-1}. The ionic conductivity of the stretched p-PBI samples was much greater than the non-stretched p-PBI-0 sample. Once again, this indicates that stretching can align the polymer backbone chains and allow for a less tortuous path, in this case for proton transport. However, a linear trend between the stretching ratio and ionic conductivity was not observed. **Figure 3.7B** shows the ionic conductivity for the various PBI chemistries before and after post-treatment without stretching. Again, the ionic conductivity was much lower after post-treatment for each type of PBI. The 2OH-PBI gel had the highest starting ionic

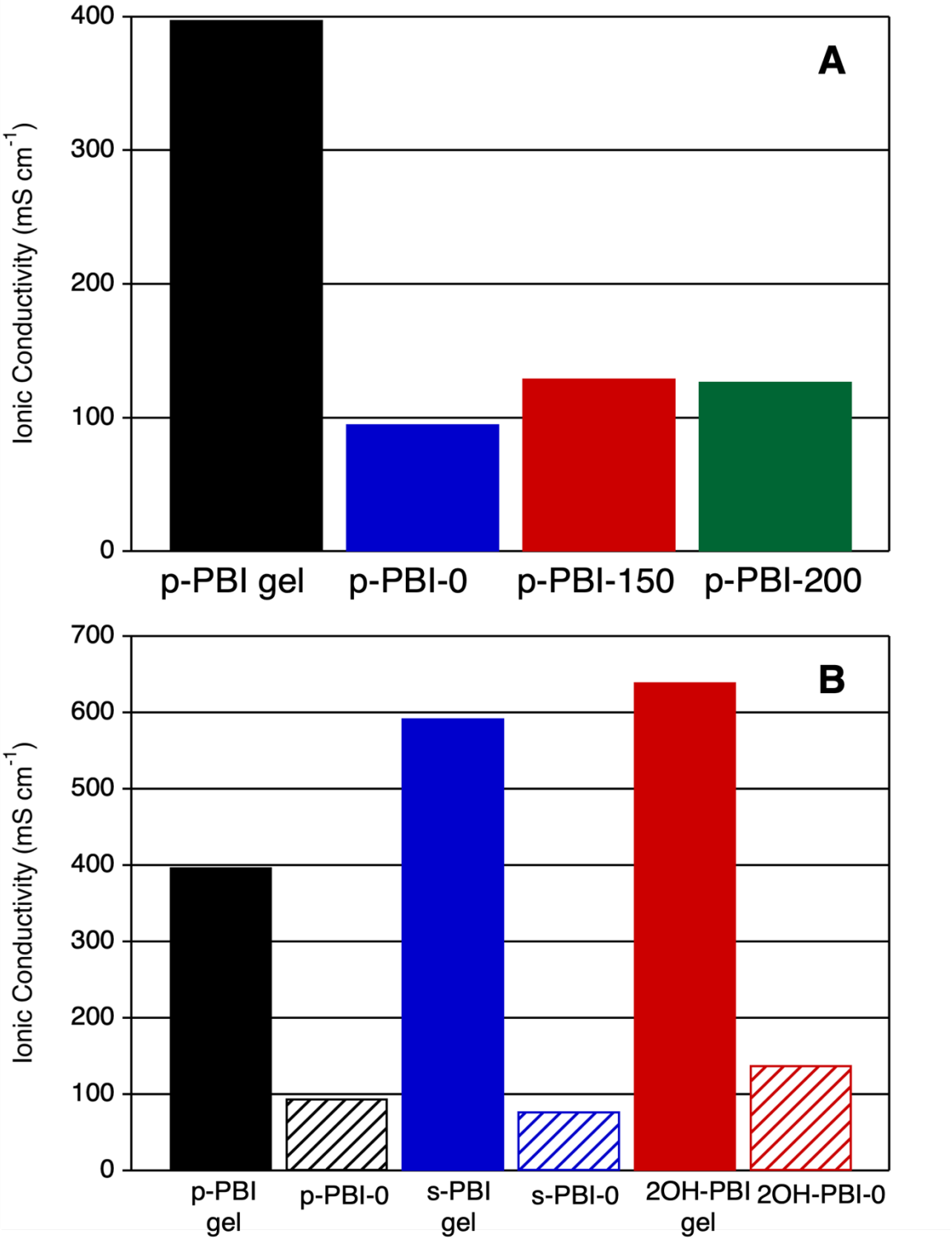

Figure 3.7. Ionic conductivity of samples in 2.6 M sulfuric acid: A) p-PBI samples as the gel membranes and after post-treatment with and without stretching and B) each type of PBI chemistry before and after post-treatment of the non-stretched samples.

conductivity of 640.4 mS cm^{-1}. After post-treatment the 2OH-PBI-0 sample exhibited the highest ionic conductivity, 139 mS cm^{-1}, of all samples that underwent post-treatment without stretching. While the ionic conductivity of each sample after post-modification was lower than the original gel PBIs, these values are still much greater than those of dense PBIs made in the conventionally imbibed method, which are typically reported below 30 mS cm^{-1}.[21-24] The dense PBI membranes prepared by post-treatment of PBI gel membranes show unprecedented ionic conductivity and indicates that there is an intrinsic morphology difference obtained with different membrane casting techniques that affects both ionic conductivity and vanadium transport.

The VRB single cell efficiency results for cells constructed with p-PBI-0, p-PBI-150, p-PBI-200 and s-PBI-0 are shown in **Figures 3.8 & 3.9**. The coulombic efficiency describes the capacity losses of a cell by calculating the ratio of discharge capacity to charge capacity. A greater coulombic efficiency obtained indicates that capacity losses from the cross-mixing of vanadium species is low. When the permeability is high, cross-mixing occurs as vanadium migrates through the membrane. The voltage efficiency is the ratio of a cell's mean discharge voltage and mean charge voltage. The discharge and charge voltages are derived from the thermodynamic reduction potential of the redox couples and the overpotential of the cell.[2] The overall energy efficiency determines how much energy is lost during charge/discharge cycling, and is a result of the combination of coulombic efficiency and voltage efficiency.

Figure 3.8 shows the VRB cell cycling efficiencies obtained for the p-PBI-0 and s-PBI-0 membranes, which underwent post-treatment without stretching. The coulombic efficiency is shown in **Figure 3.8A** and generally increased with greater current density in both cells. A coulombic efficiency of up to 99% was achieved with the p-PBI-0 sample when the current density was 483 mA cm^{-2}. At lower current densities, such as 72 mA cm^{-2}, the coulombic efficiency was greater for the s-PBI-0 cell, 91%, than the p-PBI-0 sample, 85%. s-PBI-0 had a $VOSO_4$ permeability that was much lower than the p-PBI-0, accounting for the greater coulombic efficiency of s-PBI-0 at lower current densities. However, the ionic conductivity of p-PBI-0 was greater than s-PBI-0, which account for the cells enhanced coulombic efficiency at greater current densities. At higher current densities the contribution of vanadium crossover to the coulombic efficiency is reduced, as the increased reaction speed can out-pace losses from crossover.[25]

The voltage efficiency of s-PBI-0 and p-PBI-0, **Figure 3.8B**, were relatively similar. At greater current densities, such as 483 mA cm^{-2}, the voltage efficiency for the p-PBI-0 cell was greater than the voltage efficiency measured for the s-PBI-0 cell. This can be attributed to the slightly higher conductivity of p-PBI-0. The energy efficiency at various current densities can be seen in **Figure 3.8C**. Overall, s-PBI-0 outperformed p-PBI-0 at lower current densities, due to the lower vanadium permeability of the s-PBI-0 membrane. However, at greater current densities, the performance is inverted and the p-PBI-0 cell outperformed the s-PBI-0 cell, attributed to the higher ionic conductivity of the p-PBI-0 membrane. This demonstrates that post-modification of PBI gels with various backbone

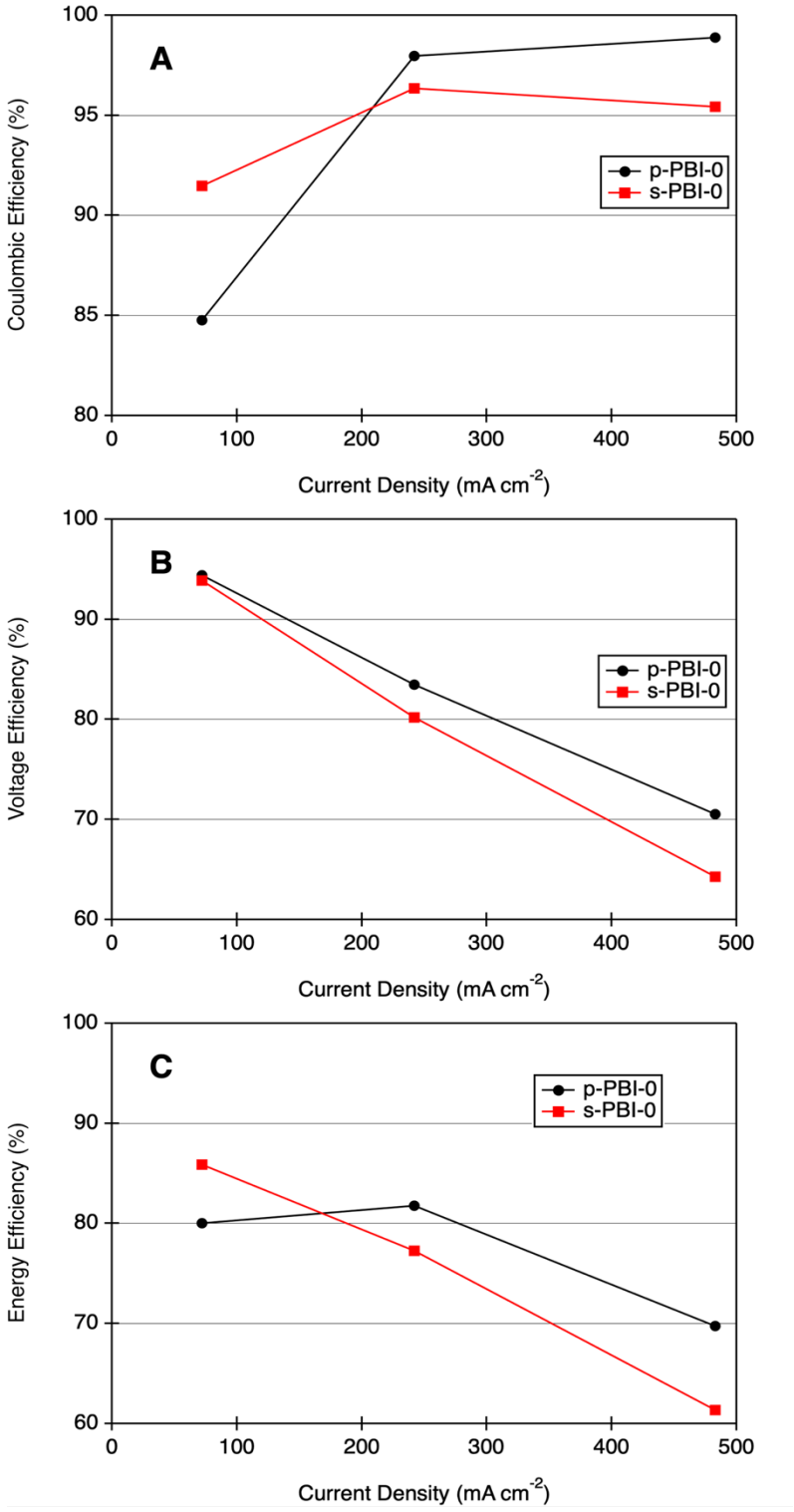

Figure 3.8. VRB cell cycling efficiencies for the s-PBI and p-PBI samples that underwent post-treatment: A) coulombic efficiency B) voltage efficiency and C) energy efficiency.

chemistries allows for tunable performance depending on the user-preferred operation conditions.

Figure 3.9 shows the VRB cell cycling efficiencies obtained for p-PBI samples that underwent post-modification. The coulombic efficiency of each cell (**Figure 3.9A)** shows that the p-PBI-150 cell had the highest coulombic efficiency at each current density that was tested. When the current density was set to 72 mA cm^{-2}, which is relatively low, the coulombic efficiency increased as the samples were stretched further. However, when the current density was increased to 583 mA cm^{-2}, the values of coulombic efficiency for each cell were very similar. The voltage efficiency (**Figure 3.9B**) of p-PBI-200 was the greatest at each current density that was tested. In **Figure 3.9C**, the range of energy efficiencies achieved for the various cells at low current density was relatively wide. As the current density was increased, the range of energy efficiencies reached by the various cells was reduced. While there does not appear to be any clear-cut trend of efficiency with measured $VOSO_4$ permeability or ionic conductivity in these samples, it is clear that stretching can be used to achieve enhanced efficiencies, particularly at lower current densities.

The VRB cell cycling results for membranes that were subjected to post-treatment demonstrate that membranes produced in this method were able to take advantage of the relatively high ionic conductivity produced in this novel technique, achieving adequate performance at current densities up to 500 mA cm^{-2}. Previous dense PBI membranes fabricated in the conventionally imbibed process were unable to perform at current densities greater than 200 mA cm^{-2} due to their intrinsically low ionic conductivity.[31] In contrast, the relatively high conductivity

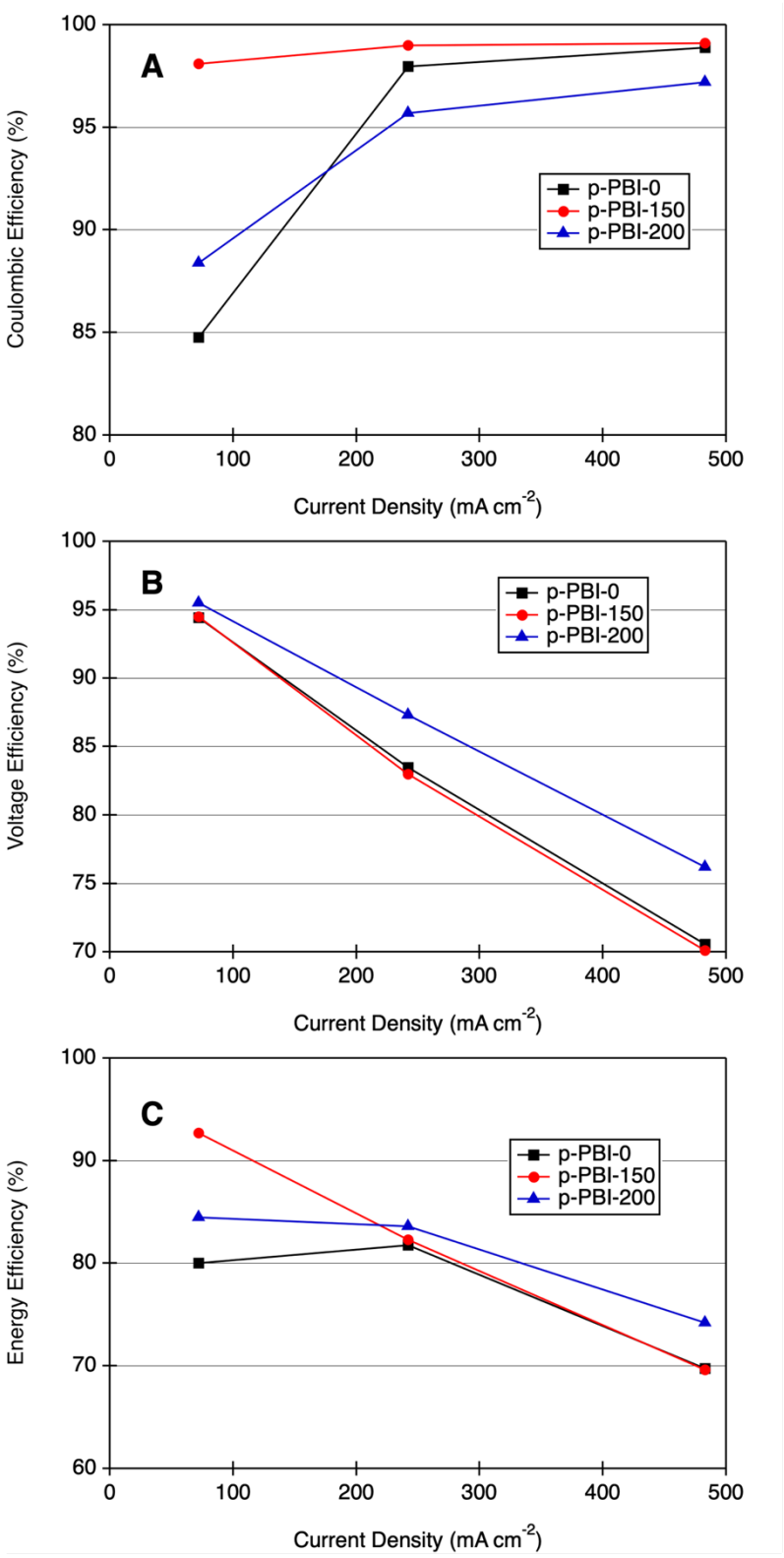

Figure 3.9. VRB cell cycling efficiencies for the p-PBI samples that underwent post-treatment: A) coulombic efficiency B) voltage efficiency and C) energy efficiency.

of the dense PBIs prepared from PBI gel membranes, and subsequent operation at greater current densities, indicates an inherent difference in membrane structure created by the different processing techniques. The post-modification method of PBI gels obtained in the PPA Process were able to realize a "best of both worlds" scenario where the ionic conductivity was high and the vanadium permeability was low, rendering cells that could operate at high current densities with minimal vanadium crossover. The results also demonstrate that the selection of PBI chemistry can be used to tune the performance of the flow battery, based on user-selected operating preferences.

The long-term cell cycling efficiency for the p-PBI-150 membrane was recorded over a period of 9 months (**Figure 3.10**). The overall energy efficiency was stable for up to 7 months. However, from 7.5 months to 9 months, the coulombic efficiency and energy efficiency was noticeably lower, particularly at lower current densities. This indicates that crossover is causing lower energy efficiencies after about 7 months of testing.

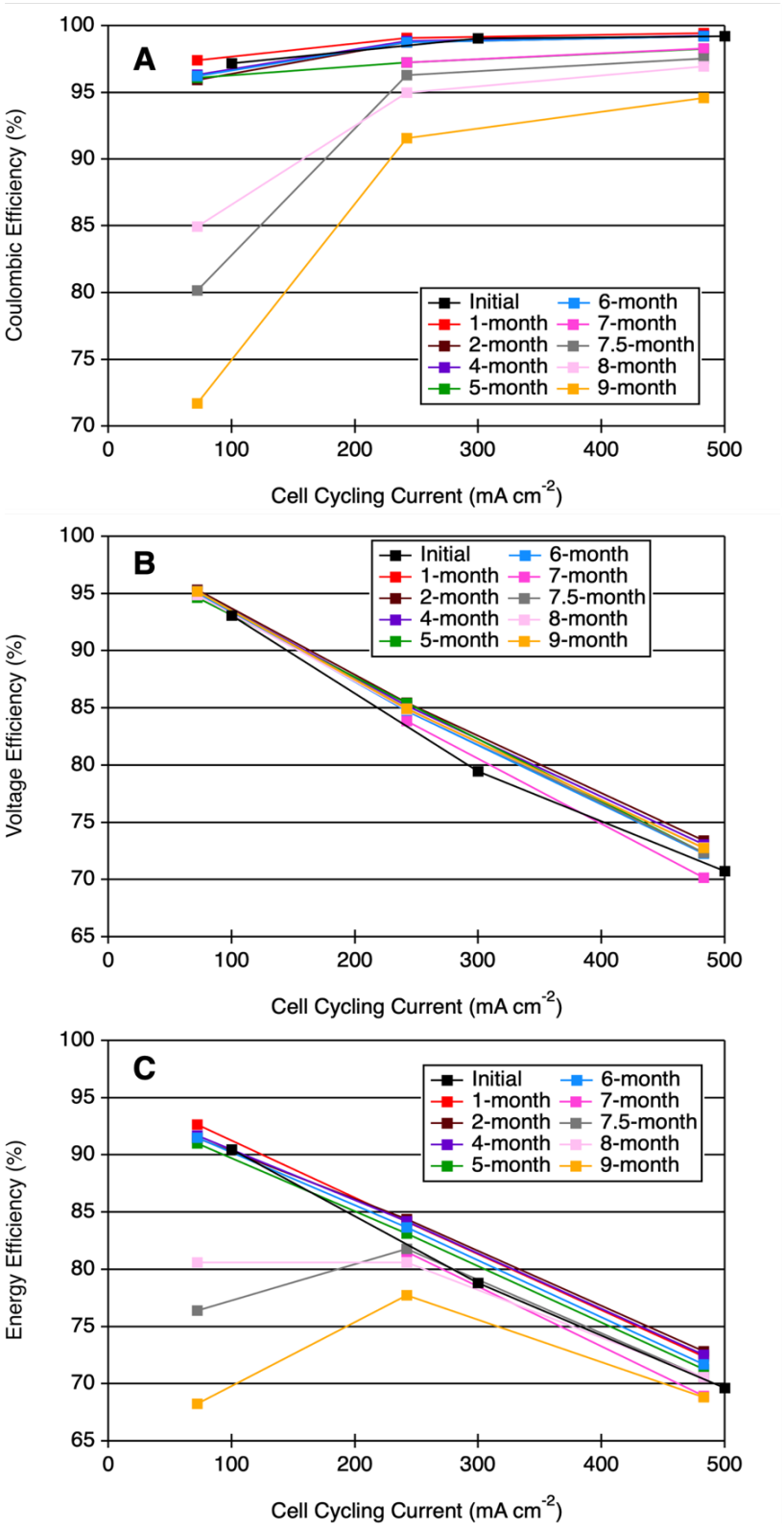

Figure 3.10. VRB cell cycling efficiencies: A) coulombic efficiency B) voltage efficiency and C) energy efficiency for the p-PBI-150 sample, tested up to 9 months after initial cell-cycling.

3.5 CONCLUSIONS

A post-polymerization modification technique has been outlined, starting with PBI gel membranes that were made in the PPA Process. The PBI gel membranes were successfully dried in a controlled manner to obtain dense PBI films with a uniform thickness. The dense PBI films in this method behaved differently than dense PBIs that have been previously made in the conventionally imbibed PBI process. The newly described procedure allows for PBI membranes with unprecedented ionic conductivity and reduced vanadium permeability. In-cell testing demonstrated that these properties work together to achieve adequately high efficiencies and operation at current densities much greater than reported for conventionally imbibed PBIs. The cell performance showed excellent stability for up to 7 months. The post-treatment described is scalable and requires no additional chemicals or reagents, establishing a new pathway for high performing VRB membranes.

3.6 ACKNOWLEDGEMENTS

The work presented in this chapter was funded in part by the Advanced Research Projects Agency – Energy (ARPA-E), U.S. Department of Energy, under Award Number DE-AR-0001478. We acknowledge United Technologies Research Center (UTRC), now Raytheon, for their support in collecting the cell-cycling data.

3.7 REFERENCES

[1] Kear, G.; Shah, A. A.; Walsh, F. C. Development of the all-vanadium redox flow battery for energy storage: a review of technological, financial and policy aspects. *International Journal of Energy Research* **2012,** *36* (11), 1105-1120.

[2] Li, X.; Zhang, H.; Mai, Z.; Zhang, H.; Vankelecom, I. Ion exchange membranes for vanadium redox flow battery (VRB) applications. *Energy & Environmental Science* **2011,** *4* (4), 1147-1160.

[3] Jones, D. J.; Rozière, J. Recent advances in the functionalisation of polybenzimidazole and polyetherketone for fuel cell applications. *Journal of Membrane Science* **2001,** *185* (1), 41-58.

[4] Skyllas-Kazacos, M.; Grossmith, F. Efficient Vanadium Redox Flow Cell. *Journal of The Electrochemical Society* **1987,** *134* (12), 2950-2953.

[5] Skyllas-Kazacos, M.; Kazacos, G.; Poon, G.; Verseema, H. Recent advances with UNSW vanadium-based redox flow batteries. *International Journal of Energy Research* **2010,** *34* (2), 182-189.

[6] Ponce de León, C.; Frías-Ferrer, A.; González-García, J.; Szánto, D. A.; Walsh, F. C. Redox flow cells for energy conversion. *Journal of Power Sources* **2006,** *160* (1), 716-732.

[7] Parasuraman, A.; Lim, T. M.; Menictas, C.; Skyllas-Kazacos, M. Review of material research and development for vanadium redox flow battery applications. *Electrochimica Acta* **2013,** *101*, 27-40.

[8] Yuan, Z.; Duan, Y.; Zhang, H.; Li, X.; Zhang, H.; Vankelecom, I. Advanced porous membranes with ultra-high selectivity and stability for vanadium flow batteries. *Energy & Environmental Science* **2016,** *9* (2), 441-447.

[9] Schwenzer, B.; Zhang, J.; Kim, S.; Li, L.; Liu, J.; Yang, Z. Membrane Development for Vanadium Redox Flow Batteries. *ChemSusChem* **2011,** *4* (10), 1388-1406.

[10] Minke, C.; Turek, T. Economics of vanadium redox flow battery membranes. *Journal of Power Sources* **2015,** *286*, 247-257.

[11] Zhang, C.; Zhang, L.; Ding, Y.; Peng, S.; Guo, X.; Zhao, Y.; He, G.; Yu, G. Progress and prospects of next-generation redox flow batteries. *Energy Storage Materials* **2018,** *15*, 324-350.

[12] Fujimoto, C.; Kim, S.; Stains, R.; Wei, X.; Li, L.; Yang, Z. G. Vanadium redox flow battery efficiency and durability studies of sulfonated Diels Alder poly(phenylene)s. *Electrochemistry Communications* **2012,** *20*, 48-51.

[13] Chen, D.; Hickner, M. A.; Agar, E.; Kumbur, E. C. Optimized Anion Exchange Membranes for Vanadium Redox Flow Batteries. *ACS Applied Materials & Interfaces* **2013,** *5* (15), 7559-7566.

[14] Luo, Q.; Zhang, H.; Chen, J.; You, D.; Sun, C.; Zhang, Y. Preparation and characterization of Nafion/SPEEK layered composite membrane and its application in vanadium redox flow battery. *Journal of Membrane Science* **2008,** *325* (2), 553-558.

[15] Sun, C.-N.; Tang, Z.; Belcher, C.; Zawodzinski, T. A.; Fujimoto, C. Evaluation of Diels–Alder poly(phenylene) anion exchange membranes in all-vanadium redox flow batteries. *Electrochemistry Communications* **2014,** *43*, 63-66.

[16] Yun, S.; Parrondo, J.; Ramani, V. Composite anion exchange membranes based on quaternized cardo-poly(etherketone) and quaternized inorganic fillers for vanadium redox flow battery applications. *International Journal of Hydrogen Energy* **2016,** *41* (25), 10766-10775.

[17] Zhang, S.; Yin, C.; Xing, D.; Yang, D.; Jian, X. Preparation of chloromethylated/quaternized poly(phthalazinone ether ketone) anion exchange membrane materials for vanadium redox flow battery applications. *Journal of Membrane Science* **2010,** *363* (1), 243-249.

[18] Xu, W.; Zhao, Y.; Yuan, Z.; Li, X.; Zhang, H.; Vankelecom, I. F. J. Highly Stable Anion Exchange Membranes with Internal Cross-Linking Networks. *Advanced Functional Materials* **2015,** *25* (17), 2583-2589.

[19] Zeng, L.; Zhao, T. S.; Wei, L.; Jiang, H. R.; Wu, M. C. Anion exchange membranes for aqueous acid-based redox flow batteries: Current status and challenges. *Applied Energy* **2019,** *233-234*, 622-643.

[20] Xie, W.; Darling, R. M.; Perry, M. L. Processing and Pretreatment Effects on Vanadium Transport in Nafion Membranes. *Journal of The Electrochemical Society* **2015,** *163* (1), A5084-A5089.

[21] Zhou, X. L.; Zhao, T. S.; An, L.; Wei, L.; Zhang, C. The use of polybenzimidazole membranes in vanadium redox flow batteries leading to increased coulombic efficiency and cycling performance. *Electrochimica Acta* **2015,** *153*, 492-498.

[22] Luo, T.; David, O.; Gendel, Y.; Wessling, M. Porous poly(benzimidazole) membrane for all vanadium redox flow battery. *Journal of Power Sources* **2016,** *312*, 45-54.

[23] Peng, S.; Yan, X.; Zhang, D.; Wu, X.; Luo, Y.; He, G. A H_3PO_4 preswelling strategy to enhance the proton conductivity of a H_2SO_4-doped polybenzimidazole membrane for vanadium flow batteries. *RSC Advances* **2016,** *6* (28), 23479-23488.

[24] Peng, S.; Wu, X.; Yan, X.; Gao, L.; Zhu, Y.; Zhang, D.; Li, J.; Wang, Q.; He, G. Polybenzimidazole membranes with nanophase-separated structure induced by non-ionic hydrophilic side chains for vanadium flow batteries. *Journal of Materials Chemistry A* **2018,** *6* (9), 3895-3905.

[25] Wang, L.; Pingitore, A. T.; Xie, W.; Yang, Z.; Perry, M. L.; Benicewicz, B. C. Sulfonated PBI Gel Membranes for Redox Flow Batteries. *Journal of The Electrochemical Society* **2019,** *166* (8), A1449-A1455.

[26] Wang, K. Y.; Chung, T.-S.; Qin, J.-J. Polybenzimidazole (PBI) nanofiltration hollow fiber membranes applied in forward osmosis process. *Journal of Membrane Science* **2007,** *300* (1), 6-12.

[27] Wang, K. Y.; Chung, T.-S. Polybenzimidazole nanofiltration hollow fiber for cephalexin separation. *AIChE Journal* **2006,** *52* (4), 1363-1377.

[28] Wang, K. Y.; Chung, T.-S. Fabrication of polybenzimidazole (PBI) nanofiltration hollow fiber membranes for removal of chromate. *Journal of Membrane Science* **2006,** *281* (1), 307-315.

[29] Rabbani, M. G.; El-Kaderi, H. M. Template-Free Synthesis of a Highly Porous Benzimidazole-Linked Polymer for CO2 Capture and H2 Storage. *Chemistry of Materials* **2011,** *23* (7), 1650-1653.

[30] Wainright, J. S.; Wang, J. T.; Weng, D.; Savinell, R. F.; Litt, M. Acid-Doped Polybenzimidazoles: A New Polymer Electrolyte. *Journal of The Electrochemical Society* **1995,** *142* (7), L121-L123.

[31] Mader, J.; Xiao, L.; Schmidt, T. J.; Benicewicz, B. C. Polybenzimidazole/Acid Complexes as High-Temperature Membranes. In *Fuel Cells II: Advances in Polymer Science,* Vol. 216; Scherer, G. G., Ed.; Springer, 2008; pp 63-124. DOI: 10.1007/12_2007_129

[32] Pingitore, A. T.; Huang, F.; Qian, G.; Benicewicz, B. C. Durable High Polymer Content m/p-Polybenzimidazole Membranes for Extended Lifetime Electrochemical Devices. *ACS Applied Energy Materials* **2019,** *2* (3), 1720-1726.

[33] Xiao, L.; Zhang, H.; Scanlon, E.; Ramanathan, L. S.; Choe, E.-W.; Rogers, D.; Apple, T.; Benicewicz, B. C. High-Temperature Polybenzimidazole Fuel Cell Membranes via a Sol−Gel Process. *Chemistry of Materials* **2005,** *17* (21), 5328-5333.

[34] Yu, S.; Zhang, H.; Xiao, L.; Choe, E.-W.; Benicewicz, B. C. Synthesis of Poly (2,2′-(1,4-phenylene) 5,5′-bibenzimidazole) (para-PBI) and Phosphoric Acid Doped Membrane for Fuel Cells. *Fuel Cells* **2009,** *9* (4), 318-324.

[35] Mader, J. A.; Benicewicz, B. C. Sulfonated Polybenzimidazoles for High Temperature PEM Fuel Cells. *Macromolecules* **2010,** *43* (16), 6706-6715.

[36] Yu, S.; Benicewicz, B. C. Synthesis and Properties of Functionalized Polybenzimidazoles for High-Temperature PEMFCs. *Macromolecules* **2009,** *42* (22), 8640-8648.

[37] Yu, S.; Xiao, L.; Benicewicz, B. C. Durability Studies of PBI-based High Temperature PEMFCs. *Fuel Cells* **2008,** *8* (3-4), 165-174.

CHAPTER 4

APPLICATION OF NOVEL POLYBENZIMIDAZOLE MEMBRANES IN HIGH TEMPERATURE POLYMER ELECTROLYTE MEMBRANE FUEL CELLS AND ELECTROCHEMICAL HYDROGEN SEPARATION

4.1 ABSTRACT

A novel processing technique was developed in which gel polybenzimidazole (PBI) membranes, produced by the Polyphosphoric Acid (PPA) Process are converted into dense polymer films and re-doped in phosphoric acid. This process, termed the PPA+ Process, provides a 5 times improvement in creep resistance due to a 2 fold increase in the solids content within the membrane. Remarkably, the dense p-PBIs re-doped in phosphoric acid also exhibit excellent ionic conductivities at high temperatures. Thus, the performance of such membranes in high-temperature polymer electrolyte membrane fuel cells (HT-PEMFCs) and electrochemical hydrogen separation (EHS) is enhanced under various operating conditions and at long lifetimes.

4.2 INTRODUCTION

Phosphoric acid doped polybenzimidazoles (PBIs) have been heavily investigated for application in high temperature polymer electrolyte membrane fuel cells (HT-PEMFCs)[1-6] and electrochemical hydrogen separation (EHS)[7-11]. PBIs are a class of wholly-aromatic polymers known for their high temperature stability, nonflammability, and excellent chemical resistance.[12]

While low-temperature polymer electrolyte membrane fuel cells (LT-PEMFCs) have been more commonly deployed than HT-PEMFCs, they typically utilize perfluorosulfonic acid (PFSA)-based membranes, which requires constant humidification and limits LT-PEMFC operating temperatures to <100 °C.[13] High temperature fuel cell operation has advantages including enhanced tolerance to fuel impurities,[13-17] faster electrode kinetics,[18-20] and simplified water

management.[21, 22] PBIs have been found to exhibit significant ionic conductivity at elevated temperatures, excellent chemical and thermal stability in the fuel cell environment, low gas permeability, and nearly zero water drag coefficient, making them suitable for use in HT-PEMFCs, which are typically operated from 120-200 °C.[1, 15, 23-30]

HT-PEMFCs in particular have shown growing promise for application in aviation and heavy duty vehicles. It has been predicted that aviation alone will account for 15% of all CO_2 emissions by 2050.[31] While battery electric vehicles (BEVs) offer a practical solution for light duty vehicles, they are not a realistic option in their current state for heavy duty vehicles and aviation applications.[32] BEVs are limited by their low driving range per charge, slow charging rate, and most significantly, the weight of the batteries required to provide the power needed for these heavy duty applications.[32-34] LT-PEMFCs application in aviation and heavy duty vehicles are mostly limited by their poor heat deflection.[35] For aviation applications, a fuel cell system must be able to operate with ambient temperatures up to 55 °C. Thus, HT-PEMFCs operating from 160 to 200 °C reject heat more effectively than LT-PEMFCs operating at 80 °C when the ambient temperature is 55 °C. Since HT-PEMFCs display an enhanced tolerance to fuel impurities, they can be operated with more readily available fuels such as methanol, dimethyl ether, impure hydrogen mixtures, etc., which can ease the extent of infrastructure that is required for large-scale deployment.[15, 36]

EHS is a technique that allows for high-purity hydrogen gas to be separated from multi-component gas mixtures with low energy consumption. In EHS, hydrogen is fed to the anode where it is oxidized, and protons at the cathode are

reduced back to hydrogen molecules by recombining with electrons instead of reacting with oxygen to produce water, as in a fuel cell.[8, 37] While a fuel cell is operated in galvanic mode, EHS is operated in electrolytic mode and requires power from an external system to drive the reactions. EHS can purify and pressurize hydrogen in one step. The applications of EHS include industrial hydrogen recycling, anode tail-gas recirculation for re-use in fuel cells or related devices, electroanalytical methods, and hydrogen compression.[8]

Most of the research on PBI membranes has been focused on the "conventionally imbibed" method of production and meta-PBI polymers.[38] In the conventionally imbibed method, PBI is polymerized, extracted, purified, and dissolved in an organic solvent such as N,N'-dimethylacetamide (DMAc). The solution is filtered to remove any undissolved PBIs and cast. The solvent is then removed from the cast solution, dried, and the PBI films are washed in boiling water to fully remove the DMAc. After drying, the dense PBI films are then doped in phosphoric acid. Membranes that were produced in the conventionally imbibed process typically achieved an acid doping level of 6-10 moles of phosphoric acid (PA) per polymer repeat unit (PRU), and ionic conductivities of 0.04 to 0.08 S cm^{-1} at 150 °C.[39] Attempts to improve the acid doping levels and ionic conductivity of PBIs membranes produced in this method have been less than fruitful, since the mechanical properties of the membranes diminished as the acid doping levels were increased. [40]

In 2005, Xiao et al. developed the Polyphosphoric Acid (PPA) Process to prepare phosphoric acid doped gel PBI membranes.[3] In the PPA Process, PBI is polymerized from tetraamines and dicarboxylic acids in PPA. Upon completion of

the polymerization, the solution of PBI in PPA is cast directly and exposed to moisture in the air, which hydrolyzes the PPA, a good solvent for PBI, to phosphoric acid, a poor solvent for many PBIs. Thus, a sol-to-gel phase transition occurs, as displayed in **Figure 4.1**, and results in a thermally stable gel PBI membrane highly doped in phosphoric acid. The PPA Process is not only simplified, more cost effective, and more environmentally friendly than the conventional imbibing process, it produces PBIs with superior electrochemical properties. For example, para-PBI can be synthesized with high acid doping levels (>20 moles PA / PRU) and high ionic conductivities (> 250 mS cm^{-2} at 160 °C). This process has been commercialized and MEAs of para-PBI membranes have demonstrated great performance at 0.2 A cm^{-2} in hydrogen and air at long lifetimes (>2 years).

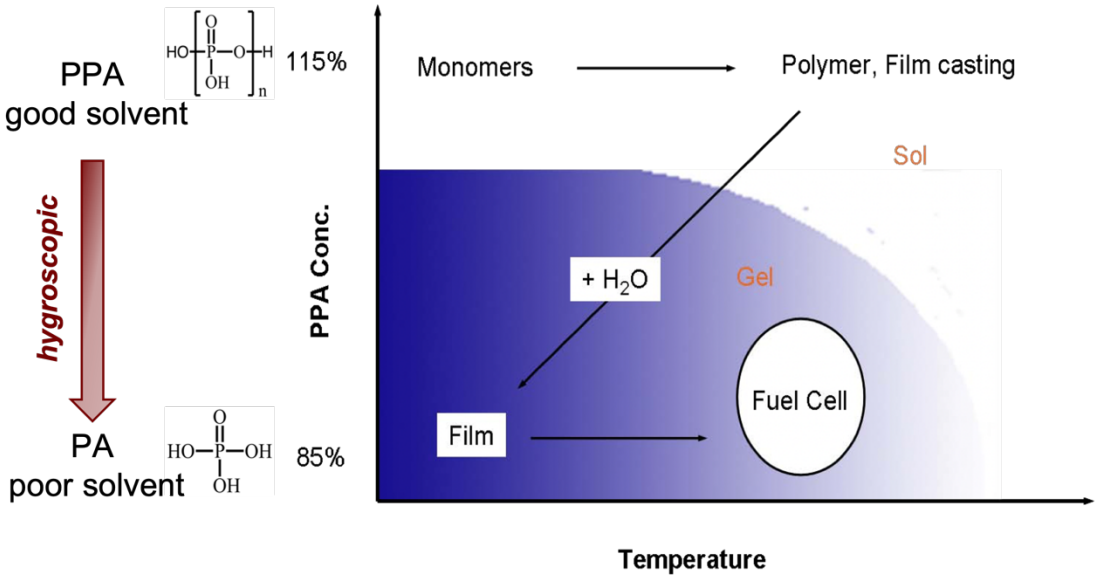

Figure 4.1. The solution-to-gel state diagram for PBIs produced in the PPA Process.

The PPA Process produces PBI membranes that have been classified as Flory type III physical gels.[41] Thus, it was previously determined that the main source of degradation in PBI gel membranes is membrane creep.[42] Creep is the time-dependent viscoelastic flow which occurs during PEMFC operation at long lifetimes as the compressive stress in the membrane relaxes. Membrane thinning results from creep and stress relaxation, leading to loss of close contact with the electrodes and gradual performance degradation. While the gel para-PBI membrane displays a high ionic conductivity at high temperatures, it contains a polymer solids content of ~5 wt% within the membrane and thus displays a high creep compliance and creep rate. The creep resistance of a polymer network should increase with polymer volume fraction, molecular weight, chain rigidity, and physical cross-linking density.[43] Unfortunately, the para-PBI cannot simply be polymerized with a higher solids content, due to solubility limits. Thus, various polymer backbone chemistries and crosslinking techniques were developed to provide PBI membranes with higher solids content and thus better creep resistance.[5, 44, 45] In 2019, a gel m/p-PBI copolymer was prepared that contained >15 wt% polymer solids and improved creep resistance that led to an excellent voltage decay rate of ~0.67 μV h^{-1} when tested at 160 °C for more than 2 years.[5] However, the membrane ionic conductivity was lower (~150 mS cm^{-1}) than gel p-PBI, and thus the voltage measured at each current density was lower. Thus, there is seemingly a trade-off between the polymer solids content in the membrane, which influences the creep resistance and long-term durability, and the ionic conductivity, which leads to better fuel cell performance.

In order to overcome this tradeoff, a new approach was developed, termed the PPA+ Process. In this process, gel p-PBI membranes undergo acid removal and controlled densification to form a dense PBI film. The dense p-PBI films are then re-doped in phosphoric acid. The properties of membranes produced in this method were explored and compared to other PBIs. There was a 2 times increase in the polymer solids content of the dense p-PBI film re-doped in phosphoric acid, compared to the gel p-PBI membrane, leading to improved creep resistance of the film. The acid doping levels and ionic conductivity at high temperatures were unexpectedly high, and provided superior performance in electrochemical devices compared to other high-solids PBIs and p-PBI. These unprecedented results indicate that we have overcome the tradeoff previously limiting the applications of PBI.

4.3. EXPERIMENTAL

4.3.1 Materials

Terephthalic acid (TPA, >99% purity) was purchased from Amoco, 3,3',4,4'-tetraaminobiphenyl (TAB, polymer grade, ~97.5%) was kindly donated by BASF Fuel Cell, Inc. Poly(phosphoric acid) (PPA, 115%) was purchased from Innophos, phosphoric acid (PA, 85%) was purchased from Oakwood Chemical, and meta-polybenzimidazole (m-PBI) was donated by PBI Performance Products. All chemicals and reagents were used as received without further purification.

4.3.2 Polymer Synthesis and Acid-Imbibed Gel Membrane Fabrication

The synthesis of para-PBI was completed as previously reported.[46] In a typical polymerization, equal molar equivalents of TPA and TAB were added to a reaction kettle followed by PPA. The mixture was stirred under a nitrogen

atmosphere using an overhead mechanical stirrer for 24 hours. A programmable temperature controller with ramp and soak features was used to control the temperature throughout the polymerization. The final polymerization temperature was between 195 and 220 °C, and the reaction was monitored by visual inspection of the viscosity. At the end of polymerization, the viscous PPA/PBI solution was cast directly onto glass substrates using a doctor blade with a controlled gate thickness of 15 mils. The glass substrates with cast polymer solution were then placed in a controlled humidity chamber set to 55% RH for 24 hours to induce hydrolysis. para-PBI gel membranes formed in the PPA Process were self-supporting and heavily imbibed in phosphoric acid.

4.3.3 Post-Polymerization Modification

para-PBI gel membranes underwent a novel post-polymerization modification technique in which they were converted into dense PBI films and re-doped in phosphoric acid. First, the phosphoric acid was removed by washing the membrane in a series of deionized water baths. Once neutralized, as determined by pH indication paper, the membrane samples were placed between porous sheets. In this study, 3.2 mm thick porous polyethylene sheets were used with an average porosity of 45-90 μm. The perimeter of the sandwiched membrane samples were clamped and left on the benchtop for 12-24 hours to allow the water to evaporate. Dense para-PBI films were removed from the porous sheets, and about 2 cm of the edges were removed. The resulting dense p-PBI films were placed in various concentrations of phosphoric acid, at different temperatures and for various time periods before characterization.

4.3.4 Membrane Composition

The relative amount of acid, water, and polymer in the membranes was determined through titration. A small membrane sample was weighed, placed in a beaker with ~50 mL of deionized water, and stirred at room temperature overnight. The following day, the beaker was titrated using a Metrohm 888 DMS Titrando autotitrator, with a standard 0.1 N sodium hydroxide solution. The polymer sample was collected after titration, washed with deionized water, and dried in a vacuum oven for 48 hours, before weighing. The polymer weight percent (*polymer wt%*) and phosphoric acid weight percent (*acid wt%*) were calculated respectively:

$$Polymer\ wt\ \% = \frac{W_{dry}}{W_{sample}} \cdot 100$$

$$Acid\ \ wt\% = \frac{M_{acid} \cdot V_{NaOH} \cdot c_{NaOH}}{W_{sample}} \cdot 100$$

Where W_{sample} was the weight of the sample before titration, W_{dry} was the weight of the final dried sample after titration, M_{acid} was the molecular weight of phosphoric acid, V_{NaOH} and C_{NaOH} was the volume and concentration of sodium hydroxide required to neutralize phosphoric acid to the first equivalence point, respectively.

The phosphoric acid doping level, or the number of moles of phosphoric acid per mole of PBI repeat unit, *X*, was calculated according to the following equation:

$$X = \frac{V_{NaOH} \cdot c_{NaOH}}{\left({W_{dry}}/{M_{polymer}}\right)}$$

Where V_{NaOH} and C_{NaOH} were the volume and concentration of sodium hydroxide needed to neutralize the phosphoric acid, W_{dry} was the weight of the final dried sample after titration, and $M_{polymer}$ was the molecular weight of the polymer repeat unit.

4.3.5 Ionic Conductivity

Through-plane ionic conductivity was measured with a four-probe electrochemical impedance spectroscopy (EIS) method. A Zahner IM6e electrochemical workstation was used over a frequency range of 1 Hz to 50 kHz and an amplitude of 5 mV. The samples were cut to roughly 1.0 cm x 4.0 cm and placed in the 4-electrode sample holder. Experimental data was fit using a two-component model with an ohmic resistance in parallel with a capacitor. The membrane resistance was obtained from the model simulation and used to calculate the membrane's ionic conductivity (σ) at different temperatures using the following equation:

$$\sigma = \frac{d}{l \cdot w \cdot R_m}$$

Where d was the distance between the two inner probes, l was the thickness of the membrane, w was the width of the membrane, and R_m was the ohmic resistance determined by model fitting. Samples were subjected to two heating ramps up to 180 °C. The first was to remove water from the membrane, and the second was to obtain results in anhydrous conditions.

4.3.6 Compression Creep and Creep Recovery

The time-dependent compression creep behavior was measured using a TA RSA III dynamic mechanical analyzer with built-in functionality. Testing first consisted of a 20 hour creep phase, where a constant compressive force equivalent to 0.1 MPa was applied to the sample. This was followed with a 3 hour recovery phase, in which the force was removed at the start of the recovery phase. Experiments were conducted at 180 °C in a temperature-controlled oven with dry air circulation.

4.3.7 Tensile Testing

Tensile testing was conducted using an Instron 5843 tensile tester equipped with a 100 N load cell. Tensile testing was performed on PBI membranes imbibed with phosphoric acid. Dumb-bell shaped samples were cut to the ASTM standard D638 (type V) specifications. Samples were pre-loaded to 0.1 N and tested with a crosshead speed of 10 mm min^{-1}. Three tensile tests were performed on each membrane type and an average modulus, stress at break, and strain at break were calculated and reported.

4.3.8 Brunauer-Emmett-Teller Measurements

A Micromeritics ASAP 2020 Plus was used to perform N_2 adsorption/desorption experiments in order to measure the Brunauer-Emmett-Teller (BET) surface area of PBI membranes. PBI samples were degassed at 120 °C for 3-8 hours under vacuum before beginning adsorption experiments.

4.3.9 Membrane Electrode Assembly (MEA) Preparation

MEAs were prepared by hot-pressing a membrane sample between two platinum carbon electrodes. Each gas diffusion electrode (GDE) contained a platinum loading of 1.0 mg cm^{-2}, acquired from BASF Fuel Cell, Inc. The GDEs were framed in Kapton to provide further stability. 10 cm^2 and 45.15 cm^2 MEAs were assembled into single-cell fuel cell test equipment. The gas flow plates were constructed from graphite with quadruple serpentine gas channels and stainless steel end plates with heaters attached were used to clamp the flow plates. Cell testing was carried out with a commercial fuel cell testing station from Fuel Cell Technologies, Inc. and controlled by home-programmed LabView software.

4.3.10 Fuel Cell Testing

Fuel cell testing was controlled by commercial fuel cell test stand (Fuel Cell Technologies, Inc.). Each MEA was broken in for 24 hours at 160 °C with a current density of 0.2 A cm^{-2} and no external humidification. Pure hydrogen was supplied to the anode with a stoichiometry of 1.2 and air was fed to the cathode with a stoichiometry of 2.0. Polarization curves were collected on 45.15 cm^2 cells with increasing temperature, and 10 cm^2 cells with increasing backpressure.

4.3.11 Electrochemical Hydrogen Separation Testing

EHS testing was carried out on standard fuel cell hardware and controlled by commercial fuel cell test stand (Fuel Cell Technologies, Inc.). Each membrane was broken in for 12 hours at 160 °C, 1.6% RH and 0.2 A cm^{-2} current density. Pure hydrogen was supplied to the anode with a stoichiometry of 1.25 and no sweep gas on the cathode. Twenty polarization curves were recorded over 3 hours at 160

°C as the initial performance. The same testing protocol was repeated at 180, and 200 °C. The temperature was then reduced back to 160 °C and the cell was operated at 0.2 A cm^{-2} for 12 hours. The final polarization behavior at 160 °C was tested to determine the recoverability.

Backpressure was applied to the anode side and controlled by the fuel cell test station. Twenty polarization curves were recorded over 3 hours at 160 °C with no backpressure, as the initial performance. The same testing protocol was repeated with 15 psi, 30 psi, and 45 psi at 160 °C. The backpressure was then removed and the cell was operated at 0.2 A cm^{-2} and 160 °C for 12 hours. The final polarization behavior with no backpressure was tested to determine the recoverability.

4.4 RESULTS AND DISCUSSION

In pursuing novel PBI membranes with enhanced mechanical stability and high ionic conductivity, a process development was invented, as shown in **Figure 4.2,** and termed the PPA+ Process. The new synthetic approach began with preparing p-PBI gel membranes according to the PPA Process.[3] The first step of the new technique was to remove the phosphoric acid by washing the gel PBI membrane in a series of water baths. When pH indication paper indicated the water bath was neutral, the samples were titrated to determine acid content remaining in the membrane. The acid doping level was 1.6 ± 0.2 mol PA/PRU and the acid content was 4.5 ± 0.7 wt% of phosphoric acid.

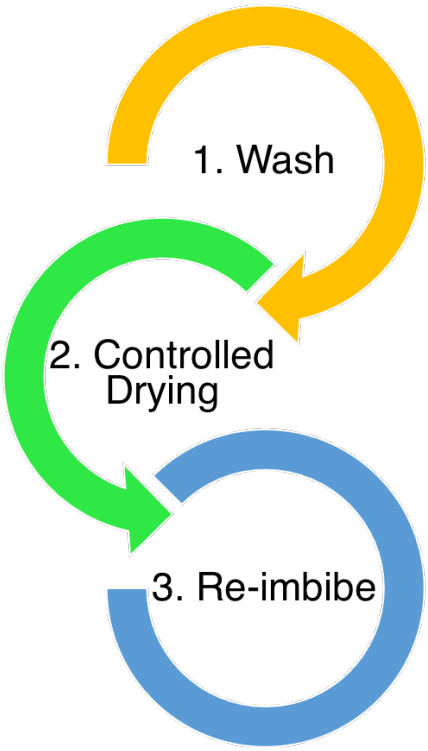

Figure 4.2. The PPA+ Process, a novel processing technique developed starting with gel PBI membranes produced in the PPA Process.

In the second step, controlled drying of the water-doped PBI gel membrane took place. This was accomplished by securing the neutralized gel membrane between two porous polyethylene sheets and clamping the perimeter with binder clips. In doing so, the membrane was restrained in the x and y direction. Water in the gel membrane was able to evaporate through the porous sheets on either side, and the sample was allowed to collapse only in the z direction as the water evaporated. The third and final step of the PPA+ Process was to re-dope the dense PBI film in phosphoric acid. Various doping conditions were investigated to determine the optimal acid bath concentration, doping time, and temperature of acid bath.

4.4.1 Concentration of Acid Doping Bath

Various concentrations of acid doping baths were investigated to optimize this step of the PPA+ Process. The dense p-PBI membranes were doped in baths containing 60, 70, 75, and 85 wt% phosphoric acid for 24 hours each at room temperature. The swelling ratio, acid uptake, ionic conductivity, and tensile properties were examined for samples doped in each concentration of phosphoric acid.

The swelling ratio of each sample is displayed below in **Table 4.1.** As the acid bath concentration increased, the volume swelling measured increased from 234% in the 60 wt% phosphoric acid bath, up to 586% in the 85 wt% phosphoric acid bath. When the acid bath concentration was between 60 to 75 wt% phosphoric acid, the swelling measured in the length and the width of each sample were less than 10% and fairly consistent. When the samples were doped in 85 wt% phosphoric acid, the swelling in the length and width increased slightly from the samples doped in lower concentrations of acid, but was still below 15% for the length and the width. Swelling occurred most significantly in the z-direction, as measured in the thickness of each sample, and increased as the concentration of the acid bath increased. The thickness swelling contributed the most to the volume swelling measured. These results indicate that PBI has a higher affinity for phosphoric acid than it does for water, and will take up more phosphoric acid as the concentration of the acid is increased.

Table 4.1. Swelling measured in each direction for each sample doped with different acid bath concentrations.

Acid Bath Concentration	Length (%)	Width (%)	Thickness (%)	Volume Swelling (%)	Thickness (um)
60 wt% PA	5.3 ± 1.7	7.6 ± 0.8	195 ± 10	234 ± 8.8	84.5 ± 2.5
70 wt% PA	8.0 ± 0.4	6.2 ± 0.8	265 ± 18	318 ± 19	97.2 ± 2.1
75 wt% PA	8.8 ± 0.2	6.9 ± 1.0	292 ± 18	356 ± 17	105 ± 1.4
85 wt% PA	13.6 ± 1.7	13.0 ± 0.3	434 ± 33	586 ± 53	151 ± 2.8

Titration was performed on each dense p-BPI sample doped from 60 to 85 wt% phosphoric acid to determine the acid loading and the composition of each sample, as shown in **Table 4.2**. As the concentration of the acid bath increased, the acid doping level measured increased. The dense p-PBI that was re- doped in 85 wt% phosphoric acid had the highest acid doping level of 24.0 moles of PA/PRU.

Table 4.2. Membrane acid doping levels and composition for dense p-PBIs re-doped in various concentrations of phosphoric acid.

Acid Bath Concentration	Acid Doping Level (PA/PRU)	PA Content (wt%)	PBI Content (wt%)	Water Content (wt%)
60 wt% PA	9.4 ± 0.9	63.2 ± 6.5	21.2 ± 0.3	15.7 ± 6.6
70 wt% PA	11.7 ± 0.6	69.4 ± 1.7	18.7 ± 0.8	11.8 ± 1.6
75 wt% PA	13.4 ± 0.5	67.8 ± 2.1	15.9 ± 0.3	16.3 ± 2.1
85 wt% PA	24.0 ± 0.5	74.8 ± 0.8	9.8 ± 0.1	15.4 ± 0.8

The composition of acid, polymer, and water measured in each sample is graphed below in **Figure 4.3.** As the concentration of the acid doping bath increased, the PBI content in the membrane decreased. While the sample doped in

60 wt% phosphoric acid contained over 20 wt% of polymer solids within the membrane, the sample that was doped in 85 wt% phosphoric acid contained only 10 wt% polymer solids. The water content measured in each membrane did not indicate any particular trend. These results indicate that the dense p-PBI samples swell more in phosphoric acid than water.

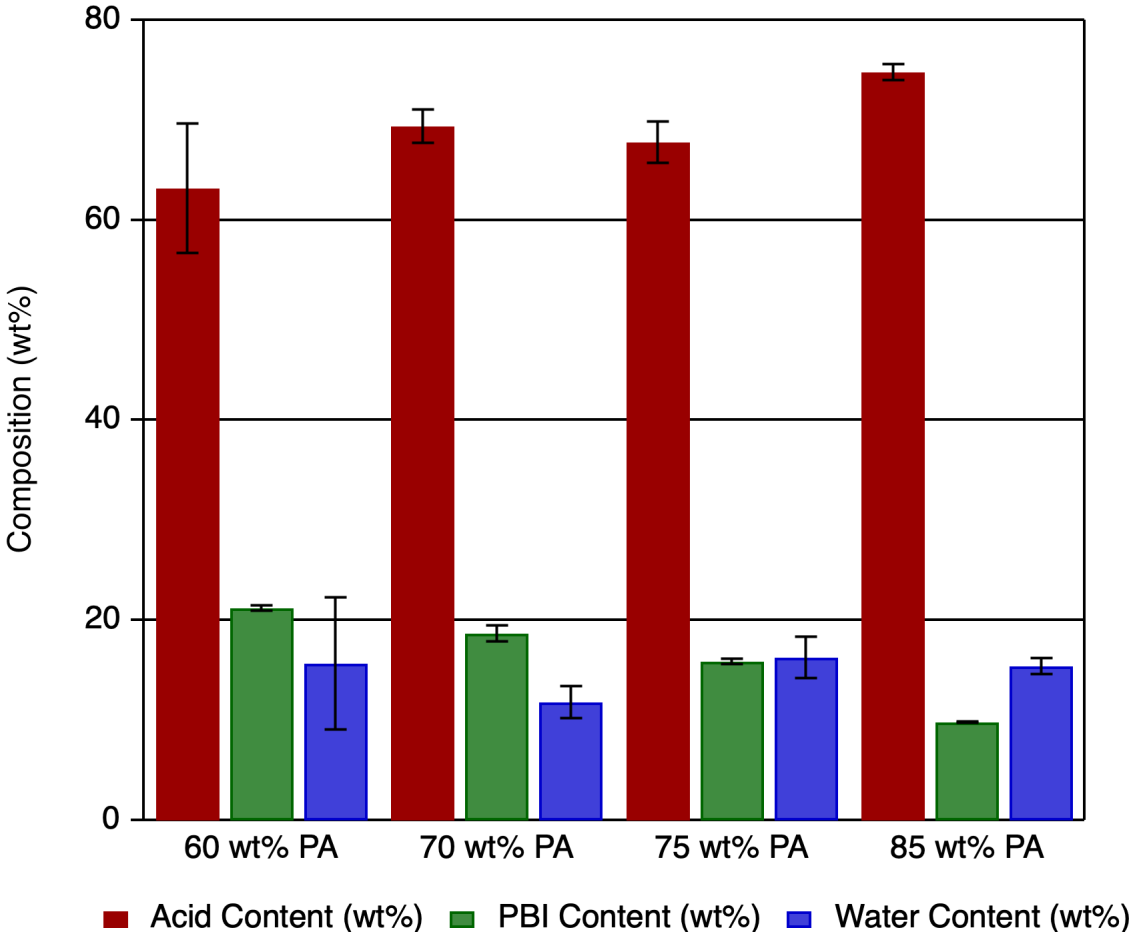

Figure 4.3. Composition of acid, polymer and water measured in dense p-PBI membranes that were re-doped in various concentrations of phosphoric acid.

The ionic conductivities were also measured as a function of acid doping bath concentration. These results were measured under anhydrous conditions, by measuring the ionic conductivity up to 180 °C, and cooling the sample without

exposure to moisture. A second measurement run was performed from 25 to 180 °C to obtain the anhydrous ionic conductivity, as displayed in **Figure 4.4**. The ionic conductivity of the dense p-PBI samples increased as the concentration of the acid doping bath increased. The samples that were doped in 60, 70, and 75 wt% phosphoric acid displayed ionic conductivities at 180 °C that slightly increased from 87 mS cm^{-1} in 60 wt% phosphoric acid to 106 mS cm^{-1} in 70 wt% phosphoric acid, followed by 125 mS cm^{-1} in 75 wt% phosphoric acid. However, when the acid bath concentration was increased from 75 wt% phosphoric acid to 85 wt% phosphoric acid, the ionic conductivity at displayed a more noticeable jump from 125 to 240 mS cm^{-1}. This represents a 92% increase in the ionic conductivity at 85 wt% phosphoric acid compared to 75 wt% phosphoric acid.

During handling of the samples re-doped in various concentrations of acid, a difference in mechanical properties could be noticed. Thus, the mechanical properties of each membrane doped in various acid concentrations were measured using tensile testing, as displayed in **Figure 4.5** and **Table 4.3**. As the concentration of the acid doping bath increased, the mechanical properties of the resulting doped PBI samples became more elastic. The sample that was re-doped in 60 wt% phosphoric acid had the highest value for Young's Modulus, which indicates it was the stiffest sample. The sample that was doped in 85 wt% phosphoric acid had a 78% lower value for Young's Modulus, compared to the sample doped in 60 wt% phosphoric acid, indicating that the concentration of the acid doping bath has a dramatic effect on the stiffness of the resulting sample. The stiffer samples, i.e. samples that were doped in baths with lower acid concentrations, also displayed

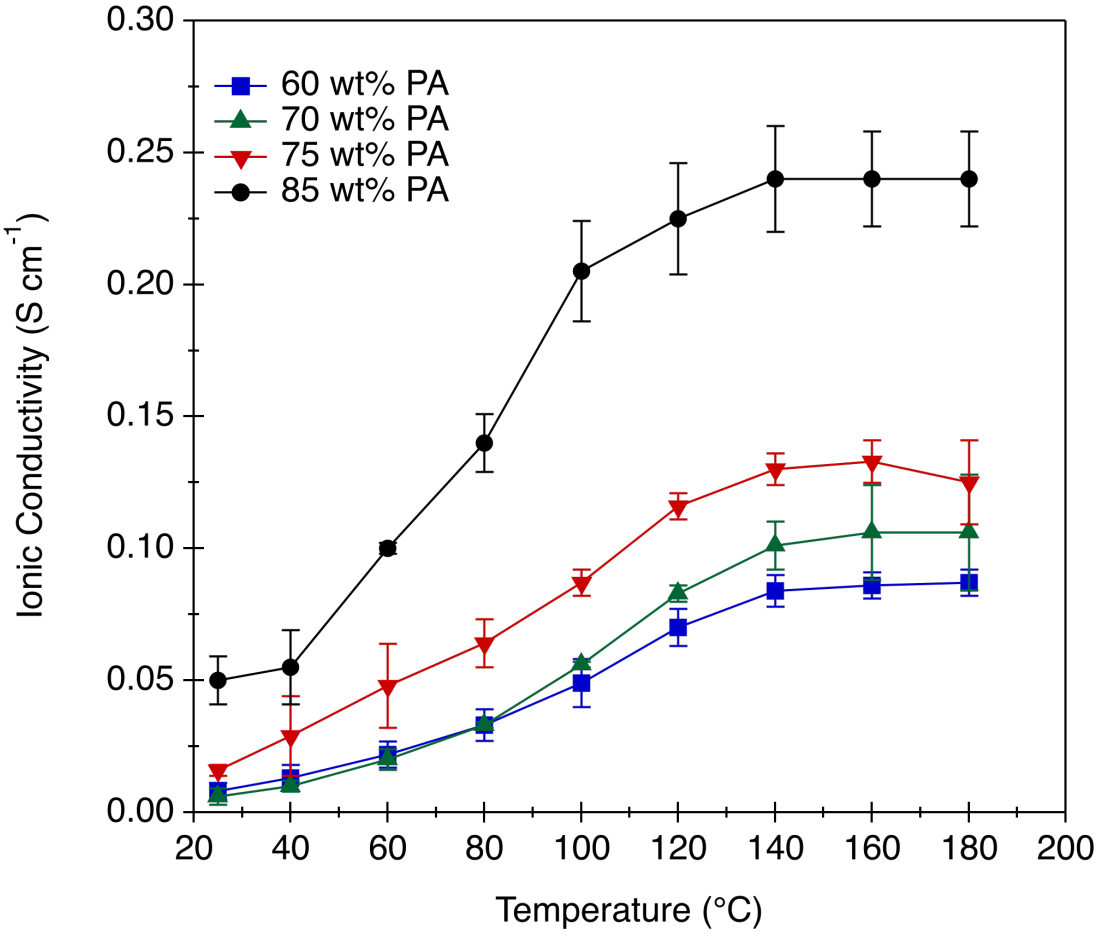

Figure 4.4. Anhydrous ionic conductivity measured from room temperature to 180 °C for dense p-PBI membranes doped in a various acid bath concentrations.

a higher tensile strength than those doped in baths with higher acid concentrations. The samples that were doped in a high acid concentration displayed more ductile properties, with strain at break increasing from about 153% when doped in 60 wt% phosphoric acid to 288% when doped in 85 wt% phosphoric acid.

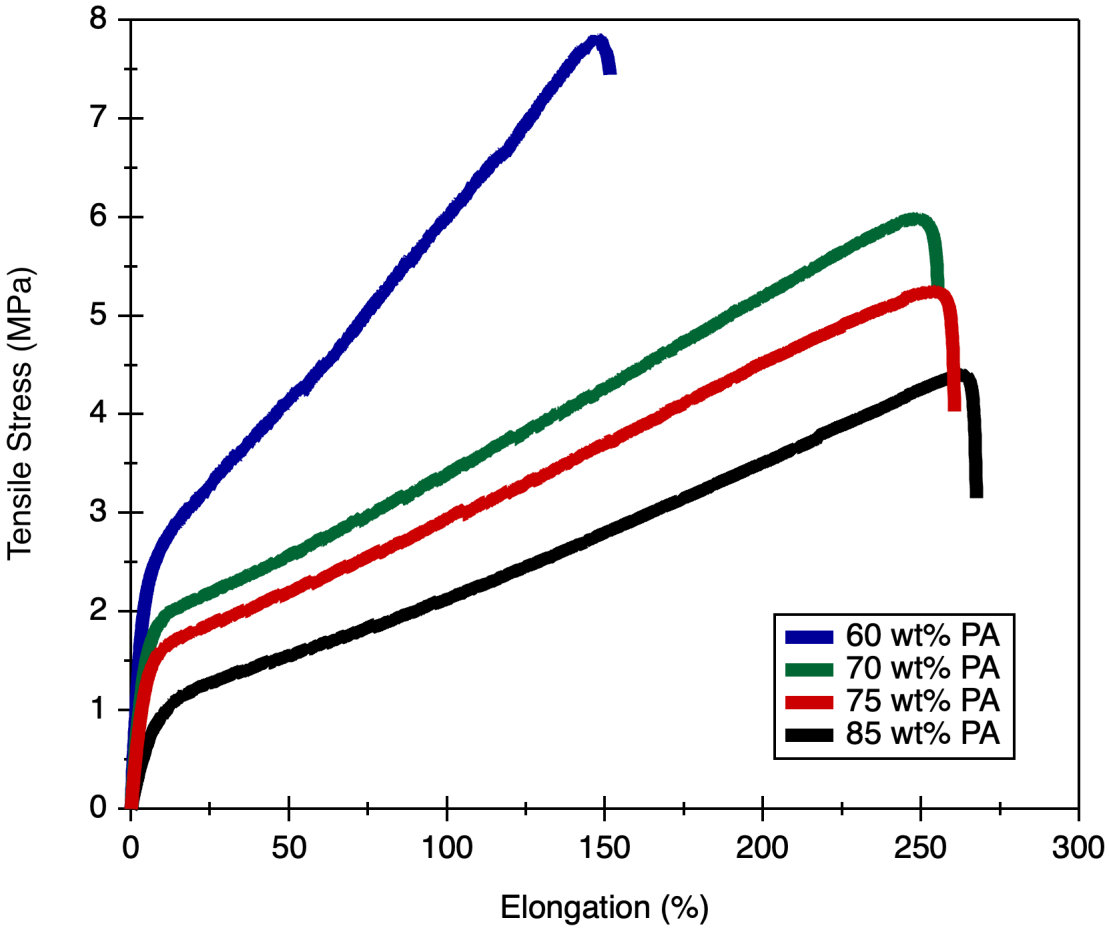

Figure 4.5. Stress-stain curves measured for each dense p-PBI membrane that was doped from 60 to 85 wt% phosphoric acid.

Table 4.3. Tensile properties measured for each dense p-PBI membrane re-doped in various acid concentration baths.

Acid Bath Concentration	Young's Modulus (MPa)	Stress at Break (MPa)	Elongation at Break (%)
60 wt% PA	74.6 ± 4.4	8.29 ± 1.1	153.4 ± 25
70 wt% PA	42.4 ± 1.3	6.16 ± 0.5	250.5 ± 24
75 wt% PA	35.5 ± 0.8	5.44 ± 0.3	254.5 ±15
85 wt% PA	16.4 ± 0.9	4.68 ± 0.5	287.8 ± 35

The acid concentration used for doping the dense p-PBI samples has a profound effect on the resulting membrane properties. Samples doped in lower acid concentrations have a lower dimensional swelling, acid doping levels and ionic conductivity. Mechanical properties also indicate that these materials are more stiff and less elastic. When the dense p-PBI PBIs were doped in high acid concentration baths, the dimensional swelling, acid uptake, and ionic conductivity increased. The results of this study indicate that the gel p-PBI samples prepared in the PPA Process can undergo densification followed by re-doping in 85 wt% phosphoric acid to yield excellent properties for application in HT-PEM Fuel Cells.

4.4.2 Acid Doping Time

Dense p-PBI samples were re-doped for 15 minutes to 24 hours in 85 wt% phosphoric acid at room temperature to determine how much time was needed for the samples to reach adequate doping levels. Titration was performed on dense p-PBI samples doped from 15 minutes to 24 hours to determine the acid loading and the composition of each sample, as shown in **Table 4.4**. As the doping time increased, the acid doping level measured increased. The sample that was doped for 15 minutes contained an acid doping level of only 13 moles of PA/PRU, which increased to 24 moles PA/PRU when doped for 24 hours.

The composition of acid, polymer, and water measured in each sample with various acid doping times are displayed below in **Figure 4.6.** As the acid doping time increased, the acid content increased slightly and the PBI content in the membrane decreased. When doped for 15 minutes, the resulting PBI contained

Table 4.4. Membrane acid doping levels and composition for dense p-PBI films re-doped in phosphoric acid for various time periods.

Acid Bath Doping Time	Acid Doping Level (PA/PRU)	PA Content (wt%)	PBI Content (wt%)	Water Content (wt%)
15 mins	13.1 ± 1.2	63.3 ± 5.2	15.2 ± 0.4	21.5 ± 5.1
30 mins	15.4 ± 0.9	64.0 ± 1.3	13.1 ± 0.7	23.0 ± 1.3
1 hour	16.4 ± 1.6	64.4 ± 5.1	12.3 ± 0.8	23.2 ± 5.1
3 hours	18.8 ± 1.9	66.7 ± 6.7	11.2 ± 0.4	22.1 ± 6.8
24 hours	24.0 ± 0.5	74.8 ± 0.8	9.8 ± 0.1	15.4 ± 0.8

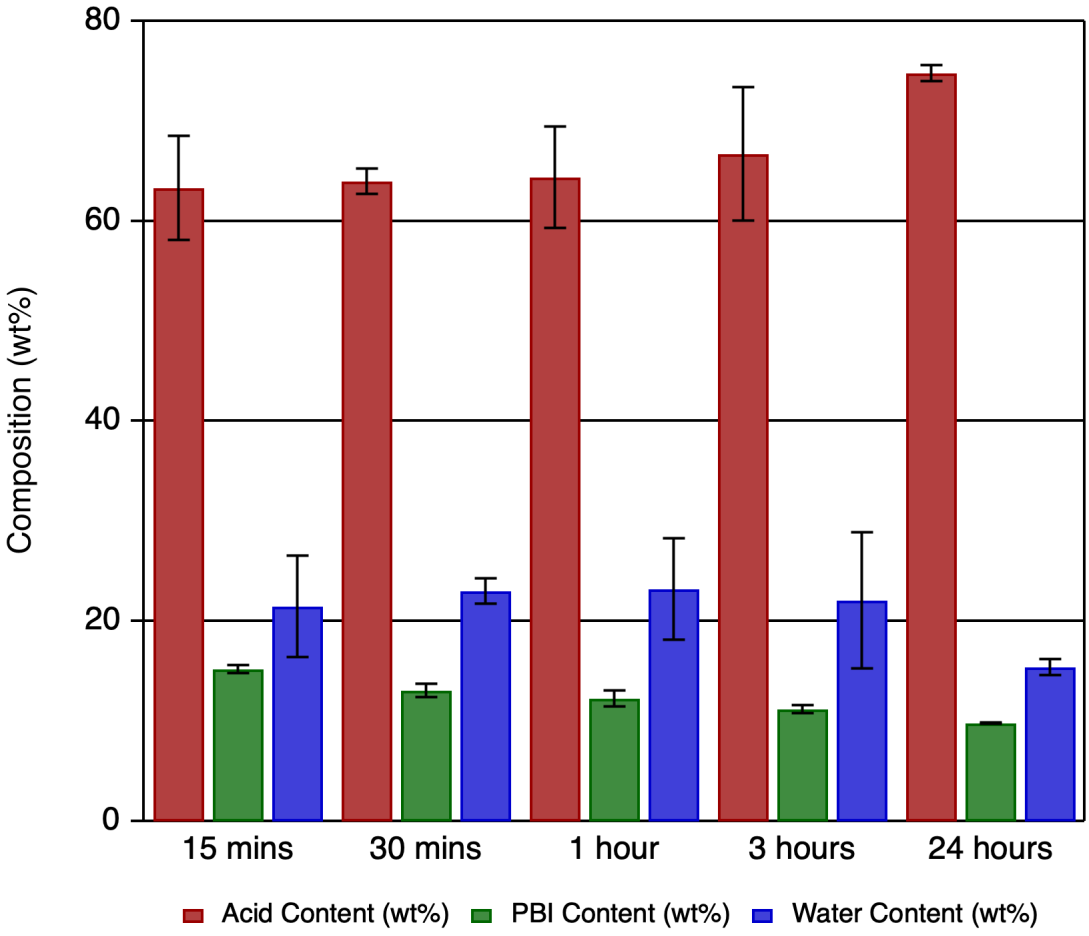

Figure 4.6. Composition of acid, polymer and water measured in each sample that was re-doped for various time periods.

15.2 wt% polymer solids, while the sample doped for 24 hours contained 9.8 wt% polymer solids, roughly a 35% decrease in polymer solids.

4.4.3 Temperature of Acid Doping Bath

The effect of the acid doping bath temperature on membrane composition, ionic conductivity and mechanical properties was investigated. The dense p-PBI membranes were doped in baths of 85 wt% phosphoric acid at 20, 40, 70, and 95 °C for 24 hours. The acid doping level, membrane composition and ionic conductivities were collected for each sample.

Titrations were completed on each sample of dense p-PBI re-doped in 85 wt% phosphoric acid at various temperatures, as shown in **Table 4.5**. The sample that was doped at 70 °C displayed the highest acid doping level of 20.5 moles PA/PRU.

Table 4.5. Acid doping levels and composition of dense p-PBI membranes re-doped at various temperatures.

Acid Bath Temperature	Acid Doping Level (PA/PRU)	PA Content (wt%)	PBI Content (wt%)	Water Content (wt%)
20 °C	18.4 ± 1.1	58.0 ± 1.0	9.9 ± 0.5	32.1 ± 1.0
40 °C	18.4 ± 1.9	62.8 ± 5.8	10.8 ± 0.2	26.5 ± 5.6
70 °C	20.5 ± 0.5	69.3 ± 1.0	10.6 ± 0.1	20.1 ± 0.9
95 °C	16.0 ± 0.9	69.2 ± 1.4	13.6 ± 0.5	17.2 ± 0.9

The composition of acid, polymer, and water measured in each sample is graphed below in **Figure 4.7.** In general, as the temperature of the acid bath was increased, the acid content and the PBI content increased while the water content

decreased. While the membrane doped at 95 °C displayed the lowest acid doping level (16.0 moles PA/PRU), it contained the highest acid content of 69%, and the highest PBI content of 13.6%.

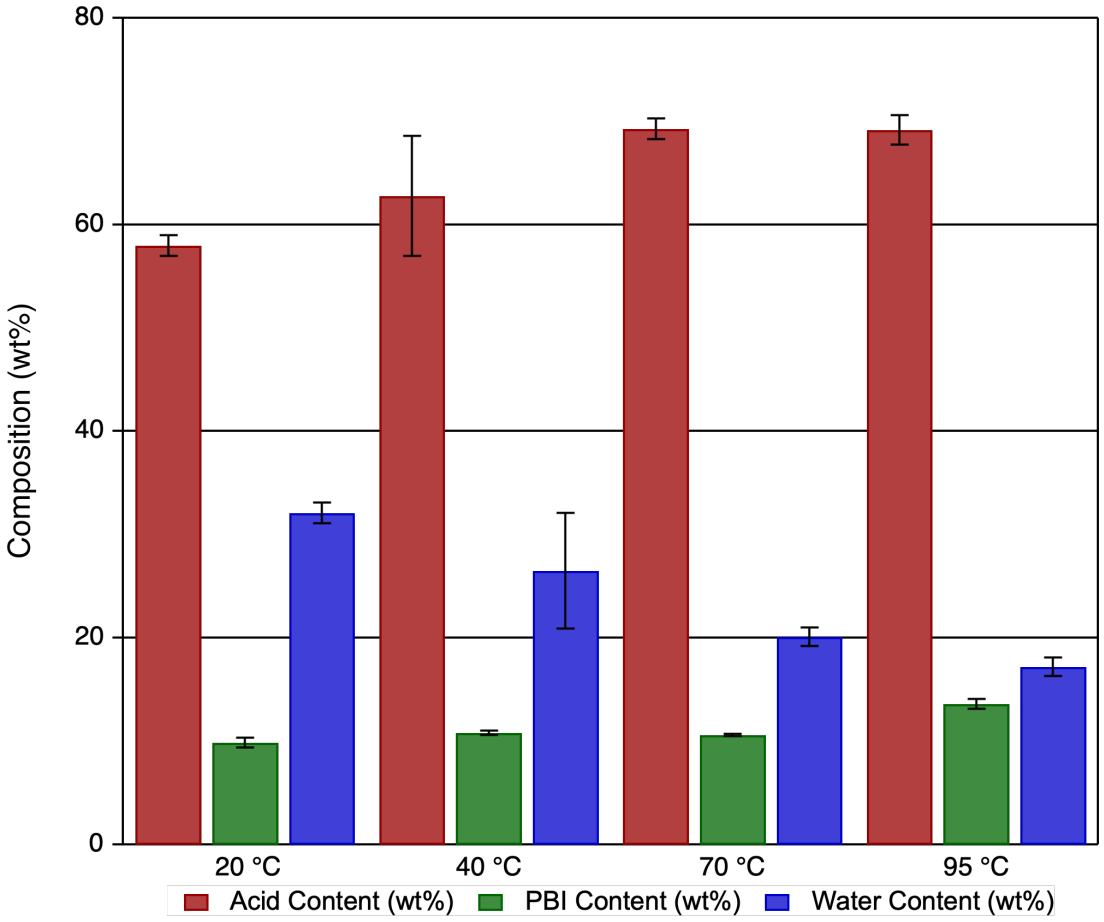

Figure 4.7. Composition of acid, polymer and water measured in each dense p-PBI sample that were re-doped at various acid bath temperatures.

The anhydrous ionic conductivity was measured for the dense p-PBI samples that were re-doped in 85 wt% phosphoric acid at various temperatures, as displayed in **Figure 4.8**. Each dense p-PBI sample that was re-doped in phosphoric acid displayed high values for ionic conductivity at high temperatures. The ionic conductivity of the dense p-PBI samples at 180 °C increased as the

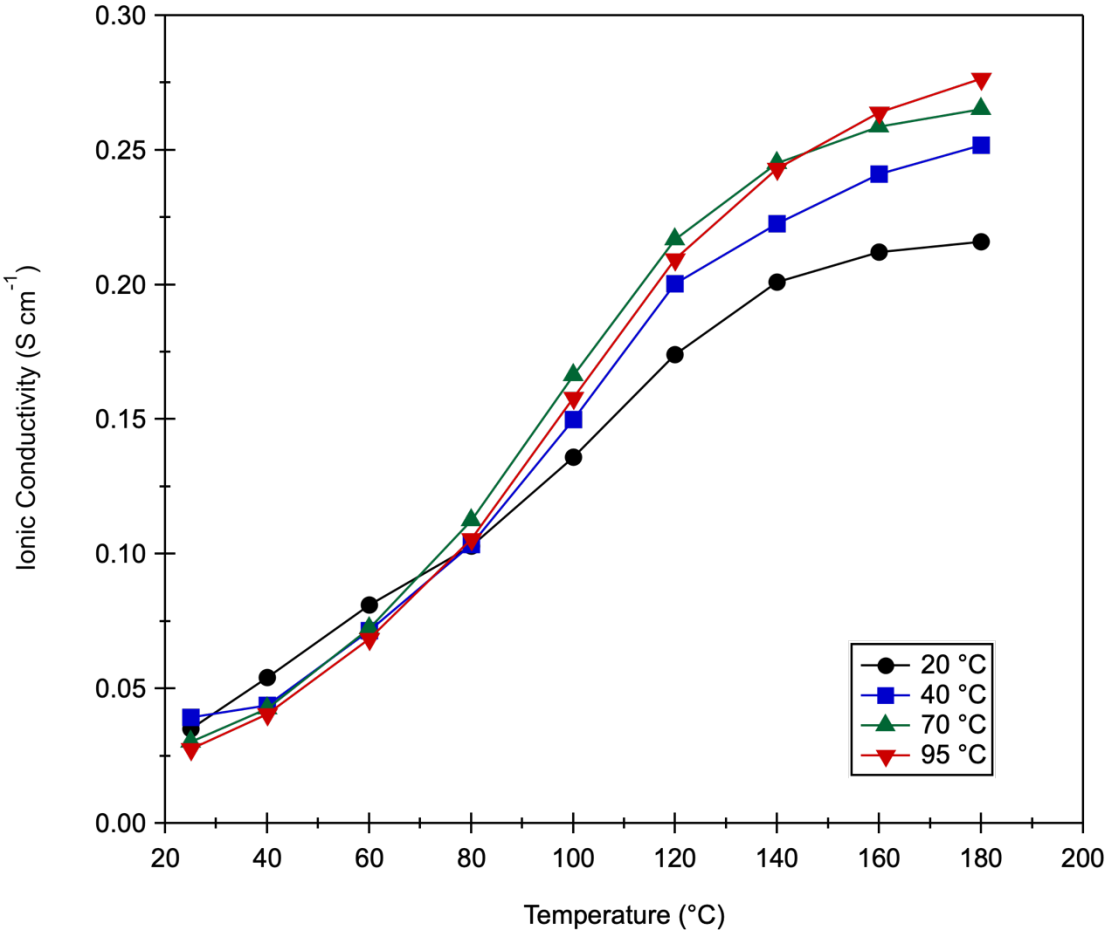

Figure 4.8. Anhydrous ionic conductivity measured from room temperature up to 180 °C for dense p-PBI membranes doped in a 85 wt% acid bath at different temperatures.

temperature of the acid doping bath increased. When the samples were re-doped at 20 °C, the ionic conductivity at 180 °C was 216 mS cm^{-1}, which is still a significantly high value for ionic conductivity. The ionic conductivity increased to 252 mS cm^{-1} when the acid doping bath temperature was increased to 40 °C. When the temperature of the acid doping bath was further raised to 70 °C, the ionic conductivity at 180 °C was slightly higher at 265 mS cm^{-1}. The highest acid doping bath temperature, 95 °C, provided the highest ionic conductivity at 180 °C of 277

mS cm^{-1}. There was a 28% increase in the ionic conductivity measured at 180 °C when acid doping bath temperature was raised from room temperature to 95 °C.

Mechanical creep was previously demonstrated to be the failure mode of gel PBI membranes produced in the PPA Process when used in a fuel cell.[42] Creep thinning of membranes causes a reduction in full contact with the electrode layers, resulting in fuel cell degradation. The compression creep and creep recovery were studied on dense p-PBI re-doped in various temperatures of acid baths. In testing, a constant compressive force is applied for 20 hours and then removed, and the recovery is measured for 3 hours. Creep testing is carried out at 180 ºC. The creep compliance is the deformation of a material under an applied stress. The creep compliance behavior is shown in **Figure 4.9** and the calculated steady-state creep compliances (J_s^0) and creep rates are displayed in **Table 4.6.** The steady-state creep compliance and creep rates for each dense p-PBI re-doped in various temperatures of acid baths were low. The sample with the lowest solids content was the sample that was re-doped at room temperature and this sample had the highest creep rate. The dense p-PBI sample that was re-doped at 95 °C displayed the highest solids content and the lowest creep rate.

Table 4.6. Creep compliance test results of PBI membranes doped in phosphoric acid at different temperatures.

Acid Doping Bath Temperature	J_s^0 (10^{-6} Pa^{-1})	Creep Rate (10^{-12} Pa^{-1} s^{-1})
20 ºC	2.00	6.94
40 ºC	2.70	3.76
70 ºC	1.35	4.58
95 ºC	1.89	3.60

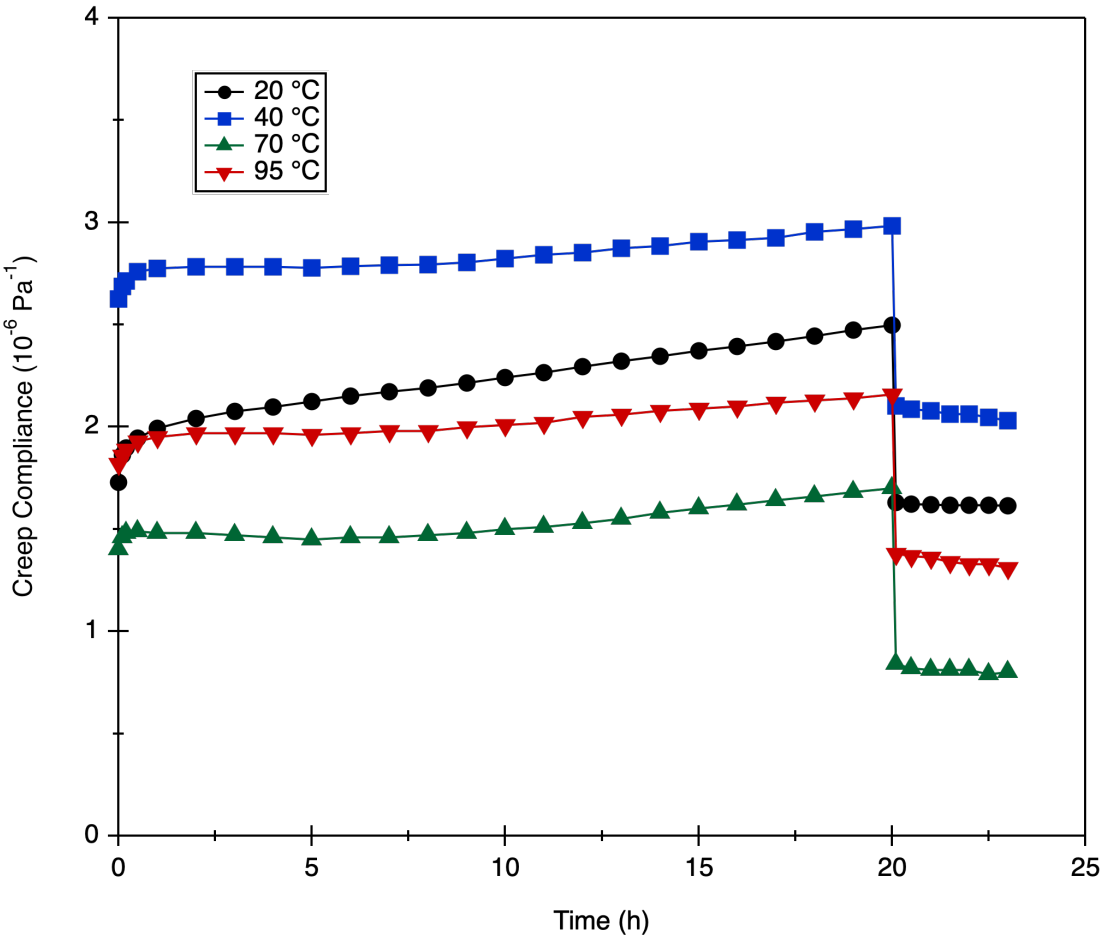

Figure 4.9. Creep compliance behavior of dense p-PBI re-doped in 85 wt% acid baths at different temperatures.

4.4.4 Ex-Situ Properties Compared to Other PBIs

With the completion of the doping studies, it is important to understand how the new dense p-PBI membranes perform when compared to other PBIs. The properties of the dense p-PBI films re-doped in phosphoric acid were compared to the original gel p-PBI membrane, the gel m/p-PBI membrane, and dense m-PBI that was prepared in the conventional imbibing process. The doping studies

established that the dense p-PBI films should be re-doped in 85 wt% phosphoric acid for at least 3 hours.

Although the higher temperature acid baths yielded higher ionic conductivities, the samples that were re-doped at room temperature still displayed sufficient electrochemical properties. In the following discussion, the dense p-PBI samples will refer to samples that were doped in 85 wt% phosphoric acid at room temperature for 24 hours. This was done to keep consistent with the dense m-PBI samples that were prepared in the conventional imbibing process, which were also doped in 85 wt% phosphoric acid at room temperature for 24 hours.

The gel p-PBI and gel m/p-PBI were both polymerized using the PPA Process. Gel m/p-PBI is a co-polymer of meta and para-PBI, and thus displays a greater solubility in PPA than p-PBI. The polymerization of m/p-PBI was carried out with a relatively high solids content of 11 wt% monomer charge and a ratio of 7:1 isophthalic acid: terephthalic acid. In contrast, p-PBI was polymerized with a 3 wt% monomer charge, due to its lower solubility in PPA.

The dense m-PBI films were prepared in the conventional imbibing process. The m-PBI powder was dissolved in DMAc to form a 20 wt% solution, which was used to cast the polymer film. The dense film is formed after removing the solvent and washing extensively. The dense m-PBI films were doped in 85 wt% phosphoric acid for 24 hours at room temperature before testing.

The titration results for gel p-PBI, gel m/p-PBI, dense p-PBI and dense m-PBI are displayed in **Table 4.7**. The gel p-PBI and gel m/p-PBI, which were both prepared in the PPA Process, displayed very different properties. The gel p-PBI

Table 4.7. Acid doping level and membrane composition of various PBIs produced in different methods.

Sample	Preparation Method	Acid Doping Level (PA/PRU)	PA Content (wt%)	PBI Content (wt%)	Water Content (wt%)
Gel p-PBI	**PPA Process**	30.0	53.7	5.6	40.6
Gel m/p-PBI	**PPA Process**	10.8	57.6	16.8	25.6
Dense p-PBI	**PPA+ Process**	24.0	74.8	9.8	15.4
Dense m-PBI	**Conventional Imbibing**	12.2	60.7	15.6	23.7

membrane displayed the highest acid doping level and the lowest PBI content. This can be attributed to the low monomer charge of the polymerization due to solubility limits of p-PBI in PPA. The gel m/p-PBI, which was polymerized with a significantly higher monomer charge, was found to contain a much higher polymer solids content compared to the gel p-PBI, but also a significantly lower acid doping level. The dense m-PBI samples displayed properties similar to the gel m/p-PBI, a low acid doping level and high polymer solids within the membrane. In the PPA+ Process, dense p-PBIs are formed used the gel p-PBI membranes. When they were re-doped in phosphoric acid, they were able to take up a significant amount of acid and the acid doping level was only a little lower than the original gel p-PBI sample. However, the dense p-PBI samples had double the PBI content within the membrane compared to the original gel p-PBI sample. These results indicate that processing conditions have a big impact on the acid

uptake of the various PBIs. It was not expected that a dense p-PBI sample would display a significantly high acid doping level compared to the dense m-PBI samples prepared in the conventional method. These unexpected ex-situ properties suggests that a superior membrane with high acid loading for significant proton transport and high solids content for mechanical stability was achieved.

The anhydrous ionic conductivity was measured for each type of PBI, and the data are plotted in **Figure 4.10**. The dense m-PBI membrane displayed the lowest ionic conductivity at each temperature, reaching only 78 mS cm^{-1} at 180 °C. The gel m/p-PBI, which was prepared in the PPA Process but had similar acid doping levels and solids content as the dense m-PBI sample, displayed a significantly higher ionic conductivity than dense m-PBI. Gel m/p-PBI reached an ionic conductivity of 170 mS cm^{-1} at 180 °C, which was 118% higher than that measured for dense m-PBI. The gel p-PBI sample displayed the highest ionic conductivity of all of the samples that were tested. At 180 °C, gel p-PBI displayed an ionic conductivity of 257 mS cm^{-1}. Interestingly, the dense p-PBI sample was able to achieve a relatively high ionic conductivity close to that of the gel p-PBI sample. The ionic conductivity of the dense p-PBI sample at 180 °C was 240 mS cm^{-1}. This result indicates that the densification of PPA Process gel membranes leads to PBIs that can retain their high proton transport properties even at lower phosphoric acid doping levels.

The temperature dependence of the measured ionic conductivities could be described by an Arrhenius equation and used to determine the activation energy. The activation energy of the gel m/p-PBI was the highest at 25.2 kJ mol^{-1}. The

dense m-PBI membrane displayed the next highest value of activation energy, 20.2 kJ mol^{-1}. The gel p-PBI membrane had a lower activation energy of 19.4 kJ mol^{-1}, and dense p-PBI had an activation energy of 15.8 kJ mol^{-1}. The higher activation energies potentially indicate that slower mechanistic pathways are dominant. The activation energy calculated for dense p-PBI is similar to activation energy of 85 wt% phosphoric acid reported in the literature as 14.29 kJ mol^{-1}.[47] These differences in activation energy can be attributed to differences in the internal structure of the PBI membranes, which can affect local proton mobility and long range transport.

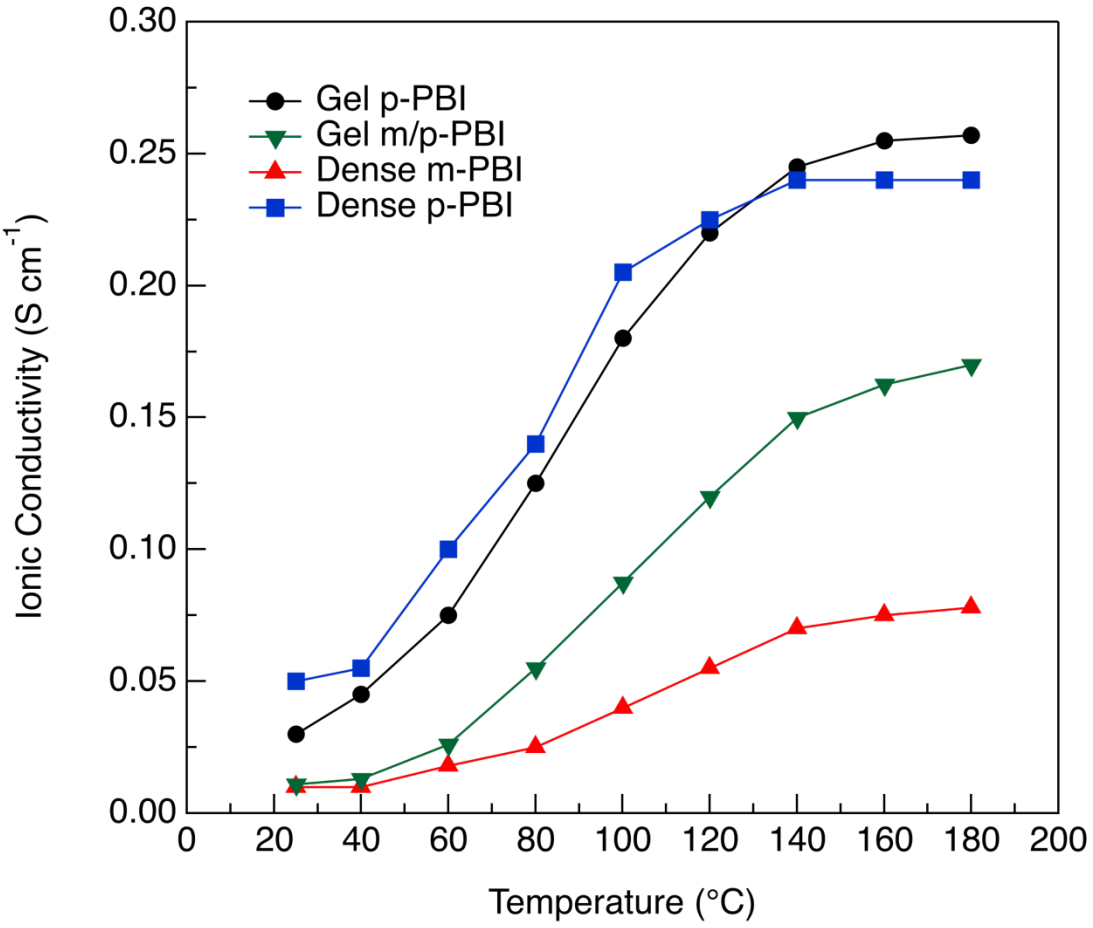

Figure 4.10. Anhydrous ionic conductivity measured from room temperature up to 180 °C for various PBI membranes.

4.4.5 Mechanical Properties

The results of the creep compression testing are shown in **Figure 4.11**. **Table 4.8** also contains the calculated values for the steady-state creep compliance (J_s^0) and the creep rate. The gel m/p-PBI sample exhibited a lower creep compliance and creep rate than the gel p-PBI sample. This is attributed to the higher polymer solids content in the gel m/p-PBI membrane, which contained 16.8 wt% PBI. The gel p-PBI sample only contained 5.6 wt% PBI in the membrane, which led to the high creep compliance and creep rate displayed. Remarkably, the dense p-PBI samples were able to achieve a low creep, very similar to the m/p-PBI sample. This is due to the higher solids content in the dense p-PBI membrane, which has twice the amount of polymer solids within the membrane compared to the gel p-PBI membrane. The ionic conductivity and creep results indicate that the dense p-PBI membrane is able to achieve both high ionic conductivity and low creep rates through densification of a gel p-PBI membrane.

Figure 4.12 and Table 4.9 show the results of tensile testing on the various PBI membranes. The gel p-PBI and gel m/p-PBI were tested as prepared from the PPA Process, with phosphoric acid still in the membrane. The dense p-PBI and dense m-PBI samples were doped in 85 wt% phosphoric acid at room temperature before testing. The gel p-PBI and gel m/p-PBI membranes both displayed more elastic properties, with low values for Young's Modulus. The gel p-PBI membrane was more ductile, with an elongation at break of about 250%. The dense m-PBI was the stiffest sample, with the highest Young's Modulus, it also had the highest stress at break (21.5 MPa). Overall, the dense m-PBI sample displayed the greatest tensile strength. Interestingly, the dense p-PBI sample displayed tensile properties

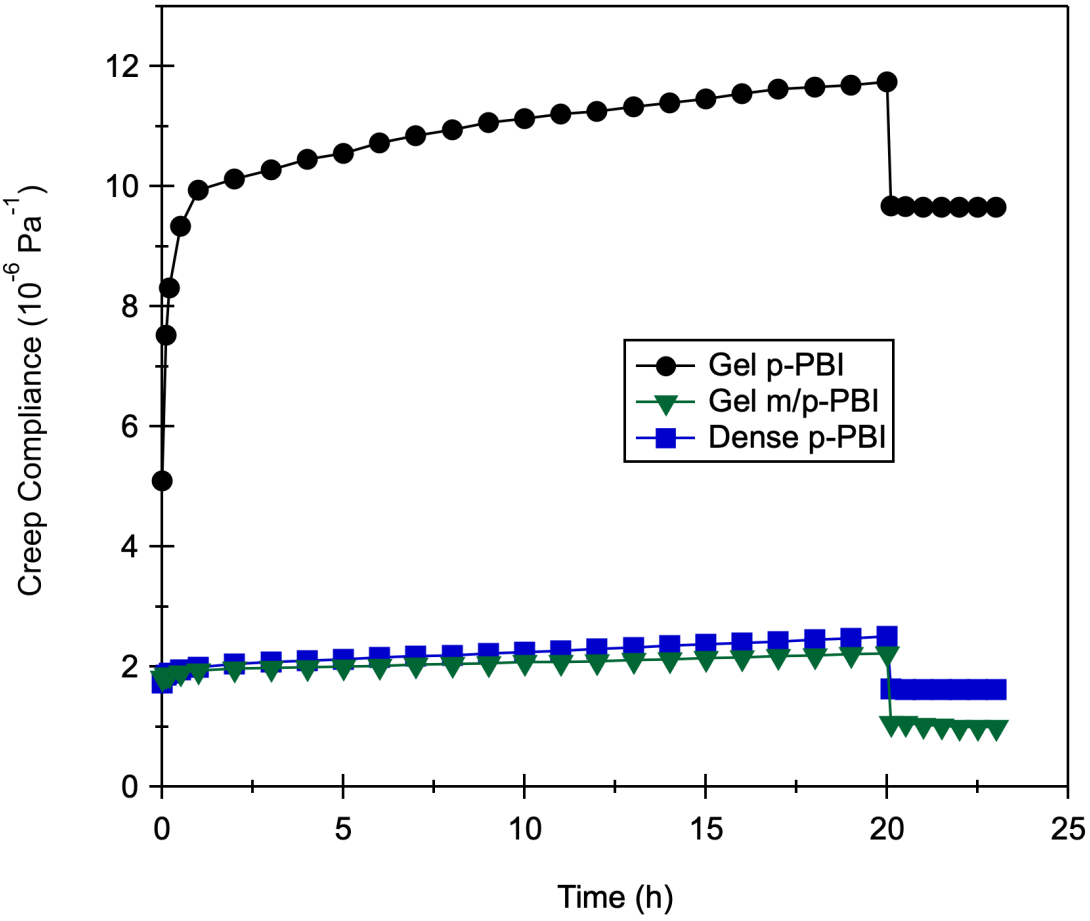

Figure 4.11. Creep compliance of gel p-PBI, gel m/p-PBI and dense p-PBI, collected at 180 °C.

Table 4.8. Steady-state creep compliance and creep rate measured for gel p-PBI, gel m/p-PBI, and dense p-PBI.

Membrane	J_s^0 (10^{-6} Pa^{-1})	Creep Rate (10^{-12} Pa^{-1} s^{-1})
Gel p-PBI	10.27	21.81
Gel m/p-PBI	1.92	4.06
Dense p-PBI	2.00	6.94

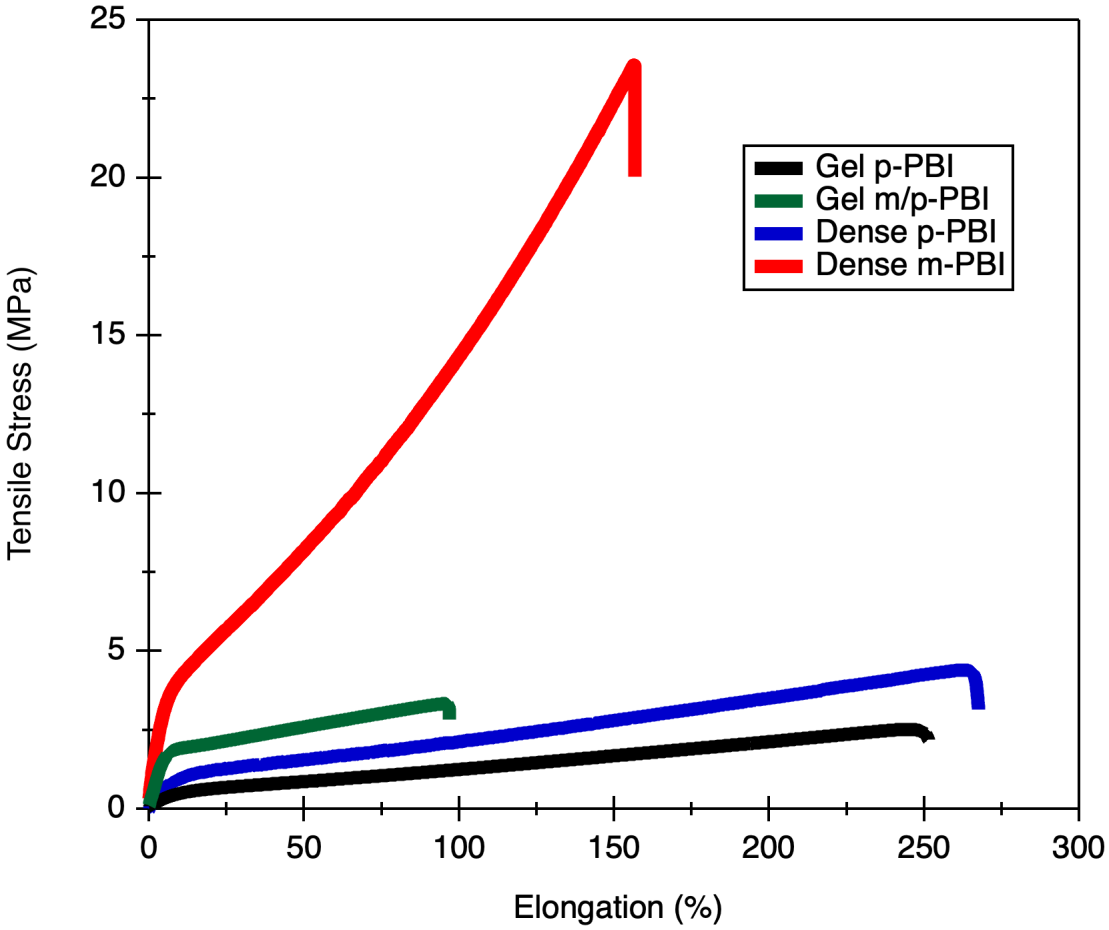

Figure 4.12. Stress-stain curves measured for dense and gel PBI membranes.

Table 4.9. Tensile properties measured for dense and gel PBI membranes.

Membrane	Young's Modulus (MPa)	Stress at Break (MPa)	Elongation at Break (%)
Gel p-PBI	14.8 ± 0.3	2.64 ± 0.3	251 ± 27
Gel m/p-PBI	49.3 ± 8.0	3.29 ± 0.1	96.5 ± 2.9
Dense p-PBI	16.4 ± 0.9	4.68 ± 0.5	288 ± 35
Dense m-PBI	106 ± 9.0	21.5 ± 2.6	154 ± 6.2

very similar to the gel p-PBI membrane. However, the dense p-PBI film had a greater tensile strength, with a larger stress at break and strength at break. The two dense PBI samples display very different tensile properties. This indicates that the different methods to prepare the two types of PBIs leads to different internal structures.

4.4.6 Dimensional Changes

The dimensional changes during each step of the densification process, as well as the overall dimensional changes are shown in **Table 4.10**. After step 1, in which the gel p-PBI membrane in phosphoric acid was neutralized and became a gel p-PBI membrane in water, there was a small reduction in the dimensions and overall volume, which was only 13.7% less than the original volume. The second step, which was the conversion of the gel p-PBI membrane in water into a dense p-PBI film, showed small changes in the length and width, but a very large (91.9%) decrease in the thickness, which led to an overall volume shrinkage of 93.2%. The shrinkage mainly occurred in the z (thickness) direction, since the membrane was constrained in the x- and y-directions during this step. In the third step, the dense p-PBI film was re-doped in 85 wt% phosphoric acid for 24 hours at room temperature, during which the length and width swelled minimally, 9-11%, while the thickness swelled by 418%. The dense p-PBI film shows anisotropic swelling, with a strong tendency to swell significantly more in the z-direction, the direction in which it was shrunk. Dense m-PBI films prepared by casting from an organic solvent have previously been reported to have a volume swelling of 150-250%, which is significantly lower than the volume swelling of the dense p-PBIs prepared in the PPA Process (527 vol%).[48]

Table 4.10. Dimensional changes during each step of the PPA+ Process, and overall.

	Length	Width	Thickness	Volume
Step 1	-5.88%	-5.98%	-2.46%	-13.7%
Step 2	-12.9%	-3.55%	-91.9%	-93.2%
Step 3	11.0%	9.15%	418%	527%
Overall	-9.08%	-1.03%	-58.9%	-63.0%

[a] **Step 1:** gel p-PBI in PA to gel p-PBI in H_2O

[b] **Step 2:** gel p-PBI in H_2O to dense p-PBI film

[c] **Step 3:** Dense p-PBI film to PA-doped p-PBI membrane

4.4.7 Brunauer-Emmett-Teller Surface Area Measurements

Investigation into the microporous structure of various PBIs was completed using Brunauer-Emmett-Teller (BET) surface areas from N_2 adsorption/desorption isotherms collected at 77 K. The gel p-PBI membranes were washed with water to remove the acid, placed in liquid nitrogen, and freeze dried to lock in the structure. The dense p-PBI and m-PBI membranes were each doped in 85 wt% phosphoric acid for 24 hours, washed in water to remove the acid, then placed in liquid nitrogen and freeze dried. The BET surface area of the m-PBI membrane prepared by casting from an organic solvent was 284.10 ± 2.4 m^2 g^{-1}. The gel p-PBI membrane had BET surface area that was double the surface area measured for the m-PBI sample, measured to be 515.59 ± 7.7 m^2 g^{-1}. Amazingly, the surface area of the dense p-PBI membrane was found to double from the gel p-PBI membrane, with a BET surface area of 997.12 ± 6.4 m^2 g^{-1}. Compared to the m-PBI prepared by casting from an organic solvent, the dense p-PBI membrane exhibited a 250% increase in the BET surface area. BET surface area measurements

were also collected on dense p-PBI samples that were not doped in acid, and measured to be 285.96 ± 2.6 $m^2 g^{-1}$.

Although more testing needs to be completed, the BET surface area measurements indicated that the internal structures vary with differing PBI processing methods. It also indicated that the PPA Process, which yields gel PBI membranes, provides more microporous volume within the membrane than samples prepared by casting from an organic solvent. Furthermore, the PPA+ Process can allow an even greater microporous volume within the membrane for acid uptake. This might be correlated with the higher conductivity results observed. Further detailed characterization on the relationship between microporous volume and surface area, and ionic conductivity is needed to provide a more complete understanding of proton mobilities in PBI membranes.

4.4.8 Fuel Cell Testing

The dense p-PBI samples re-doped in 85 wt% phosphoric acid at room temperature for 24 hours and the gel p-PBI samples were selected for further studies in fuel cells. Membrane samples were constructed into a membrane electrode assembly (MEA) by hot pressing between an anode and a cathode electrodes. The anode electrode was Pt/C with a 1 mg cm^{-2} Pt loading, and the cathode electrode was Pt/C with a 1 mg cm^{-2} Pt alloy loading. The MEA was assembled into a single cell and tested at various conditions.

Figure 4.13 shows the polarization curves of the gel p-PBI membrane and the dense p-PBI membrane tested at 160 °C with hydrogen and oxygen at 1.2 and 2.0 stoichiometric flow, respectively. The performance of the dense p-PBI

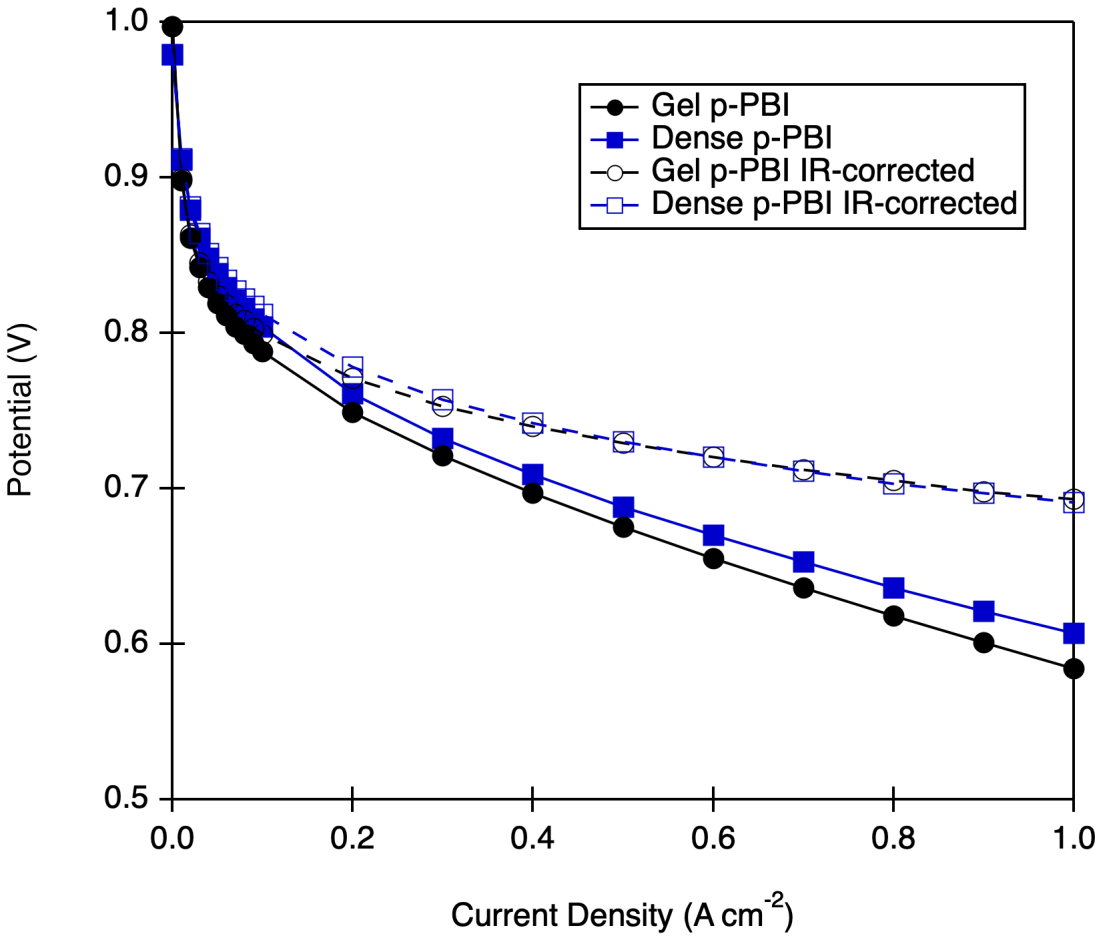

Figure 4.13. Polarization curves measured at 160 °C for gel p-PBI MEA (black) and dense p-PBI MEA (blue). The unfilled symbols represent the IR-corrected data. The test cell active area was 45.15 cm^{-2}, H_2/O_2 = 1.2/2.0 stoichiometric flows, no external humidification.

membranes was slightly higher than the gel p-PBI membrane, especially at higher current densities. At 160 °C, the potential of the dense p-PBI membrane was 0.761 V at 0.2 A cm^{-2}. The gel p-PBI sample displayed a potential of 0.749 V at 0.2 A cm^{-2} and 160 °C. The high-frequency resistance (HFR) was measured at 0.2 A cm^{-2} at 1 kHz. The HFR is related to ohmic losses, and thus the performance at higher current densities is related to the HFR. The HFR of the dense p-PBI MEA was 83.5 mΩ cm^2 and 108.4 mΩ cm^2 for the gel p-PBI MEA. When the IR-corrected

polarization curves are plotted, the performance difference at high current densities of the two MEAs is negligible.

Figure 4.14 shows the polarization curves and power density curves of the gel p-PBI MEA and the dense p-PBI MEA tested from 160 to 200 °C with hydrogen and air at 1.2 and 2.0 stoichiometric flow, respectively. At 160 °C, the performance of the two MEAs are very similar. At 0.2 A cm^{-2} the potential was 0.680 V for the gel p-PBI MEA, while the dense p-PBI MEA recorded a potential of 0.682 V at 0.2 A cm^{-2}. When the temperature of the cell was raised to 180 °C, gel p-PBI MEA reached a potential of 0.690 V at 0.2 A cm^{-2}, while the dense p-PBI MEA experienced a larger increase in potential, which measured 0.700 V at 0.2 A cm^{-2}. When the temperature was increased further to 200 °C, the potential of the gel p-PBI MEA increased once again to 0.703 V at 0.2 A cm^{-2}. The dense p-PBI MEA experienced greater improvements with increasing temperature, at 200 °C it had a potential of 0.714 V at 0.2 A cm^{-2}. This is likely due to the creep behavior of the gel p-PBI membrane, which becomes even "softer" as the temperature increases. This is supported by the HFR measured during testing of each MEA. In the gel p-PBI sample, as the temperature increased from 160 to 200 °C, the HFR increased from 103 mΩ cm^2 to 117 mΩ cm^2. However, in the dense p-PBI MEA, as the temperature increased from 160 to 200 °C, the HFR decreased from 81.3 mΩ cm^2 to 76.8 mΩ cm^2. Thus, the gel p-PBI membrane is not able to take advantage of faster electrode kinetics at higher temperatures due to creep of the membrane. Conversely, the dense p-PBI has a higher solids content and better (lower) creep properties, and it is able to take advantage of the faster electrode kinetics at higher temperatures with improved performance each time the temperature is raised.

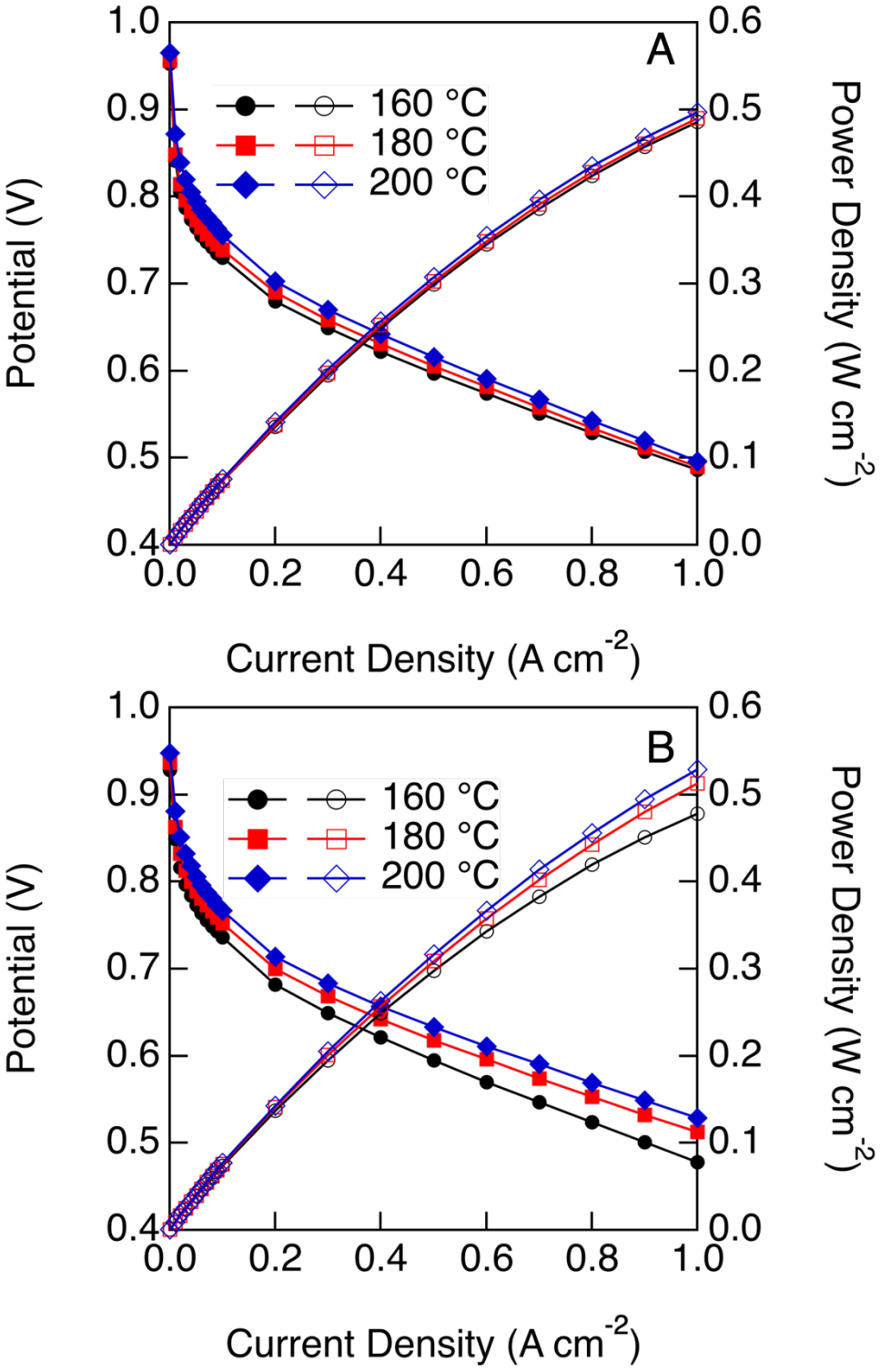

Figure 4.14. Polarization (filled symbols) and power density (unfilled symbols) curves for A) gel p-PBI MEA and B) dense p-PBI MEA tested in a 45.15 cm^2 cell. H_2/Air = 1.2/2.0 stoichiometric flows, no external humidification.

One of the many benefits of high temperature fuel cell operation is enhanced tolerance to fuel impurities such as carbon monoxide.[15] At low temperatures, small amounts of carbon monoxide (~10 ppm) in the fuel stream poison the cell rapidly due carbon monoxide binding to the platinum catalyst, resulting in reduced open platinum sites for the hydrogen fuel to react.[49] However, the binding of carbon monoxide to the platinum catalyst is a reversible reaction at high temperatures.[17] Thus, HT-PEMFCs can operate with comparatively large concentrations of carbon monoxide in the fuel stream.

The two MEAs were further tested under reformate conditions with a fuel stream containing 2.1% carbon monoxide, 70% hydrogen and a nitrogen balance. **Figure 4.15** displays the polarization curves and power density curves of the gel p-PBI MEA and the dense p-PBI MEA tested from 180 to 200 °C with reformate and air at 1.2 and 2.0 stoichiometric flow, respectively. The performance of the dense p-PBI MEA was slightly better than the gel p-PBI MEA. At 180 °C, the potential of the gel p-PBI MEA at 0.2 A cm^{-2} was 0.668 V, while the dense p-PBI MEA had a potential of 0.681 V at the same operating conditions. At 200 °C, the potential of the gel p-PBI MEA at 0.2 A cm^{-2} was 0.684 V, and the dense p-PBI MEA had a potential of 0.698 V under the same operating conditions.

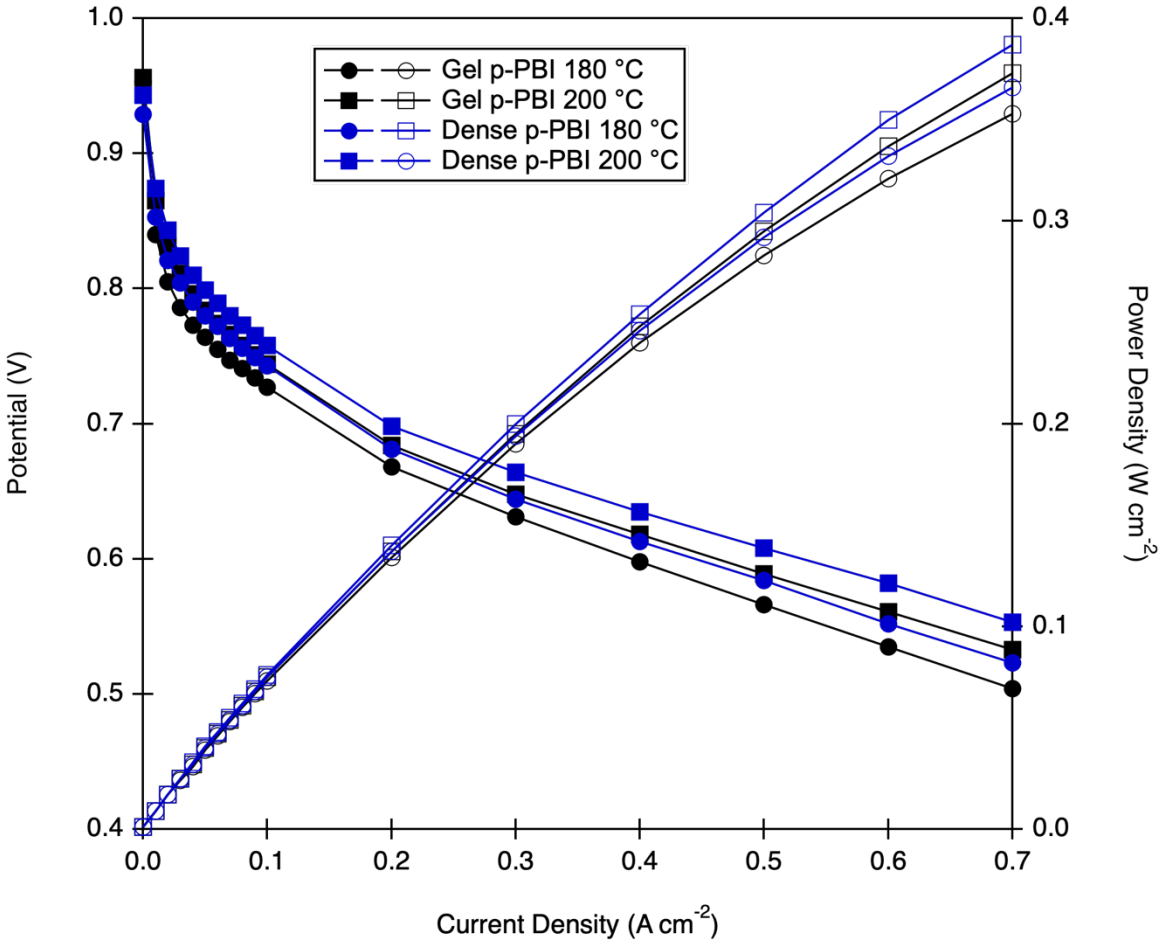

Figure 4.15. Polarization (filled symbols) and power density (unfilled symbols) curves for gel p-PBI membrane (black) and dense p-PBI membrane (blue) tested in a 45.15 cm^2 cell. Reformate / Air = 1.2 / 2.0 stoichiometric flows, no external humidification. Reformate = 2.1% CO, 70% H_2, N_2 balance.

4.4.9 Effect of Pressure

Greater performance, in terms of voltage and power density, of PEM fuel cells can be achieved by increasing the gas operating pressure. This can be attributed to lower diffusion polarization and a decrease in the activation potential. Higher pressures increase the partial pressures of the gas reactants and accelerate reactions, as well as increase the ionic conductivity. The polarization

and power density curves of the gel p-PBI membrane and the dense p-PBI membrane tested with various back pressures at 180 ºC with hydrogen and air at 1.2 and 2.0 stoichiometric flow, respectively, are shown in **Figure 4.16**.

Table 4.11 contains the voltage measured at 0.2 A cm^{-2} as well as the maximum power density achieved at each back pressure. On the top, in **Figure 4.16A**, the gel p-PBI membrane displayed enhanced performance with up to 30 psi back pressure (3.0 atm, absolute) applied. The maximum power density achieved increased from 0.372 W cm^{-2} with no back pressure (1 atm, absolute), to 0.624 W cm^{-2} with 30 psi back pressure (3.0 atm, absolute). However, when the back pressure was further increased to 45 psi (4.0 atm, absolute), there was no significant performance enhancement, and the maximum power density achieved was lower than that achieved at 30 psi (3.0 atm, absolute). When the back pressure was removed and the final polarization curve was obtained, there was roughly a 6.2% lower maximum power achieved after operating the gel p-PBI MEA with back pressure.

As previously discussed, the gel p-PBI membrane has a higher creep rate and creep compliance, and membrane creep effects the interface of the membrane with the electrodes. As the back pressure increased in the cell, the membrane creep was accelerated at high temperatures. Thus, although back pressure can improve fuel cell performance, it is limited and must be balanced for the gel p-PBI membrane, especially if it were to be operated at long lifetimes under these conditions. The graph on the bottom**, Figure 4.16B,** shows the dense p-PBI membrane performance with up to 45 psi (4.0 atm, absolute) back pressure

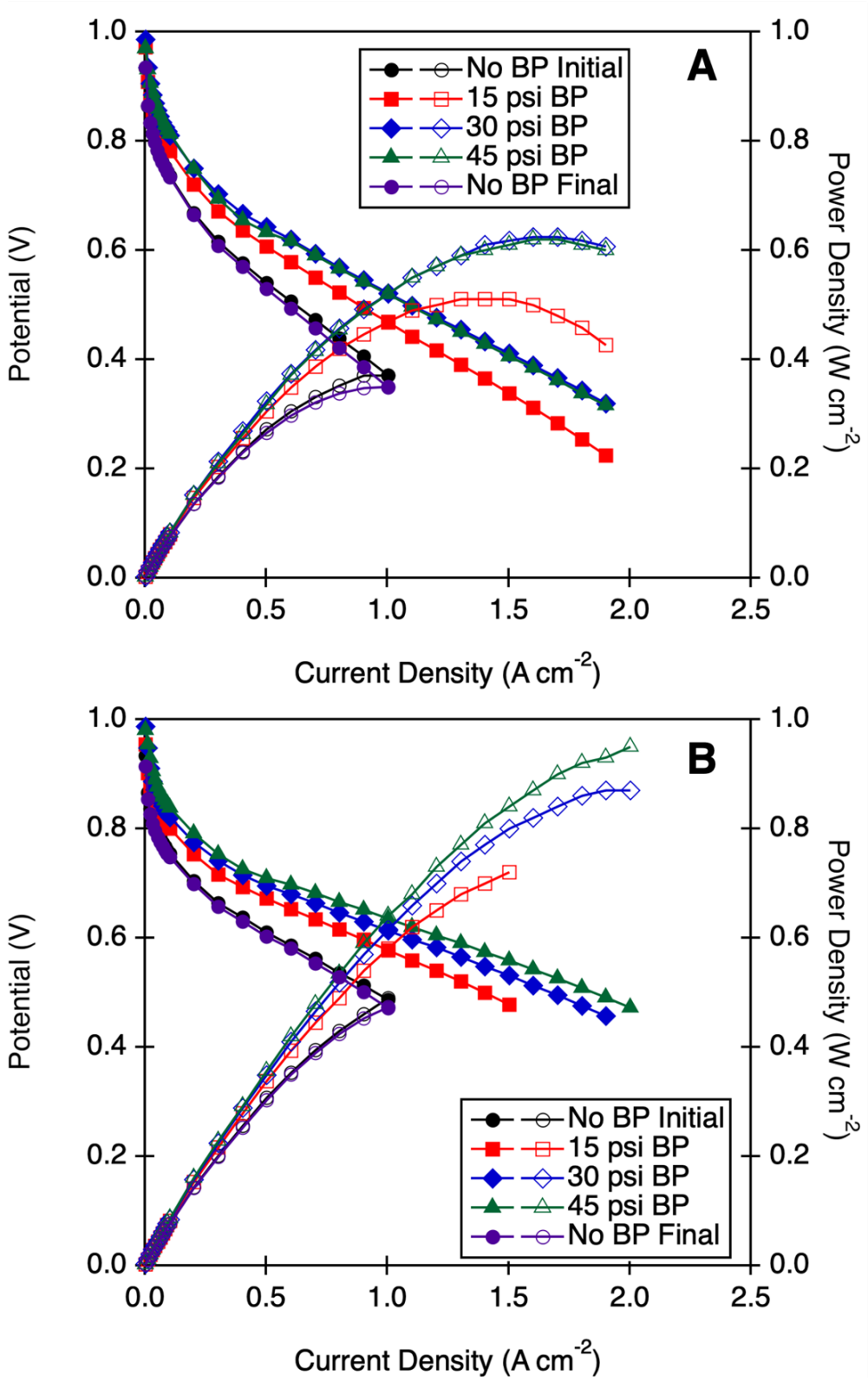

Figure 4.16. Polarization (filled symbols) and power density (unfilled symbols) curves measured at 180 °C for A) gel p-PBI membrane and B) dense p-PBI membrane. H_2/Air = 1.2/2.0 stoichiometric flows, no external humidification.

Table 4.11. Potential measured at 0.2 A cm^{-2} and maximum power density for gel and dense p-PBI operated at 180 °C with H_2/Air and various back pressures.

	Gel p-PBI Potential @ 0.2 A cm^{-2} (V)	Gel p-PBI Max Power Density (W cm^{-2})	Dense p-PBI Potential @ 0.2 A cm^{-2} (V)	Dense p-PBI Max Power Density (W cm^{-2})
No BP Initial	0.668	0.372	0.704	0.488
15 psi	0.720	0.511	0.753	0.717
30 psi	0.750	0.624	0.775	0.873
45 psi	0.749	0.616	0.792	0.945
No BP Final	0.664	0.349	0.698	0.473

applied. As the back pressure increased, there was a noticeable enhancement in the voltage and maximum power density achieved. Since the dense p-PBI membrane has a lower creep compliance and creep rate, it does not undergo deformation as readily due to creep when back pressure is applied. The maximum power density increased from 0.488 W cm^{-2} with no back pressure applied (1 atm, absolute), up to 0.945 W cm^{-2} with 45 psi (4.0 atm, absolute) back pressure applied. This represents a 51% increase in the maximum power density achieved when switching from the gel p-PBI to the dense p-PBI. An experimental equation was developed to determine the change in voltage (ΔV) for PAFC's with a temperature range of 177 and 218 °C and a pressure range of 1 to 10 atm, based on the Nernst equation[50]:

$$\Delta V\ (mV)\ =\ 146\ log\ \frac{P_2}{P_1}$$

Where P_1 and P_2 are different cell pressures. Using this equation, it is predicted that there will be a 87.9 mV potential increase when 45 psi (4.0 atm, absolute) back pressure is applied. The potential difference measured at 0.2 A cm^{-2} from the initial performance with no backpressure (1 atm, absolute) and 45 psi

(3.0 atm, absolute) back pressure was 81 mV for the gel p-PBI membrane and 88 mV for the dense p-PBI membrane. This further indicated that the creep effects in the gel p-PBI membrane limited it from reaching the predicted potential increase with 45 psi (4.0 atm, absolute) back pressure applied. The back pressure was then removed and the recovery polarization curve without back pressure was collected. The final polarization curve achieved a maximum power density that was only 3.1% lower than the initial performance for the dense p-PBI membrane.

The dense p-PBI membrane, with its better creep properties, was also operated at 200 °C with H_2/Air and various back pressures, as displayed in **Figure 4.17**. **Table 4.12** summarizes the potential at 0.2 A cm^{-2} and maximum power density achieved for the dense p-PBI membrane operated up to 45 psi at 200 °C. Once again, as the back pressure increased, the voltage measured at 0.2 A cm^{-2} increased as well as the maximum power density. When no back pressure was applied, the maximum power density was only 504 W cm^{-2}, however when 45 psi back pressure was applied, the maximum power density increased to 1.010 W cm^{-2}. The back pressure was then removed and a polarization curve was collected to measure the performance recovery with no back pressure. The maximum power density of the final no back pressure curve was only 2% lower than the initial performance, indicating little to no degradation took place by operating the MEA at 200 ºC and 45 psi back pressure.

The dense p-PBI MEA was also tested at 200 ºC with H_2 and O_2 fed to the cell at various back pressures, as shown in **Figure 4.18.** The voltage measured at 0.2 A cm^{-2} is given in **Table 4.13**, as well as the maximum power density achieved. Under these conditions, the maximum power density increased from

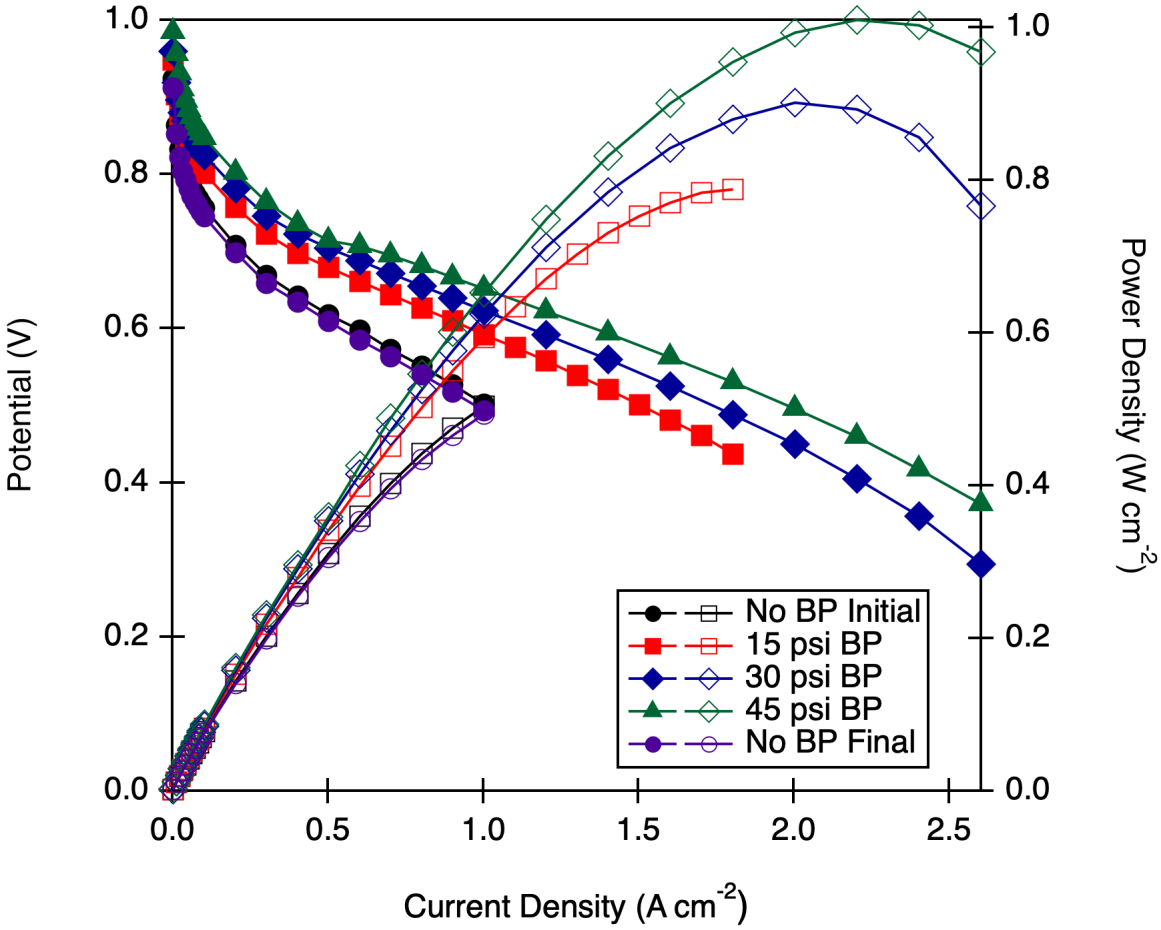

Figure 4.17. Polarization (filled symbols) and power density (unfilled symbols) curves measured at 200 °C for dense p-PBI membrane. H_2/Air = 1.2/2.0 stoichiometric flows, no external humidification.

Table 4.12. Potential measured at 0.2 A cm^{-2} and maximum power density for dense p-PBI operated at 200 °C with H_2/Air and various back pressures.

	Dense p-PBI Potential @ 0.2 A cm^{-2} (V)	**Dense p-PBI Max Power Density (W cm^{-2})**
No BP Initial	0.708	0.504
15 psi	0.757	0.788
30 psi	0.781	0.902
45 psi	0.802	1.010
No BP Final	0.698	0.494

0.635 W cm^{-2} with no back pressure, up to 1.809 W cm^{-2} when 45 psi back pressure was applied to the anode and the cathode. The back pressure was removed and the performance without back pressure was measured to study the recovery of the MEA after operation with up to 45 psi back pressure applied. There was only a 1.6% decrease in the maximum power density achieved after operation with 45 psi back pressure at 200 ºC, demonstrating the excellent robustness of the dense p-PBI membrane and durability under high temperature and high pressure operation.

The long-term performance of the new membrane was also investigated. The performance of gel p-PBI, gel m/p-PBI and dense p-PBI membranes when operated at a constant current of 0.6 A cm^{-2} for 5000 hours with hydrogen and air is shown in **Figure 4.19**. The gel p-PBI membrane displays a high electrochemical performance, but the performance starts to degrade rapidly at 0.6 A cm^{-2} after approximately 2000 hours. The m/p-PBI membrane exhibited lower initial electrochemical performance, but the performance was more stable, with a degradation rate of 8.1 μV h^{-1}. However, the dense p-PBI membrane was able to achieve high initial electrochemical performance at 0.6 A cm^{-2} as well as stable performance, with a degradation rate of 7.2 μV h^{-1} for more than 4000 hours. These results indicate that the ex-situ properties measured in the dense p-PBI membrane, including high ionic conductivity and low creep, allows for improved cell performance.

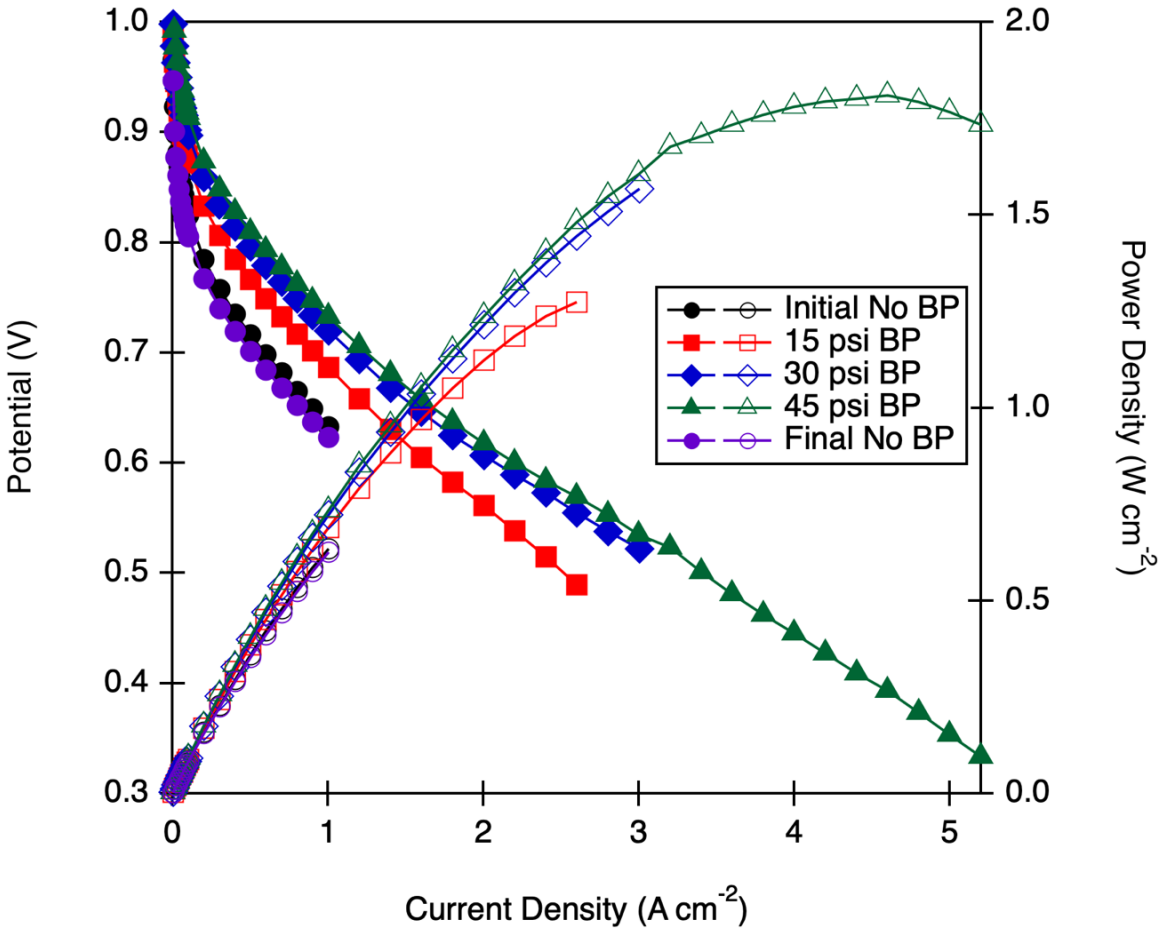

Figure 4.18. Polarization (filled symbols) and power density (unfilled symbols) curves measured at 200 °C for dense p-PBI membrane. H_2/O_2 = 1.2/2.0 stoichiometric flows, no external humidification.

Table 4.13. Potential measured at 0.2 A cm^{-2} and maximum power density for dense p-PBI operated at 200 °C with H_2/O_2 and various back pressures.

	Dense p-PBI Potential @ 0.2 A cm^{-2} (V)	**Dense p-PBI Max Power Density (W cm^{-2})**
No BP Initial	0.785	0.635
15 psi	0.833	1.274
30 psi	0.859	1.568
45 psi	0.874	1.809
No BP Final	0.767	0.625

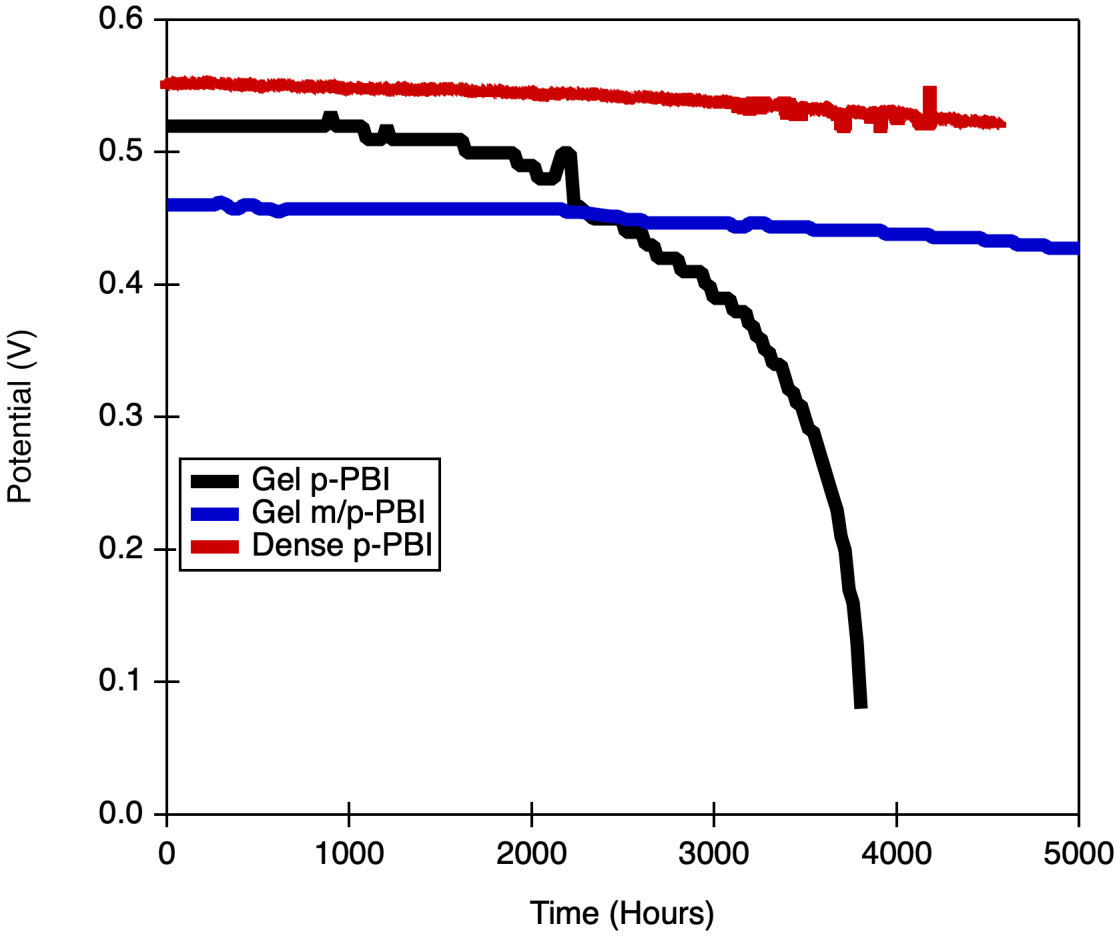

Figure 4.19. Potential measured under constant current of 0.6 A cm^{-2} over a period of 5000 hours for gel p-PBI, gel m/p-PBI and dense p-PBI. Measured at 160 °C, H_2/Air = 1.2/2.0 stoichiometric flows, no external humidification.

4.4.10 Electrochemical Hydrogen Separation Cell Testing

The p-PBI samples were also investigated for their application in electrochemical hydrogen separation. In EHS operation, the polarization curve provides the voltage required from an external power source to pump hydrogen across the membrane. The performance of gel p-PBI and dense p-PBI was investigated using pure hydrogen as a fuel stream at various operating temperatures, as illustrated in **Figure 4.20**. Higher temperature operation should lead to performance improvements due to increased kinetics and faster proton

transport. However, this was not observed for the gel p-PBI membrane. When the temperature was increased from 160 °C to 180 °C, the voltage at each current density was slightly lower, but when the temperature increased again to 200 °C, the voltage was higher than the 160 °C run, meaning more energy was required to pump hydrogen across the membrane. When the temperature is increased, creep thinning occurs and affects the interfacial contact between the membrane and the electrodes, resulting in performance degradation. When the sample was returned to 160 °C, the voltage measured at each current density was higher than the initial 160 °C performance, indicating that permanent membrane degradation had taken place.

The dense p-PBI sample, however, showed improved performance with increasing temperature. The voltage measured at each current density was lower as the temperature increased, which indicates that the membrane with improved creep properties is able to take advantage of faster electrode kinetics and proton transport at higher temperatures. When the temperature was lowered back to 160 °C, the polarization curve was nearly identical to the initial 160 °C curve, indicating that no permanent degradation of the membrane occurred during operation at high temperatures.

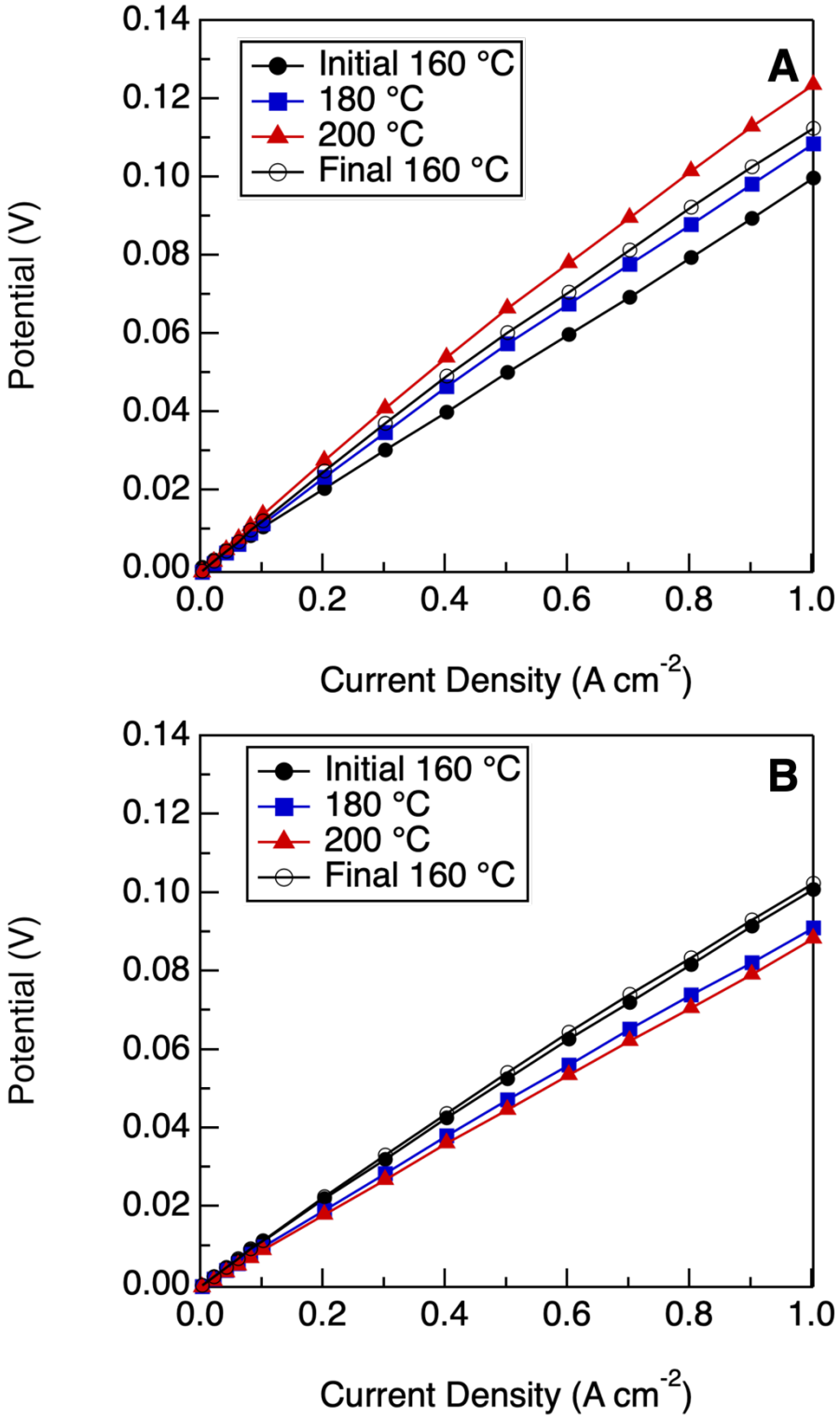

Figure 4.20. EHS polarization curves of A) gel p-PBI membrane and B) dense p-PBI membrane as a function of operating temperature using humidified pure hydrogen with 1.25 stoichiometry and constant RH of 1.6%.

Performance under high differential pressures for long lifetimes is important for current and future industrial hydrogen markets. According to the Nernst equation, a higher pressure at the anode and a lower pressure at the cathode could reduce the voltage and power requirements. In a certain range of current densities, the hydrogen pressure differential applied across the membrane can actually generate power instead of consuming power.

$$E_{required} = E_{polarization} + E_{ohmic} - \frac{RT}{2F} \ln \frac{p_{anode}}{p_{cathode}}$$

The performance of gel p-PBI and dense p-PBI was investigated using pure hydrogen as a fuel stream at various differential pressures, as illustrated in **Figure 4.21**. For the gel p-PBI membrane, when the back pressure on the anode was increased to 30 psi, the performance at low current density was enhanced, however there was no improvement at higher current densities. When the anode back pressure was increased further to 45 psi the performance at higher current densities was lower than without a back pressure differential. When the anode back pressure was removed and the performance without back pressure was tested again, it was found to be lower than the initial performance, with a higher voltage at each current density. This indicates that the gel p-PBI sample undergoes permanent degradation due to membrane creep at high pressure differentials.

The dense p-PBI sample, however, showed improved performance with increasing pressure differentials, up to 45 psi back pressure on the anode. The voltage measured at each current density was lower as the anode back pressure increased. When the anode back pressure was removed and tested again at atmospheric pressures, the polarization curves were nearly identical with the

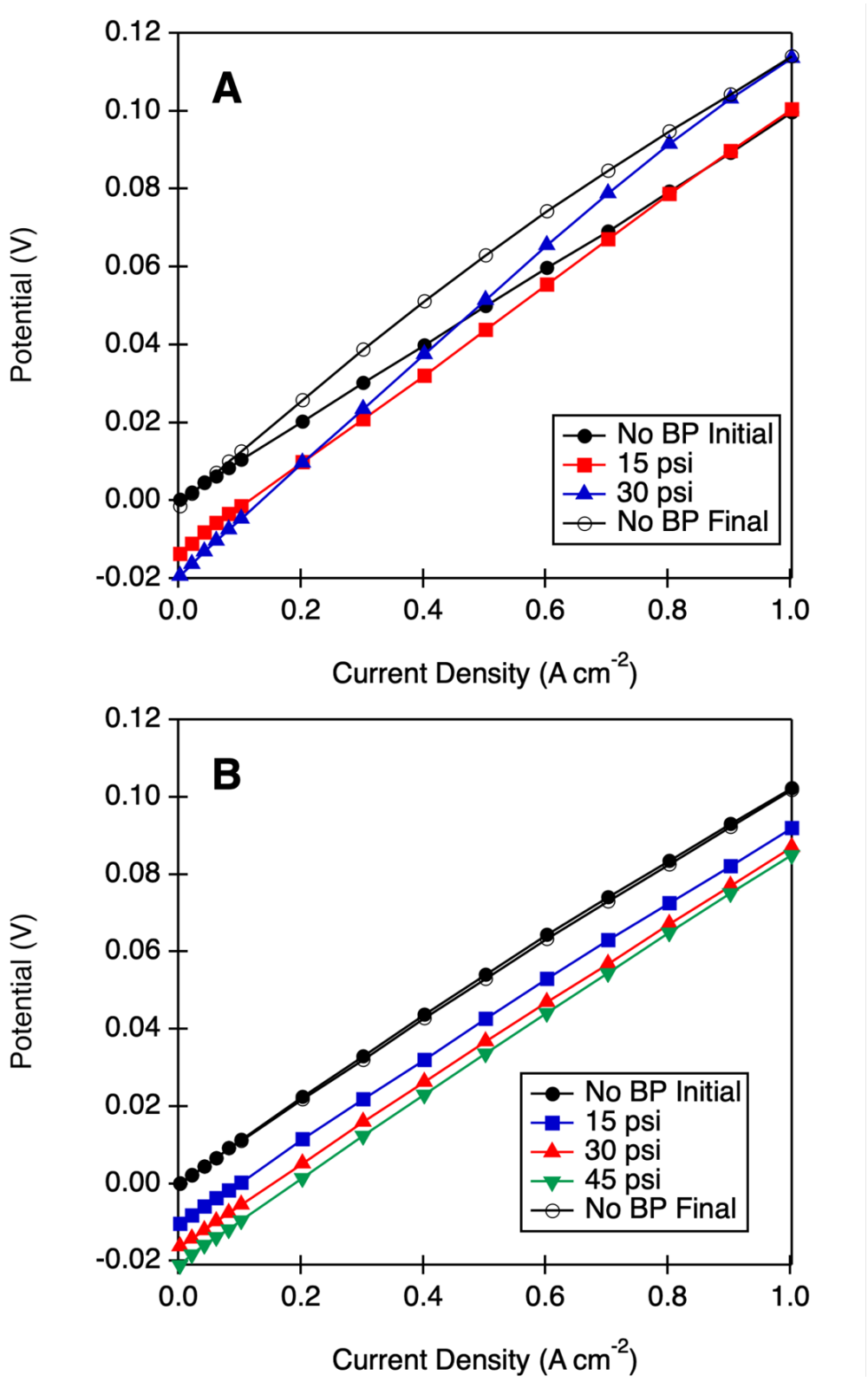

Figure 4.21. EHS polarization curves of A) gel p-PBI membrane and B) dense p-PBI membrane as a function of differential pressures using humidified pure hydrogen with 1.25 stoichiometry and constant RH of 1.6% at 160 °C.

initial curves, indicating that the dense p-PBI membrane can be operated at high differential pressures up to 45 psi without permanent membrane degradation.

4.5 CONCLUSIONS

A novel PPA+ Process was developed in which gel p-PBI membranes produced in the PPA Process were converted into dense PBI films and re-doped in phosphoric acid. The controlled densification that was developed allows gel PBI membranes to collapse almost exclusively in the z-direction to yield dense PBI films with high mechanical properties and a homogeneous thickness. It was found that re-doping the dense p-PBI films in phosphoric acid led to swelling primarily in the z-direction, which indicates some reversibility of the original gel membrane structure.

The effects of the various acid doping conditions on membrane properties were tested and it was determined that an acid doping bath containing 85 wt% phosphoric acid doped for at least 3 hours was needed to attain high doping levels. It was also determined that while increasing the temperature of the acid doping bath led to even higher ionic conductivities, it was not necessary to achieve good fuel cell performance.

Importantly, the PPA+ Process led to PBI membranes that are able to overcome the tradeoff previously encountered between high acid doping and good mechanical properties. By using the existing gel structure created in the PPA Process as a template, the new PBI membranes were able to re-establish high ionic conductivity upon doping in phosphoric acid. The densification also provides a 2x increase in the polymer solids in the p-PBI membrane, which leads to improved

mechanical properties and creep resistance. Cell testing confirmed what was expected based on ex-situ results. In fuel cell testing, the dense p-PBI membranes performed better at higher temperatures and with greater back pressures applied to the membranes, achieving a power density >1.0 W cm^{-2} with H_2/Air at 200 °C and 45 psi back pressure applied to the anode and the cathode. The cell was able to achieve a maximum power density of >1.8 W cm^2 when operated with H_2/O_2 at 200 °C and 45 psi back pressure applied to the anode and cathode. The dense p-PBI membranes also demonstrated excellent long-term (5000 hr) stability at 0.6 A cm^{-2}, with a degradation rate of 7.2 μV h^{-1}. EHS testing revealed that the dense p-PBI samples were more stable at higher temperatures and with a differential backpressure applied. Moreover, the dense p-PBI performance was recoverable under both of these conditions, which indicated that no permanent degradation of the membrane took place. These results demonstrate the utility of the new processing technique in achieving excellent electrochemical performance in HT-PEMFCs and EHS devices.

4.6 REFERENCES

[1] Wainright, J. S.; Wang, J. T.; Weng, D.; Savinell, R. F.; Litt, M. Acid-Doped Polybenzimidazoles: A New Polymer Electrolyte. *Journal of The Electrochemical Society* **1995,** *142* (7), L121-L123.

[2] Jones, D. J.; Rozière, J. Recent advances in the functionalisation of polybenzimidazole and polyetherketone for fuel cell applications. *Journal of Membrane Science* **2001,** *185* (1), 41-58.

[3] Xiao, L.; Zhang, H.; Scanlon, E.; Ramanathan, L. S.; Choe, E.-W.; Rogers, D.; Apple, T.; Benicewicz, B. C. High-Temperature Polybenzimidazole Fuel Cell Membranes via a Sol−Gel Process. *Chemistry of Materials* **2005,** *17* (21), 5328-5333.

[4] Jung, J.; Ku, J.; Park, Y. S.; Ahn, C.-H.; Lee, J.-H.; Hwang, S. S.; Lee, A. S. Advances in Ion Conducting Membranes and Binders for High Temperature Polymer Electrolyte Membrane Fuel Cells. *Polymer Reviews* **2022**, 1-37.

[5] Pingitore, A. T.; Huang, F.; Qian, G.; Benicewicz, B. C. Durable High Polymer Content m/p-Polybenzimidazole Membranes for Extended Lifetime Electrochemical Devices. *ACS Applied Energy Materials* **2019,** *2* (3), 1720-1726.

[6] Molleo, M.; Schmidt, T. J.; Benicewicz, B. C. Polybenzimidazole Fuel Cell Technology. In *Encyclopedia of Sustainability Science and Technology;* Meyers, R. A., Ed.; Springer, 2012; pp 8173-8201. DOI: 10.1007/978-1-4419-0851-3

[7] Perry, K. A.; Eisman, G. A.; Benicewicz, B. C. Electrochemical hydrogen pumping using a high-temperature polybenzimidazole (PBI) membrane. *Journal of Power Sources* **2008,** *177* (2), 478-484.

[8] Fishel, K.; Qian, G.; Eisman, G.; Benicewicz, B. C. Electrochemical Hydrogen Pumping. In *High Temperature Polymer Electrolyte Membrane Fuel Cells*; Li, Q.; Aili, D.; Hjuler, H. A.; Jensen, J. O., Eds.; Springer, 2016; pp 527-540. DOI: 10.1007/978-3-319-17082-4_24

[9] Grigoriev, S.; Shtatniy, I.; Millet, P.; Porembsky, V.; Fateev, V. Description and characterization of an electrochemical hydrogen compressor/concentrator based on solid polymer electrolyte technology. *International Journal of Hydrogen Energy* **2011,** *36* (6), 4148-4155.

[10] Huang, F.; Pingitore, A. T.; Benicewicz, B. C. High Polymer Content m/p-Polybenzimidazole Copolymer Membranes for Electrochemical Hydrogen Separation under Differential Pressures. *Journal of The Electrochemical Society* **2020,** *167* (6), 063504.

[11] Huang, F.; Pingitore, A. T.; Benicewicz, B. C. Electrochemical hydrogen separation from reformate using high-temperature polybenzimidazole (PBI) membranes: the role of chemistry. *ACS Sustainable Chemistry & Engineering* **2020,** *8* (16), 6234-6242.

[12] Vogel, H.; Marvel, C. S. Polybenzimidazoles, new thermally stable polymers. *Journal of Polymer Science* **1961,** *50* (154), 511-539.

[13] Garsany, Y.; Gould, B. D.; Baturina, O. A.; Swider-Lyons, K. E. Comparison of the Sulfur Poisoning of PBI and Nafion PEMFC Cathodes. *Electrochemical and Solid-State Letters* **2009,** *12* (9), B138.

[14] Song, C.; Hui, S.; Zhang, J. High-temperature PEM Fuel Cell Catalysts and Catalyst Layers. In *PEM Fuel Cell Electrocatalysts and Catalyst Layers: Fundamentals and Applications*, Zhang, J., Ed. Springer, 2008; pp 861-888. DOI: 10.1007/978-1-84800-936-3_18

[15] Li, Q.; He, R.; Gao, J.-A.; Jensen, J. O.; Bjerrum, N. J. The CO Poisoning Effect in PEMFCs Operational at Temperatures up to 200°C. *Journal of The Electrochemical Society* **2003,** *150* (12), A1599.

[16] Asensio, J. A.; Sánchez, E. M.; Gómez-Romero, P. Proton-conducting membranes based on benzimidazole polymers for high-temperature PEM fuel cells. A chemical quest. *Chemical Society Reviews* **2010,** *39* (8), 3210-3239.

[17] Bose, S.; Kuila, T.; Nguyen, T. X. H.; Kim, N. H.; Lau, K.-t.; Lee, J. H. Polymer membranes for high temperature proton exchange membrane fuel cell: Recent advances and challenges. *Progress in Polymer Science* **2011,** *36* (6), 813-843.

[18] Chandan, A.; Hattenberger, M.; El-kharouf, A.; Du, S.; Dhir, A.; Self, V.; Pollet, B. G.; Ingram, A.; Bujalski, W. High temperature (HT) polymer electrolyte membrane fuel cells (PEMFC) – A review. *Journal of Power Sources* **2013,** *231*, 264-278.

[19] Clouser, S. J.; Huang, J. C.; Yeager, E. Temperature dependence of the Tafel slope for oxygen reduction on platinum in concentrated phosphoric acid. *Journal of Applied Electrochemistry* **1993,** *23* (6), 597-605.

[20] Zhu, Y.; Zhu, W. H.; Tatarchuk, B. J. Performance comparison between high temperature and traditional proton exchange membrane fuel cell stacks using electrochemical impedance spectroscopy. *Journal of Power Sources* **2014,** *256*, 250-257.

[21] Zhang, C.; Zhang, L.; Zhou, W.; Wang, Y.; Chan, S. H. Investigation of water transport and its effect on performance of high-temperature PEM fuel cells. *Electrochimica Acta* **2014,** *149*, 271-277.

[22] He, R.; Li, Q.; Xiao, G.; Bjerrum, N. J. Proton conductivity of phosphoric acid doped polybenzimidazole and its composites with inorganic proton conductors. *Journal of Membrane Science* **2003,** *226* (1), 169-184.

[23] Kim, H.-J.; Lim, T.-H. PBI Derivatives: Polymer Electrolyte Fuel Cell Membrane for High Temperature Operation. *Journal of Industrial and Engineering Chemistry* **2004,** *10* (7), 1081-1085.

[24] Samms, S. R.; Wasmus, S.; Savinell, R. F. Thermal Stability of Proton Conducting Acid Doped Polybenzimidazole in Simulated Fuel Cell Environments. *Journal of The Electrochemical Society* **1996,** *143* (4), 1225-1232.

[25] Kerres, J.; Ullrich, A.; Meier, F.; Häring, T. Synthesis and characterization of novel acid–base polymer blends for application in membrane fuel cells. *Solid State Ionics* **1999,** *125* (1), 243-249.

[26] Cassidy, P. E. Polybenzimidazoles. In *Thermally Stable Polymers, Synthsis and Properties*; Marcel Dekker, 1980; pp 163-173.

[27] Ma, Y. L.; Wainright, J. S.; Litt, M. H.; Savinell, R. F. Conductivity of PBI Membranes for High-Temperature Polymer Electrolyte Fuel Cells. *Journal of The Electrochemical Society* **2004,** *151* (1), A8.

[28] Bouchet, R.; Siebert, E. Proton conduction in acid doped polybenzimidazole. *Solid State Ionics* **1999,** *118* (3), 287-299.

[29] Mekhilef, S.; Saidur, R.; Safari, A. Comparative study of different fuel cell technologies. *Renewable and Sustainable Energy Reviews* **2012,** *16* (1), 981-989.

[30] Zeis, R. Materials and characterization techniques for high-temperature polymer electrolyte membrane fuel cells. *Beilstein Journal of Nanotechnology* **2015,** *6*, 68-83.

[31] Olsthoorn, X. Carbon dioxide emissions from international aviation: 1950–2050. *Journal of Air Transport Management* **2001,** *7* (2), 87-93.

[32] Çabukoglu, E.; Georges, G.; Küng, L.; Pareschi, G.; Boulouchos, K. Battery electric propulsion: An option for heavy-duty vehicles? Results from a Swiss case-study. *Transportation Research Part C: Emerging Technologies* **2018,** *88*, 107-123.

[33] Zhang, L.; Brown, T.; Samuelsen, S. Evaluation of charging infrastructure requirements and operating costs for plug-in electric vehicles. *Journal of Power Sources* **2013,** *240*, 515-524.

[34] Forrest, K.; Mac Kinnon, M.; Tarroja, B.; Samuelsen, S. Estimating the technical feasibility of fuel cell and battery electric vehicles for the medium and heavy duty sectors in California. *Applied Energy* **2020,** *276*, 115439.

[35] Waiblinger, W.; Kallo, J.; Schirmer, J.; Friedrich, K. A. High Temperature Polymer Electrolyte Fuel Cell Systems for Aircraft Applications. In *High Temperature Polymer Electrolyte Membrane Fuel Cells;* Li, Q.; Aili, D.; Hjuler, H. A.; Jensen, J. O., Eds. Springer, 2016; pp 511-525. DOI: 10.1007/978-3-319-17082-4_23

[36] Rosli, R. E.; Sulong, A. B.; Daud, W. R. W.; Zulkifley, M. A.; Husaini, T.; Rosli, M. I.; Majlan, E. H.; Haque, M. A. A review of high-temperature proton exchange membrane fuel cell (HT-PEMFC) system. *International Journal of Hydrogen Energy* **2017,** *42* (14), 9293-9314.

[37] Maget, H. J. R. Process for Gas Purification. U.S. Patent #3,489,670. January 13, 1970.

[38] Aili, D.; Jensen, J. O.; Li, Q. Polybenzimidazole Membranes by Post Acid Doping. In *High Temperature Polymer Electrolyte Membrane Fuel Cell*s; Li, Q.; Aili, D.; Hjuler, H. A.; Jensen, J. O., Eds. Springer, 2016; pp 195-215. DOI: 10.1007/978-3-319-17082-4_9

[39] Mader, J.; Xiao, L.; Schmidt, T. J.; Benicewicz, B. C. Polybenzimidazole/Acid Complexes as High-Temperature Membranes. In *Fuel Cells II: Advances in Polymer Science,* Vol. 216; Scherer, G. G., Ed.; Springer, 2008; pp 63-124. DOI: 10.1007/12_2007_129

[40] He, R.; Li, Q.; Bach, A.; Jensen, J. O.; Bjerrum, N. J. Physicochemical properties of phosphoric acid doped polybenzimidazole membranes for fuel cells. *Journal of Membrane Science* **2006,** *277* (1-2), 38-45.

[41] Flory, P. J. Introductory lecture. *Faraday Discussions of the Chemical Society* **1974,** *57* (0), 7-18.

[42] Chen, X.; Qian, G.; Molleo, M. A.; Benicewicz, B. C.; Ploehn, H. J. High temperature creep behavior of phosphoric acid-polybenzimidazole gel membranes. *Journal of Polymer Science Part B: Polymer Physics* **2015,** *53* (21), 1527-1538.

[43] Graessley, W. W. *Polymeric Liquids and Networks: Structure and Properties*, 1st ed.; Garland Science, 2003. DOI: 10.4324/9780203506127

[44] Molleo, M.; Chen, X.; Ploehn, H. J.; Fishel, K.; Benicewicz, B. C. High Polymer Content 3, 5-Pyridine-Polybenzimidazole Copolymer Membranes with Improved Compressive Properties. *Fuel Cells* **2014,** *14* (1), 16-25.

[45] Molleo, M.; Chen, X.; Ploehn, H. J.; Benicewicz, B. C. High Polymer Content 2, 5-Pyridine-Polybenzimidazole Copolymer Membranes with Improved Compressive Properties. *Fuel Cells* **2015,** *15* (1), 150-155.

[46] Yu, S.; Zhang, H.; Xiao, L.; Choe, E.-W.; Benicewicz, B. C. Synthesis of Poly (2,2′-(1,4-phenylene) 5,5′-bibenzimidazole) (para-PBI) and Phosphoric Acid Doped Membrane for Fuel Cells. *Fuel Cells* **2009,** *9* (4), 318-324.

[47] Chin, D.-T.; Chang, H. H. On the conductivity of phosphoric acid electrolyte. *Journal of Applied Electrochemistry* **1989,** *19* (1), 95-99.

[48] Aili, D.; Allward, T.; Alfaro, S. M.; Hartmann-Thompson, C.; Steenberg, T.; Hjuler, H. A.; Li, Q.; Jensen, J. O.; Stark, E. J. Polybenzimidazole and sulfonated polyhedral oligosilsesquioxane composite membranes for high temperature polymer electrolyte membrane fuel cells. *Electrochimica Acta* **2014,** *140*, 182-190.

[49] Springer, T. E.; Rockward, T.; Zawodzinski, T. A.; Gottesfeld, S. Model for polymer electrolyte fuel cell operation on reformate feed: effects of CO, H_2 dilution, and high fuel utilization. *Journal of the Electrochemical Society* **2001,** *148* (1), A1.

[50] *Fuel Cell Handbook (Sixth Edition)*; EG&G Technical Services, Inc. Science Applications International Corporation, 2002.

CHAPTER 5

NOVEL SULFONATED POLYBENZIMIDAZOLE COPOLYMERS FOR USE IN ELECTROCHEMICAL DEVICES

5.1 ABSTRACT

Novel copolymers of meta-polybenzimidazole (PBI) and sulfonated meta-PBI were synthesized with various copolymer compositions. Copolymerization was further optimized by investigating various monomer charges. The copolymer series was characterized and studied for their application in high temperature polymer electrolyte membrane fuel cells (HT-PEMFCs) and vanadium redox flow batteries (VRBs). Previous work demonstrated that meta-oriented PBIs are more soluble in PPA and allow for a higher solids content within the membrane. Thus, meta-oriented PBIs can provide mechanical enhancement needed for HT-PEMFC performance and to reduce vanadium permeability for VRB applications. The copolymer series was investigated to determine if higher solids content and high ionic conductivity could be achieved. The membranes were evaluated for HT-PEM applications using acid content, conductivity, and creep resistance, as well as fuel cell performance. The membranes were also evaluated for application in VRBs using acid content, ionic conductivity, and vanadium permeability.

5.2 INTRODUCTION

An increasing demand for green energy solutions has led to the development of new electrochemical devices to meet these needs. Polymer electrolyte membranes (PEMs) are utilized in many of these applications and represent an important area that needs to be developed in order to meet our energy needs.[1] Two of these applications include hydrogen fuel cells and vanadium redox flow batteries (VRBs). Sulfonated polybenzimidazoles (s-PBIs) were been previously investigated for their application in electrochemical devices including

high temperature polymer electrolyte membrane fuel cells (HT-PEMFCs) and VRBs.[2-6] PBIs are well known for their high temperature stability, chemical resistance, and excellent oxidative stability.[7] Sulfonated PBIs can provide higher acid doping levels and ionic conductivities than non-functionalized PBIs.[2, 5]

Fuel cells convert the chemical energy of a fuel, such as hydrogen into chemical energy using electrochemical reactions. Thus, fuel cells are used to generate electricity. HT-PEMFCs are operated from 120-200 °C and rely on a polymer membrane, most commonly PBI, doped in phosphoric acid. High temperature fuel cell operation provides certain benefits including fast electrode kinetics, enhanced tolerance to fuel impurities, and simplified water/heat management.[8-17] For this type of application, a membrane must display great thermal stability, high ionic conductivity, low gas permeability, and excellent durability during cell operation at long lifetimes.

VRBs are rechargeable, all liquid batteries for application in large-scale energy storage.[18] VRBs utilize the four oxidation states of vanadium (V^{2+}, V^{3+}, V^{4+}, and V^{5+}) to convert between chemical energy and electrical energy to charge and discharge the battery. The vanadium redox couples (2+/3+ and 4+/5+) are dissolved in a supporting electrolyte of sulfuric acid, and stored in tanks separated by the cell stack at the center.[19] Oxidation or reduction reactions of the active vanadium species allows the battery to undergo charge-discharge processes through conversion of chemical and electrical energy.[20] The VRB is a great candidate for large scale energy storage devices due to their liberation from energy and power rankings, active thermal management, and longevity.[21, 22] VRBs contain a polymer membrane in the cell stack which is responsible for proton conduction

and limiting vanadium crossover. Thus, membranes candidates for VRBs must display high ionic conductivity, low vanadium permeability, excellent resistance to the oxidative V^{5+} species, and long-term durability.

PBI membranes have been prepared by a few different methods. The most common method is called the "conventional imbibing process" where PBI is dissolved in an organic solvent, such as N,N'-dimethylacetamide (DMAc) to form a dense PBI film that is then imbibed in the selected electrolyte.[23] In 2005, Xiao et al. reported a one-pot method to polymerize PBI and form membranes, termed the Polyphosphoric acid (PPA) Process.[24] In the PPA Process, PBI is polymerized in PPA and the solution is cast directly onto a substrate. Exposure to moisture induces a sol-to-gel phase transition and subsequent formation of gel PBI membranes that are highly swollen in phosphoric acid.

In HT-PEMFC applications, membranes produced in the PPA Process have displayed superior acid doping levels, and higher ionic conductivities than PBI membranes prepared in the conventional imbibing process.[25] However, gel PBIs produced in the PPA Process have a very low solids content, and high liquid content (water + acid). Thus, during long-term fuel cell testing, degradation occurs due to a low creep resistance of the low solids gel PBI.[26]

Application of PBIs in VRBs has been more recently investigated. Most of the publications on PBIs in VRBs utilize PBIs prepared by the conventional imbibing process. Conventionally imbibed PBIs have a small pore size of 0.5 to 2.0 nm, which provides very low permeability of vanadium ions.[27] However, the smaller pore size and reduced interstitial space also provides very low ionic

conductivities for the conventionally imbibed PBIs (<20 mS cm^{-1}). [28] Thus, there is a trade-off between the ionic conductivity and vanadium permeability in these PBIs.

There has only been one report on gel PBI membranes produced in the PPA Process applied to VRBs.[2] In this report, sulfonated para-orientated gel PBIs with a sulfonic acid group attached to the backbone were prepared using the PPA Process and terephthalic acid monomer with a sulfonic acid group attached to the aromatic ring. The membrane underwent acid switching from phosphoric acid to sulfuric acid for application in VRBs. While the gel PBI membrane, containing a more porous and open structure, was significantly better at conducting protons (ionic conductivities of about 593 mS cm^{-1}), the vanadium permeability was also much higher.

In the current work, a series of meta-oriented PBI copolymers composed of various ratios of unfunctionalized monomers and monomers functionalized with sulfonic acid, were produced in the PPA Process. The meta-orientated PBIs display greater solubility in PPA than para-oriented PBIs, and thus a higher solids content of the resulting membrane was achieved. The greater solids content and incorporation of sulfonic acid in the backbone led to enhanced creep resistance and high ionic conductivities for HT-PEMFC applications. In VRB applications, the higher solids content of the meta-oriented sulfonated copolymer gel PBI membranes led to reduced vanadium permeability, while maintaining relatively high ionic conductivity. In this report, various copolymer were prepared with different monomer charges, as well as various compositions of meta-PBI and

sulfonated meta-PBI to investigate the effects of copolymer composition and polymer solids content on membrane properties for both applications.

5.3 EXPERIMENTAL

5.3.1 Materials

Isophthalic acid (IPA, >99% purity) was purchased from Amoco, 5-sulfoisophthalic acid monosodium salt (5S-IPA, >98% purity) was purchased from TCI America, and 3,3',4,4'-tetraaminobiphenyl (TAB, polymer grade, ~97.5%) was kindly donated by BASF Fuel Cell, Inc. Poly(phosphoric acid) (PPA, 115%) was purchased from Innophos, vanadium (IV) sulfate hydrate was purchased from BeanTown Chemicals, and technical grade sulfuric acid was purchased from Fisher Chemical. All chemicals and reagents were used as received without further purification.

5.3.2 Polymer Synthesis and Membrane Fabrication

Polymerizations were conducted by charging a reaction kettle with the desired amount of monomers and PPA, as shown **in Figure 5.1**. For example, in the polymerization of 50 *m*-PBI/50 s*m*-PBI at 8 wt% monomer concentration, 5.0599 g (27.82 mmol) TAB, 2.3104 g (13.91 mmol) IPA, and 3.7297 g (13.91 mmol) 5S-IPA were added to a reaction kettle in a nitrogen atmosphere glove box. Once removed from the glove box, 138 g PPA was added to the kettle. The reaction kettle was equipped with a nitrogen inlet, outlet, and overhead mechanical stirrer with a glass stir shaft. Reactions were started at room temperature with a stir speed of 60 rpm, and heated following a heat/soak profile. This was adjusted slightly for each polymerization by monitoring the viscosity. Polymerizations were cast

immediately onto glass substrates and placed into a controlled humidity chamber set to 55% RH for 24 hours.

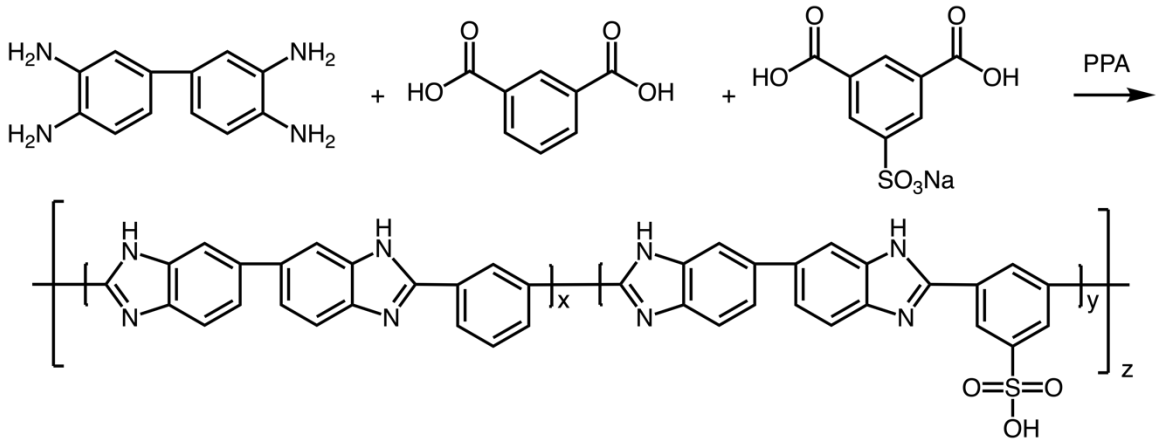

Figure 5.1. Polymerization scheme for copolymers of meta-PBI and sulfonated meta-PBI.

5.3.3 Inherent Viscosity

The viscosity of a solution describes its resistance to flow, which is dependent on solvent, polymer, molecular weight of the sample, temperature, and pressure. Inherent viscosity (IV) measurements were obtained for PBI by isolating a small amount of polymer in water. Then the sample was pulverized and neutralized with concentrated ammonium hydroxide. Polymer pieces were isolated and the sample was washed with distilled water to remove any salts and ensure neutrality. After vacuum drying, the polymer samples were dissolved in concentrated sulfuric acid to achieve a concentration of ~0.2 g dL^{-1}. The solution was pushed through a 0.45 μm syringe filter into a 200 μm Ubbelohde viscometer, which was placed in a water bath set at 30 °C for 30 minutes for the temperature to equilibrate. The flow time was measured and recorded for three runs. A control

flow time was also measured and recorded three times using pristine concentrated sulfuric acid. The average flow time obtained for the sample was compared to the average flow time of the control using the following equation to calculate the inherent viscosity:

$$\eta_{inh} = \frac{\ln\left(t/t_o\right)}{c}$$

Where t was the sample flow time (s), t_o was the control flow time (s), c was the concentration of polymer sample dissolved in sulfuric acid (g dL^{-1}), and η_{inh} was the calculated inherent viscosity (dL g^{-1}). Typically, inherent viscosity can be used in the Mark-Houwink equation to determine molecular weight. However, PBI is not a typical polymer and normal characterization techniques are limited due to polymer solubility restrictions. IVs are commonly reported in PBI literature, typically an IV greater than 1.0 dL g^{-1} is considered to be high molecular weight.

5.3.4 Elemental Analysis

Polymer samples were pulverized and neutralized with ammonium hydroxide. After washing with water and drying in vacuo, samples were sent to Midwest Microlabs to conduct elemental analysis.

5.3.5 Membrane Composition

There are three components in acid-doped PBI membranes: acid, water, and polymer. The relative amount of each were determined through titration. A small membrane sample was isolated using a hole puncher and weighed out in a beaker. After adding ~50 mL of deionized water, the beaker was covered in parafilm and

stirred at room temperature overnight. Mixtures were then titrated with a standard 0.1 N sodium hydroxide solution using a Metrohm® 888 DMS Titrando autotitrator. After titration, the samples were washed with deionized water and dried in vacuo at 120 °C overnight. The dried sample was reweighed to obtain dry polymer weight. The phosphoric acid (PA) or sulfuric acid (SA) doping level *X*, was calculated according to the following equations:

$$PA\ X = \frac{V_{NaOH} \cdot C_{NaOH}}{W_{dry}/_{PRU}}$$

$$SA\ X = \frac{V_{NaOH} \cdot C_{NaOH}}{2 \cdot \left(W_{dry}/_{PRU}\right)}$$

Where V_{NaOH} and C_{NaOH} were the volume (L) and concentration (mol L^{-1}) of sodium hydroxide needed to neutralize the phosphoric or sulfuric acid, W_{dry} was the weight (g) of the dried polymer sample after titration, and *PRU* was the molecular weight (g mol^{-1}) of the polymer repeat unit. The average molecular weight of the repeat unit was calculated based on the molar ratios in which each polymerization was conducted. The polymer weight percent was calculated using the following equation:

$$Polymer\ wt\% = \frac{W_{dry}}{W_{membrane}} \cdot 100$$

Where W_{dry} was the weight of the dried polymer sample after titration, and $W_{membrane}$ was the weight of the polymer sample before titration. The acid weight percent for phosphoric acid (*PA wt%*) and sulfuric acid (*SA wt%*), respectively, was then calculated as shown:

$$PA\ wt\% = \frac{V_{NaOH} \cdot C_{NaOH} \cdot MW_{acid}}{W_{membrane}} \cdot 100$$

$$SA\ wt\% = \frac{V_{NaOH} \cdot C_{NaOH} \cdot MW_{acid}}{2 \cdot W_{membrane}} \cdot 100$$

In phosphoric acid doped PBI, the first equivalence point was used in calculations, while in sulfuric acid doped PBI, the second equivalence point was used.

5.3.6 Through-Plane Ionic Conductivity

Through-plane proton conductivity was measured with a four-probe electrochemical impedance spectroscopy method using a Zahner IM6e electrochemical workstation in the frequency range of 1 Hz to 100 KHz and an amplitude of 5 mV. The experimental data was fit using a two-component model with an ohmic resistance in parallel with a capacitor. The membrane resistance was obtained from the model simulation and used to calculate the membrane conductivity (σ) at different temperatures with the following equation:

$$\sigma = \frac{d}{l \cdot w \cdot R_m}$$

Where d was the distance between inner probes, l was the thickness of the membrane, w was the width of the membrane, and R_m was the ohmic resistance obtained by model fitting. Samples underwent heating ramps to 180 °C twice. The first was to remove water from the membrane, and the second was to obtain anhydrous ionic conductivity results.

5.3.7 Compression Creep and Creep Recovery

A TA RSA III dynamic mechanical analyzer with built-in in functionality was used to measure the time-dependent compression creep behavior. Testing occurred in two phases (1) a 20 hour creep phase, where a constant compressive force equivalent to 0.1 MPa was applied to the sample and (2) a 3 hour recovery phase, where the force was removed and the recovery was measured. Each experiment was conducted at 180 °C in a temperature-controlled oven with dry air circulation.

5.3.8 MEA Fabrication and Fuel Cell Testing

Single cells with an active area of 45.15 cm^2 were used to measure the performance of the PBI membranes in HT-PEMFCs. Membrane electrode assemblies (MEAs) were fabricated by hot-pressing the membranes between the anode and cathode electrodes at 150 °C for 45 seconds using 4500 lbs of force and compressing to 75-80% its original thickness. Electrodes were received from BASF Fuel Cell, Inc. and contained 1.0 mg cm^{-2} Pt/C on the anode and 1.0 mg cm^{-2} Pt/C alloy on the cathode. Fuel cells were assembled with gaskets to compress the MEA 20-25%. The cells were controlled by stations assembled by Fuel Cell Technologies. The fuel cells were broken-in for 24 hours at 160 ºC and 0.2 A cm^{-2} with hydrogen and air. Polarization curves were obtained at 160 ºC with 1.2 stoichiometric flow of H_2 with a minimum flow rate of 75 sccm, and 2.0 stoichiometric flow of air with a minimum flow rate of 300 sccm. Break-in and polarization curves were conducted under non-humidified conditions.

5.3.9 Acid Exchange

Phosphoric acid doped PBI membranes synthesized in the PPA Process needed to be doped in a 2.6 M sulfuric acid solution for further characterization as VRB membranes. This was achieved by first soaking the phosphoric acid doped membranes in deionized water baths. The water was exchanged every couple hours while monitoring the acidity with pH strips until a pH of 7 was observed. Acid-free membranes were then placed in a 2.6 M sulfuric acid bath for at least 24 hours to ensure equilibrium of acid doping was reached.

5.3.10 In-Plane Ionic Conductivity

After acid exchange, in-plane conductivity was measured using a four-probe electrochemical impedance spectroscopy (EIS) method. A FuelCon (TrueData EIS PCM) electrochemical workstation was used over a frequency range of 1 Hz to 50 kHz. Samples were cut to be roughly 1.0 cm x 4.0 cm and placed in the 4-electrode sample holder. Conductivity (σ) was calculated using the following equation:

$$\sigma = \frac{d}{l \cdot w \cdot R_m}$$

Where d was the distance between the two inner probes, l was the thickness of the membrane, w was the width of the membrane, and R_m was the ohmic resistance determined by the model fitting. In-plane conductivity measurements were conducted at room temperature.

5.3.11 Vanadium Permeability

The vanadium ($VOSO_4$) permeability was measured for each sample with using a PermeGear "side-by-side" direct permeation cell. The cell contained two chambers, each with a volume of 45 mL separated by the membrane under test. A recirculating water bath regulated the temperature during testing to 25 °C. In each experiment, 1.5 M $VOSO_4$ in 2.6 M sulfuric acid was added to the donor chamber and 1.5 M $MgSO_4$ in 2.6 M sulfuric acid was added to the receptor chamber. Vanadium (IV) displays a strong UV absorption characteristic at 248 nm, thus the concentration of the receptor chamber was measured with a Shimadzu UV-2450 UV/Vis spectrometer at various time intervals. The VO^{2+} permeability was calculated using Fick's law of diffusion:

$$P_s t = \ln\left[1 - 2\frac{c_r(t)}{c_r(0)}\right]\left[-\frac{V_d}{A}\right]$$

Where $c_r(0)$ was the initial concentration of $VOSO_4$ in the donor chamber, V was the volume of solution added to each chamber, d was the membrane thickness, A was the active area of the membrane, $c_r(t)$ was the concentration of $VOSO_4$ in the receptor chamber at time t, and P_s was the calculated salt permeability.

5.4 RESULTS AND DISCUSSION

5.4.1 Polymer Synthesis and Membrane Fabrication

The investigation began by polymerizing various copolymer compositions with an overall monomer charge of 8 wt%, as displayed in **Table 5.1** and **Figure 5.2**. A small addition of sulfonated dicarboxylic acid (DCA) monomer content (20 wt%) led to lower IV measurements. However, when the composition of the

Table 5.1. Copolymerizations carried out at 8 wt% monomer charge.

Notebook #	IPA (molar % of DCA)	5S-IPA (molar % of DCA)	Monomer charge (wt%)	IV (dL g^{-1})
LM1-010	100	0	8	1.02
LM1-011	100	0	8	1.03
LM1-023	80	20	8	0.90
LM1-033	60	40	8	1.64
LM1-027	60	40	8	1.05
LM1-019	50	50	8	0.88
LM1-021	40	60	8	0.45
LM1-025	20	80	8	0.48

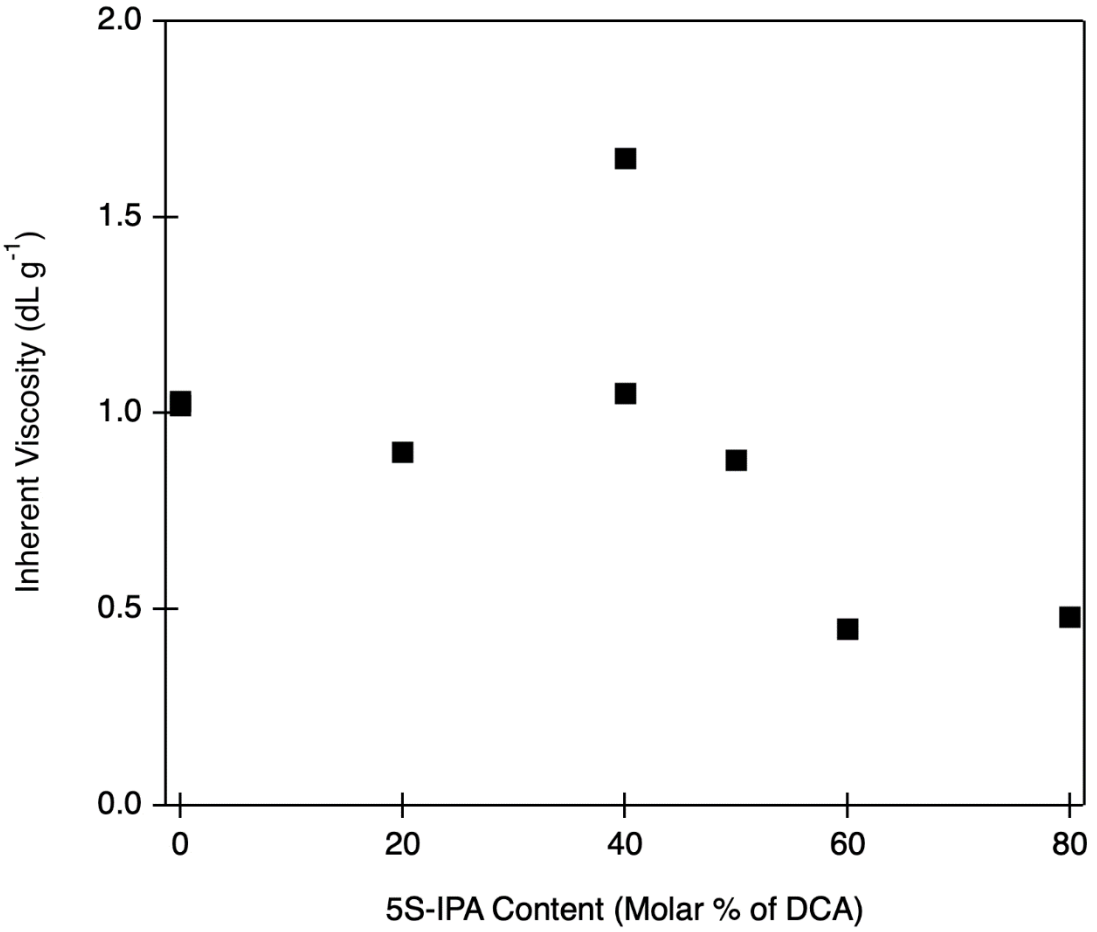

Figure 5.2. IV's of various compositions of m/sm-PBI copolymers, polymerized with an 8 wt% monomer charge.

sulfonated monomer increased further, to 40 and 50 wt%, the inherent viscosity increased. When the sulfonated monomer content was increased further, the inherent viscosities dropped rapidly. Although the 100 m/0 sm-PBI polymerization displayed an IV that was over 1.0 dL g^{-1}, the membrane formed from this polymer was not mechanically strong enough to be handled. However, the membranes of 60 m/40 sm-PBI and 50 m/50 sm-PBI polymerized with a monomer charge of 8 wt% were mechanically strong enough to be handled and further examined.

The monomer charge of the polymerizations was increased to 9 wt% and the copolymers listed in **Table 5.2** were synthesized, with IV data shown in **Figure 5.3**. The 100 m/0 sm-PBI sample displayed a higher IV when polymerized with a monomer charge of 9 wt% than with a monomer charge of 8 wt%. The same general trend was observed for the various copolymers polymerized with a 9 wt% monomer charge and 8 wt% monomer charge. Initially, a small addition of sulfonated monomer content led to a lower IV. However, when the compositions of sulfonated monomer were increased further to 40 and 50 wt%, the IV increased. Polymerizations of 0 m/100 sm-PBI were unsuccessful and led to very low IVs.

The m/sm-PBI composition containing 50 wt% IPA and 50 wt% 5S-IPA produced high IV's and was studied further by polymerizing at different monomer charges, as shown in **Table 5.3** and **Figure 5.4**. As the monomer charge increased from 8 wt% to 9 wt%, the IV increased. However, IV's decreased when the monomer charge was further increased to 10 and 12 wt%. This indicated that the solubility limit had been reached at a monomer charge of 9 roughly wt%. This

Table 5.2. Copolymerizations carried out at 9 wt% monomer charge.

Notebook #	IPA (molar % of DCA)	5S-IPA (molar % of DCA)	Monomer charge (wt%)	IV (dL g^{-1})
LM1-029	100	0	9	1.2
LM1-039	80	20	9	0.71
LM1-035	60	40	9	0.90
LM1-058	60	40	9	1.45
LM1-031	50	50	9	1.19
LM1-043	50	50	9	1.04
LM1-048	50	50	9	1.15
LM1-051	50	50	9	1.06
LM1-054	50	50	9	1.3
LM1-064	50	50	9	1.25
LM1-078	0	100	9	0.21

was supported by the observations of the reaction medium becoming very viscous and the complete loss of stirring at the highest monomer charge of 12 wt%.

The copolymerization of 50 m/50 sm-PBI with a monomer charge of 9 wt% was further studied to investigate monomer reactivity and determine how the monomers were being incorporated. Four copolymerizations (**Table 5.4**) were conducted and stopped at various times**.** Each copolymer was isolated, neutralized, and tested for IV as well as sulfur content using elemental analysis. As the polymerization progressed, the sulfur content measured in the PBI samples decreased. This indicated that there was some compositional drift during polymerization, and the sulfonated monomer was more reactive and preferentially incorporated earlier in the polymerization.

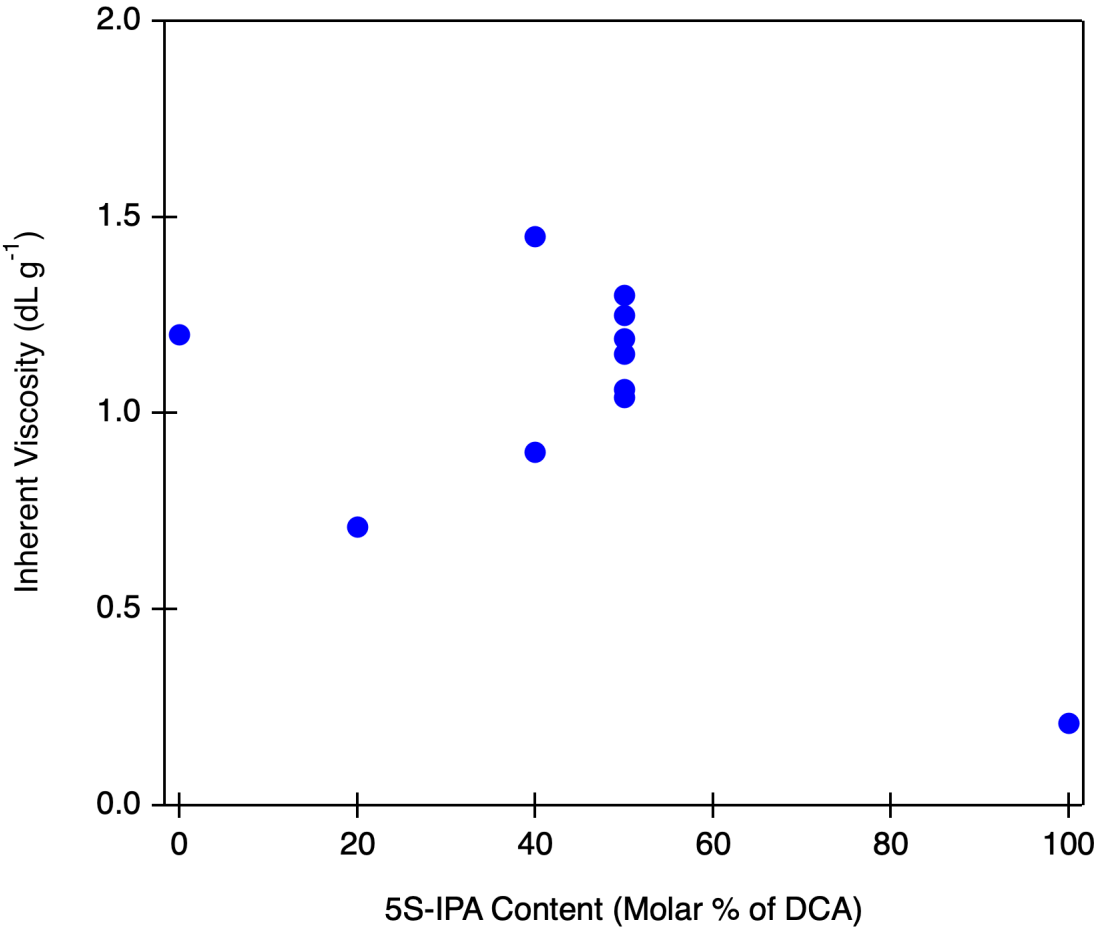

Figure 5.3. IV's of various compositions of m/sm-PBI copolymers, polymerized with an 9 wt% monomer charge.

Table 5.3. Polymerizations of 50 molar % IPA, 50 molar % 5S-IPA with various monomer charges.

Notebook #	IPA (molar % of DCA)	5S-IPA (molar % of DCA)	Monomer charge (wt%)	IV (dL g^{-1})
LM1-019	50	50	8	0.88
LM1-090	50	50	8.5	1.02
LM1-031	50	50	9	1.19
LM1-043	50	50	9	1.04
LM1-048	50	50	9	1.15
LM1-051	50	50	9	1.06
LM1-054	50	50	9	1.3
LM1-064	50	50	9	1.25
LM1-095	50	50	10	0.89
LM1-37	50	50	12	0.69

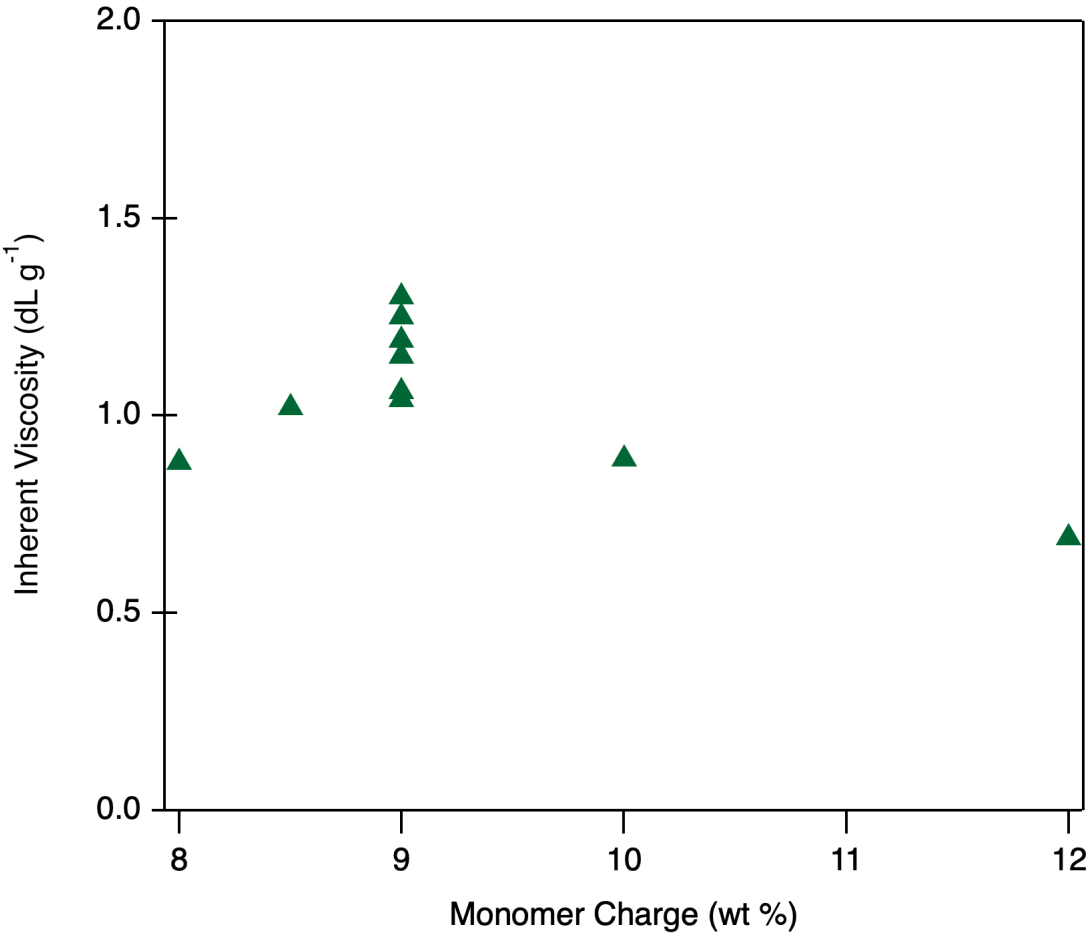

Figure 5.4. Polymerizations of 50 molar % IPA, 50 molar % 5S-IPA at various monomer charges.

Table 5.4. Polymerization of 50 m/50 sm-PBI copolymers, 9 wt% monomer charge, stopped at various times, data includes IV's and S% from elemental.

Notebook #	Total time (h)	Time at 190° C (h)	IV (dL g^{-1})	S (element %)
LM1-073	8	1	0.33	3.04
LM1-072	9	2	0.26	3.09
LM1-070	11	4	0.47	2.41
LM1-071	15	8	0.45	1.86

5.4.2 Characterization for Fuel Cell Applications

The copolymer membranes that displayed enough mechanical integrity to handle were titrated to determine the acid doping level and composition of each copolymer (**Table 5.5**). Each PBI sample contained polymer solids content of at least 13 wt%. It was generally found that increasing the sulfonated monomer content led to higher acid doping levels. At 8 wt% monomer charge, increasing the sulfonated monomer content from 60 m/40 sm-PBI to 50 m/50 sm-PBI led to an almost 2x increase in the acid doping levels measured. At 9 wt% monomer charge, increasing the sulfonated monomer content from 100 m/0 sm-PBI up to 50 m/50 sm-PBI led to a 33% increase in the acid doping level measured. There appeared to be an anomaly with the 50 m/50 sm-PBI sample polymerized with a monomer charge of 8.5 wt%, as it had a lower acid doping level than the same composition polymerized at higher and lower monomer charges.

Table 5.5. Acid doping level and membrane composition of phosphoric acid imbibed PBI membranes.

Composition	Monomer Charge (wt%)	Acid Doping Level (PA/PRU)	PA Content (wt%)	PBI Content (wt%)	Water Content (wt%)
60 m/40 sm	8	7.84 ± 1.8	34.5 ± 7.4	15.3 ± 0.34	50.2 ± 7.0
50 m/50 sm	8	17.7 ± 0.69	68.5 ± 0.49	13.8 ± 0.47	17.7 ± 0.41
50 m/50 sm	8.5	10.9 ± 0.81	50.3 ± 2.8	16.4 ± 0.32	33.3 ± 2.5
100 m/0 sm	9	11.6 ± 0.21	62.6 ± 1.3	16.9 ± 0.06	20.4 ± 1.4
60 m/40 sm	9	14.0 ± 0.08	60.0 ± 2.8	14.9 ± 0.60	25.1 ± 3.4
50 m/50 sm	9	15.4 ± 0.20	65.1 ± 0.70	15.1 ± 0.07	19.8 ± 0.67

The data in **Figure 5.5** show the anhydrous ionic conductivity measured for the copolymer membranes from room temperature to 180 °C. Although the ionic conductivities were measured during the second run when all of the water should have been removed, the samples containing some content of sulfonated PBI showed a drop in ionic conductivity when the temperature reached 100 °C. This indicates that either the water was not fully removed after the first run, or that some water was absorbed by the sulfonic acid groups between the two runs. The membranes that were polymerized with the 60 m/40 sm-PBI composition showed the lowest ionic conductivity at 180 °C. The 100 m/0 sm-PBI exhibited a high ionic conductivity of 152 mS cm^{-1}. The 50 m/50 sm-PBIs with a monomer charge of 8.5 and 9 wt% had a higher ionic conductivity than the 100 m/0 sm-PBI. The 50 m/50 sm-PBI with a monomer charge of 9 wt% exhibited the highest ionic conductivity of 170 mS cm^{-1} at 180 °C, which indicated that incorporating sulfonated components in the copolymers could increase the ionic conductivity by as much as 11% with proper choice of polymer composition and polymerization conditions.

The results of the compression creep and creep recovery tests are shown in **Figure 5.6**. The steady-state creep compliance and creep rate values for the membranes tested are given in **Table 5.6**. The creep is defined as the deformation of a material under a constant compressive force. The creep compliance (J(t)) is a measurement of the amount of creep at time t. The steady-state creep compliance (J_s^0) and creep rate were determined by plotting the creep compliance as a function of time in the linear region (t = 4 h to t = 20 h) and applying a linear regression analysis. The slope of the line corresponds to the creep rate while the y-intercept corresponds to the steady-state creep compliance. Thus, a lower value of creep

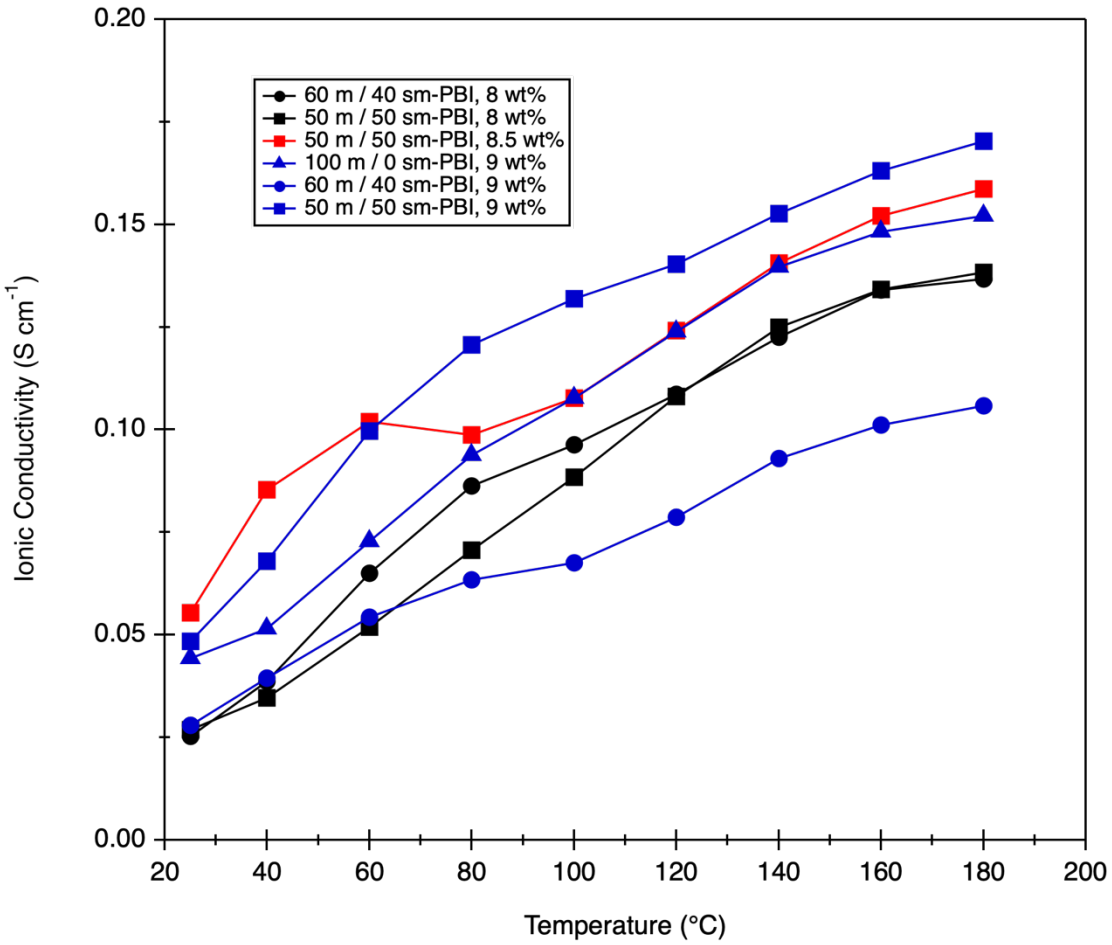

Figure 5.5. Anhydrous ionic conductivity measured for PBI copolymers containing sulfonated monomers.

compliance, steady-state creep compliance, and creep rate represents a material with a high creep resistance.

Each PBI membrane tested exhibited good creep resistance, with creep compliance values less than 2.5 x 10^{-6} Pa^{-1}. The steady-state creep compliance values were very similar and ranged from 1.56 to 1.80 x 10^{-6} Pa^{-1}. However, there were larger differences in the creep rate. The 100 m/0 sm-PBI polymerized with a monomer charge of 9 wt% and the 50 m/50 sm-PBI polymerized with an 8.5 wt% monomer charge displayed the lowest creep rates that were fairly similar, 5.63 x

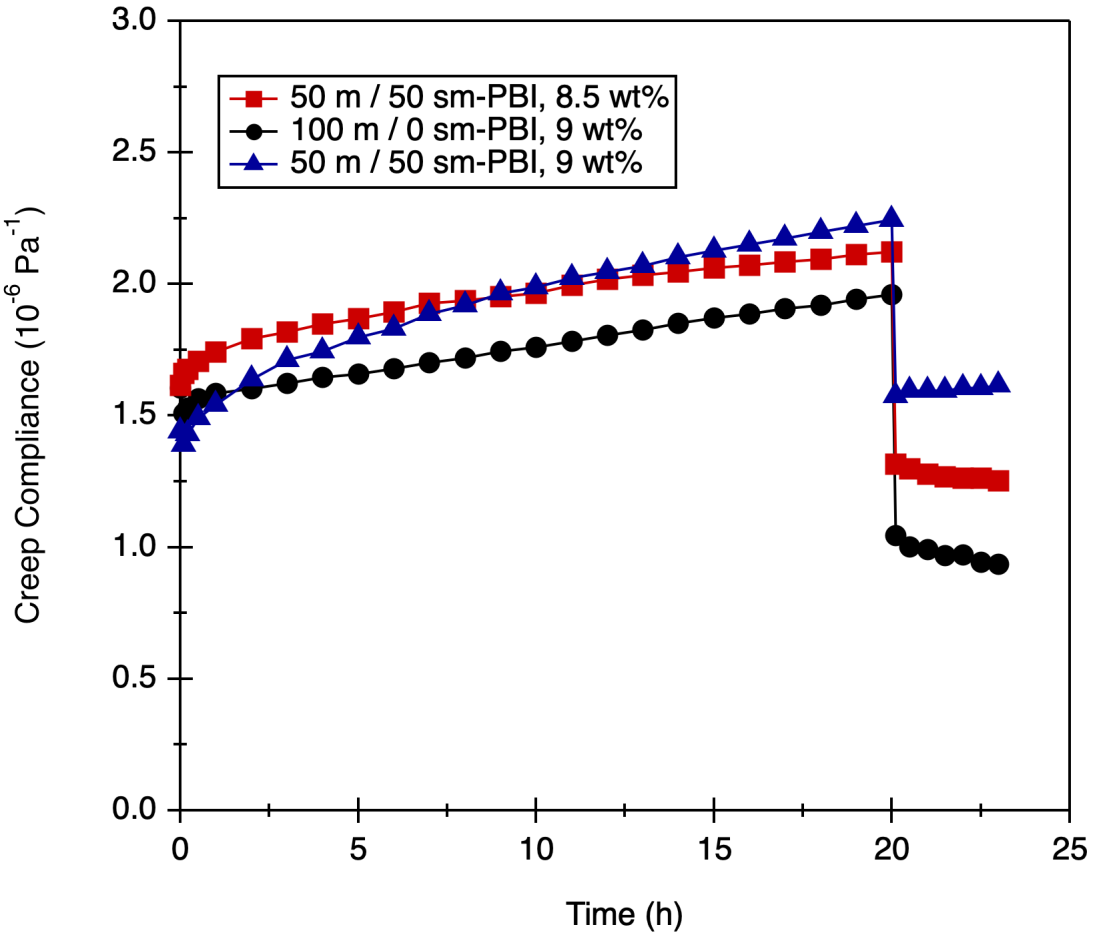

Figure 5.6. Creep compliance of 50 m/50 sm-PBI polymerized with a monomer charge of 8.5 wt%, 100 m/0 sm-PBI polymerized with a monomer charge of 9 wt% and 50 m/50 sm-PBI polymerized with a monomer charge of 9 wt%.

Table 5.6 Steady-state creep compliance and creep rate.

Sample	J_s^0 (10^{-6} Pa^{-1})	Creep Rate (10^{-12} Pa^{-1} s^{-1})
50 m/50 sm-PBI, 8.5 wt%	1.80	4.72
100 m/0 sm-PBI, 9 wt%	1.56	5.63
50 m/50 sm-PBI, 9 wt%	1.67	8.36

10^{-12} Pa^{-1} s^{-1} and 4.72 x 10^{-12} Pa^{-1} s^{-1}, respectively. These two samples also contained the highest polymer content of the membranes tested. The 50 m/50 sm-PBI polymerized with a monomer charge of 9 wt% had a higher creep rate, meaning it was less resistant to creep than the other samples. Titration data of this sample indicated it had slightly lower polymer content within the membrane, which explains the slightly higher creep rate measured. Overall, the copolymers displayed excellent creep resistance, and the creep rate was lower as the polymer content within the membrane increased, as previously reported.[26]

Although the 50 m/50 sm-PBI membrane polymerized with a monomer charge of 9 wt% exhibited the highest ionic conductivity, the sample unfortunately continually suffered from bubbles within the membrane, which would have resulted in pinholes within the membrane and fuel crossover during fuel cell testing. Fuel cell performance was thus evaluated for the 100 m/0 sm-PBI membrane and the 50 m/50 sm-PBI membrane with a monomer charge of 8.5 wt%.

The polarization curves shown in **Figure 5.7** were collected at 160 °C at various current densities using hydrogen and air. Both samples were able to operate up to 160 °C without any external humidification. The 50m/50 sm-PBI membrane showed higher performance than the 100 m/0 sm-PBI sample. Although the 100 m/0 sm-PBI membrane had a lower ionic conductivity than the 50 m/50 sm-PBI membrane, the difference between the polarization curves appear larger than can be attributed to only the small differences in ionic conductivity. The 100 m/0 sm-PBI membrane performance was significantly lower at higher current densities, which indicates mass transfer losses. Minimal optimization of

the MEA preparation was conducted, which could contribute to the performance differences observed in these limited studies.

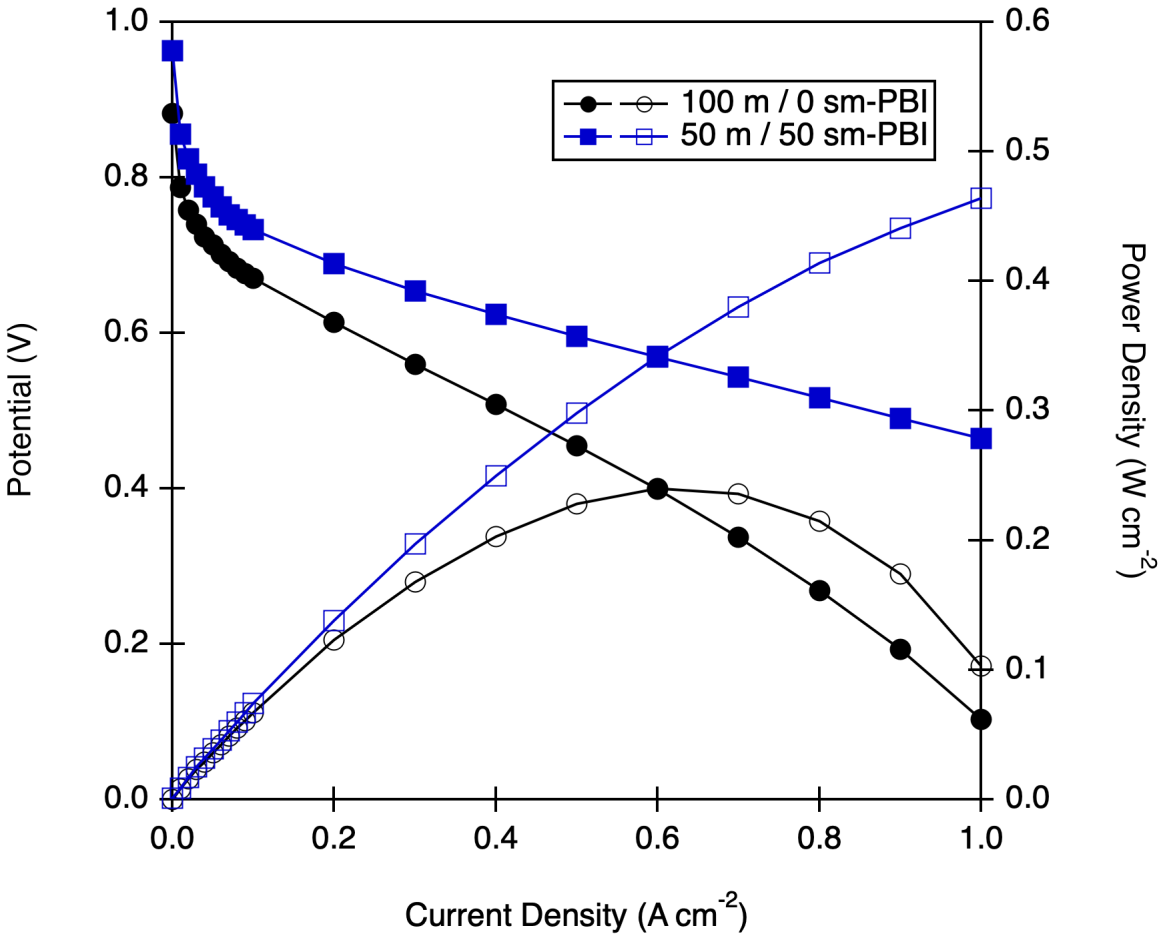

Figure 5.7. Polarization (filled symbols) and power density (unfilled symbols) curves for the 100 m/ 0 sm-PBI polymerized at 9 wt% monomer charge (black) and 50 m/50 sm-PBI polymerized with 8.5 wt% monomer charge (blue) tested in a 45.15 cm^2 cell. H_2/Air = 1.2/2.0 stoichiometric flows, no external humidification.

5.4.3 Characterization for VRB Applications

For VRB evaluation, membrane samples were subjected to acid switching by placing the PA-doped PBI gel membranes in a series of water bathes until pH indication paper was neutral indicating that the PA was removed. The samples

were then placed in 2.6 M sulfuric acid, and titrated to determine the acid doping level and membrane composition (**Table 5.7**). While the samples that were polymerized with a monomer charge of 9 wt% contained a higher solids content than samples polymerized with a monomer charge of 8 wt%, the sample polymerized with a monomer charge of 8.5 wt% contained the highest overall solids content. However, there were no clear trends observed with the various PBI polymerizations or the monomer charge on the acid doping level or membrane composition measured.

Table 5.7. Acid doping levels and membrane compositions of PBIs doped in 2.6 M sulfuric acid.

Composition	Monomer Charge (wt%)	Acid Doping Level (SA/PRU)	SA Content (wt%)	PBI Content (wt%)	Water Content (wt%)
60 m/40 sm	8	2.93 ± 0.05	21.0 ± 0.22	24.8 ± 0.20	66.5 ± 0.71
50 m/50 sm	8	3.81 ± 0.03	24.8 ± 0.14	23.1 ± 0.16	54.7 ± 0.66
50 m/50 sm	8.5	2.03 ± 0.13	25.5 ± 2.9	45.3 ± 2.4	29.1 ± 5.1
60 m/40 sm	9	4.36 ± 0.09	28.6 ± 0.55	34.1 ± 0.23	37.2 ± 0.55
50 m/50 sm	9	2.81 ± 0.01	24.0 ± 0.9	30.9 ± 1.1	45.0 ± 2.0
0 p/100 sp	4	10.5 ± 2.1	20.9 ± 0.3	8.24 ± 1.6	70.8 ± 1.5

Table 5.8 shows the results of the in-plane ionic conductivity and vanadium permeability measurements. The 50 m/50 sm-PBI samples polymerized at 8, 8.5, and 9 wt% monomer charge each displayed about the same ionic conductivity of ~110 mS cm^{-1}. The permeability, however, varied with monomer charge. The 50 m/50 sm-PBI polymerized with 8.5 wt% monomer charge contained the highest solids content within the membrane (45.3 wt% PBI) and the lowest permeability.

The 50 m/50 sm-PBI polymerized with 9 wt% monomer charge had the second highest solids content within the membrane (30.9 wt%) and its permeability fell between that 50 m/50 sm-PBI polymerized at 8 and 8.5 wt%. Thus while their conductivities were similar, their permeabilities varied with the solids content measured in each membrane.

Table 5.8. Ionic conductivity and vanadium permeability of PBI samples doped in 2.6 M H_2SO_4.

Composition	Monomer Charge (wt%)	Ionic Conductivity (mS cm^{-1})	Permeability (10^{-8} cm^2 s^{-1})
60 m/40 sm	8	280	20.0
50 m/50 sm	8	109	55.9
50 m/50 sm	8.5	112	9.94
60 m/40 sm	9	150	29.0
50 m/50 sm	9	110	36.9
0 p/100 sp[a]	4	593	57.4

[a] Data from literature[2]

The 60 m/40 sm-PBI membranes polymerized at 8 and 9 wt% monomer charge displayed different values for ionic conductivity and permeability. The sample polymerized with a monomer charge of 8 wt% exhibited a higher ionic conductivity and a lower vanadium permeability than the sample polymerized at 9 wt% monomer charge. This was not expected as the 9 wt% monomer charge sample contained a higher acid doping level and a higher solids content than the sample polymerized with an 8 wt% monomer charge.

Overall, there was no correlation with the acid doping level or the composition of sulfuric acid measured in each sample with the measured ionic conductivity. However, the two 60 m/40 sm-PBI membranes exhibited higher ionic conductivities than the 50 m/50 sm-PBI membranes. For permeability, the sample with the highest PBI content (50 m/50 sm-PBI, 8.5 wt% monomer charge) had the lowest permeability, while the sample with the lowest PBI content (50 m/50 sm-PBI, 8 wt% monomer charge) exhibited the highest vanadium permeability.

Compared to the 0 p/100 sp-PBI from the literature, the m/sm-PBIs are able to achieve a greater range of properties (**Figure 5.8**). The vanadium permeability was reduced by an order of magnitude with the 50 m/ 50 sm-PBI polymerized with a monomer charge of 8.5 wt%. Although the ionic conductivity was also reduced to 112 mS cm^{-1} from 593 mS cm^{-1} for the 0 p/100 sp-PBI, the ionic conductivity was still significantly higher than conventionally imbibed PBIs (<20 mS cm^{-1}).[28]

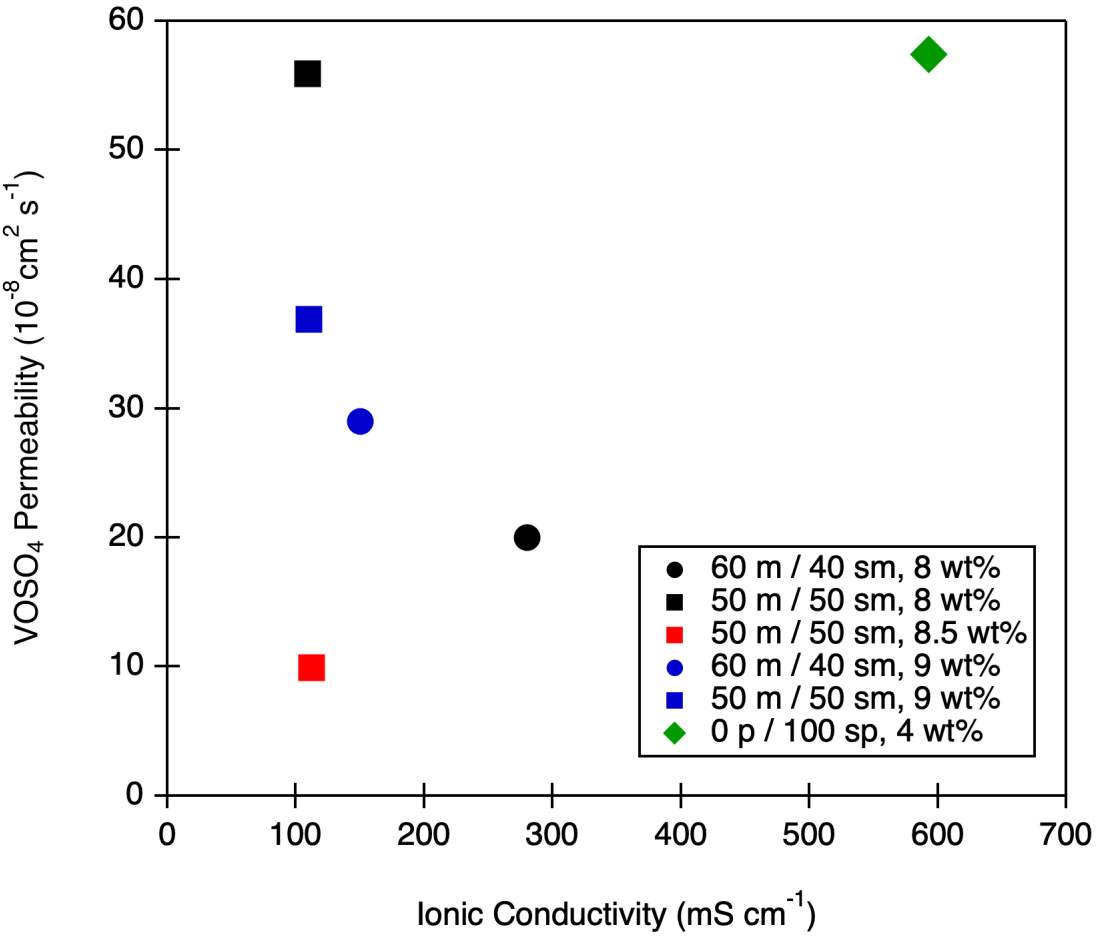

Figure 5.8. Comparison of ionic conductivity and vanadium permeability for various PBI membranes doped in 2.6 M H_2SO_4.

5.5 CONCLUSIONS

A series of novel m/sm-PBI copolymers were synthesized and characterized to determine their potential application in HT-PEMFCs and VRBs. It was found that copolymer compositions of 60 m/40 sm-PBI and 50 m/50 sm-PBI provided the best film forming properties and monomer charges of 8-9 wt% were excellent for attaining high IV polymers and solutions that could be readily processed into membranes. Copolymers that incorporated more sulfonated monomer did not yield polymers with good mechanical properties and displayed

low IV's. Furthermore, it was found that the composition of sulfur in the membranes decreased as the polymerization time increased, which potentially indicated some compositional drift.

For HT-PEMFC applications, the 50 m/50 sm-PBIs polymerized with a monomer charge of 8.5 and 9 wt% exhibited ionic conductivities above 100 mS cm^{-1} at 180 °C. Each of these membranes displayed a high solids content and good creep resistance. The membrane formed from 50 m/50 sm-PBI polymerized with a monomer charge of 8.5 wt% was tested in a fuel cell and found to perform higher than 100 m/ 0 sm-PBI membrane. However, the initial testing was fairly limited and MEA optimization needs to be conducted to provide full evaluation.

There was a wide range of properties observed with the vanadium permeability and conductivity for the PBI membranes tested for application in VRBs. Higher solids content within the membrane generally led to lower vanadium permeability, but also lower ionic conductivity. Compared to 0 p/100 sp-PBI, which was polymerized at a monomer concentration of 4 wt%, the 50 m/50 sm-PBI polymerized at a monomer content of 8.5 wt% displayed an order of magnitude decrease in vanadium permeability. Unfortunately, the ionic conductivity was also 81% lower than the 0 p/100 sp-PBI. However, further testing needs to be completed to determine if the lower vanadium permeability makes a significant impact in cell testing.

5.6 REFERENCES

[1] Steele, B. C. H.; Heinzel, A. Materials for fuel-cell technologies. *Nature* **2001,** *414* (6861), 345-352.

[2] Wang, L.; Pingitore, A. T.; Xie, W.; Yang, Z.; Perry, M. L.; Benicewicz, B. C. Sulfonated PBI Gel Membranes for Redox Flow Batteries. *Journal of The Electrochemical Society* **2019,** *166* (8), A1449-A1455.

[3] Mader, J. A.; Benicewicz, B. C. Synthesis and properties of segmented block copolymers of functionalised polybenzimidazoles for high-temperature PEM fuel cells. *Fuel Cells* **2011,** *11* (2), 222-237.

[4] Mader, J.; Benicewicz, B. Synthesis and properties of random copolymers of functionalised polybenzimidazoles for high temperature fuel cells. *Fuel Cells* **2011,** *11* (2), 212-221.

[5] Mader, J. A.; Benicewicz, B. C. Sulfonated Polybenzimidazoles for High Temperature PEM Fuel Cells. *Macromolecules* **2010,** *43* (16), 6706-6715.

[6] Staiti, P.; Lufrano, F.; Aricò, A. S.; Passalacqua, E.; Antonucci, V. Sulfonated polybenzimidazole membranes — preparation and physico-chemical characterization. *Journal of Membrane Science* **2001,** *188* (1), 71-78.

[7] Vogel, H.; Marvel, C. S. Polybenzimidazoles, new thermally stable polymers. *Journal of Polymer Science* **1961,** *50* (154), 511-539.

[8] Garsany, Y.; Gould, B. D.; Baturina, O. A.; Swider-Lyons, K. E. Comparison of the Sulfur Poisoning of PBI and Nafion PEMFC Cathodes. *Electrochemical and Solid-State Letters* **2009,** *12* (9), B138.

[9] Song, C.; Hui, S.; Zhang, J. High-temperature PEM Fuel Cell Catalysts and Catalyst Layers. In *PEM Fuel Cell Electrocatalysts and Catalyst Layers: Fundamentals and Applications*, Zhang, J., Ed. Springer, 2008; pp 861-888. DOI: 10.1007/978-1-84800-936-3_18

[10] Li, Q.; He, R.; Gao, J.-A.; Jensen, J. O.; Bjerrum, N. J. The CO Poisoning Effect in PEMFCs Operational at Temperatures up to 200°C. *Journal of The Electrochemical Society* **2003,** *150* (12), A1599.

[11] Asensio, J. A.; Sánchez, E. M.; Gómez-Romero, P. Proton-conducting membranes based on benzimidazole polymers for high-temperature PEM fuel cells. A chemical quest. *Chemical Society Reviews* **2010,** *39* (8), 3210-3239.

[12] Bose, S.; Kuila, T.; Nguyen, T. X. H.; Kim, N. H.; Lau, K.-t.; Lee, J. H. Polymer membranes for high temperature proton exchange membrane fuel cell: Recent advances and challenges. *Progress in Polymer Science* **2011,** *36* (6), 813-843.

[13] Chandan, A.; Hattenberger, M.; El-kharouf, A.; Du, S.; Dhir, A.; Self, V.; Pollet, B. G.; Ingram, A.; Bujalski, W. High temperature (HT) polymer electrolyte membrane fuel cells (PEMFC) – A review. *Journal of Power Sources* **2013,** *231*, 264-278.

[14] Clouser, S. J.; Huang, J. C.; Yeager, E. Temperature dependence of the Tafel slope for oxygen reduction on platinum in concentrated phosphoric acid. *Journal of Applied Electrochemistry* **1993,** *23* (6), 597-605.

[15] Zhu, Y.; Zhu, W. H.; Tatarchuk, B. J. Performance comparison between high temperature and traditional proton exchange membrane fuel cell stacks using electrochemical impedance spectroscopy. *Journal of Power Sources* **2014,** *256*, 250-257.

[16] Zhang, C.; Zhang, L.; Zhou, W.; Wang, Y.; Chan, S. H. Investigation of water transport and its effect on performance of high-temperature PEM fuel cells. *Electrochimica Acta* **2014,** *149*, 271-277.

[17] He, R.; Li, Q.; Xiao, G.; Bjerrum, N. J. Proton conductivity of phosphoric acid doped polybenzimidazole and its composites with inorganic proton conductors. *Journal of Membrane Science* **2003,** *226* (1), 169-184.

[18] Kear, G.; Shah, A. A.; Walsh, F. C. Development of the all-vanadium redox flow battery for energy storage: a review of technological, financial and policy aspects. *International Journal of Energy Research* **2012,** *36* (11), 1105-1120.

[19] Skyllas-Kazacos, M.; Kazacos, G.; Poon, G.; Verseema, H. Recent advances with UNSW vanadium-based redox flow batteries. *International Journal of Energy Research* **2010,** *34* (2), 182-189.

[20] Ponce de León, C.; Frías-Ferrer, A.; González-García, J.; Szánto, D. A.; Walsh, F. C. Redox flow cells for energy conversion. *Journal of Power Sources* **2006,** *160* (1), 716-732.

[21] Li, X.; Zhang, H.; Mai, Z.; Zhang, H.; Vankelecom, I. Ion exchange membranes for vanadium redox flow battery (VRB) applications. *Energy & Environmental Science* **2011,** *4* (4), 1147-1160.

[22] Skyllas-Kazacos, M.; Grossmith, F. Efficient Vanadium Redox Flow Cell. *Journal of The Electrochemical Society* **1987,** *134* (12), 2950-2953.

[23] Perry, K. A.; L. More, K.; Payzant, E. A.; Meisner, R. A.; Sumpter, B. G.; Benicewicz, B. C. A comparative study of phosphoric acid-doped m-PBI membranes. *Journal of Polymer Science Part B: Polymer Physics* **2014,** *52* (1), 26-35.

[24] Xiao, L.; Zhang, H.; Scanlon, E.; Ramanathan, L. S.; Choe, E.-W.; Rogers, D.; Apple, T.; Benicewicz, B. C. High-Temperature Polybenzimidazole Fuel Cell Membranes via a Sol−Gel Process. *Chemistry of Materials* **2005,** *17* (21), 5328-5333.

[25] Xie, W.; Darling, R. M.; Perry, M. L. Processing and Pretreatment Effects on Vanadium Transport in Nafion Membranes. *Journal of The Electrochemical Society* **2015,** *163* (1), A5084-A5089.

[26] Chen, X.; Qian, G.; Molleo, M. A.; Benicewicz, B. C.; Ploehn, H. J. High temperature creep behavior of phosphoric acid-polybenzimidazole gel membranes. *Journal of Polymer Science Part B: Polymer Physics* **2015,** *53* (21), 1527-1538.

[27] Zeng, Y. K.; Zhao, T. S.; An, L.; Zhou, X. L.; Wei, L. A comparative study of all-vanadium and iron-chromium redox flow batteries for large-scale energy storage. *Journal of Power Sources* **2015,** *300*, 438-443.

[28] Peng, S.; Yan, X.; Wu, X.; Zhang, D.; Luo, Y.; Su, L.; He, G. Thin skinned asymmetric polybenzimidazole membranes with readily tunable morphologies for high-performance vanadium flow batteries. *RSC Advances* **2017,** *7* (4), 1852-1862.

CHAPTER 6

SUMMARY AND OUTLOOK

This dissertation focuses on the synthesis, characterization and application of novel PBI membranes. A new processing technique was developed which allowed dense PBIs with more rigid backbone structures to be prepared for the first time. This new process paves the way to superior membranes for electrochemical devices. The applications of novel PBI membranes were studied for their application in high temperature polymer electrolyte membrane fuel cells, electrochemical hydrogen separation, and vanadium redox flow batteries.

Chapter 2 of this dissertation focuses on the development of the new processing technique to produce dense films and their properties. Various para-oriented PBIs were synthesized and characterized for thermal stability and mechanical properties. The PBIs prepared in the new method were compared to dense m-PBI films that are commercially produced from the solvent-casting method. Using this new method, dense PBI films were produced for the first time without the use of organic solvents by controlled drying of a gel PBI membrane into a dense PBI film. Films made from the more rigid p-PBI displayed higher thermal stability and better mechanical properties than m-PBI films produced from the organic solvent-casting method.

Chapter 3 expands on the novel processing technique outlined in Chapter 2 and explores the dense PBI membranes for application in vanadium redox flow batteries. Different types of PBIs were produced as dense PBI films from the new solvent-free process and doped in sulfuric acid. Ex-situ characterization was completed to gain an understanding of the membrane properties and acid uptake. Cell testing was also completed to understand the practical application and limitation of these membranes. The properties of the acid-doped dense PBI films

were compared to the original gel PBI membrane. Membranes produced in the new process were able to achieve an order of magnitude reduction in vanadium permeability, while maintaining relatively high ionic conductivity. Cell testing showed that membranes produced in the new process had stable performance for about 7 months and couple be operated at higher current densities than previously reported.

Chapter 4 further expands on the processing technique by investigating applications of the dense PBI membranes in high temperature polymer electrolyte membrane fuel cells and electrochemical hydrogen separation. The doping of dense p-PBI was investigated by varying the acid bath concentration, temperature, and duration of doping. Ex-situ properties were investigated including acid doping level, ionic conductivity, and mechanical properties. The doped membrane after optimization was compared to various types of PBIs produced both in the PPA Process and the conventional imbibing method. The dense p-PBI membrane doped in phosphoric acid displayed high ionic conductivity and excellent mechanical properties, which was not expected. We hypothesized that the novel process led to changes in the morphology of the PBI, and was responsible for the improved properties. Additional testing such as BET measurements provided preliminary data that support the hypothesis. Fuel cell and electrochemical hydrogen separation testing was completed to study the in-cell performance of the new membranes. Compared to the gel p-PBI membrane, which is a commercial product, the dense p-PBI membranes displayed equal or better electrochemical performance under a wide variety of operating conditions. This indicated that the

novel processing technique led to superior membranes that are more durable for next-level energy applications, such as aviation and heavy-duty vehicles.

Chapter 5 is a departure from the novel processing technique outlined in Chapter 1 and instead focuses on the synthesis of novel copolymer sulfonated gel PBI membranes. The copolymers were prepared in the PPA Process and various copolymer compositions as well as monomer charges were investigated to optimize the membrane synthesis. The application of the copolymers in redox flow batteries and fuel cells were explored. In fuel cell testing, it was found that the copolymers could provide higher ionic conductivity than m-PBI homopolymers and displayed excellent mechanical properties. In flow battery applications, the copolymers showed lower vanadium permeability than para-oriented gel PBIs, and lower ionic conductivities. However, further testing needs to be completed to study the effects of the ex-situ properties during cell testing.